

**X-612-67-479**

NASA TM X-55944

# THE GEOMAGNETIC SECULAR VARIATION 1900-1965

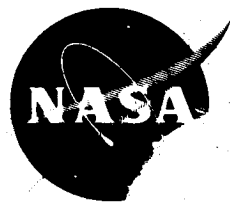
# **JOSEPH C. CAIN**

# **SHIRLEY J. HENDRICKS**

FACILITY FORM 602	N67-37398 (ACCESSION NUMBER) 231-
	(PAGES)
	TMX-55944 (NASA CR OR TMX OR AD NUMBER)

(THRU) *P*  
(CODE) *13*  
(CATEGORY)

ÜBER 1967



# **GODDARD SPACE FLIGHT CENTER**

## **GREENBELT, MARYLAND**

THE GEOMAGNETIC SECULAR VARIATION

1900 - 1965

Joseph C. Cain

Shirley J. Hendricks

September 1967

## ABSTRACT

The GSFC(12/66) model of the main geomagnetic field uses linear and parabolic terms in time to represent secular change over the interval 1900-1965. The predicted field is compared with observatory annual means to investigate systematic residuals. Deviations of the order of 100γ are noted for short spans of years and are observed to occur only in limited regions. Otherwise, the trends of the computed field parallel the observations. Comparisons of secular change charts with those drawn by earlier analyses show good agreement.

The westward drift is generally noted in the vector representation of the harmonic coefficients except that a few terms are seen to undergo predominantly an amplitude change. The components below ( $g_6^6$ ,  $h_6^6$ ) that show a recognizable eastward drift are the (3,2) and (5,2) terms.

Both dip poles are noted to move smoothly northwestward over the interval whereas the dipole position initially drifts eastward, reverses direction near 1920, and then moves westward at a rate up to about 0.7°/year. Its 1965 position is found to be 78.8°N and 70.0°W.

## Introduction

Over the last few centuries there have literally been hundreds of papers written concerning the main geomagnetic field and its secular variation. These past research efforts follow two main lines of approach in their analyses: 1) the data from fixed observatories or relocatable positions (repeat stations) are differenced over a period of a year or two and the differences by components are contoured on charts. These secular change, or isoporic, charts can be compared at intervals of decades to learn how the patterns are altering with time. 2) Magnetic charts for given epochs are constructed using survey observations that are reduced to the epoch of the chart. These charts are subjected to a spherical harmonic analysis and the results compared for several epochs (Mauersberger, 1952; McDonald and Gunst, 1967).

Recently, however, we have elected to take a different approach to the problem of representing the field and its secular change by attempting to perform a numerical fitting to all of the observational data available to us through the Magnetic Division of the United States Coast and Geodetic Survey for the period 1900-1964 plus some recent global satellite data acquired by the OGO-2 satellite. The result of this work, designated the GSFC(12/66) field model (Cain et al., 1967), is intended to be used as an initial tool for aiding in the evaluations of the time variations in the field observed by OGO-2. A set of 120 spherical harmonics of the internal potential were obtained, including their first and second time derivatives.

The accuracy of this expansion in matching the observational data was expressed in terms of the residuals of fit by type of data, component, and epoch. It was shown that the non-satellite data scattered about the fit with a distribution that was gaussian ( $\sigma \sim 120\gamma$ ) except for higher-than-gaussian tails. Over half of the data of a given component lay within  $100\gamma$ , 75% within  $200\gamma$  and 95% within  $500\gamma$  of the fit. The distribution by component varied slightly, with the gaussian "core" of the  $\Delta Z$  distribution being the widest at  $210\gamma$  whereas the total field distribution, with a  $100\gamma$  core was the narrowest. Inspection of the data makes it clear that the large non-gaussian excursions of the survey data about the fitting surface are due to crustal anomalies. Considering the fact that the distributions were obtained without any selection (on our part) of the observations, and no time corrections were made, it is remarkable that only 5% of the data fall outside of the  $500\gamma$  limit.

The satellite data are free from the influence of these crustal anomalies and scatter a much smaller amount from the fitting surface. The OGO-2 total field data used were taken from a magnetically quiet period (October 29-November 15, 1965) and deviated with an almost gaussian distribution whose constant was  $12\gamma$ .

The root-mean-square residuals (data differing by more than  $2000\gamma$  were rejected) of the survey data was found to be of the order of  $180$ - $260\gamma$  for individual years over the interval 1906-1964 after

decreasing from a peak of 320γ at 1900. It was suggested in the previous paper that there may thus be systematic deviations of the secular change estimates from the fitting surface.

In this paper we will show the way in which the parabolic series in time for the spherical harmonic coefficients matches the field variations measured at a selection of magnetic observatories and also will comment on some of the features of secular change compared with those made in past papers. In reviewing the past work on secular changes we have been surprised to find few displays of the comparisons between the observational data and the results of analysis.

### The Use of Secular Change "Data" In the Fit

Consideration was previously given to the possibility of using the year-to-year differences at the observatories and repeat stations as separate information which would help determine the secular change coefficients along with the main field terms. Such an analysis was attempted and the results reported at the IUGG meeting in Berkeley in 1963. It was noted that the secular change could only be entered as a constraint to the fitting equations in an artificial way and that the relative importance of the secular change "data" compared with the effect of the rest of the observations had to be entered as an arbitrary factor. Separate considerations of using secular change were then discontinued.

In creating the GSFC(12/66) field model, a deviation was made from the practice mentioned in a past work in that no special heavy weighting was given to the observatory data included in the fit. As explained in the discussion of the GSFC(12/66) derivation it was noted that the earlier determinations (Cain et al., 1965; Hendricks and Cain, 1966; and Cain, 1966) used very heavy relative weights for the observatory data because the accuracy is higher than the field survey data. However, it was noted in reviewing the results of these analyses that the scatter of the observatory data was not appreciably different from that of the rest of the observations since the main disturbing factor is the presence of crustal anomalies and not the inaccuracies of measurement. The observatory annual means were thus entered into the fit with the same relative weights as the other surface data.

Comparison With Observatory Annual Means

The results of comparing the field components computed from the GSFC(12/66) model with annual means observed at a selection of magnetic observatories is given in Appendix A. These graphs (plotted automatically) are ordered alphabetically by observatory name. An observatory is deleted only if fewer than five annual means are available. Noted under each name is the observatory's latest location, longitude (positive east), geodetic latitude in decimal degrees, and the altitude in kilometers, if known and above 100 meters. The vertical scales are arranged from left to right, H and Z are in gammas with  $1000\gamma$  between abscissa (Z positive down), and D is in degrees (positive eastward) at  $2^\circ$  intervals. The computed values are traced by the solid lines and are labeled on the right side according as they are H, D, or Z. There is a break in the computed curves if the observatory was moved. The calculations are made as appropriate to the site of observation.

The observed annual means are plotted as  $\otimes$  for H,  $\odot$  for D, and  $\square$  for Z. The computed values are fed to the (cathode ray tube) plotter for each year for which there are observations of a component. The plotter beam is left on between points and traces out a straight line. The continuous curves thus appear lighter for those years for which observed means are missing since the beam moves more quickly, and, whereas a continuous set of points appears to give a smooth curve, large gaps in the data (e.g. Chelyuskin, Hel) result in a straight line connecting the points.

One other idiosyncrasy is that on occasion the observed data disappear from the top or bottom of the plots. This problem arose in imperfections in the computer algorithm to choose a scale suitable to all graphs. Since it affected but a few plots and the algorithm was already quite complex it was decided to omit the worst offenders and leave the rest. Thus in a few instances (e.g. Dombas Z before 1928) there are more observed data than appear on the graphs.

The fact that there are numerous instances where the observed and measured data appear to parallel each other with up to a few hundred gammas displacement (e.g. Alibag) suggests that the absolute differences are due to crustal anomalies. This view is strengthened by such examples as Honolulu where the observed values are seen to hop from one side of the computed D and H curves when the station was moved near 1947.

The question then arises as to whether the total observed secular change represents that of the main field or whether it includes a contribution from crustal matter with a "soft" permeability. At this juncture we assume that the changes in the anomaly field with time are of small consequence. Such changes are likely to be of the order of the percentage secular change multiplied by the size of the anomaly. Thus for the 95% of the data within 500', variations of the anomaly field due to a few percent change of the

main field would represent only a few gammas. An inspection of the graphs in the appendix indicates that the oscillations of the data from the fitting surface is more often of the order of 100γ.

One other factor in regard to the influence of anomalies has been pointed out by Eleman (1966). He notes that if a constant anomaly causes the observed annual means  $H$  and  $D$  to deviate from the normal field  $H_N$  and  $D_N$ , then a representation of secular change in terms of  $\dot{H}$  and  $\dot{D}$  can be in error. Letting  $\delta = D_N - D$ , the secular change of the normal field is given by

$$\dot{D}_N \cong (H/H_N)\dot{D} - (\dot{H}/H_N)\delta$$

$$\dot{H}_N = \dot{H} + H\dot{D}\delta$$

if  $\delta$  is sufficiently small that  $\cos\delta \approx 1$  and  $\sin\delta \approx \delta$ . Eleman (1966) showed that for Kiruna (1954-1955) the second terms amount to about 1'/year for  $\dot{D}$  and 4γ/year for  $\dot{H}$ .

Although a plot of the data in the orthogonal components X, Y, and Z would eliminate any concern over this geometric interaction, we have chosen to make the comparison here in terms of the observed values. At this stage such refinements are not essential.

If the displacement due to crustal anomalies is taken into account, the trends of the curves can be compared with the observations to inspect the degree of comparability in secular change.

Considering that the fit was made to a selection of all data without any corrections for storm variations or other transient effects such as the diurnal variations, the agreement is seen to be generally quite good. For most observatories the computed and measured H component trends are not only very nearly parallel but also show relatively little absolute displacement. Trends in declination agree a little less well. The vertical intensity curves show the largest displacements, the poorest agreement, and the largest scatter of observational data.

The major discrepancies between the predicted and observed data are seen to be at the western edge of the Indian Ocean. For the two stations Mauritius and Tananarive the declination data appears to have a smooth parabolic shape which is considerably different from the computed curves. Alibag declination also shows an increasing deviation from the computed values at recent epochs after tracking very well for the first 40 years.

For most of the other graphs the deviations from the computed curves are sufficiently greater than any errors of measurement that they must be real, but generally can be regarded as second order perturbations from the main trend of secular change. The reality of such deviations can of course be important if one is attempting to use the field model to compute a reference field, particularly for extrapolations beyond 1965, and also for theoretical considerations as to their cause.

One correlation to be noted later herein is that of changes of rotation rate of the earth with trends in secular change (Dicke, 1966). In the period 1900-1920, for example, there may have been a short lived reversal of the slowing of the earth's rotation rate that has otherwise appeared to be almost constant from 1800 through 1950 (Munk and MacDonald, 1960). The high residuals of fit from 1900 to 1910 noted in the previous paper (Cain et al., 1967) may have been related to this phenomena. Without having survey data available to us for the eighteenth century we could never be sure that such an increase was not merely the result of the numerical process of least squares where the residuals sometimes are largest near the fringes of the data set, particularly when the data distribution is relatively thin as it is for 1900-1910.

However, the graphs in Appendix A do show that there does appear to be a definite trend away from the parabolic curves for the interval 1900-1910 for some components and stations. An inspection of the plots for all English and European observatories (e.g. Bochum, Stonyhurst, Kew, DeBilt, Greenwich, etc.) shows that the measured secular change in H is significantly more positive than that computed. Likewise, for the same area the secular change in declination is more negative than that predicted. The boundaries of this phenomena are somewhat vague but it is clearly not present in the Pacific, South America, and Asia (e.g. Melbourne, Hong Kong, Kakioka, Christchurch, Kodaikanal, Huancayo, Santiago, Colaba ---).

In the United States (Cheltenham, Baldwin, Sitka) and central Russia (Sverdlovsk) the higher secular change in H from that computed is evident, but without the corresponding disparity in declination. It is undoubtedly such irregularities that have led to past conclusions (e.g. Chapman and Bartels, 1940, p. 130) that secular variation is a regional phenomena. Although the deviations do seem to correlate for observing stations over a given region so that a very accurate mathematical model would require their inclusion in some way, it is apparent that the general character of secular change is well represented by the model.

Of interest to those intending to use the field model as a reference for the period after 1965 is the degree to which the observed and computed trends in secular change diverge. An inspection of the diagrams again reveals that the residuals are somewhat correlated by area. The major discrepancies are summarized graphically in Figure 1. Shown here is the order of magnitude of the deviation of the observed from the computed secular change in gammas/year for H and Z and in minutes/year for D. The difference is taken in the sense of "observed-minus-computed". The numbers plotted are taken from averaging the secular change differences for the observatories indicated as dots. The boundaries of the areas are sometimes unknown since the stations are not very dense. However, in some cases nearby stations show little deviation. For example, the declination difference over northeastern Scandinavia and northwestern

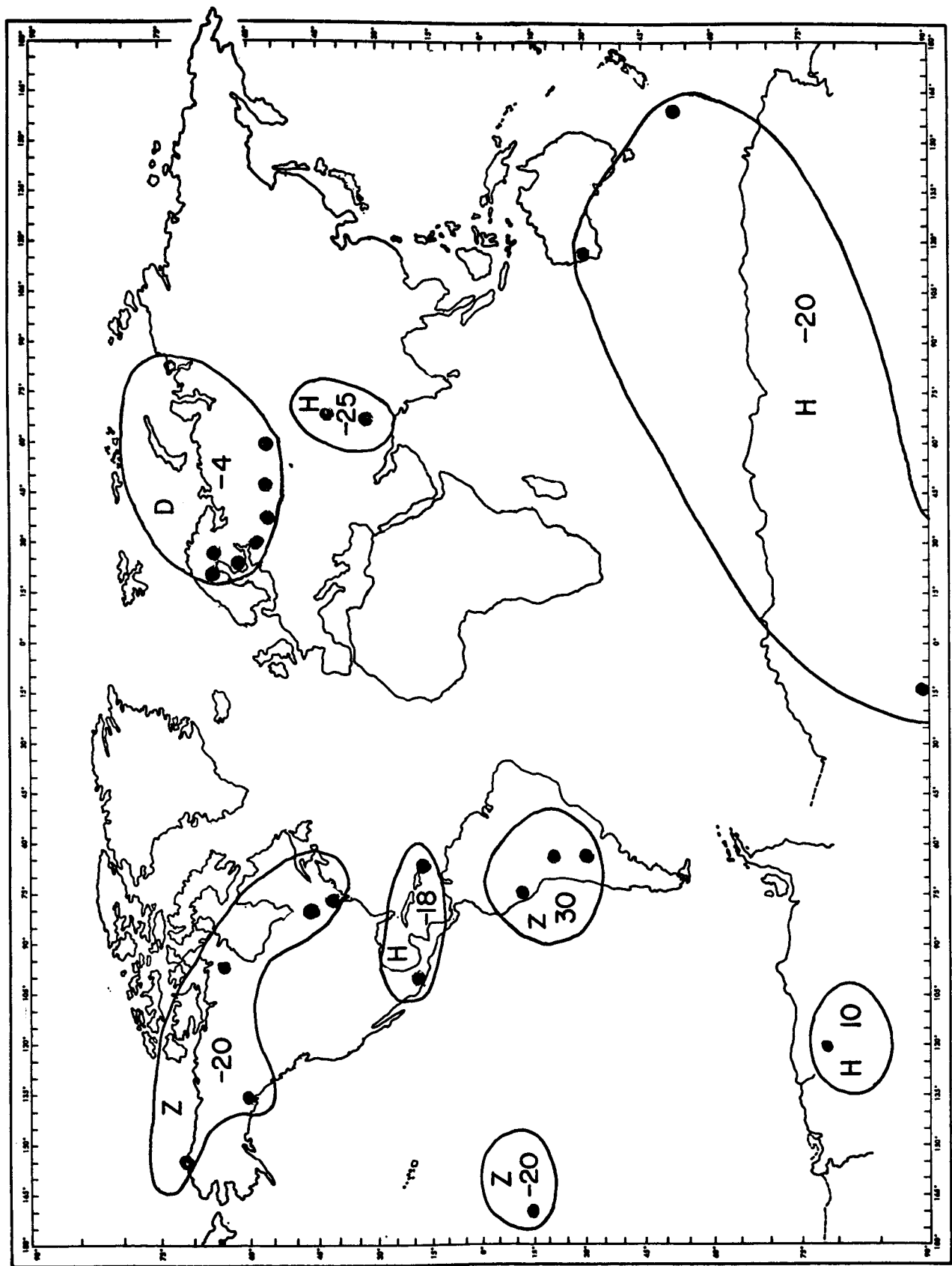


FIGURE 1:  
Deviation of observatory secular change after 1960 from GSFC(12/66) model.  
( $Z, H$  in gammas/year,  $D$  in minutes/year.)

Russia does not appear in Europe. Also, the deviation in Z at Apia and northern America does not appear at Honolulu or in the central United States. The positive Z discrepancy is largest at Huancayo ( $\sim 50\gamma/\text{yr}$ ) and smallest at Pilar ( $16\gamma/\text{yr}$ ).

Comparisons With Earlier Isoporic Charts

Using the GSFC(12/66) coefficients it is possible to compute the secular change of the components at any epoch. Although this could theoretically be done in a straightforward way for the orthogonal components by differentiating the expressions for those components and evaluating  $-\nabla \dot{V}$ , the representation of the  $\dot{H}$ ,  $\dot{D}$ , and  $\dot{I}$  would require special expansions. It is therefore computationally simpler to compute the field for a small increment of time on either side of an epoch (e.g. 0.5 years) and take the difference. This procedure was carried out for the epochs 1912.5, 1922.5, 1932.5, and 1942.5 for the components H, I, X, Y, Z, and F and isoporic charts plotted using an automatic contouring procedure similar to that described by Cain and Neilon (1963). These charts appear in Appendix B along with reproductions of the corresponding ones from Vestine et al. (1959). These charts may also be compared with those for 1922 by Fisk (Chapman and Bartels, 1940, p. 115-119).

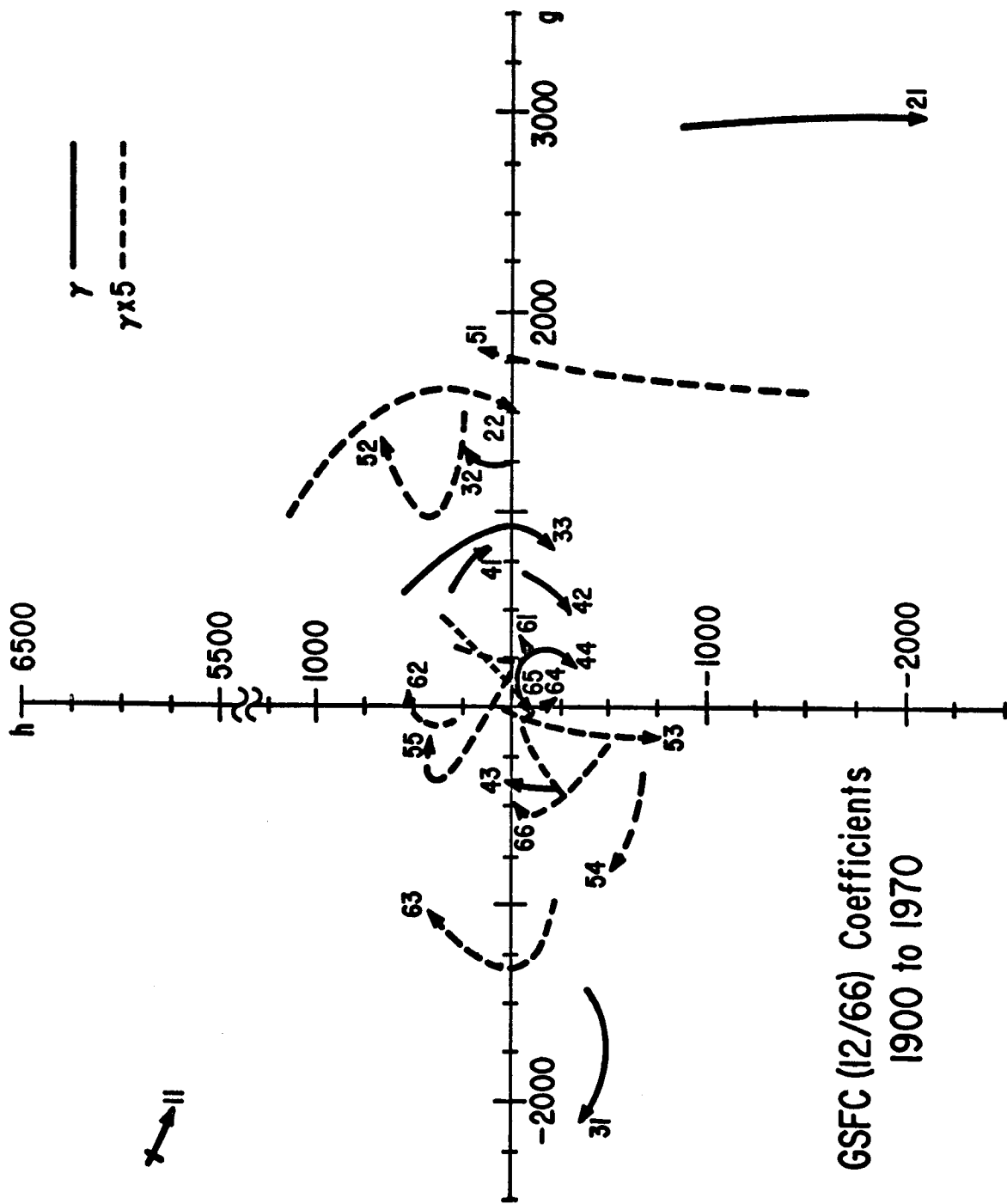
The comparison with the earlier charts shows that in all instances the basic cell structure is identical. The GSFC map extreme values do vary for the force components a few tens of gammas per year from the values given by Vestine et al. and generally have a smaller absolute magnitude. For inclination, the agreement is within a few minutes per year for the center cells. Comparison with the diagrams by Fisk for 1922 also leads to the conclusion

that the GSFC extreme values are of smaller absolute value than those on the earlier works. This fact would seem to imply that the analysis using only 120 spherical harmonics may have produced an unnecessarily smooth picture of the secular change patterns.

Field at 1965

Since the recent field is of interest to those wishing to use the GSFC(12/66) model as a reference at current epochs we have compiled in Appendix C a set of surface charts for 1965.0. These may be compared with the U. S. World Magnetic Charts for the same epoch and shown to be in close agreement. However, as previously noted in the comparison with the earlier isoporic charts, the GSFC(12/66) patterns are slightly broader and less intense. If the positive residuals given in Figure 1 for the Z component over South America are added to the contour values in that area on the Z isoporic chart, there would tend to be a sharpening of the cell pattern over South America to more closely resemble that presented in the U.S. Charts. Also, adding the negative H residual noted on Figure 1 north of India to the H isoporic chart would bring about a better agreement with the U.S. Charts.

Thus it is likely that the present method of representation produces patterns which may in general be smoother than the observed changes. However, more work would be needed in this area to determine whether the representation could be realistically improved for the whole sphere with the present set of data. These comparisons do suggest that the user of the GSFC(12/66) model as a reference beyond 1965 should be wary of possible deviations of the order of magnitude indicated in Figure 1.



# GSFC (I2/66) Coefficients 1900 to 1970

FIGURE 2

Drift of Harmonic Components

In order to display one aspect of secular change we plot the  $g, h$  harmonic vectors in Figure 2. The trace of the individual components is given from 1900 to 1970, with the arrow at the later date, for the components  $(g_1^1, h_1^1)$  through  $(g_6^6, h_6^6)$ . The scale is in gammas and must be divided by 5 for the  $(g_5^1, h_5^1)$  through  $(g_6^6, h_6^6)$  traces. Also, the scale is broken for the large  $h_1^1$  component. This figure is very similar to that given by Cain and Hide (1966) using the results of an earlier analysis. Although the traces are given by a single curved arrow for the whole interval without indicating the location of the points for the years between 1900 and 1970, a detailed inspection of the data revealed that the years fall almost uniformly along each path.

Consideration of the westward drift in terms of harmonic components was first discussed by Carlheim-Gyllensköld who deduced that the harmonic components of the first few terms drifted westward at an increasing rate according to the degree of the expansion. Bartels disagreed with this deduction on the basis of his analysis of data for the period 1902-1920 (cf. Chapman and Bartels, 1940, p. 666). Phase changes for the spherical harmonics are also discussed in several later works (cf. Nagata, 1962) which conclude that all components up to  $(4,4)^*$  drift westward with the exception of  $(3,2)$ .

---

\* The notation  $(n,m)$  is used here to denote the components  $(g_n^m, h_n^m)$ .

Figure 2 tends to support the general pattern of westward drift as indicated by the number of components moving clockwise about the origin. The components showing a predominantly westward motion are (2,1), (2,2), (3,3), (4,1), (4,2), (4,3), (5,4), (6,1), (6,2), (6,3) whereas those with a dominant eastward pattern are (3,2) and (5,1). The others tend to be special cases. For example (3,1) and (4,4) and (6,5) combine a large relative amplitude change with a predominantly westerly drift while (5,2), (5,3), and (6,4) also undergo large changes in amplitude but exhibit an overall eastward motion.

The dipole term (1,1) is drawn with a bar across at the 1900 starting point. It traces out from 1900 to about 1920 in an increasing-amplitude, eastward direction and then suddenly reverses and overlays itself with a slight westward motion. As pointed out earlier, it would be unwise to infer too much significance from this reversal until a systematic analysis is performed which includes pre-1900 data.

The more constant and characteristic feature of this diagram, which was also discussed by Cain and Hide (1966) is that with the sole exception of the (6,1) trace, both the east and westward moving components exhibit a clockwise curl. Each trace appears to be a segment of an ellipse.

### Changes in Surface Features

Bullard et al. (1950) treated the question of the westward drift by considering the "non-dipole" field as defined by vectorially subtracting the eccentric dipole from the results of Vestine et al. (1959). This subtraction is commonly done because of the dipole component is so much larger than the smaller scale features, appears to change differently and thus may have a different physical basis. However, as we have seen in Figure 2 the absolute change in the (1,1) component is not disproportionate to that of the other harmonic terms. According to this figure the small angular change in its phase is due to the fact that its amplitude is relatively large and there is a reversal of trend. We thus prefer at this juncture to discuss features pertaining to the whole field rather than dismembering it for an inspection of its parts.

A cursory inspection of some of the surface features confirms the general westerly motion of the field depicted by our model. The  $0.23^{\circ}$ /year drift of the Brazilian minimum in total field for this model at the present epoch has already been discussed (Cain, Langel, and Hendricks, 1967). The Siberian high in F at the surface is estimated by the model to be located at  $61.8^{\circ}\text{N}$ ,  $107.6^{\circ}\text{E}$  in 1960 and moving at a rate of  $0.03^{\circ}/\text{yr}$  north in latitude and  $0.1^{\circ}/\text{yr}$  west in longitude. The Canadian high is also moving north from its 1960 position of  $56.7^{\circ}\text{N}$ ,  $98.0^{\circ}\text{W}$  at a rate of  $0.08^{\circ}/\text{yr}$ . However, it appears to evidence an easterly drift of about  $0.03^{\circ}/\text{yr}$ .

Position of Poles

The GSFC(12/66) model shows both the north and south dip poles to be moving northwesterly. The change in position of these two points for the period of the data is shown in Table 1.

TABLE 1

Drift of Dip Poles [GSFC(12/66) Model]

<u>Date</u>	<u>North</u>		<u>South</u>	
1900	71.2N	96.9W	72.3S	153.2E
1930	72.6N	99.0W	68.8S	144.7E
1960	75.1N	100.7W	66.7S	140.7E
1965	75.5N	101.0W	65.5S	140.3E

The 1965 values for the latitudes agree exactly with those adopted for the U.S. (Hurwitz et al., 1966) and British (Leaton, Malin, and Evans, 1965) World Magnetic Charts but differ a few tenths of a degree in longitude.

Although the positions of the computed dip poles varied smoothly over the 1900-1965 interval, the direction of motion of the dipole appeared to reverse as already indicated on Figure 2. The positions of the boreal point are given in Table 2. It is seen that after the reversal near 1920 the pole has begun to move westward at a current rate of about  $0.07^{\circ}/\text{yr}$ .

TABLE 2

North Dipole Location - GSFC(12/66) Model

	<u>Latitude</u>	<u>Longitude</u>	Westward <u>Drift Rate</u> (degrees/year)
1900	79.0N	69.0W	-.03
1910	78.8	68.6	-.01
1920	78.7	68.5	.01
1930	78.7	68.6	.02
1940	78.7	68.8	.04
1950	78.7	69.2	.05
1960	78.7	69.7	.07
1965	78.8	70.0	

The 1965 location given here can be compared with the 78.6N,  
70.4W position given by Leaton, Malin, and Evans (1965) and the 78.6N,  
70.0W values of Hurwitz et al.(1966).

Conclusions

Since the GSFC(12/66) field analysis was performed on survey data without correcting them for short period fluctuations such as Dst and Sq, it is remarkable that the main patterns of secular change represented agree so closely with earlier analyses in which the data were subjected to a careful screening and correction process. The main defects of the model result from the irregular regional changes superimposed on the general trends and the use of a parabolic representation over too long an interval. For these reasons it is apparent that an extrapolation of the model to epochs beyond the last data used (1965.8) will be increasingly in error by as much as a few tens of gammas per year in some areas. Although this deviation may seem large it is unlikely that better forecasts can be made until there is an evaluation of recent satellite survey data taken over a period of a year or more to allow for a more accurate global estimate of secular change. This work does indicate that there is no special need for fixed repeat stations for monitoring the secular change. Although data from such stations were indeed a valuable addition to the data set, the fact that they remained in one location was not used in the analysis. It may be possible in the future to monitor the main field using only satellite data corrected for time variations as derived from the fluctuations observed at the surface observatories.

The observation that most of the spherical harmonic vectors move westward supports previous work that there is a basic pattern of westward

Decrease in Magnetic Moment of Dipole

The first three terms of the expansion can be used to compute an equivalent dipole moment and equatorial field (Chapman and Bartels, 1940, p. 642). Using a value of  $a = 6.3712 \times 10^8$  cm for a mean radius, the value of  $M$  and  $H_o$  are given in Table 3.

TABLE 3

Dipole Moment and Horizontal Field Of Equivalent Dipole

	<u><math>M \times 10^{-25}</math> cgs</u>	<u><math>H_o (\Gamma)</math></u>	<u><math>H_o (\gamma/year)</math></u>
1900	8.298	.3209	
1920	8.197	.3170	-20
1940	8.105	.3134	-18
1960	8.023	.3102	-16

Although it has become popular recently (Leaton and Malin, 1967; McDonald and Gunst, 1967) to speculate on the demise (about 3700-4000 A.D.) of the main field dipole by extrapolating a linear trend from such data as the above [since field reversals are believed to have occurred in geological time (Cox et al., 1967)], one should note the tendency in the above results for a reduction in rate of decrease. Since our analysis included data for a time span during which there is only a 3% change in  $M$ , extrapolations to zero are very speculative.

drift. The constancy of a clockwise curvature pattern for almost all components is noted for the first time as a curious and unexplained result.

The sudden reversal of the eastward drift of the dipole poles near 1920 may possibly be due to inaccuracies in the analysis resulting in part from the poor data distribution. On the other hand one is tempted to join those who speculate that such a change coincides with the reversal in the rate of decrease of the earth's rate of rotation. The slight, but apparently real, slowing of the rate of decrease of the moment of the earth's main dipole is in a direction that suggests that the field is not beginning a cycle of reversal. Such suggestions could be checked only by obtaining a much longer span of magnetic field observations and subjecting them to a consistent analysis.

## References

- Bullard, E. C., C. Freedman, H. Gellman and J. Nixon, The westward drift of the earth's magnetic field, Phil. Trans. Roy. Soc., 243A, 67-92, 1950.
- Cain, Joseph C., and James R. Neilon, Automatic mapping of the geomagnetic field, J. Geophys. Res., 68, 4689-4698, 1963.
- Cain, J. C., W. E. Daniels, Shirley J. Hendricks, and Duane C. Jensen, An evaluation of the main geomagnetic field, 1940-1962, J. Geophys. Res., 70, 3647-3674, 1965.
- Cain, J. C., and Raymond Hide, The secular change of the geomagnetic field, (Abst.) Trans. AGU 47, 57 (1966).
- Cain, J. C., Models of the earth's magnetic field, Radiation Trapped in the Earth's Magnetic Field, p. 1, D. Reidel, 1966.
- Cain, J. C., S. J. Hendricks, R. G. Langel, and W. V. Hudson, A proposed model for the international geomagnetic reference field, NASA X-612-67-173, 1967.
- Cain, J. C., R. A. Langel, and S. J. Hendricks, Magnetic chart of the Brazilian anomaly - A verification, NASA/GSFC Rept. X-612-67-373, 1967.
- Chapman, S. and J. Bartels, Geomagnetism, Oxford University Press, London, 1940.
- Cox, A., G. B. Dalrymple, and R. R. Doell, Reversals of the earth's magnetic field, Scient. Am., 216, 44, 1967.
- Dicke, R. H., The secular acceleration of the earth's rotation and cosmology, The Earth Moon System, pp. 141, Plenum Press, New York, 1966.

Eleman, Folke, Time variations of geomagnetic H and D at disturbed stations, Nature, 209, 1120-1121, 1966.

Hendricks, S. J. and J. C. Cain, Magnetic field data for trapped particle evaluations, J. Geophys. Res. 71, 346, 1966.

Hide, R. Free hydromagnetic oscillations of the earth's core and the theory of the geomagnetic secular variation, Phil. Trans. Royal Soc., A259, 615-647, 1966.

Hurwitz, L., D. G. Knapp, J. H. Nelson and D. E. Watson, Mathematical model of the geomagnetic field, J. Geophys. Res., 71, 2373, 1966.

Leaton, B. R., S. R. C. Malin, and Margaret J. Evans, An analytical representation of the estimated geomagnetic field and its secular change for the epoch 1965.0, J. Geomag. Geoelec., 17, 187-194, 1965.

Leaton, B. R. and S. R. C. Malin, Recent changes in the magnetic dipole moment of the earth, Nature, 213, 1110, 1967.

Mauersberger, P., A discussion of the variation with time of the parameters of the geomagnetic field based on the existing potential analysis, Abhandlungen des Geophysikalische Instituts Potsdam, No. 5, 9-58, 1952, (trans. NASA TT-F-8443, 1963).

McDonald, K. L. and R. H. Gunst, An analysis of the earth's magnetic field from 1835 to 1965, ESSA Technical Rept. IER 46-IES 1, 1967.

Munk, W. H. and G. J. F. MacDonald, The Rotation of the Earth, Cambridge University Press, 1960.

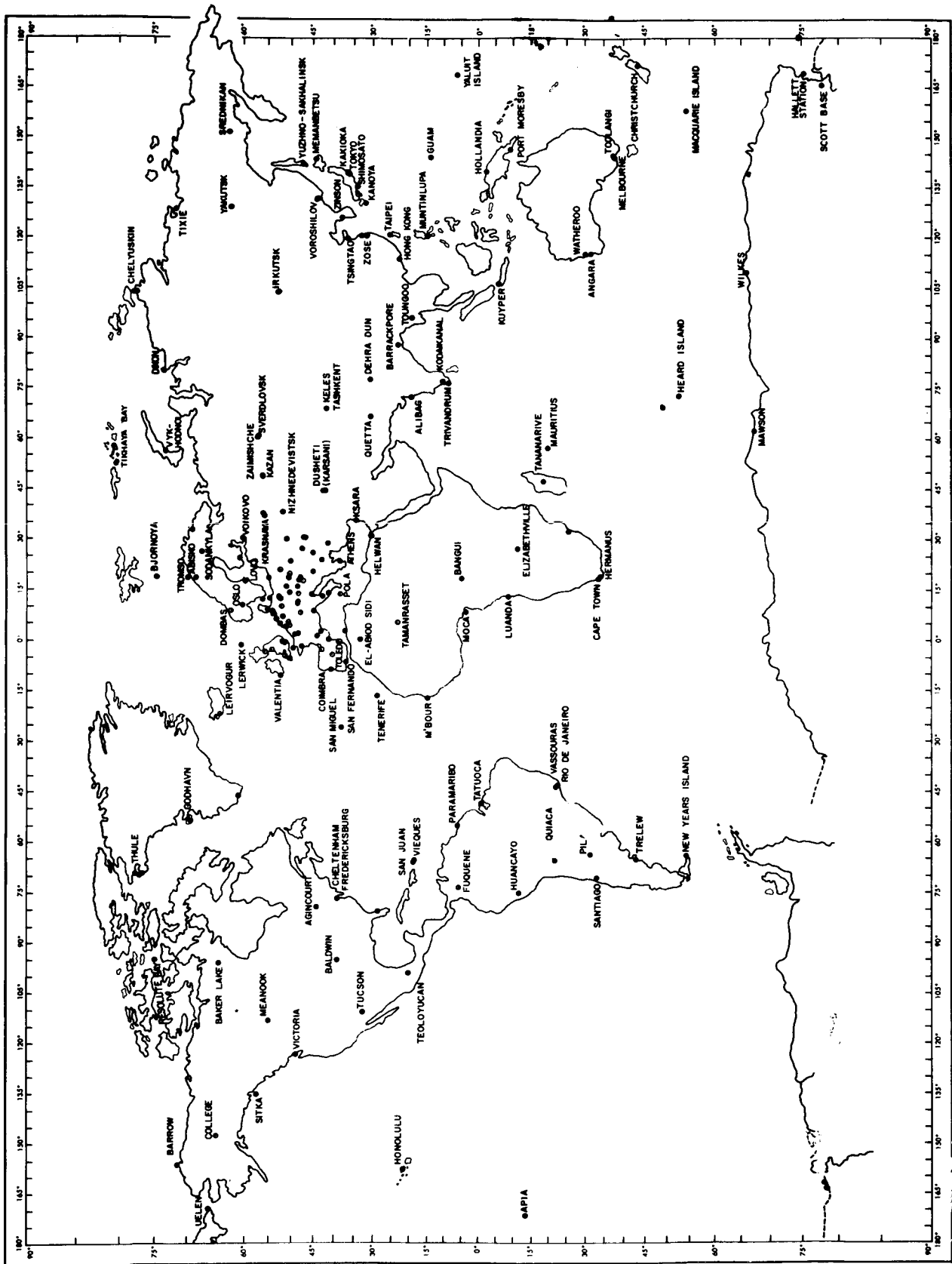
Nagata, T., Two main aspects of geomagnetic secular variation - westward drift and non-drifting components, Benedum Earth's Magnetism Symposium, U. of Pittsburgh Press, 1962.

Vestine, E. H., I. Lange, L. Laporte, and W. E. Scott, The geomagnetic field, its description and analysis, Carnegie Institution of Washington, Publication 580, 1947, reprinted 1959.

APPENDIX A

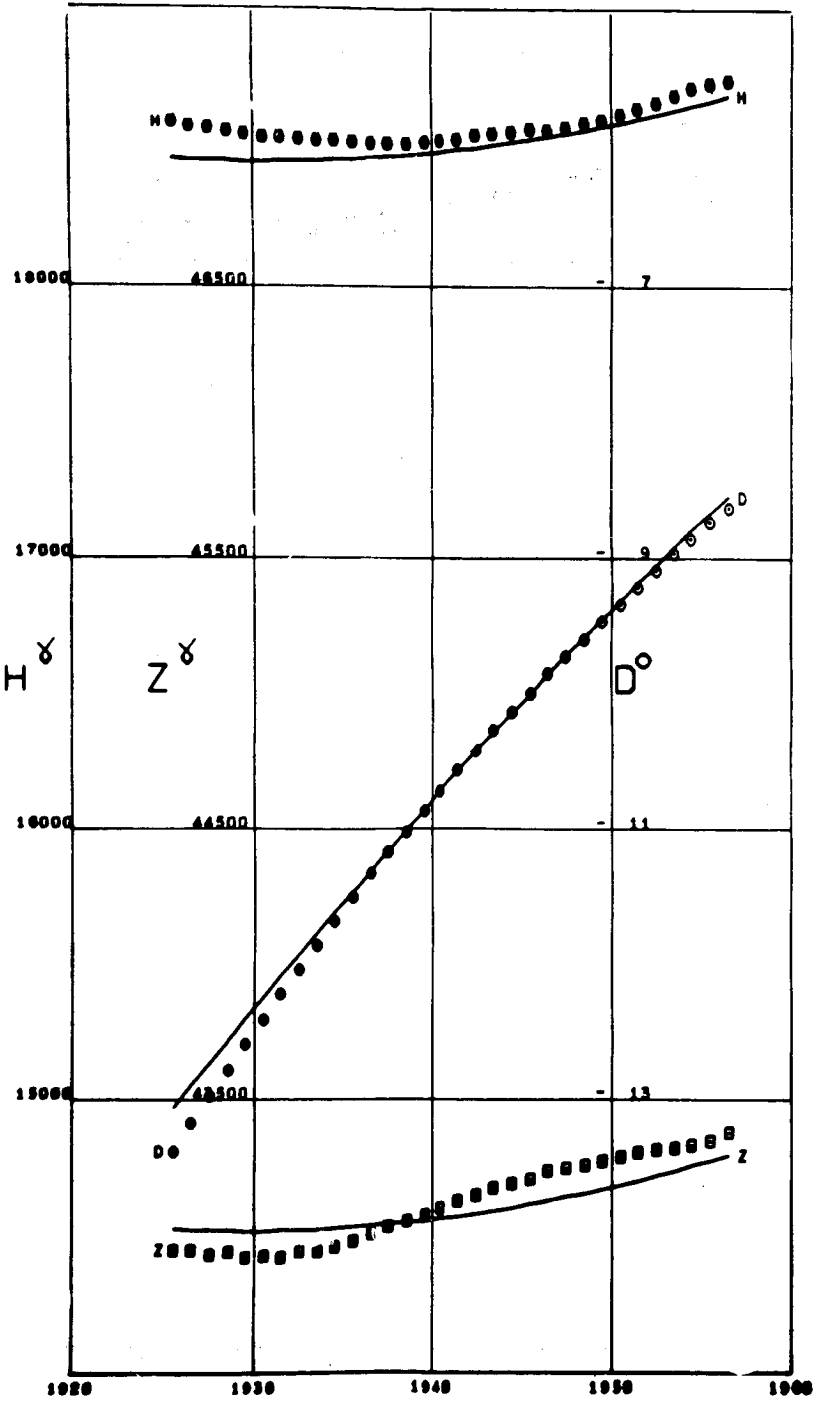
Comparison of observatory annual mean values

1900-1965 with elements computed from GSFC(12/66)

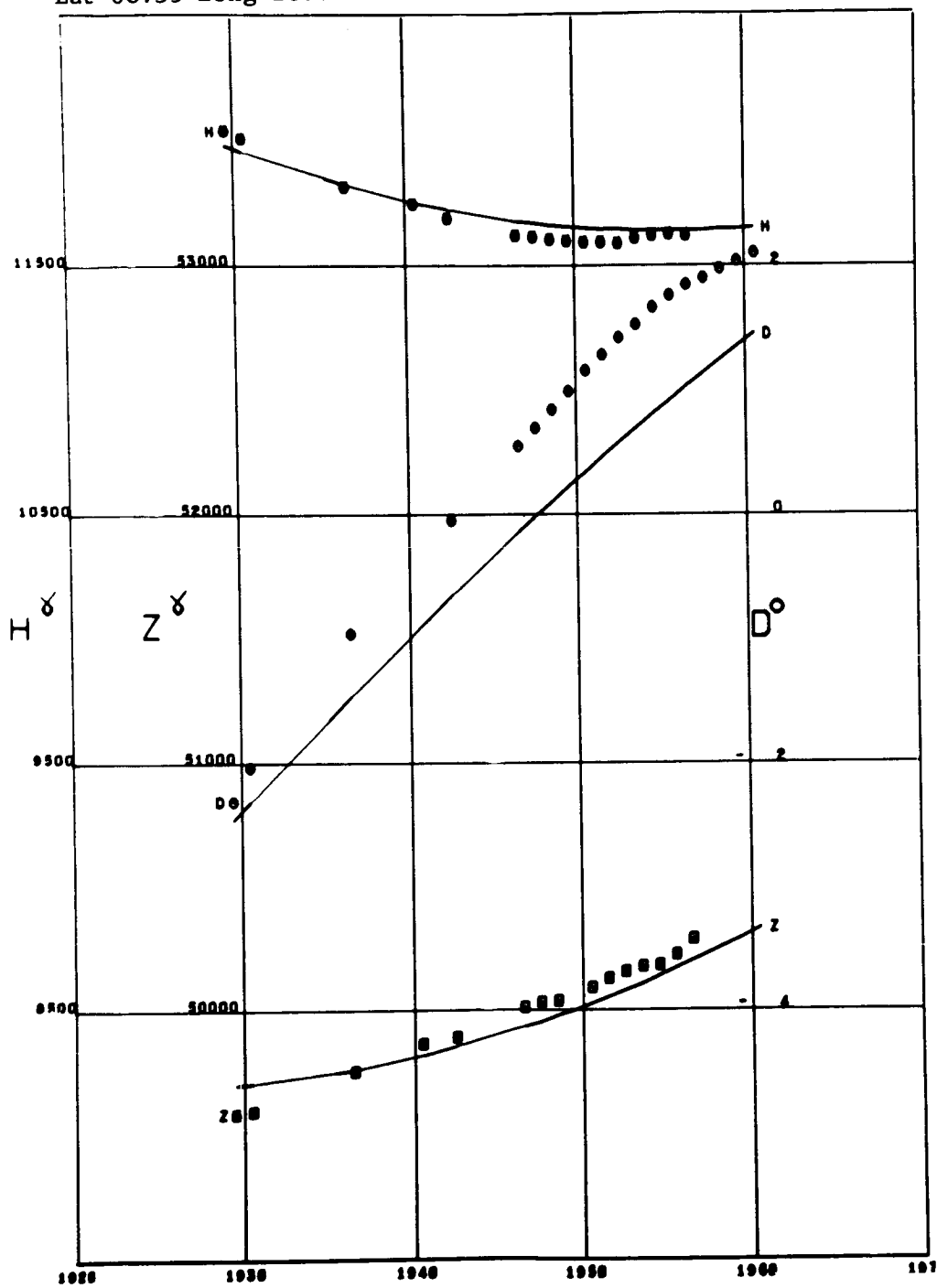


ABINGER

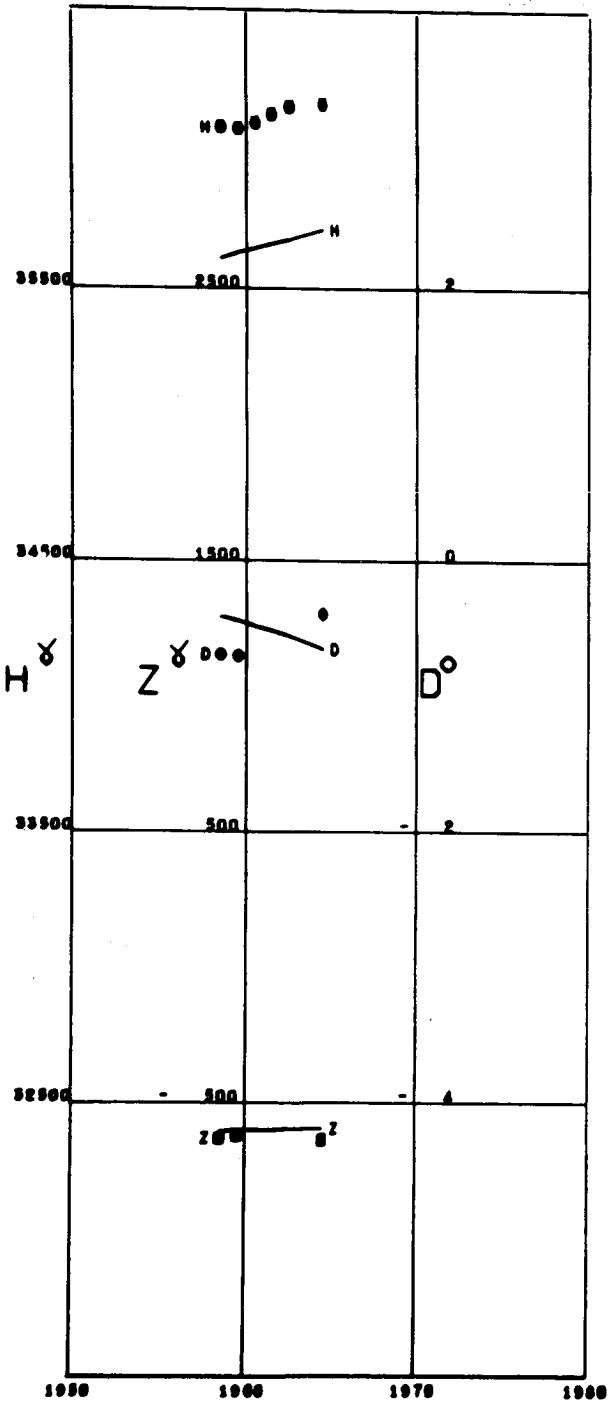
Lat 51.18 Long -0.38



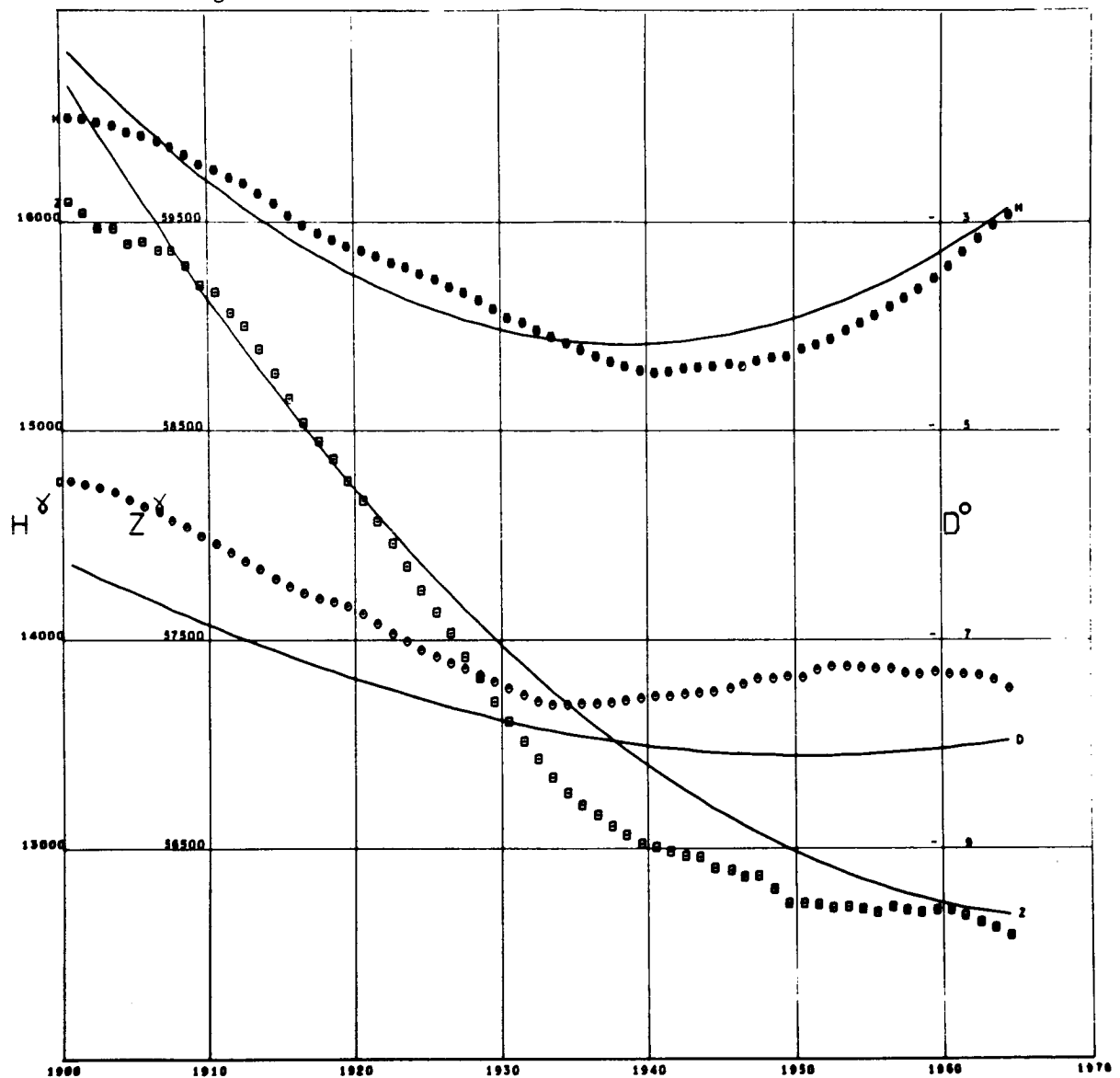
ABISKO  
Lat 68.35 Long 18.82



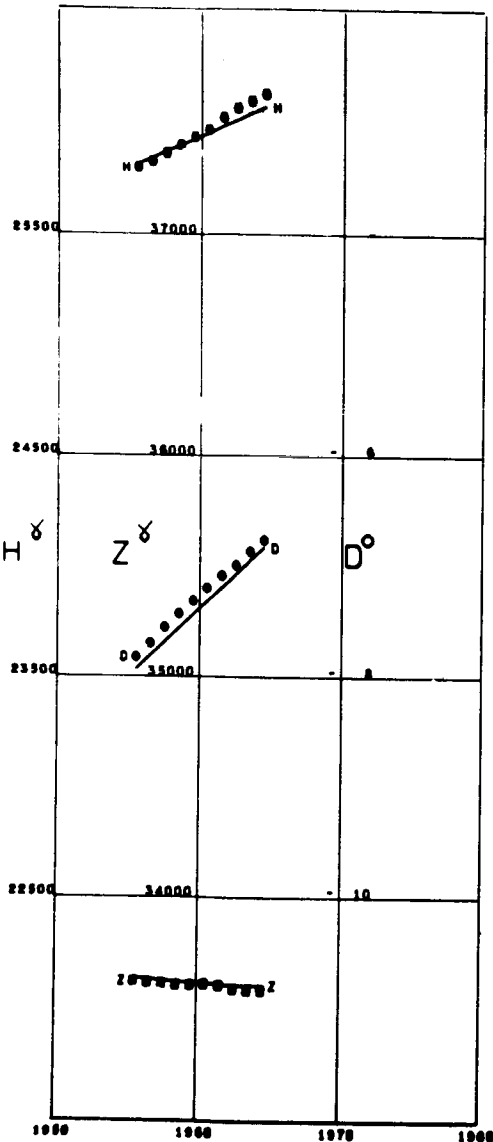
ADDIS ABABA  
Lat 9.03 Long 38.76 Alt 2.44



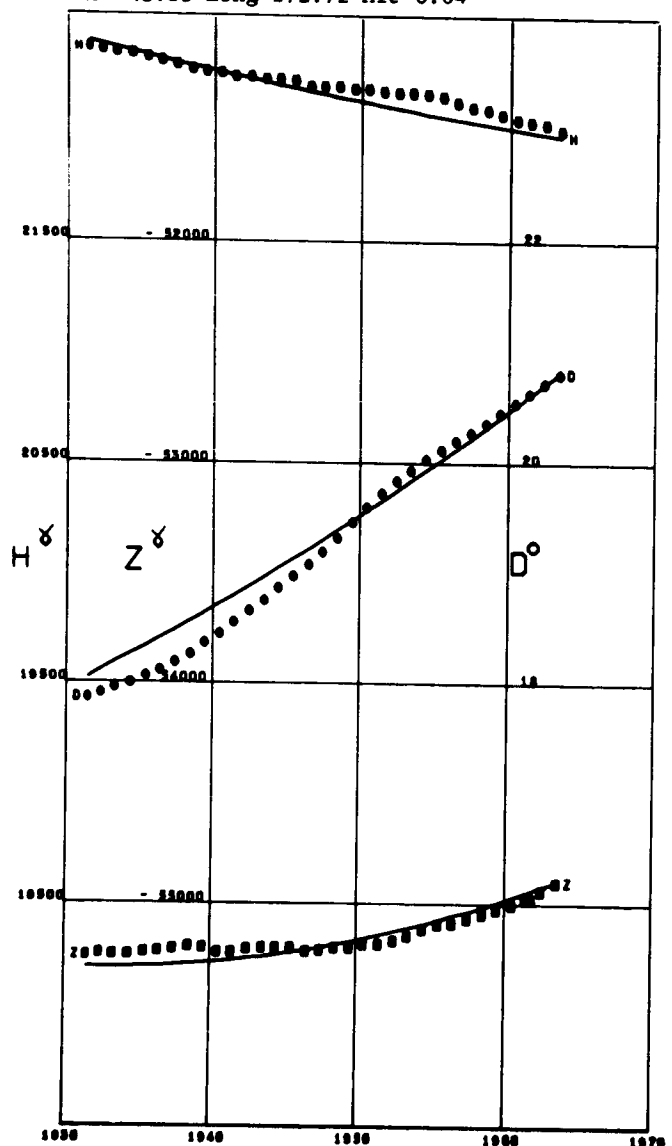
AGINCOURT  
Lat 43.78 Long -79.26 Alt 0.18



ALMERIA  
Lat 36.85 Long -2.46

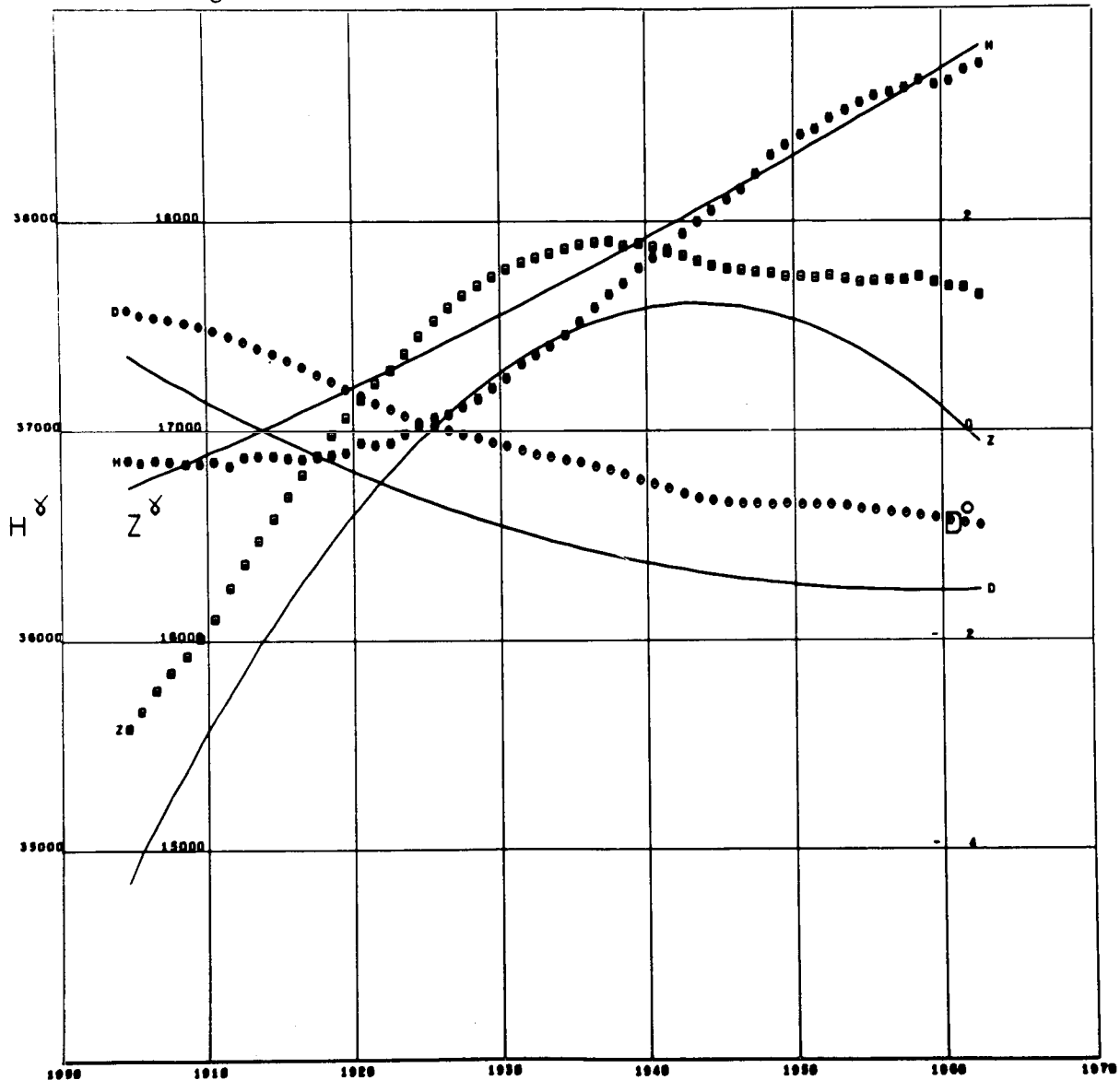


AMBERLEY  
Lat -43.15 Long 172.72 Alt 0.04

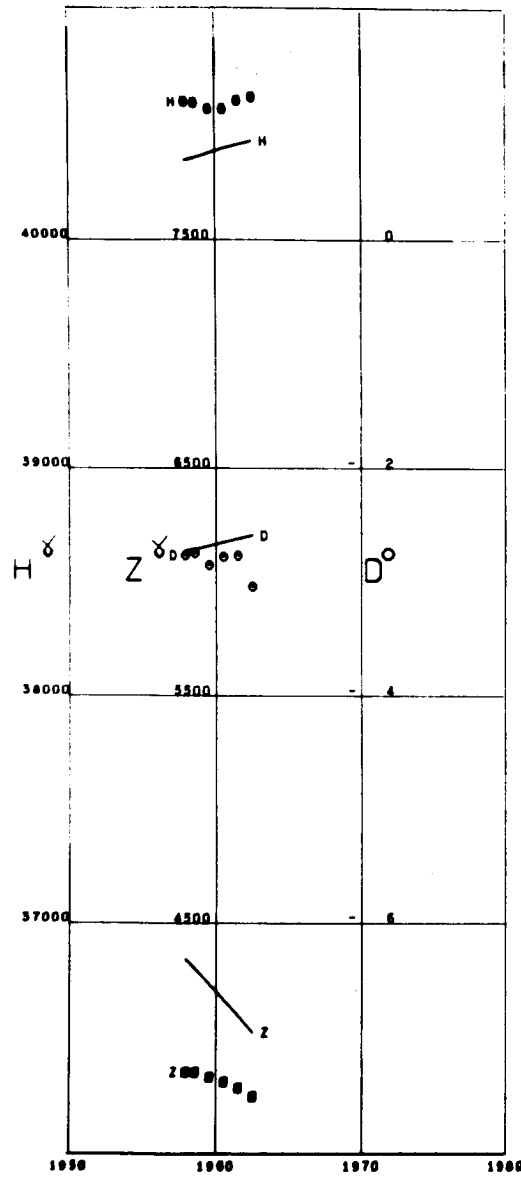


ALIBAG

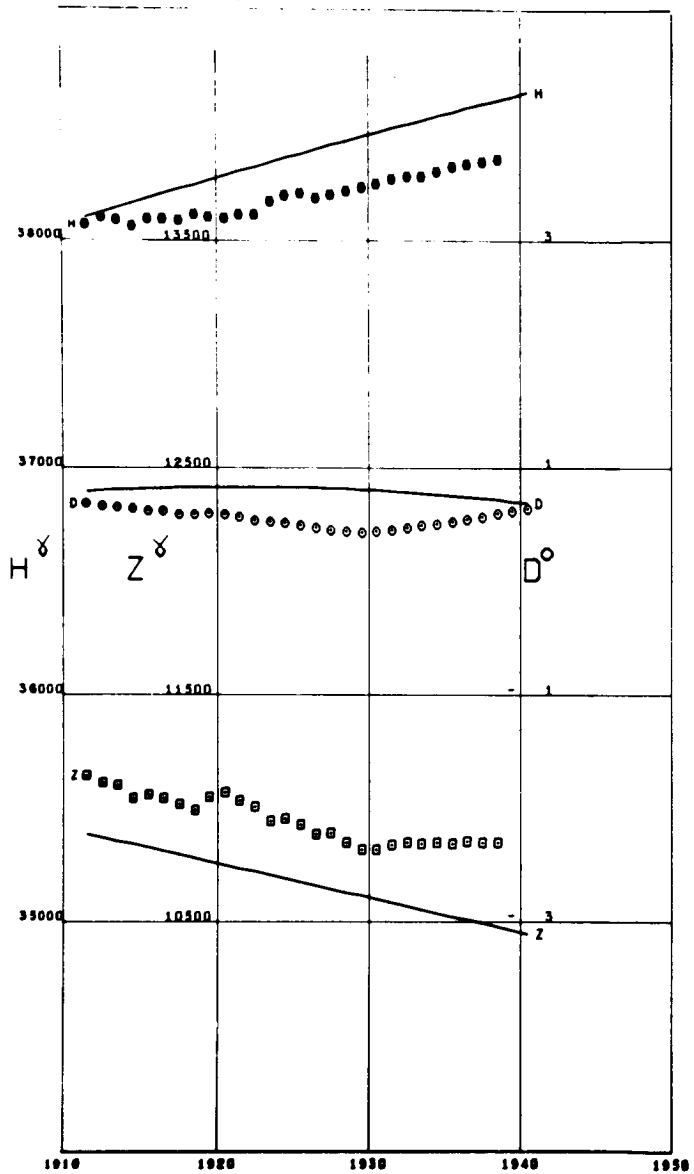
Lat 18.63 Long 72.87 Alt 0.01



ANNAMALAINAGAR  
Lat 11.40 Long 79.68

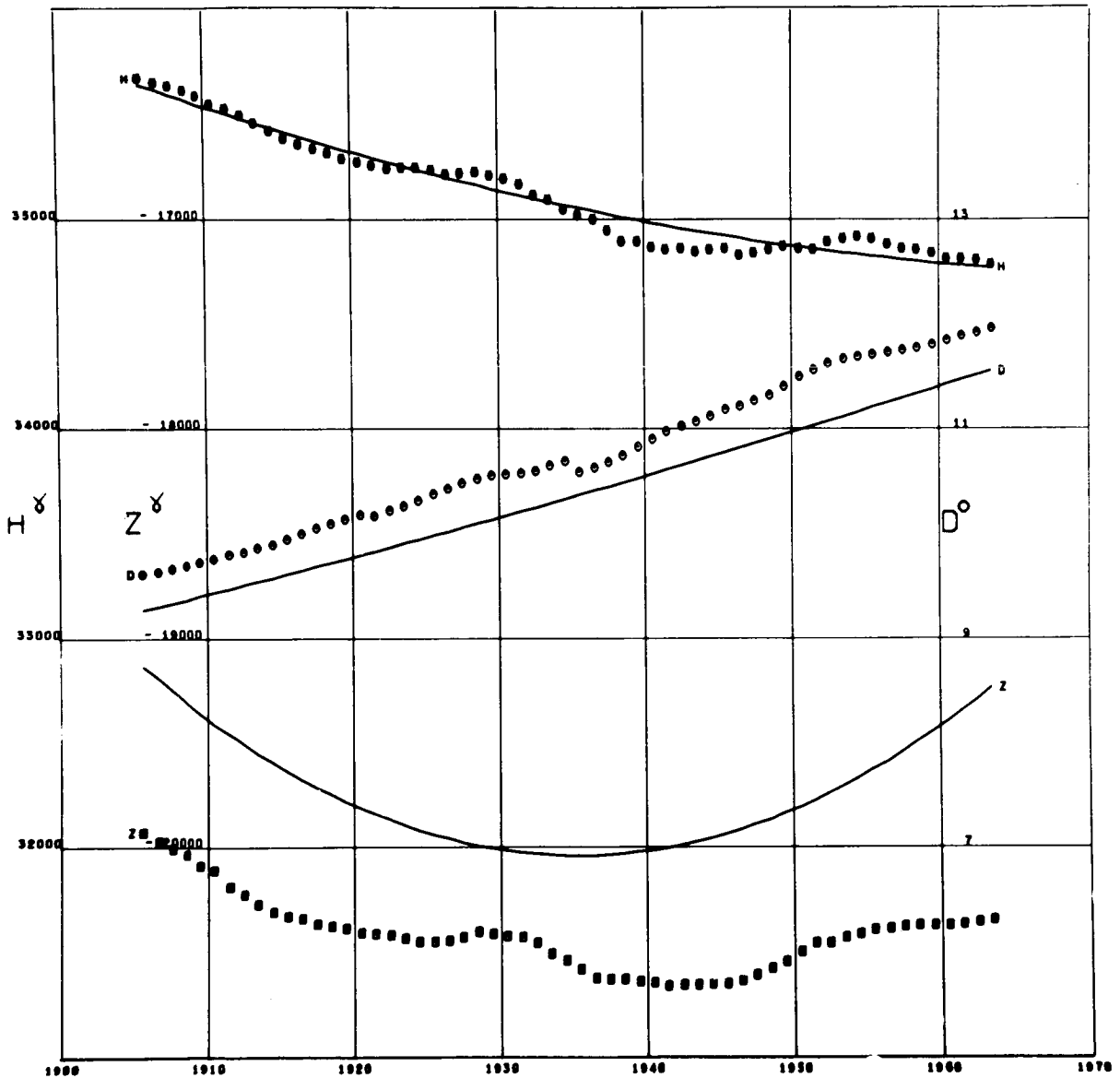


ANTIPOLLO  
Lat 14.60 Long 121.16

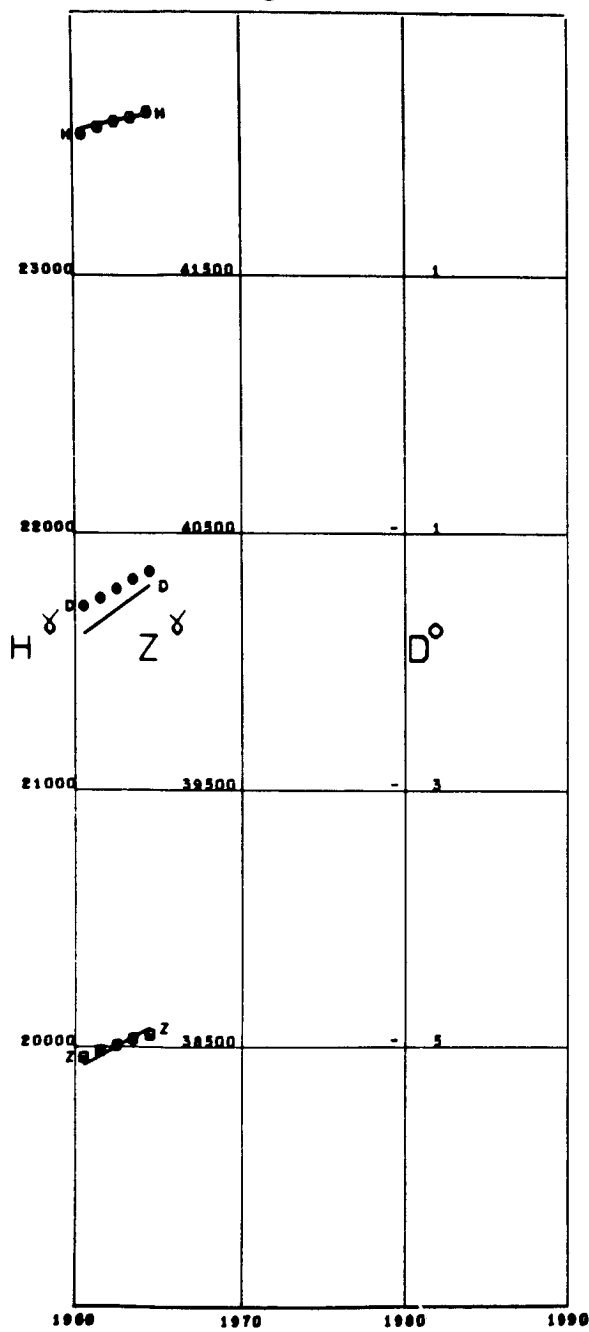


APIA

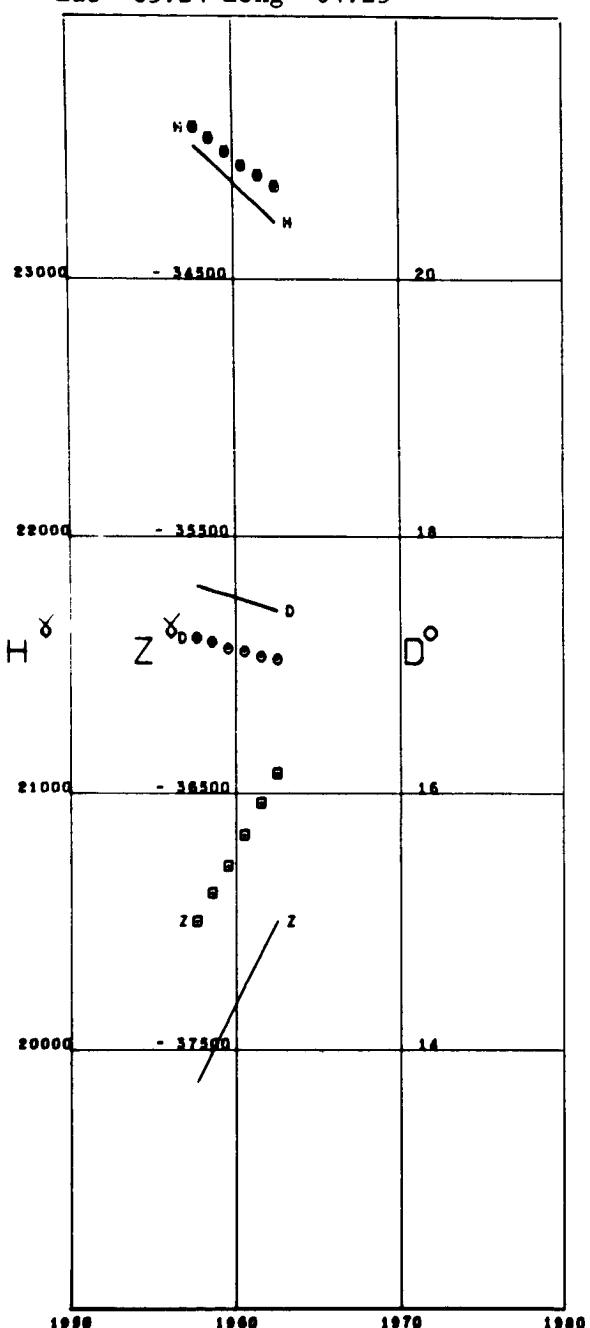
Lat -13.80 Long -171.77



AQUILA  
Lat 42.38 Long 13.31

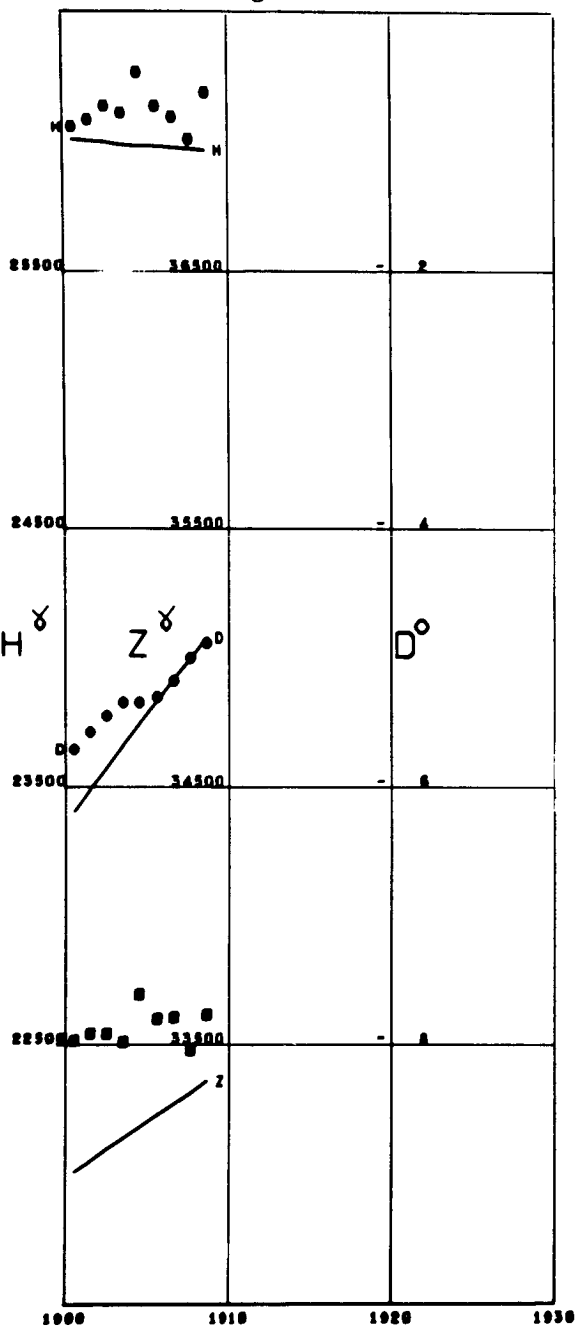


ARGENTINE ISLAND  
Lat -65.24 Long -64.25



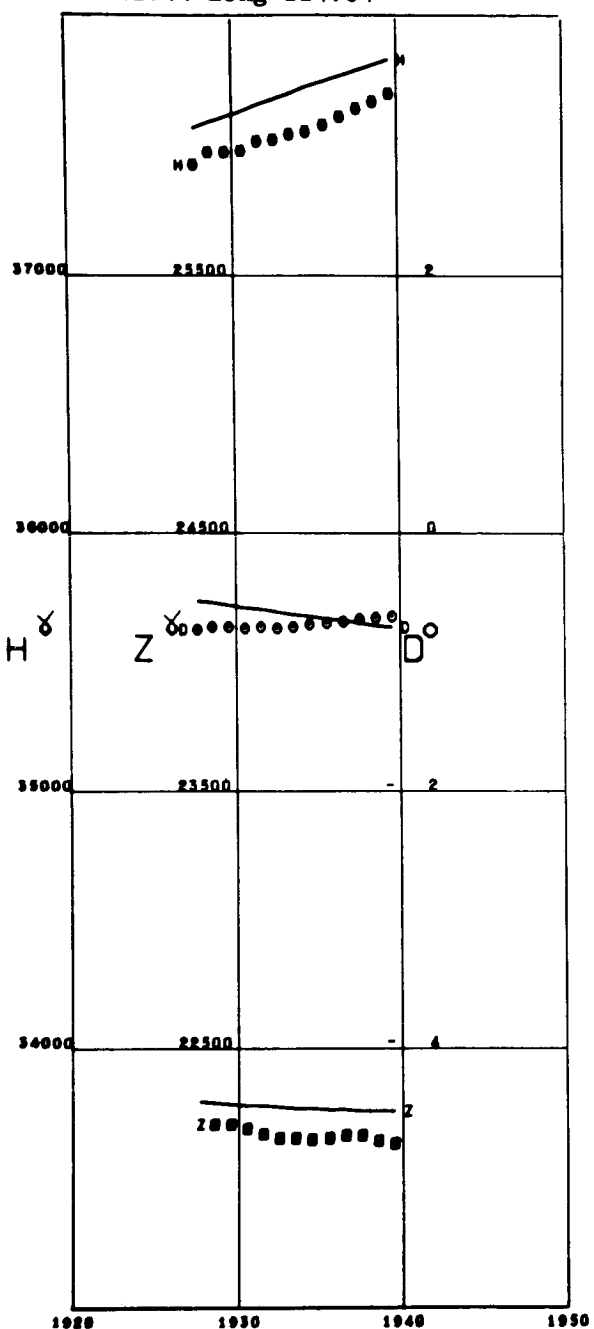
**ATHENS**

Lat 37.97 Long 23.72

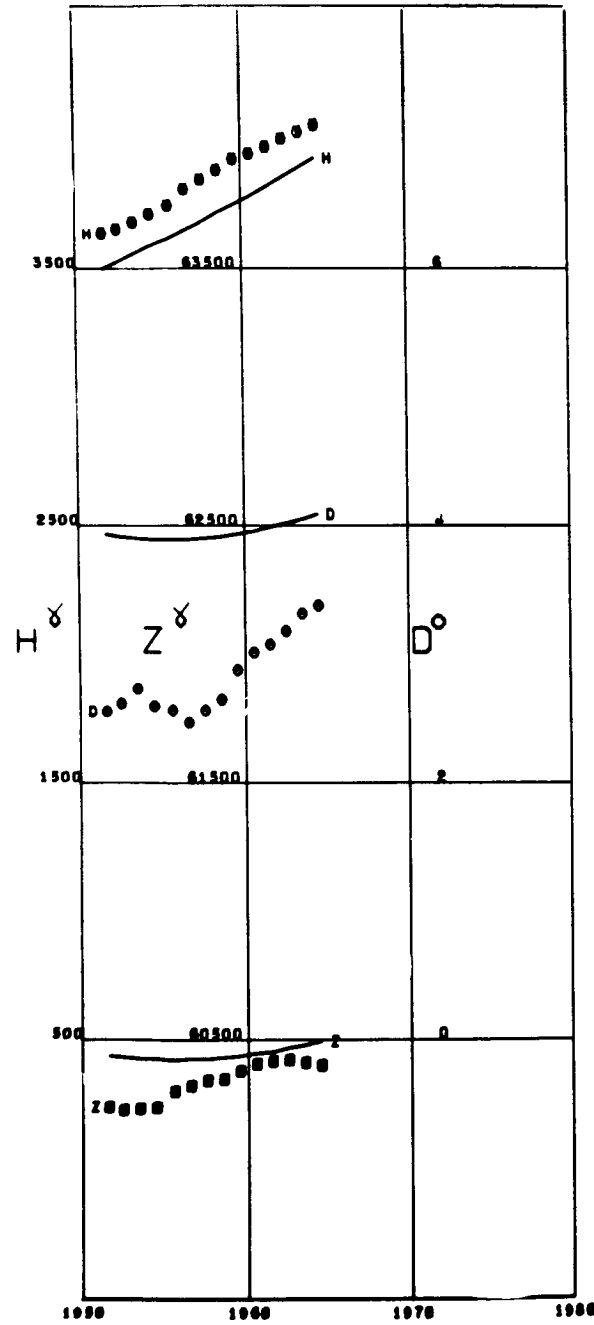


**AU TAU**

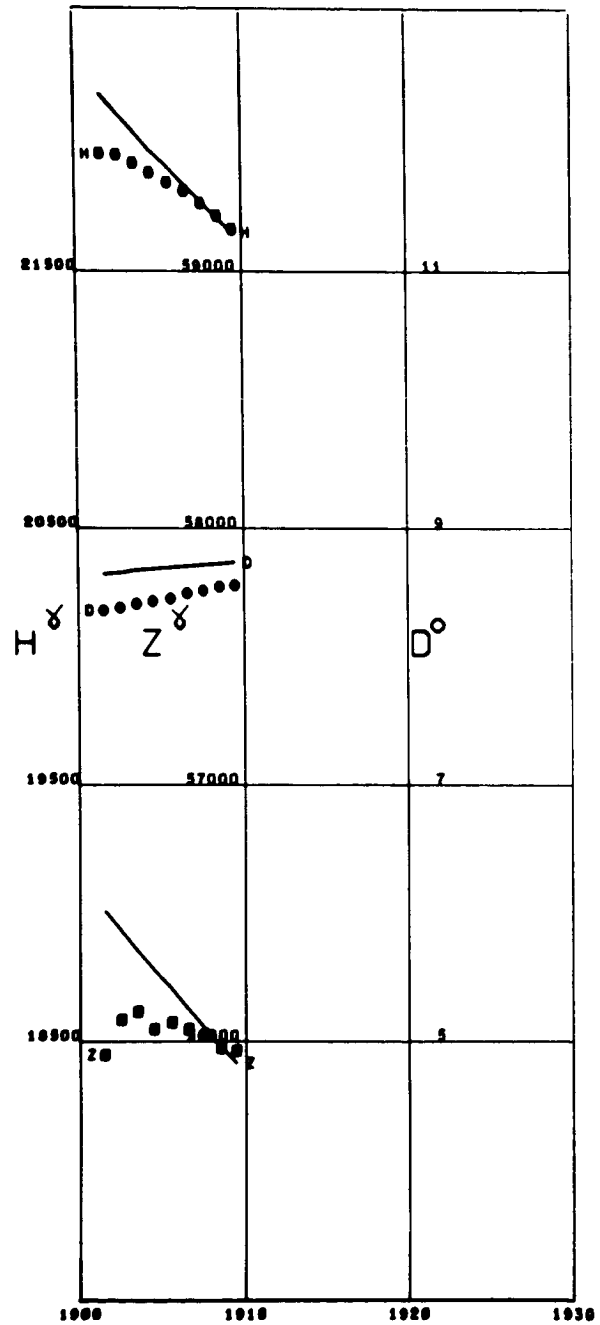
Lat 22.44 Long 114.04



BAKER LAKE  
Lat 64.33 Long -96.03 Alt 0.04

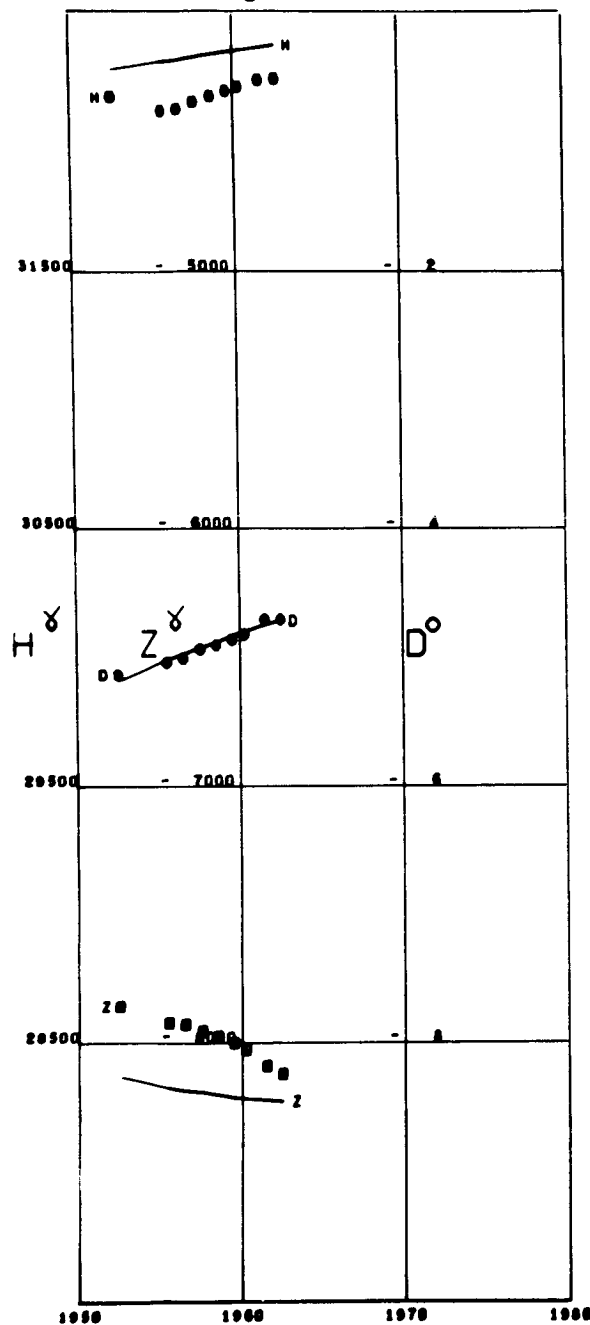


BALDWIN  
Lat 38.78 Long -95.16



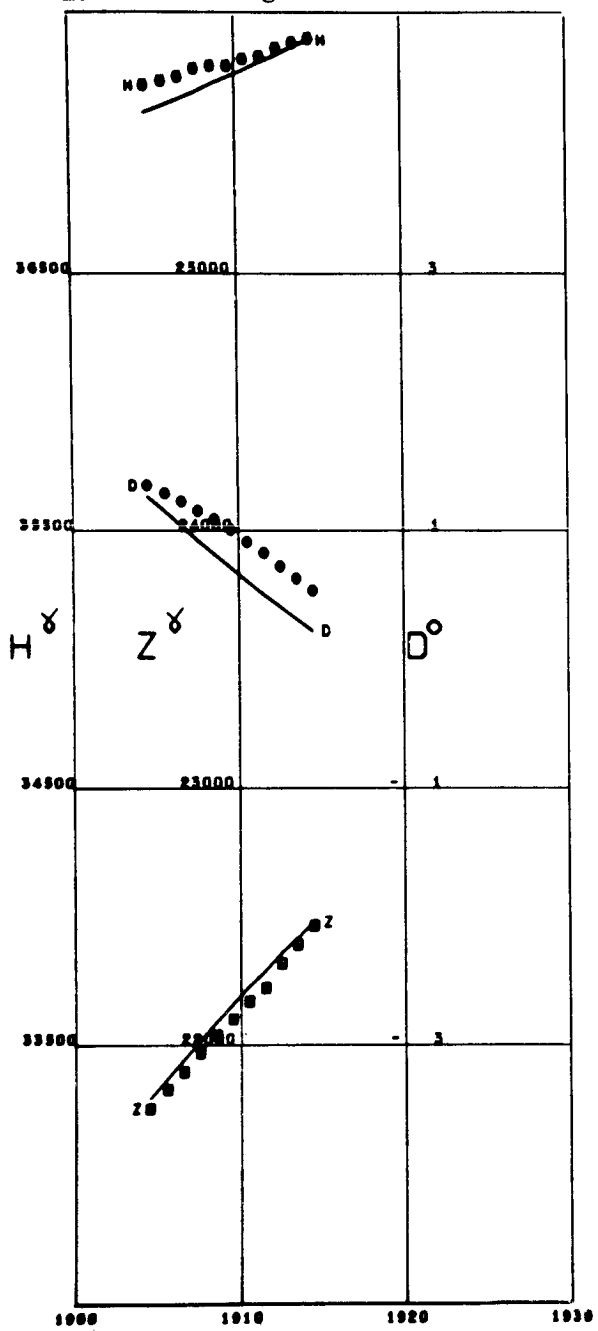
BANGUI

Lat 4.43 Long 18.56 Alt 0.44



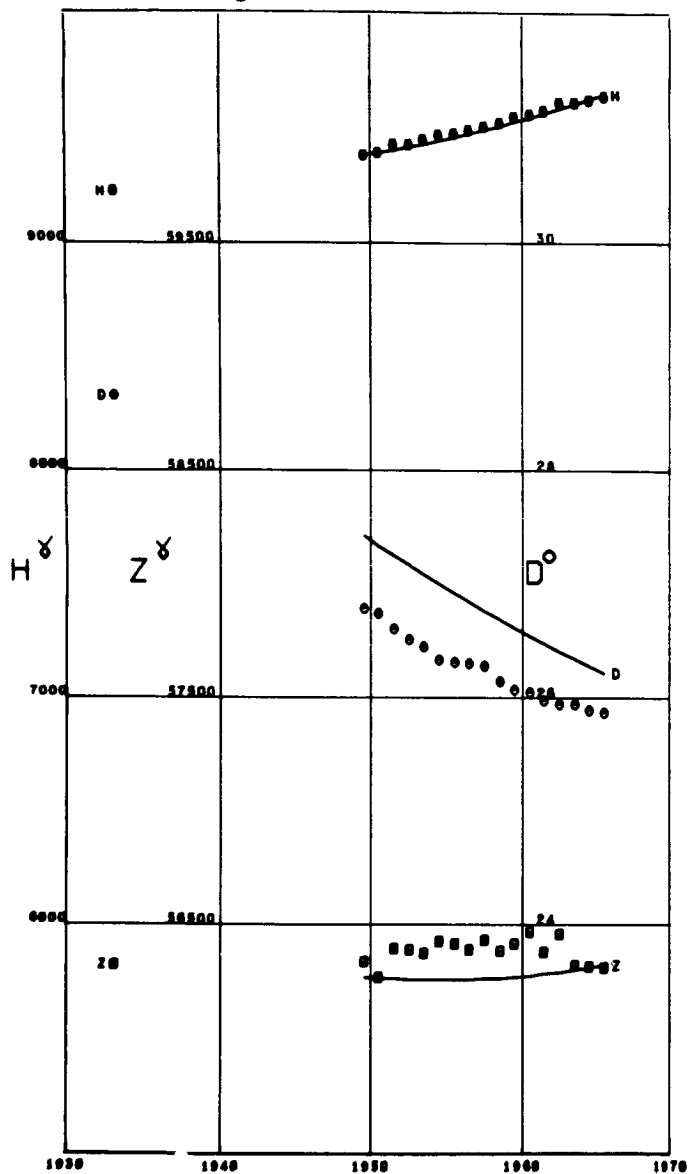
BARRACKPORE

Lat 22.77 Long 88.36

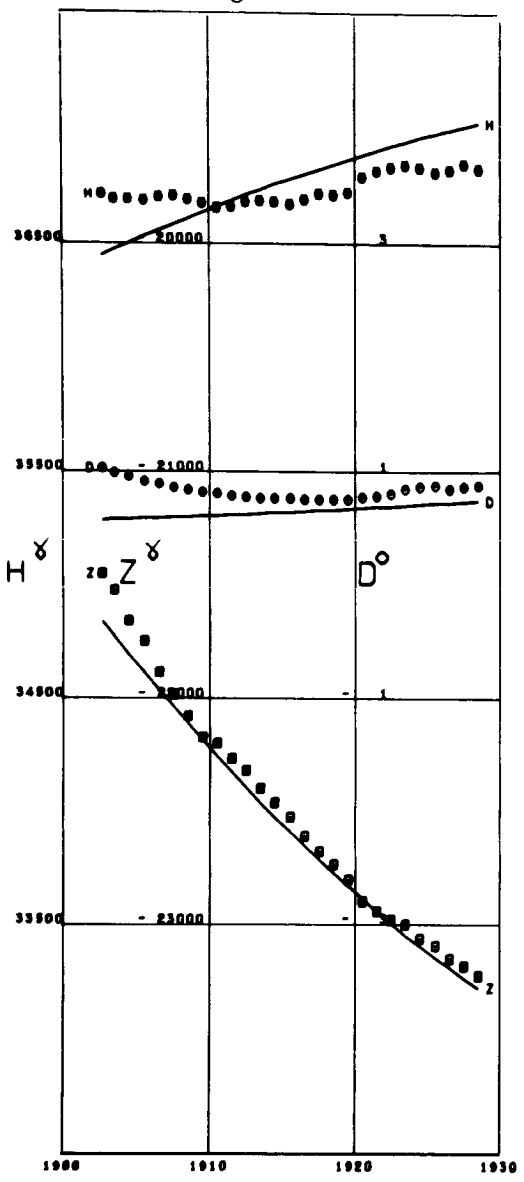


**BARROW**

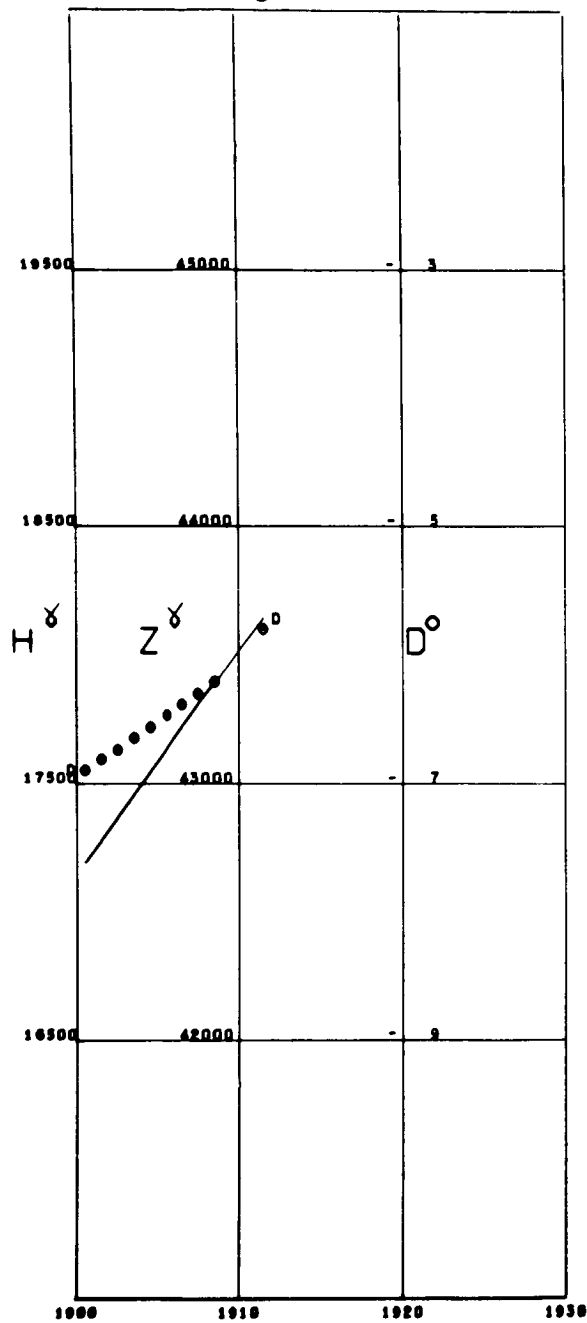
Lat 71.30 Long -156.74

**BATAVIA**

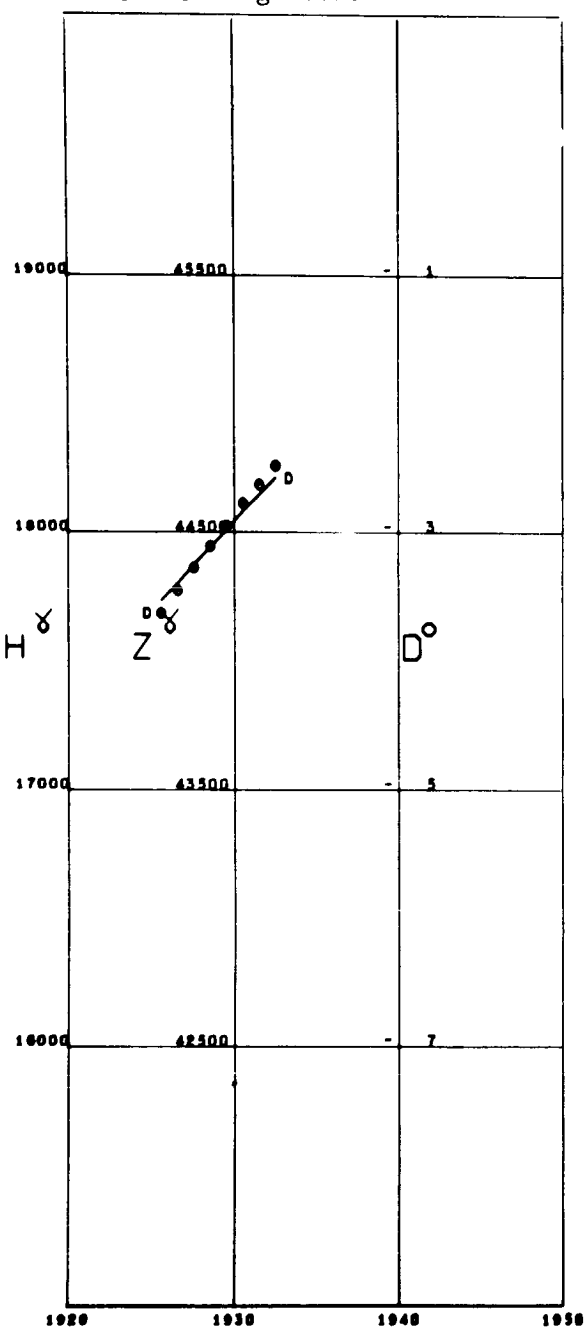
Lat -6.18 Long 106.83



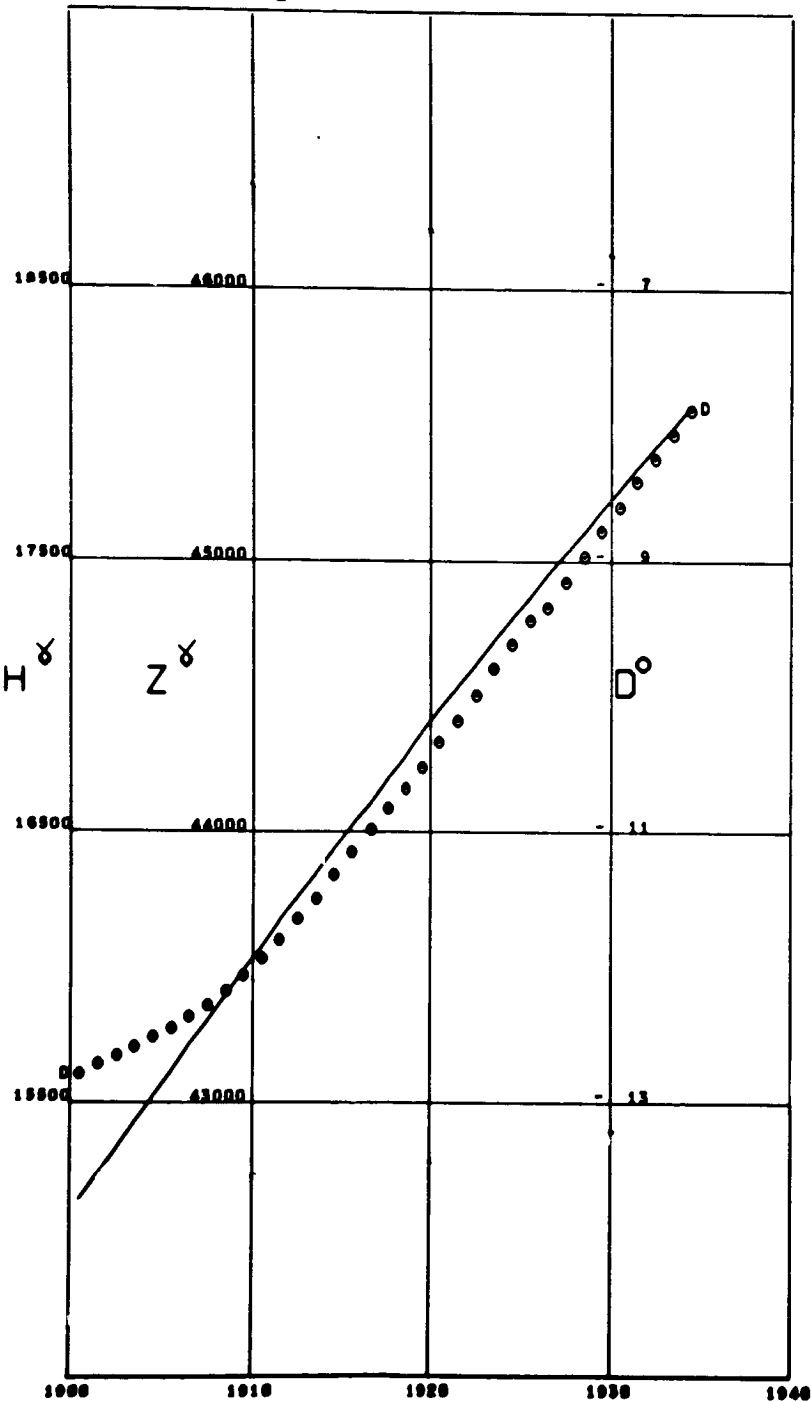
BEUTHEN  
Lat 50.35 Long 18.92



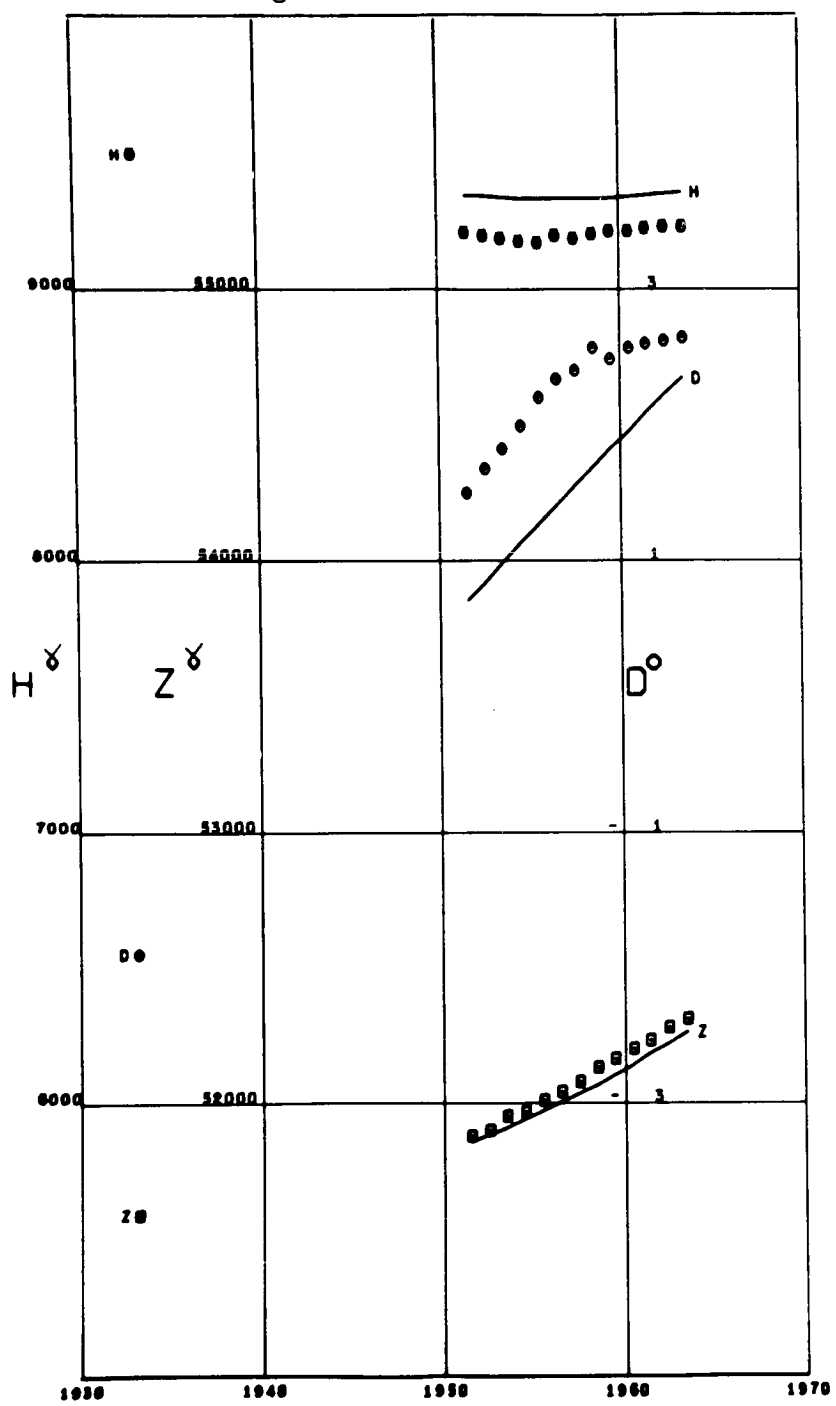
BEUTHEN MIKILOW  
Lat 50.15 Long 18.90



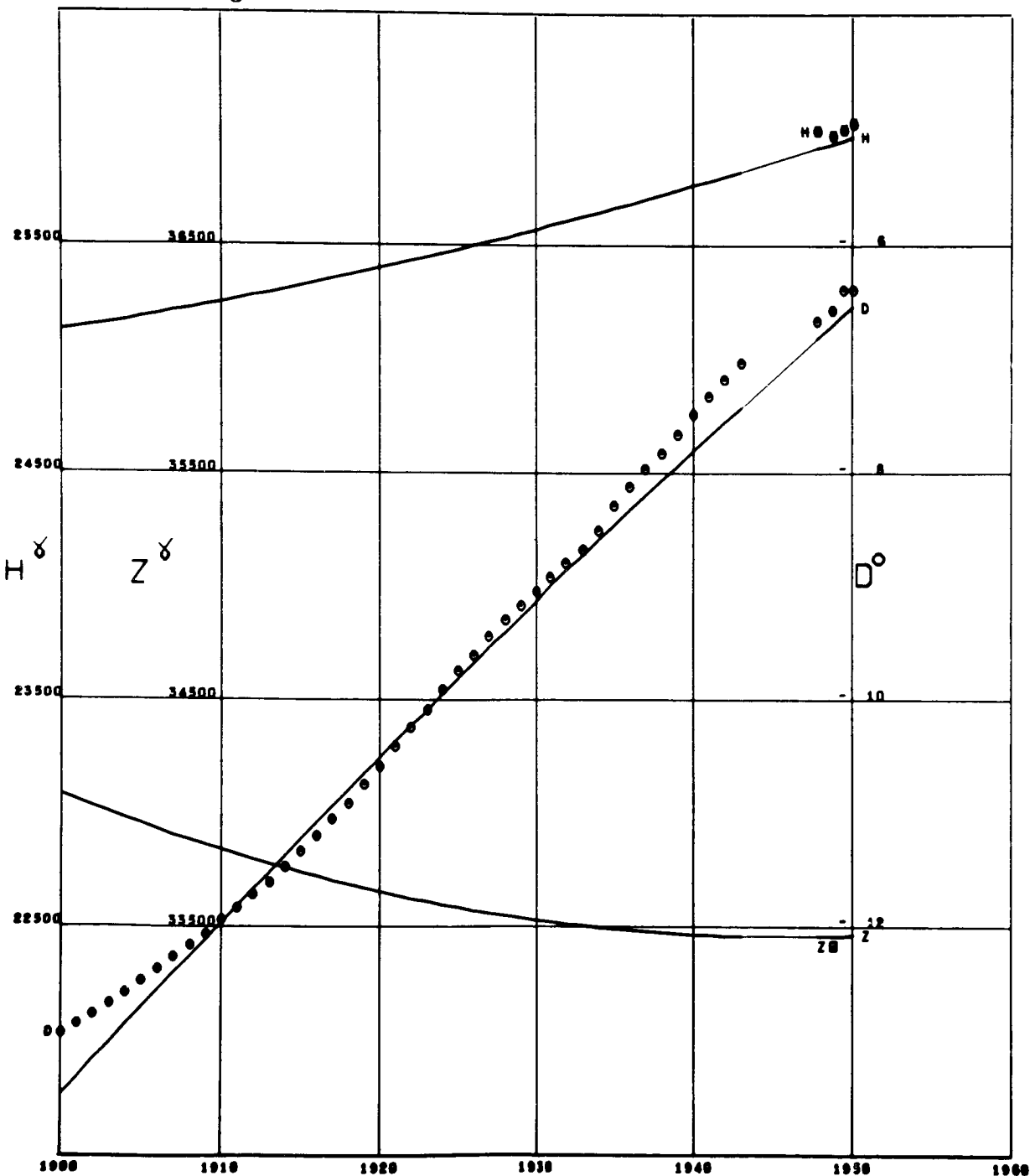
BOCHUM  
Lat 51.49 Long 7.23



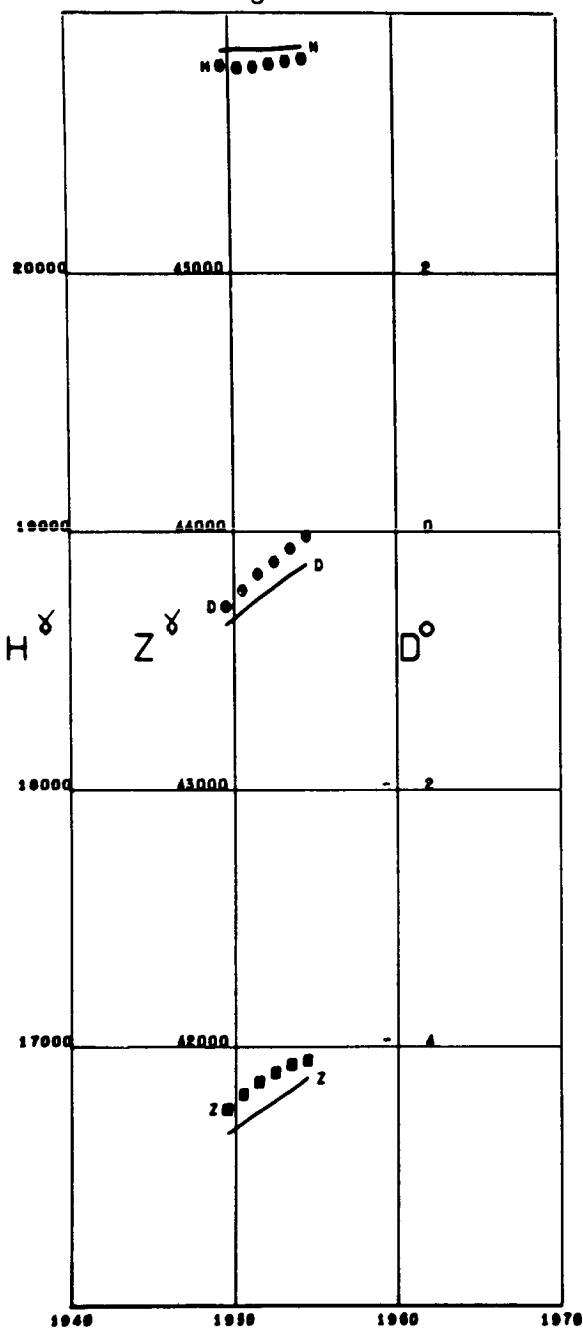
BJORNOYA  
Lat 74.50 Long 19.20



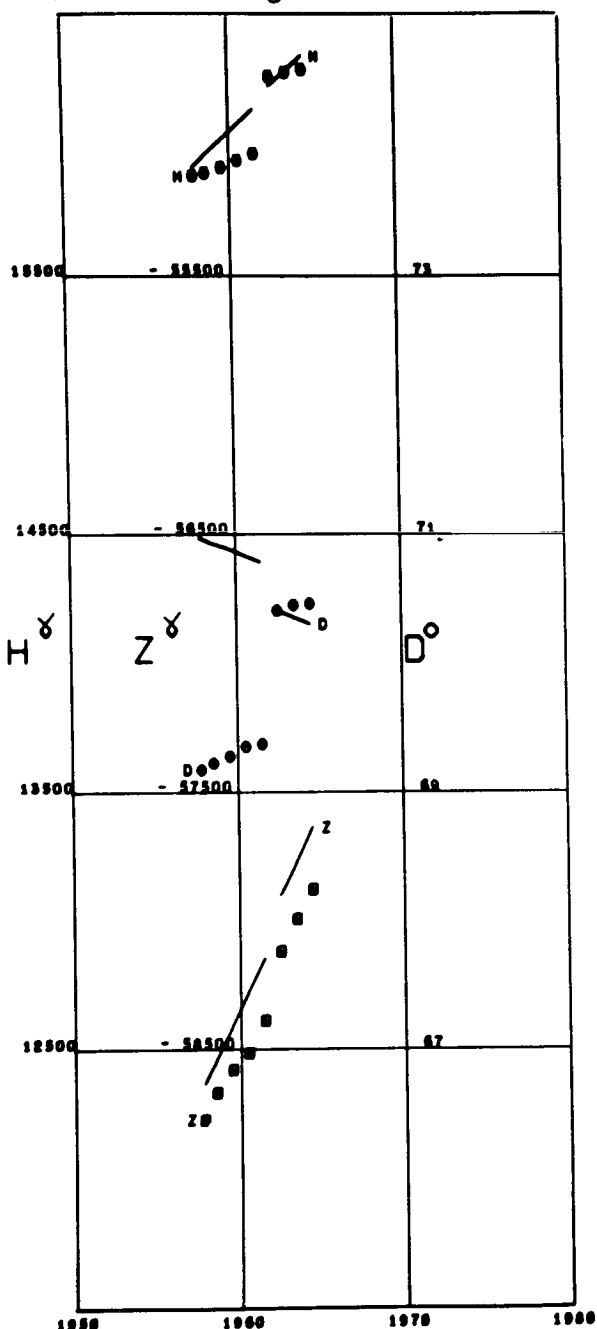
BOUZAREAH  
Lat 36.80 Long 3.01



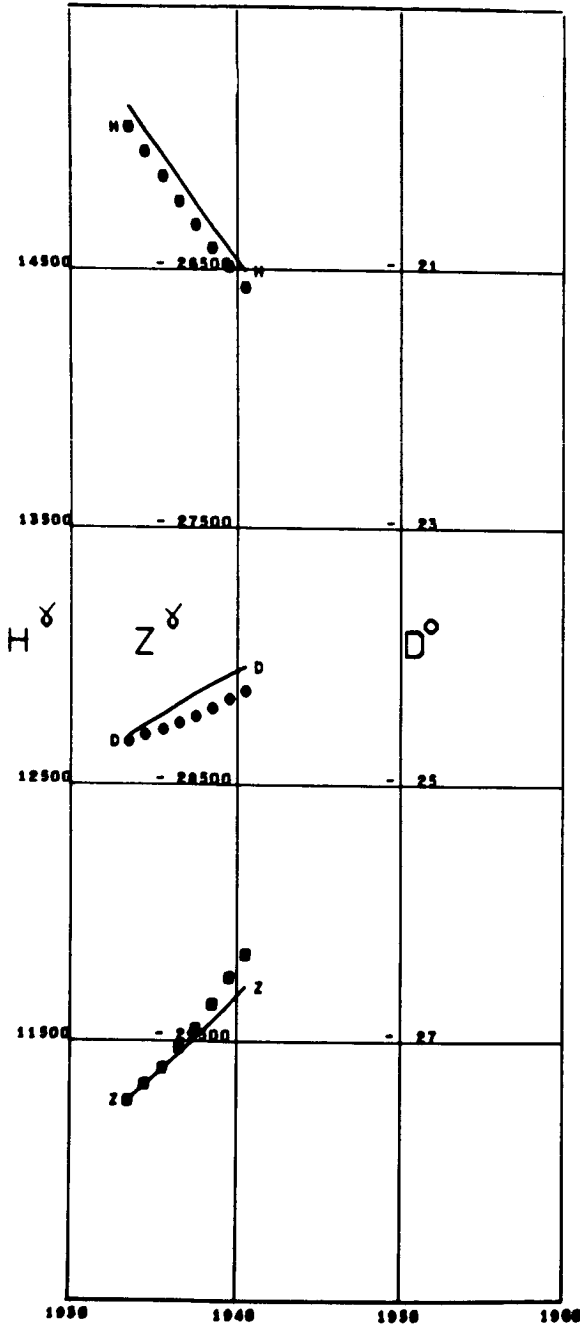
BUDAKESZI  
Lat 47.52 Long 18.89



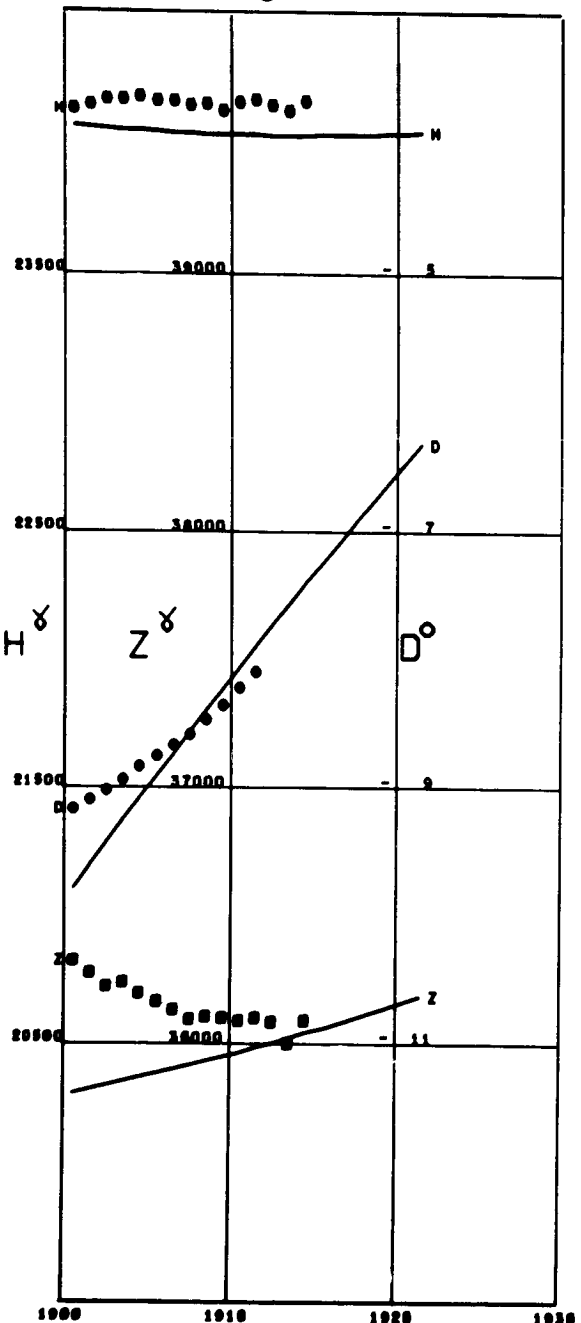
BYRD  
Lat -80.01 Long -119.51 Alt 1.52



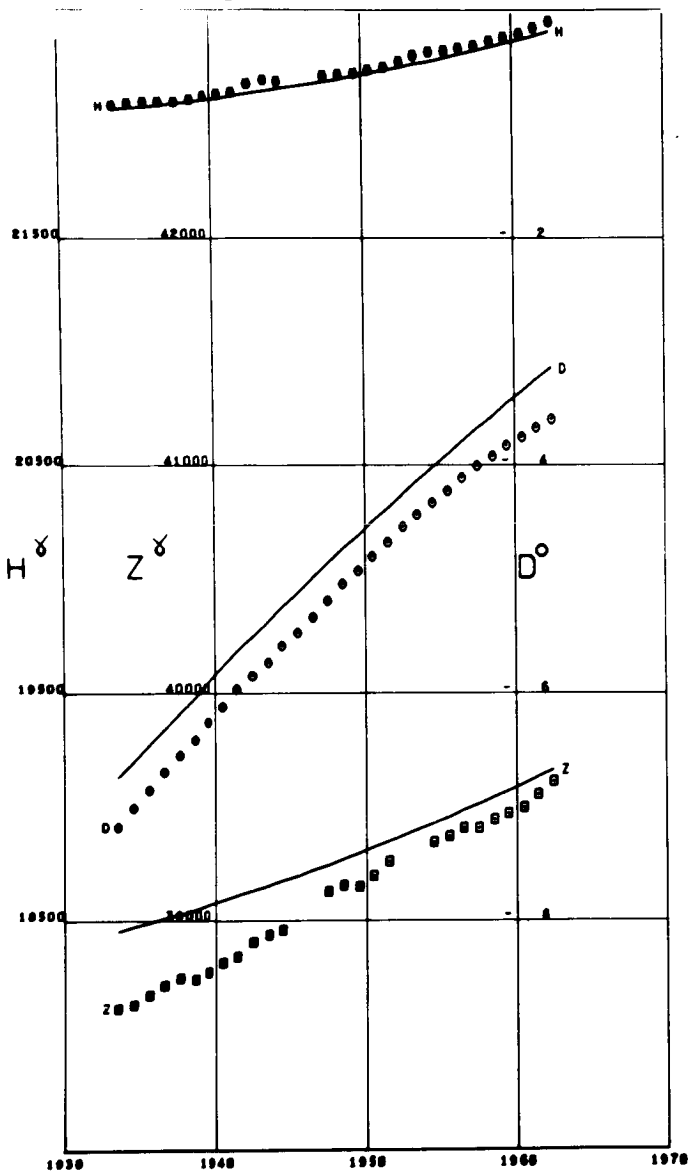
CAPETOWN  
Lat -33.95 Long 18.46



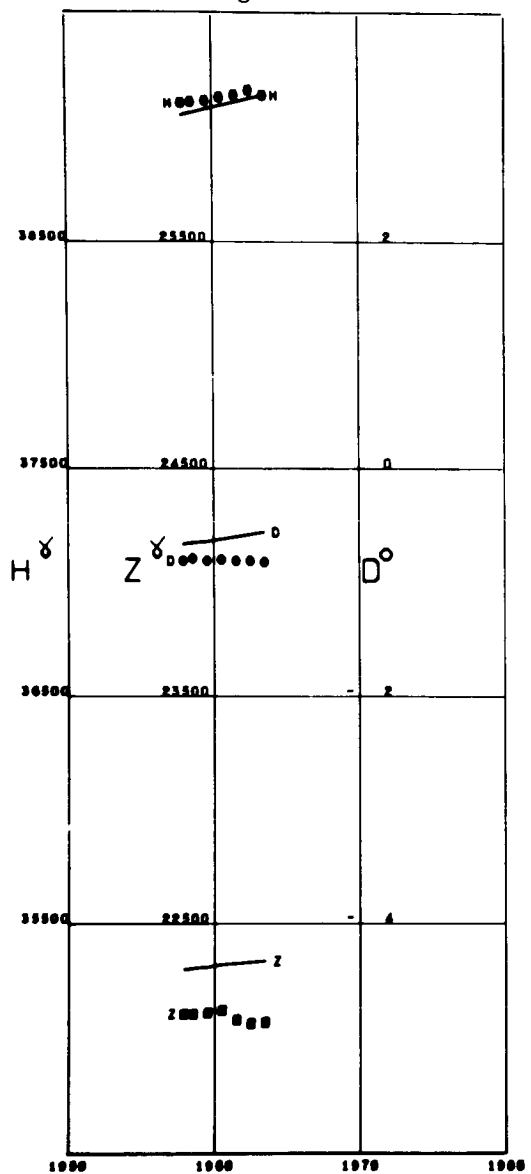
CAPODIMONTE  
Lat 40.86 Long 14.25



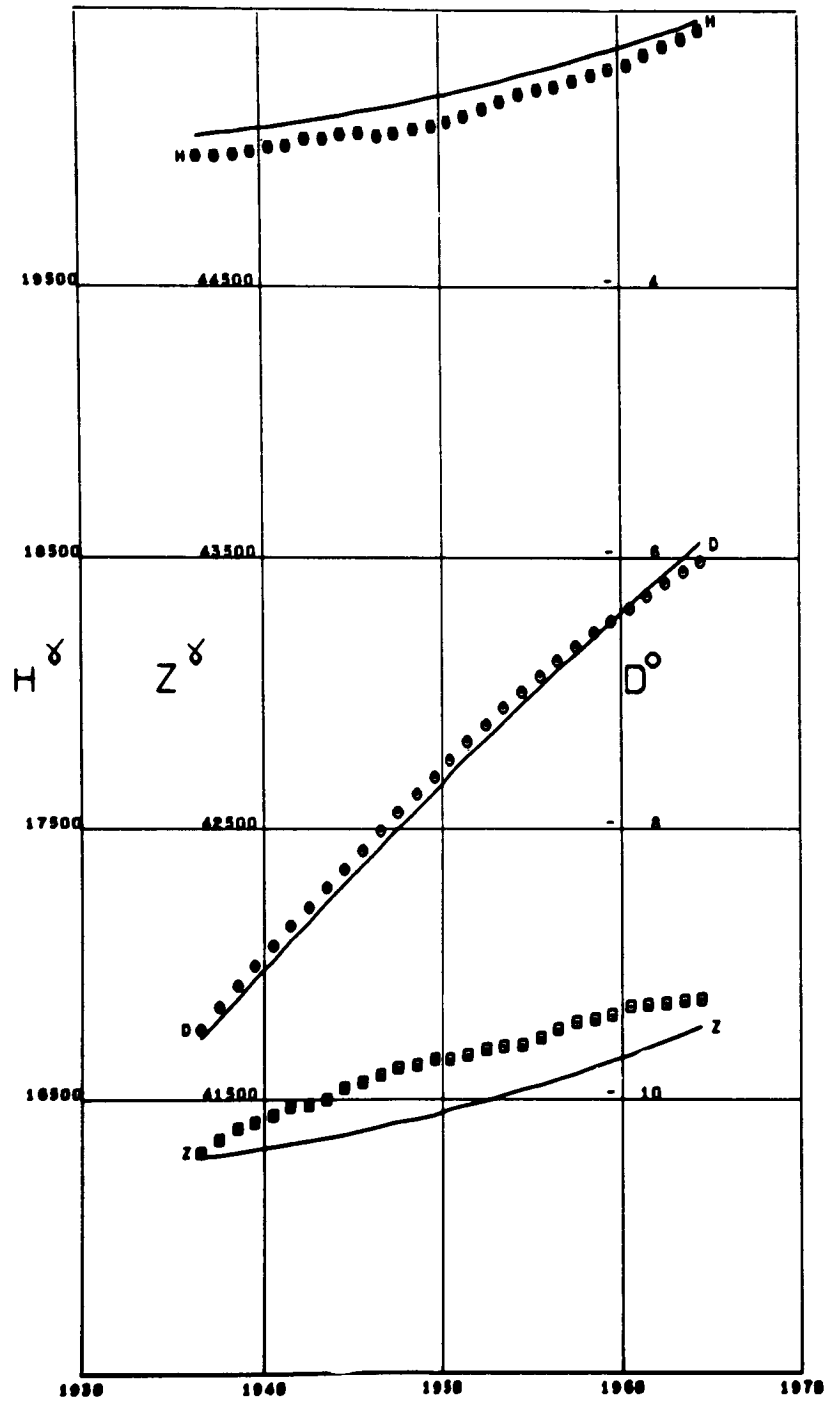
CASTELLACCIO  
Lat 44.43 Long 8.93



CHA PA  
Lat 22.35 Long 103.83

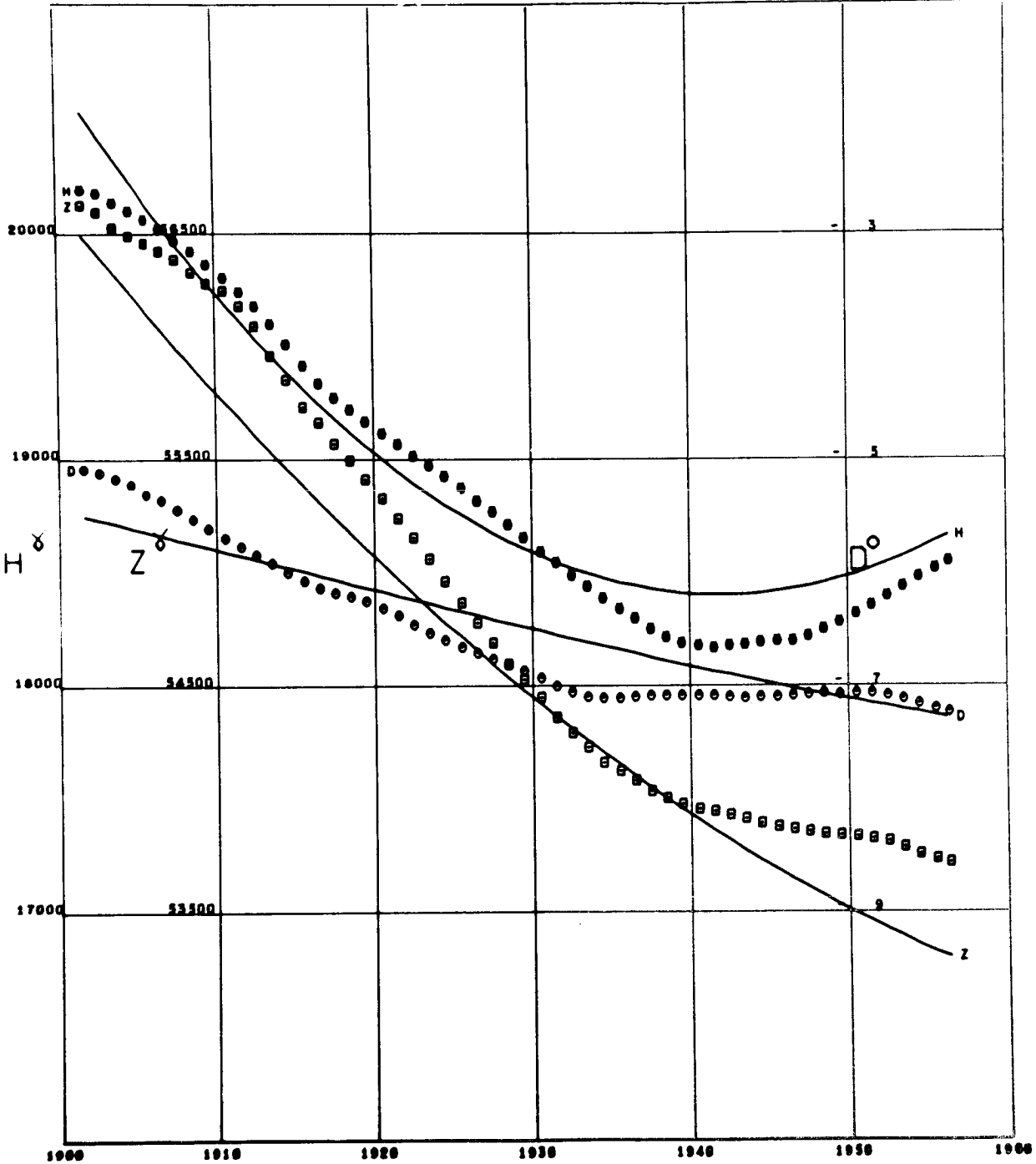


CHAMBON-LA-FORET  
Lat 48.02 Long 2.26

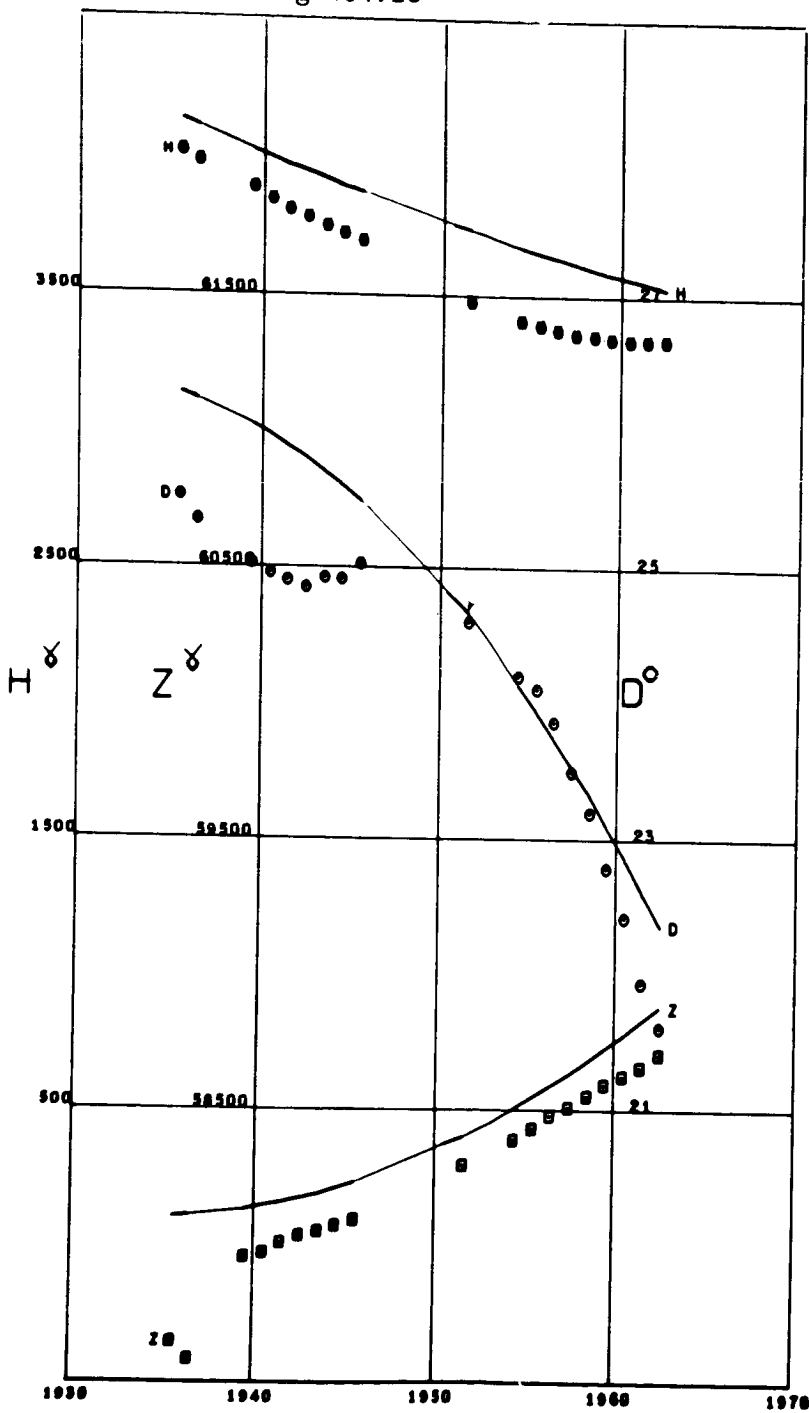


CHELTENHAM

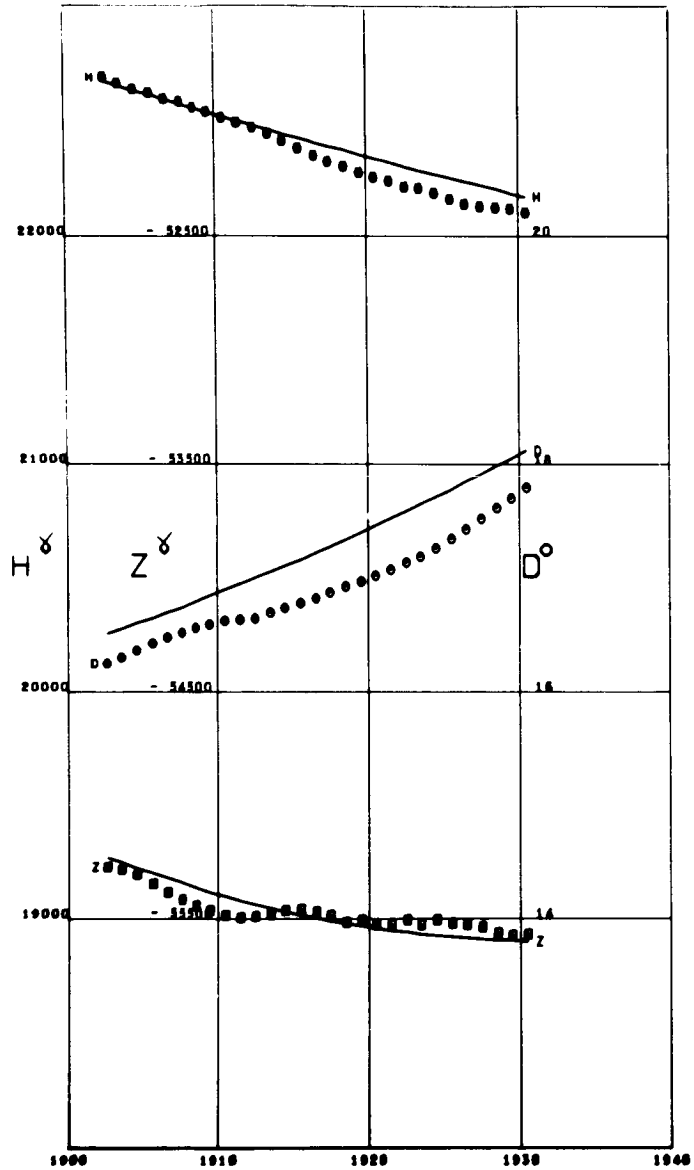
Lat 38.73 Long -76.84



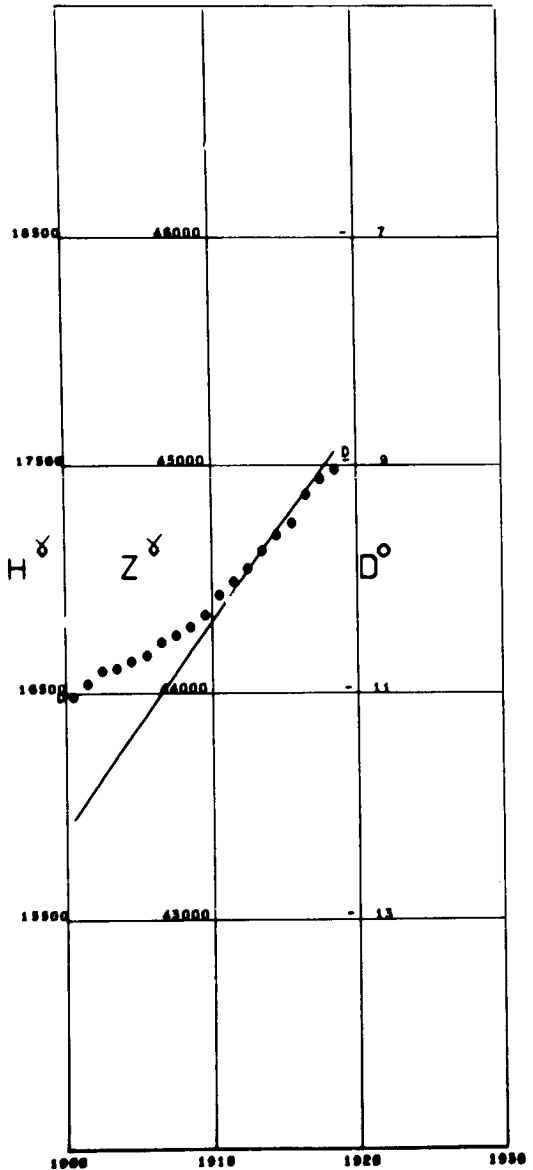
CHELYUSKIN  
Lat 77.71 Long 104.28



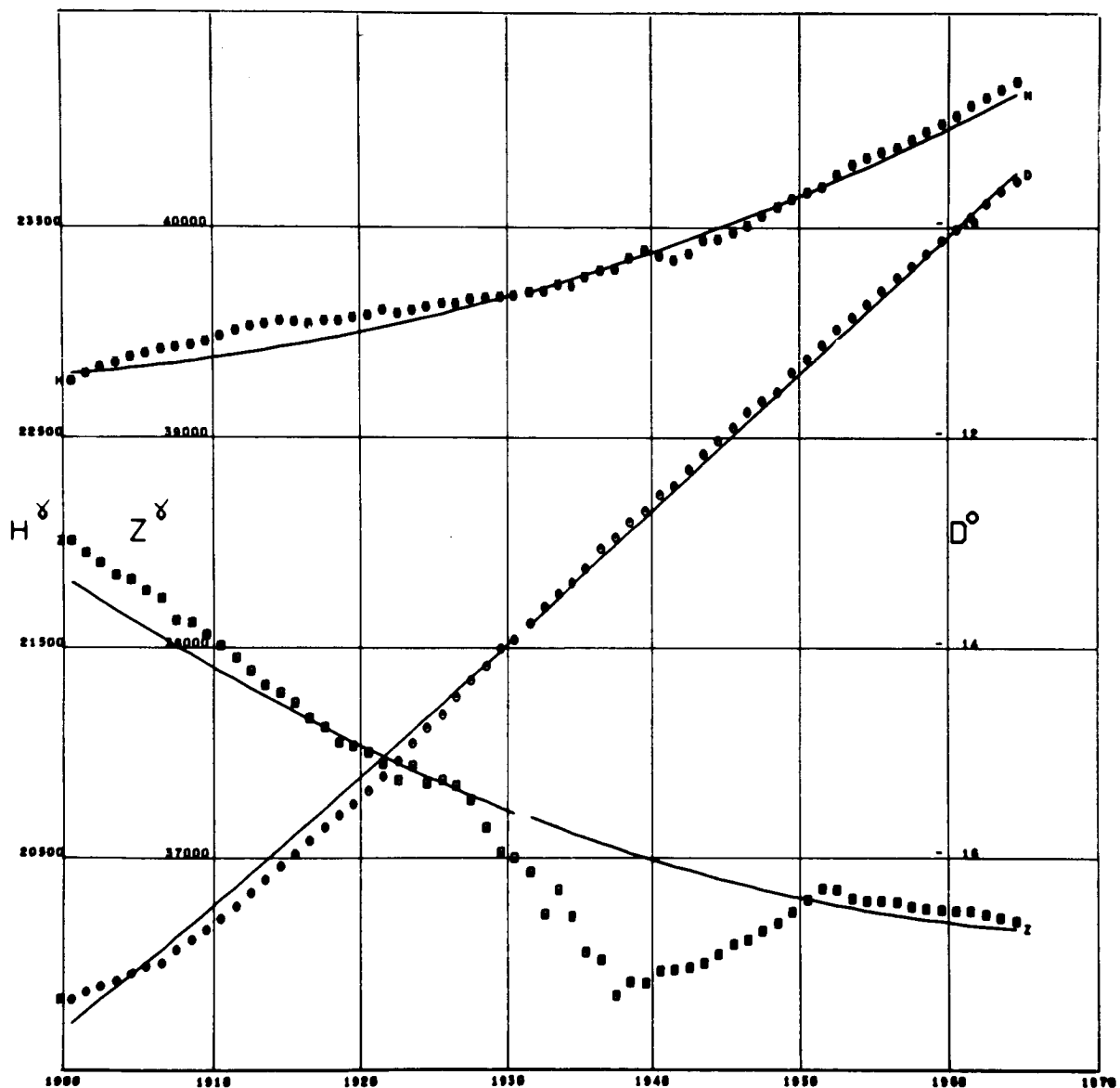
CHRISTCHURCH  
Lat -43.53 Long 172.62



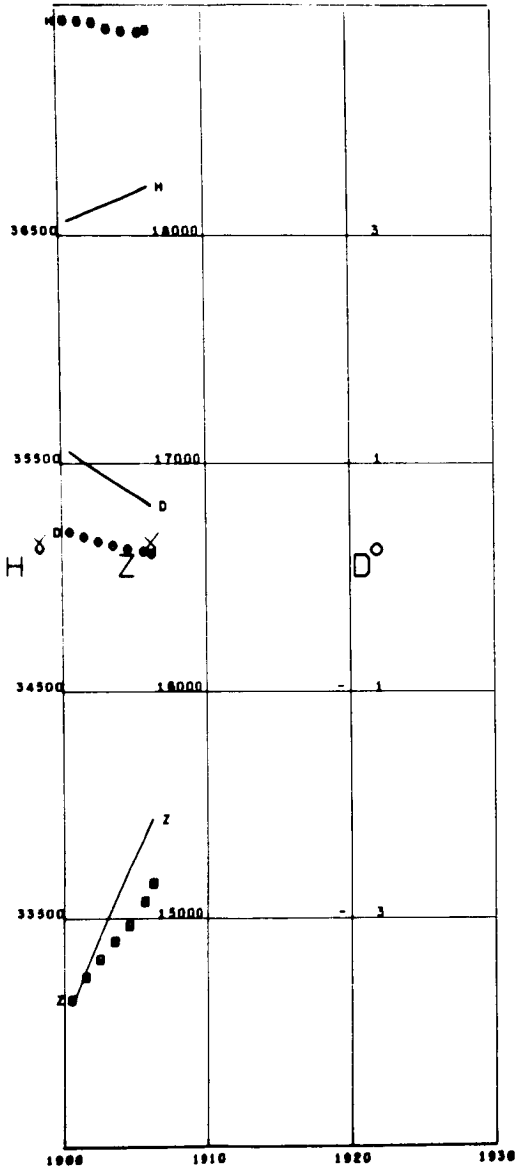
CLAUSTHAL  
Lat 51.80 Long 10.33



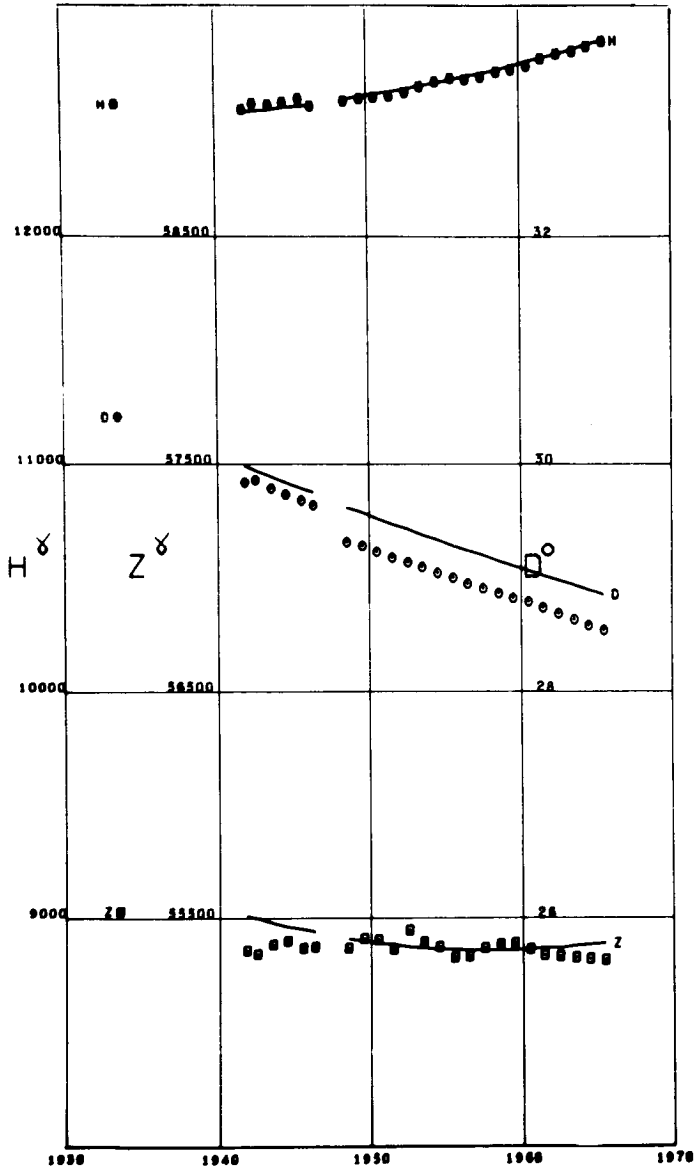
COIMBRA  
Lat 40.22 Long -8.42



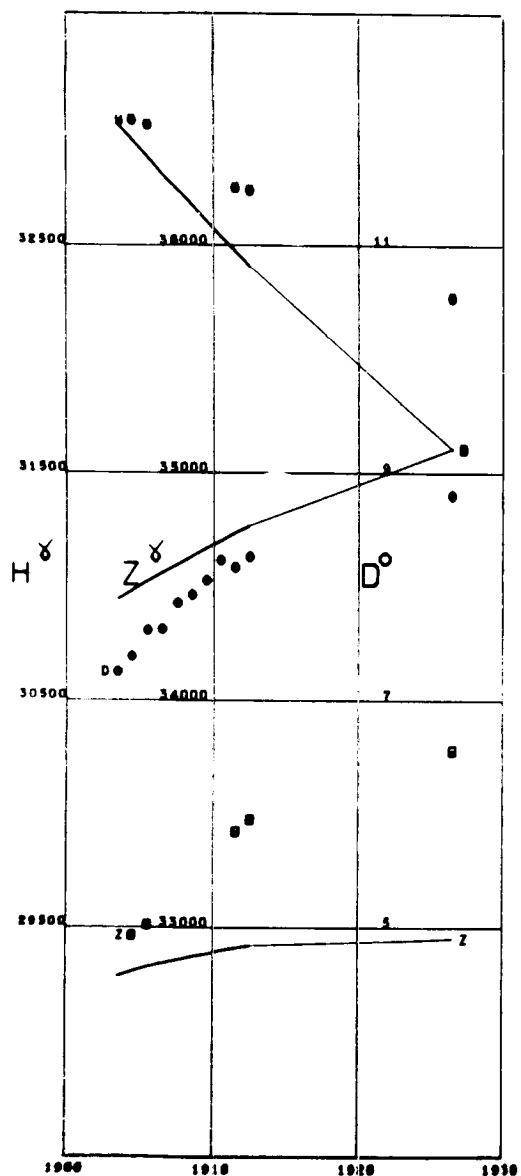
COLABA  
Lat 18.89 Long 72.81



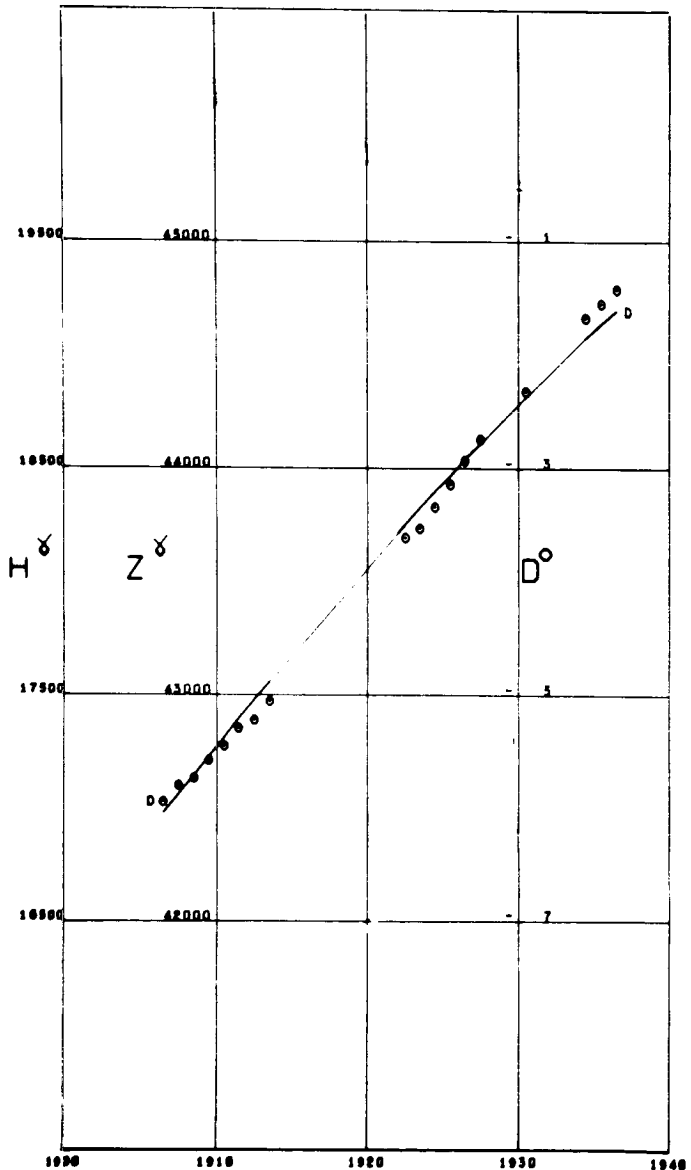
COLLEGE  
Lat 64.86 Long -147.85 Alt 0.20



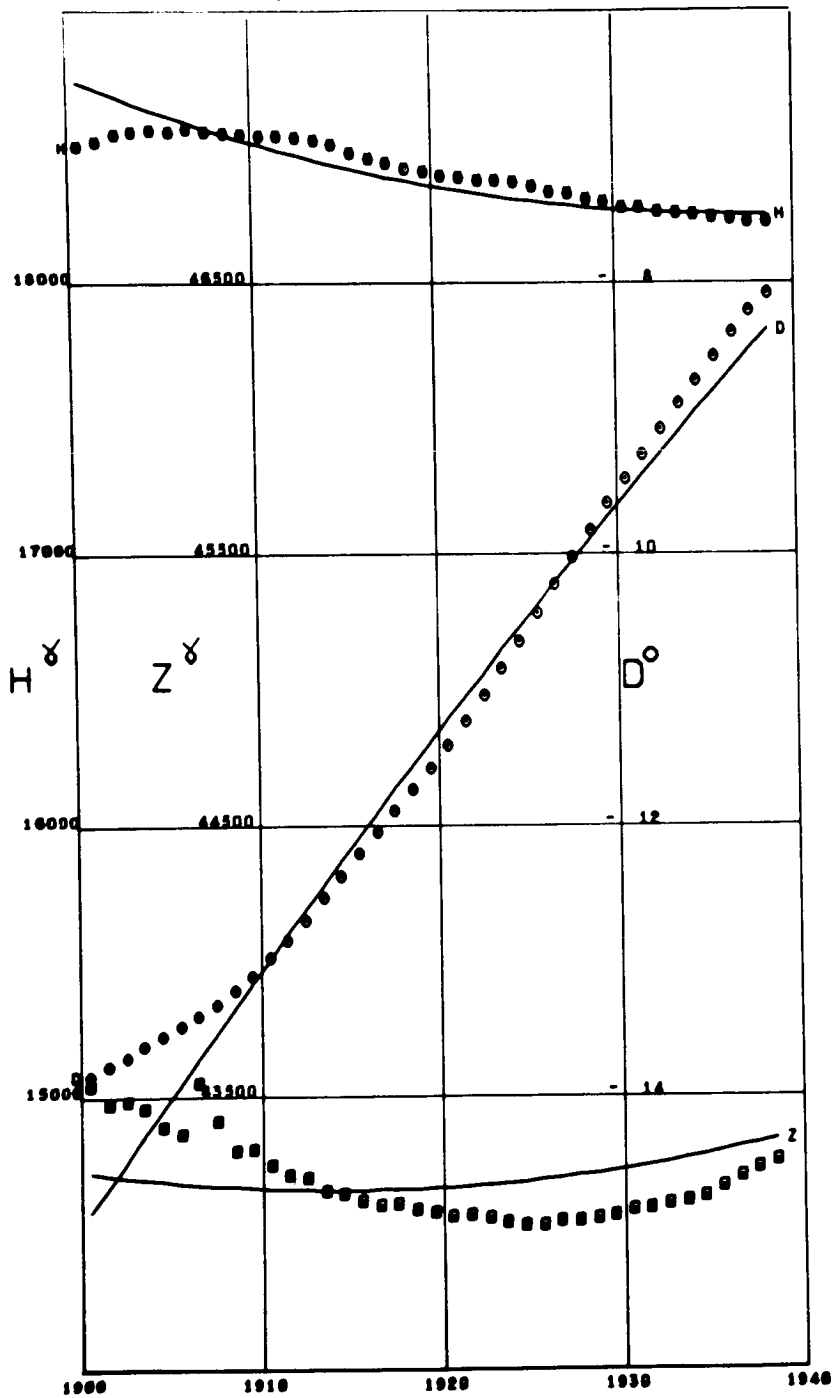
CUAJIMALPA  
Lat 19.37 Long -99.28



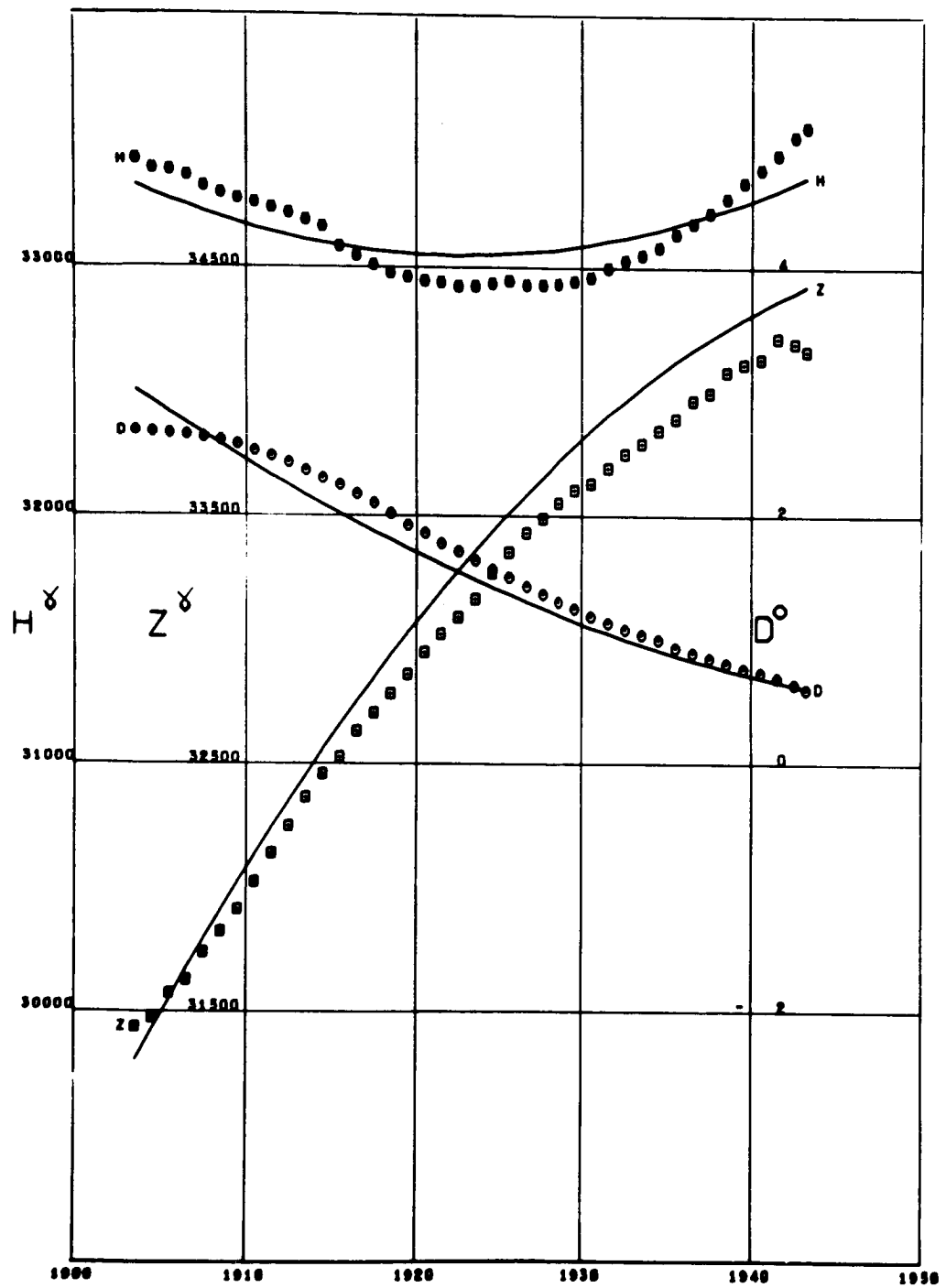
CRACOW  
Lat 50.05 Long 19.95



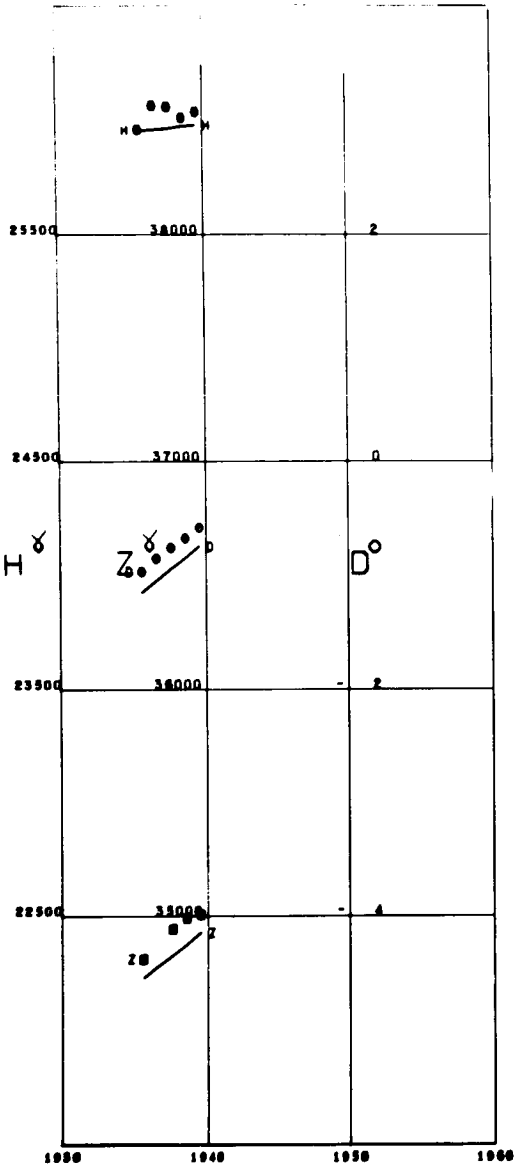
DE BILT  
Lat 52.10 Long 5.17



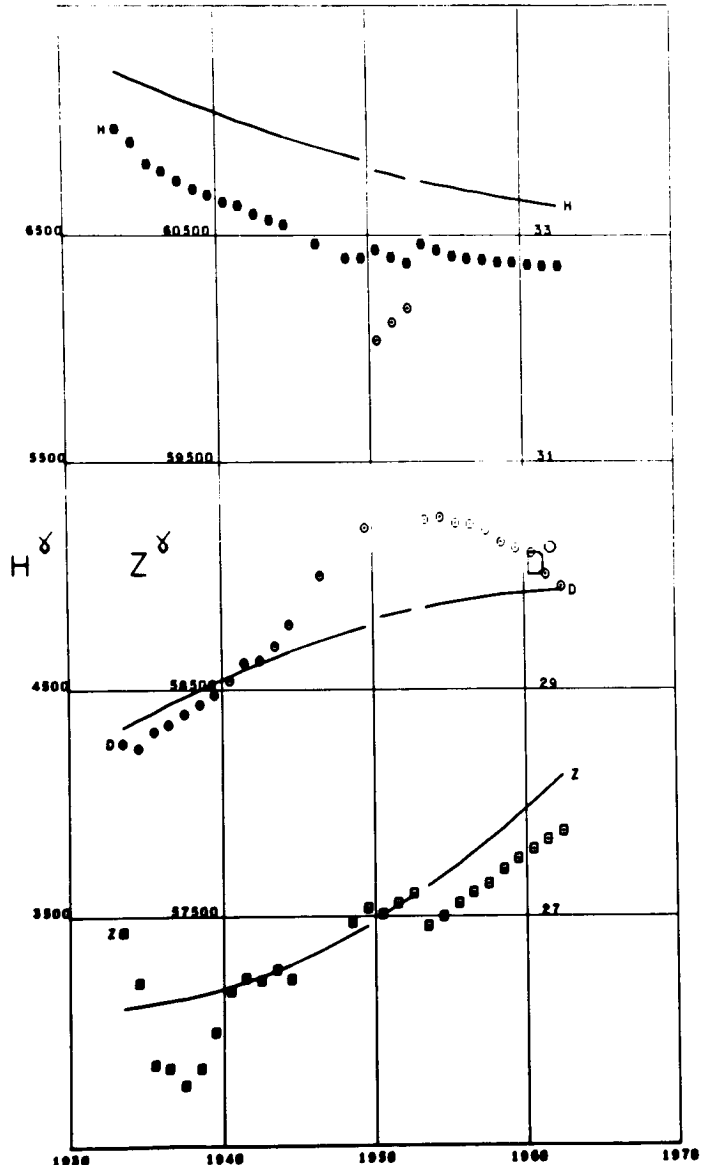
DEHRA DUN  
Lat 30.32 Long 78.05



DEKELEIA  
Lat 38.10 Long 23.77

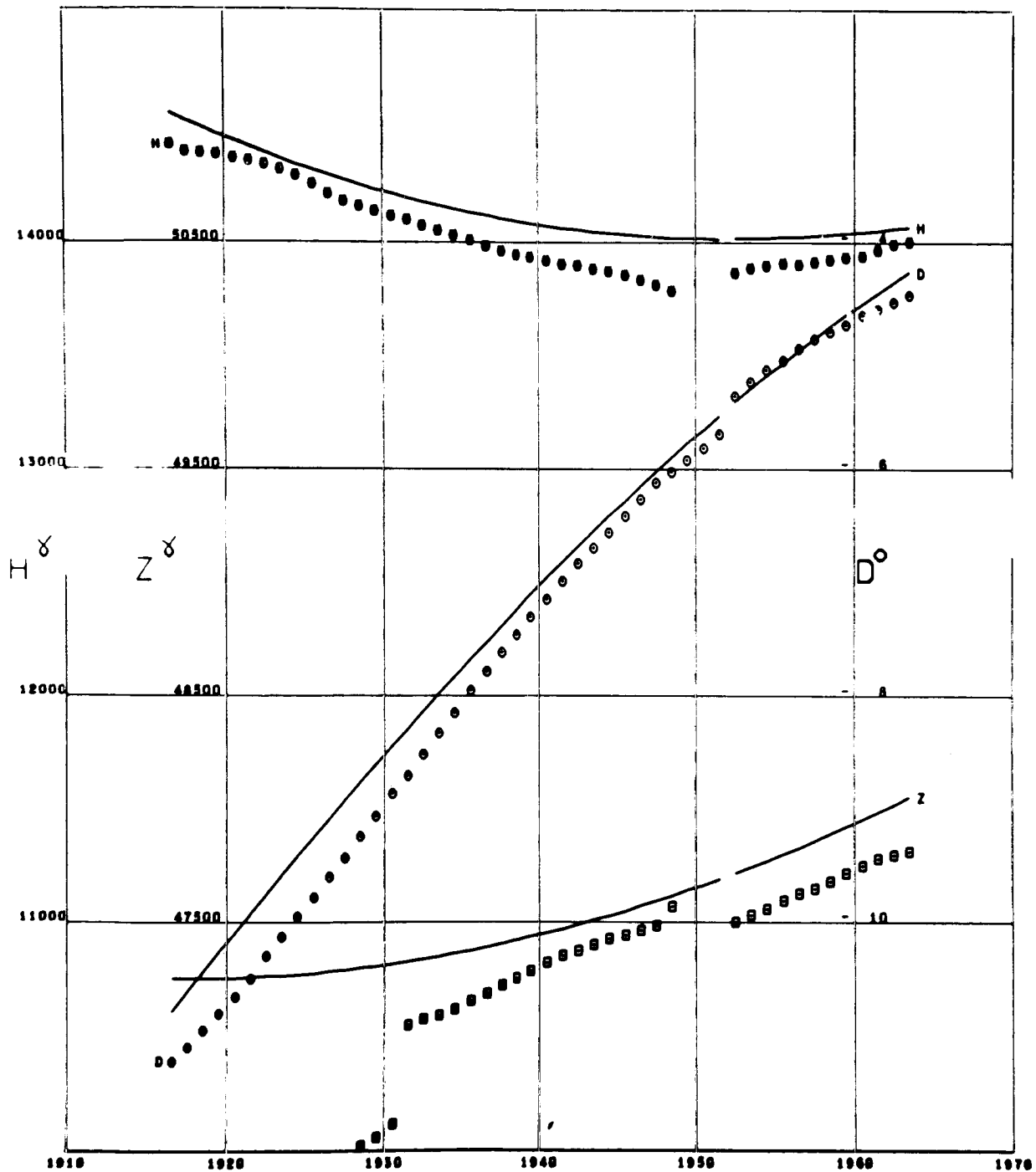


DIKSON  
Lat 73.54 Long 80.56

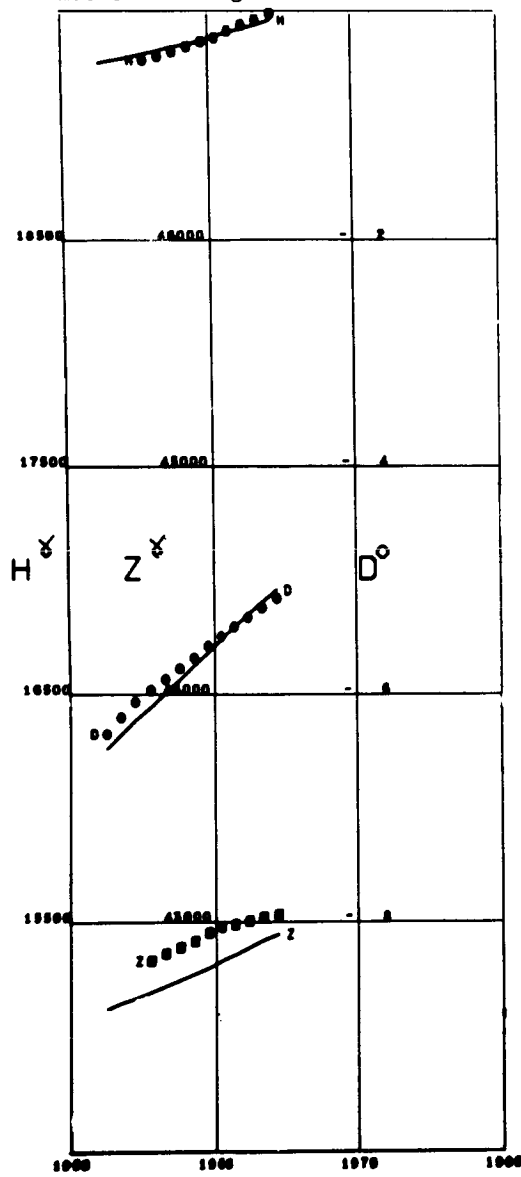


DOMBAS

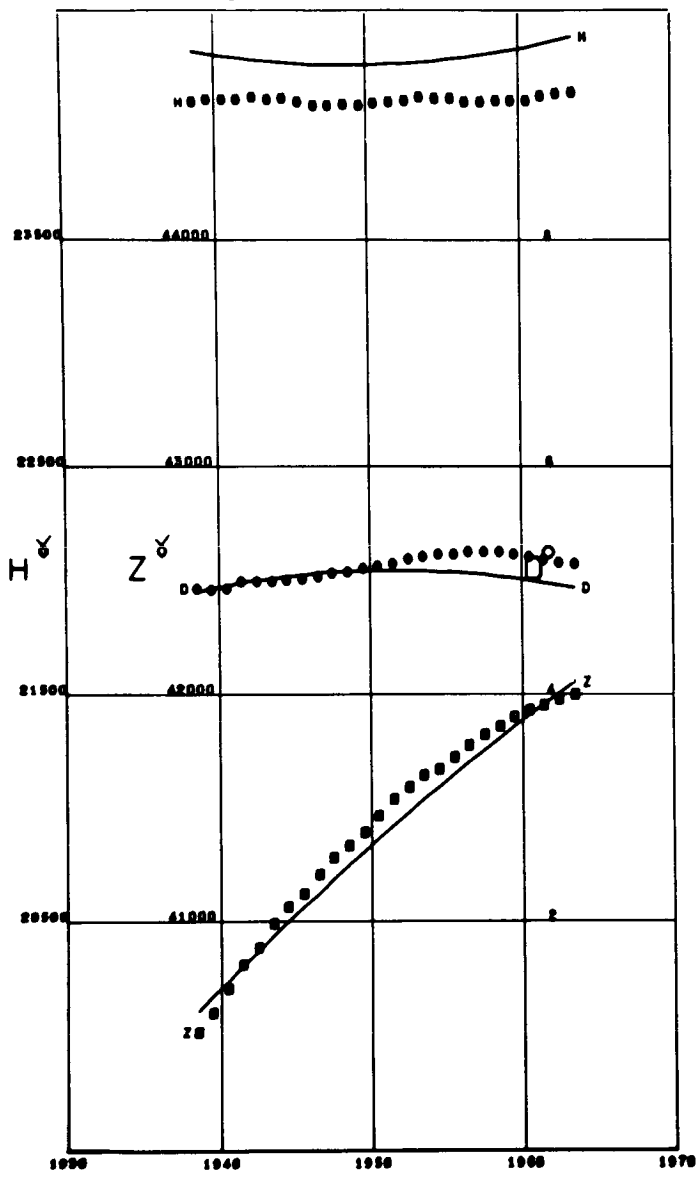
Lat 62.07 Long 9.11



DOURBES  
Lat 50.09 Long 4.59

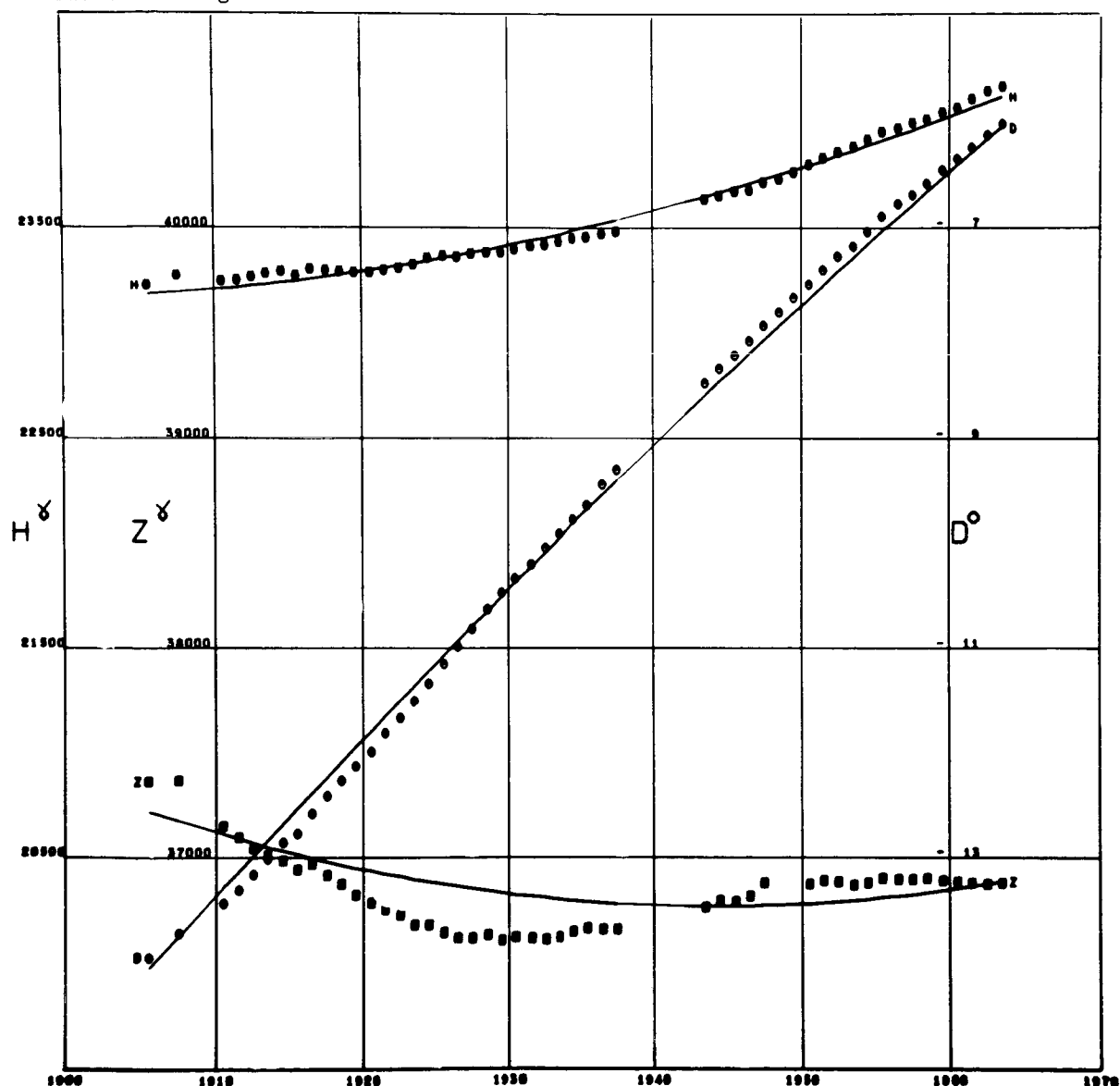


DUSHETI  
Lat 42.09 Long 44.70

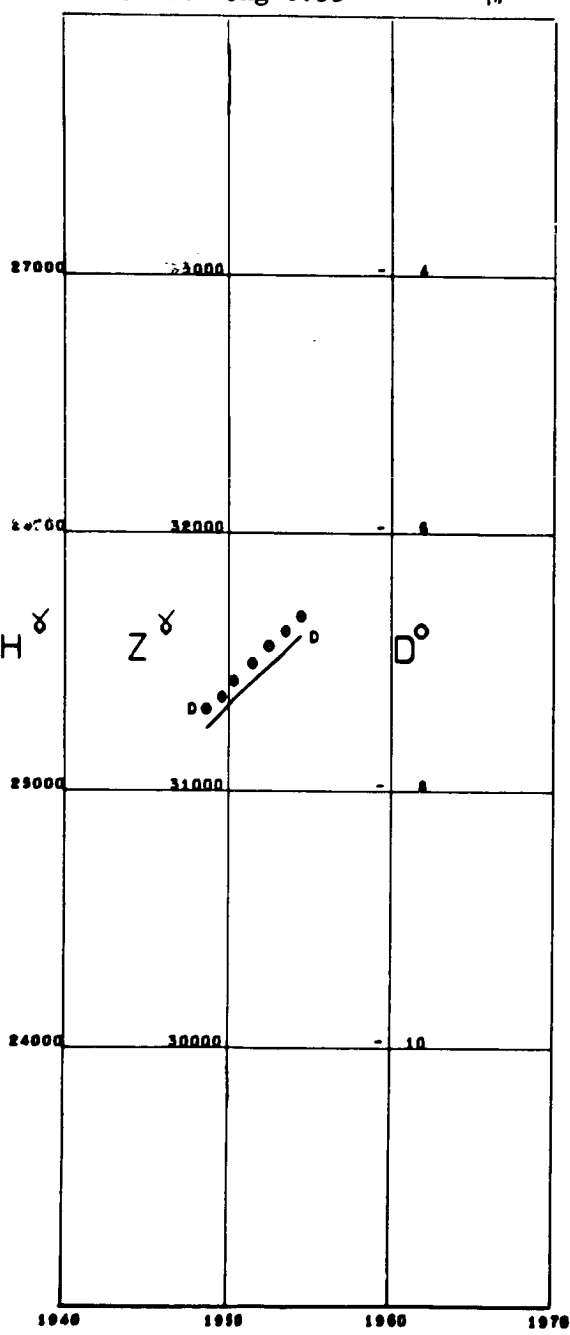


EBRO

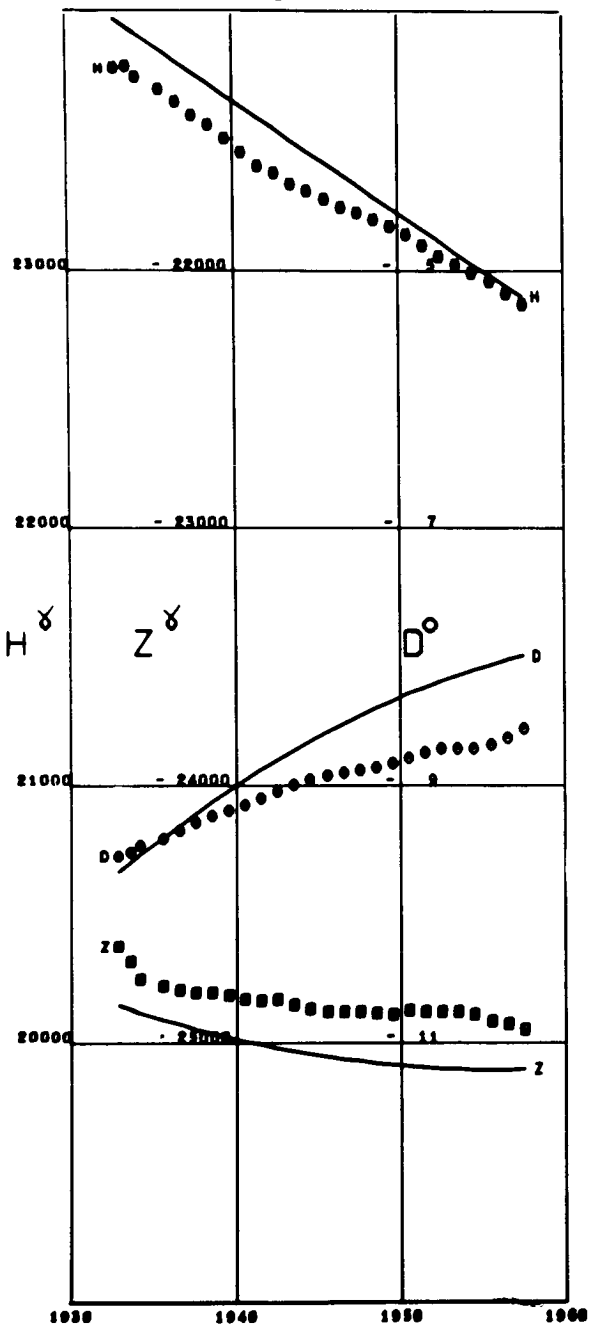
Lat 40.82 Long 0.49 Alt 0.05



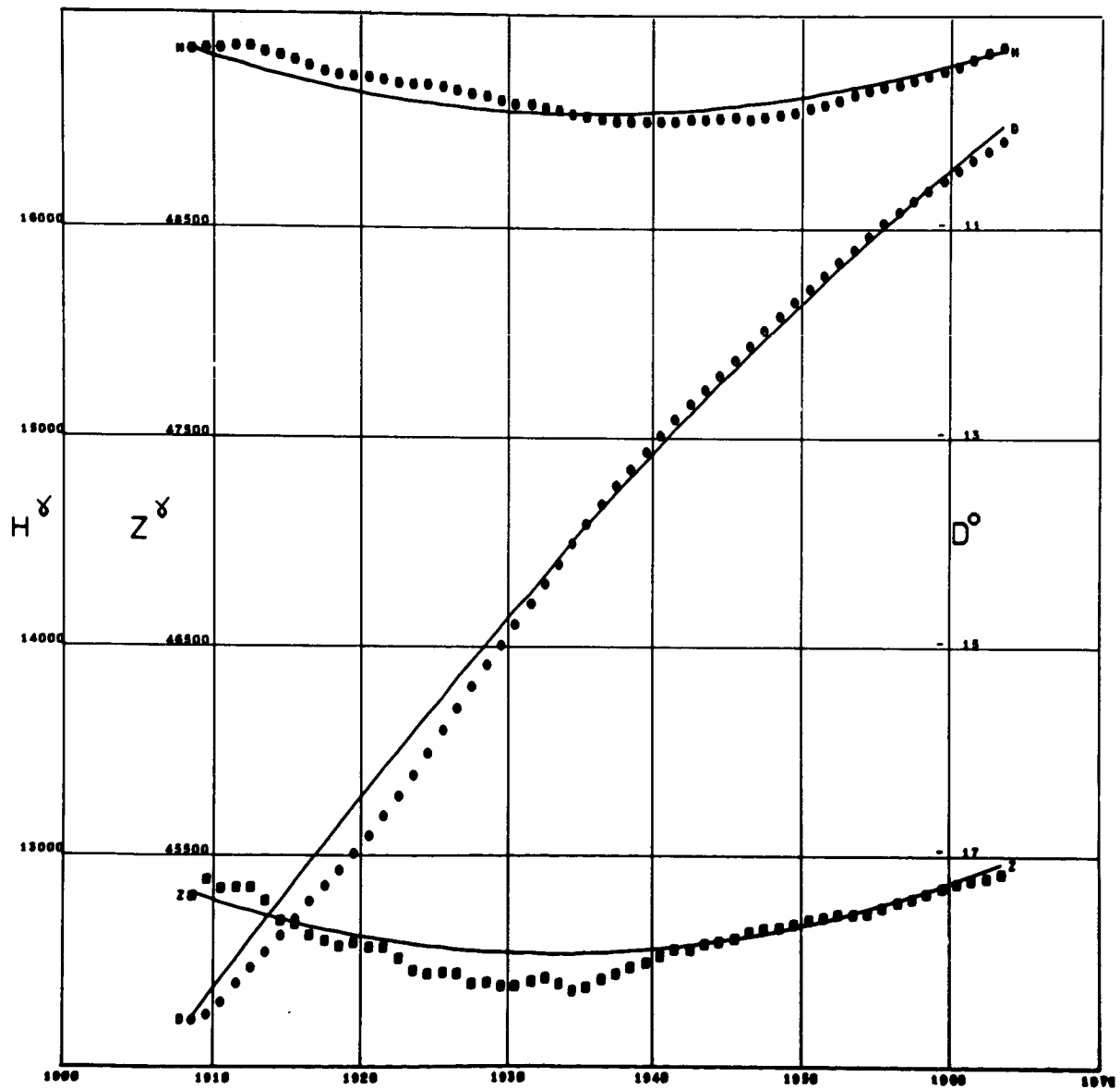
EL ABIOD SIDI  
Lat 32.90 Long 0.55



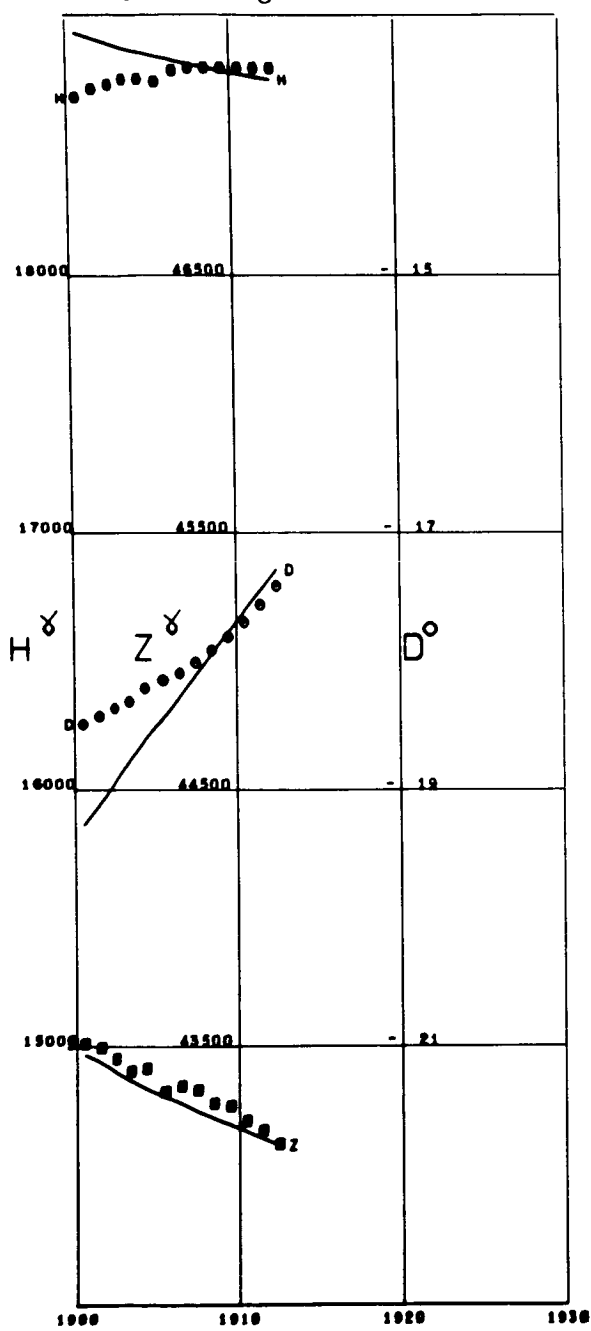
ELISABETHVILLE  
Lat -11.65 Long 27.46



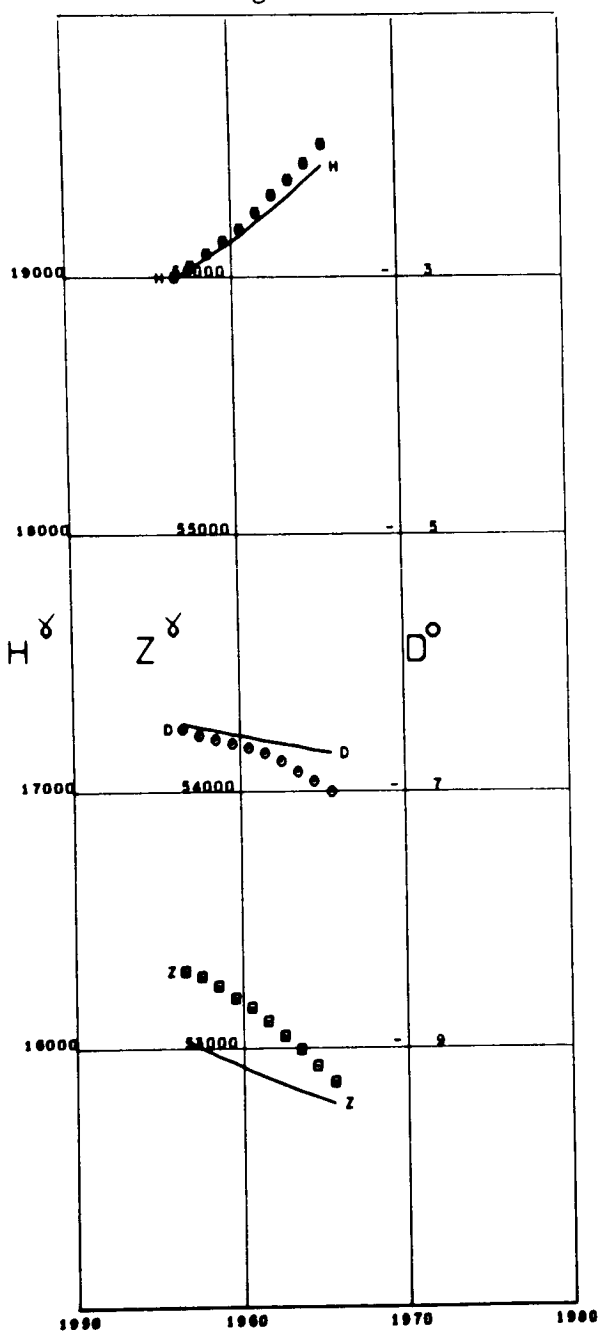
ESKDALEMUIR  
Lat 55.31 Long -3.20



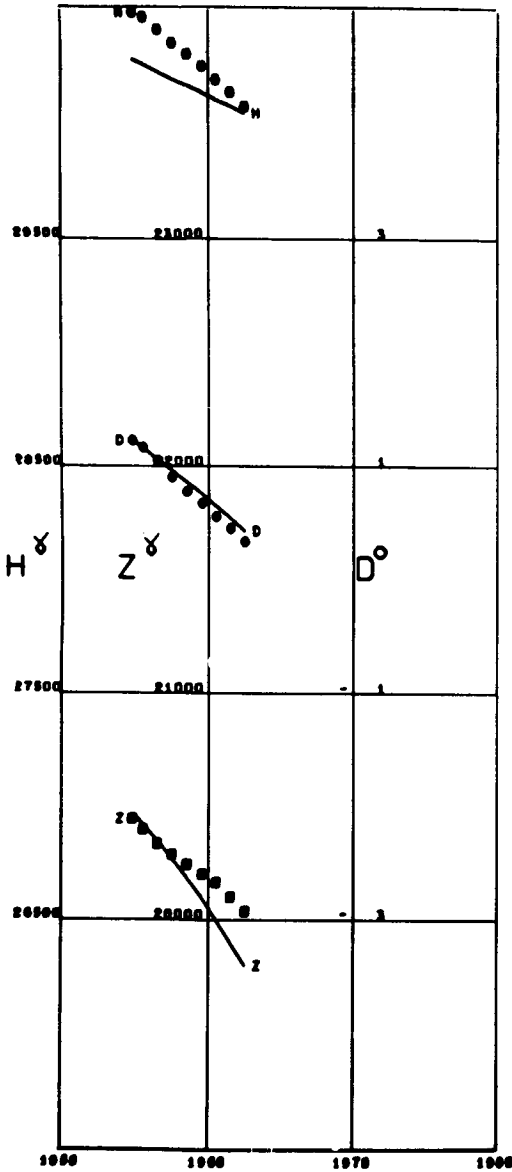
FALMOUTH  
Lat 50.15 Long -5.07



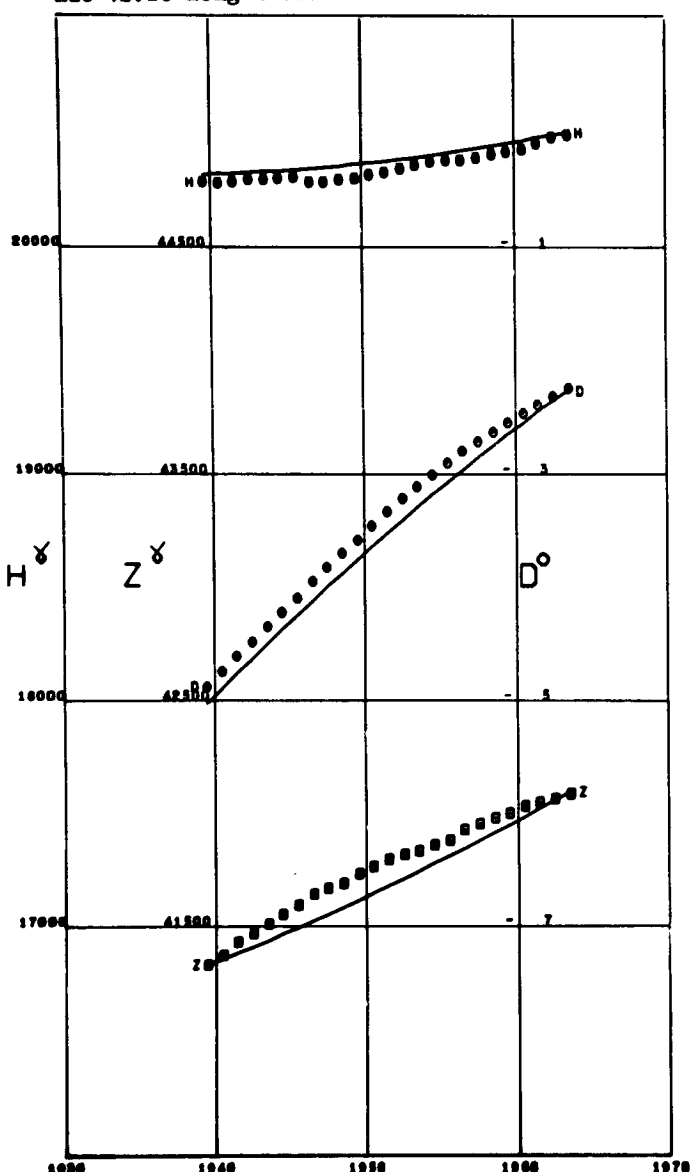
FREDERICKSBURG  
Lat 38.20 Long -77.37 Alt 0.07



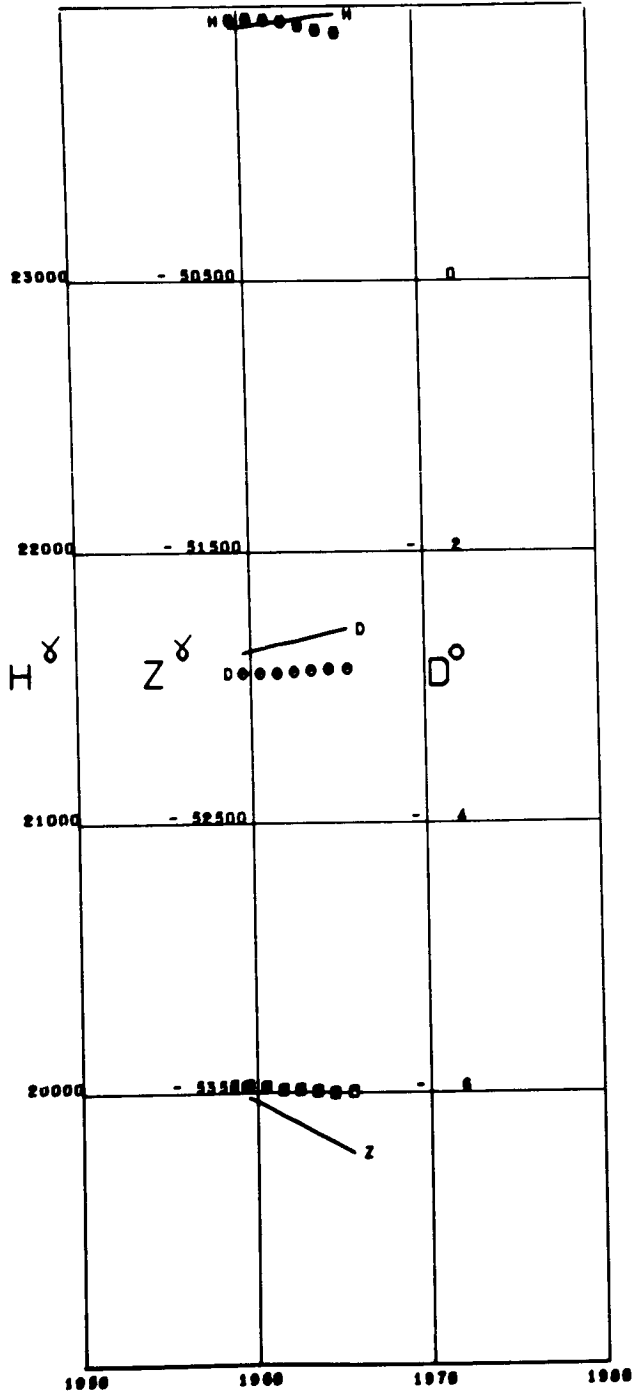
FUQUENE  
Lat 5.47 Long -73.73 Alt 2.54



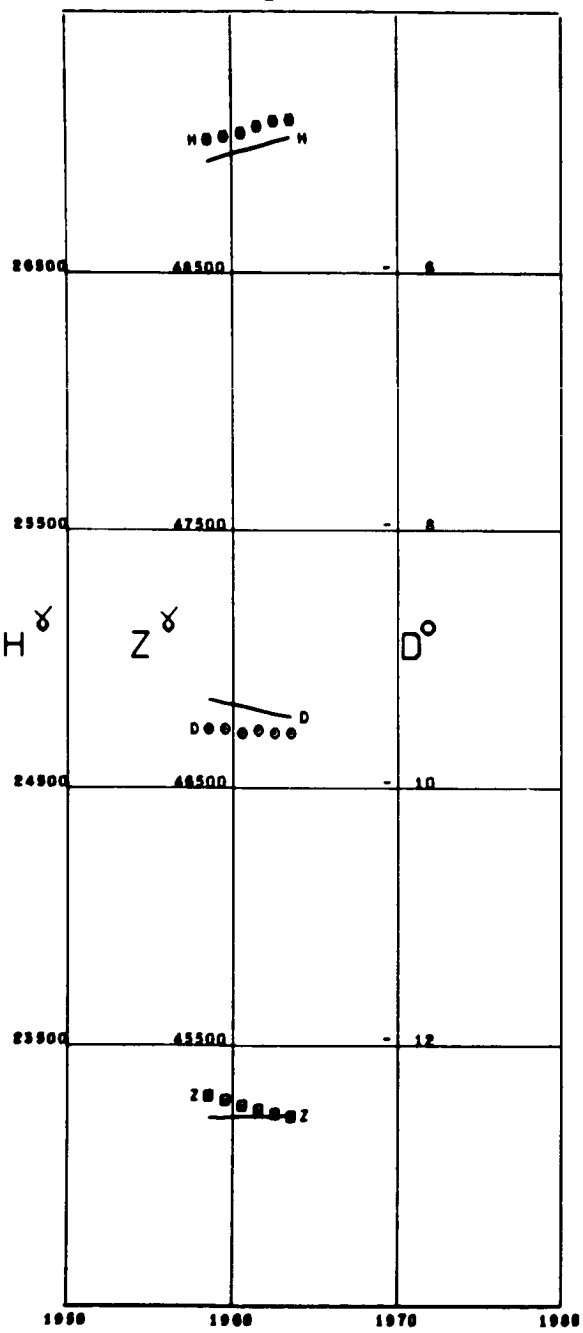
FURSTENFELDBRUCK  
Lat 48.16 Long 11.27 Alt 0.57



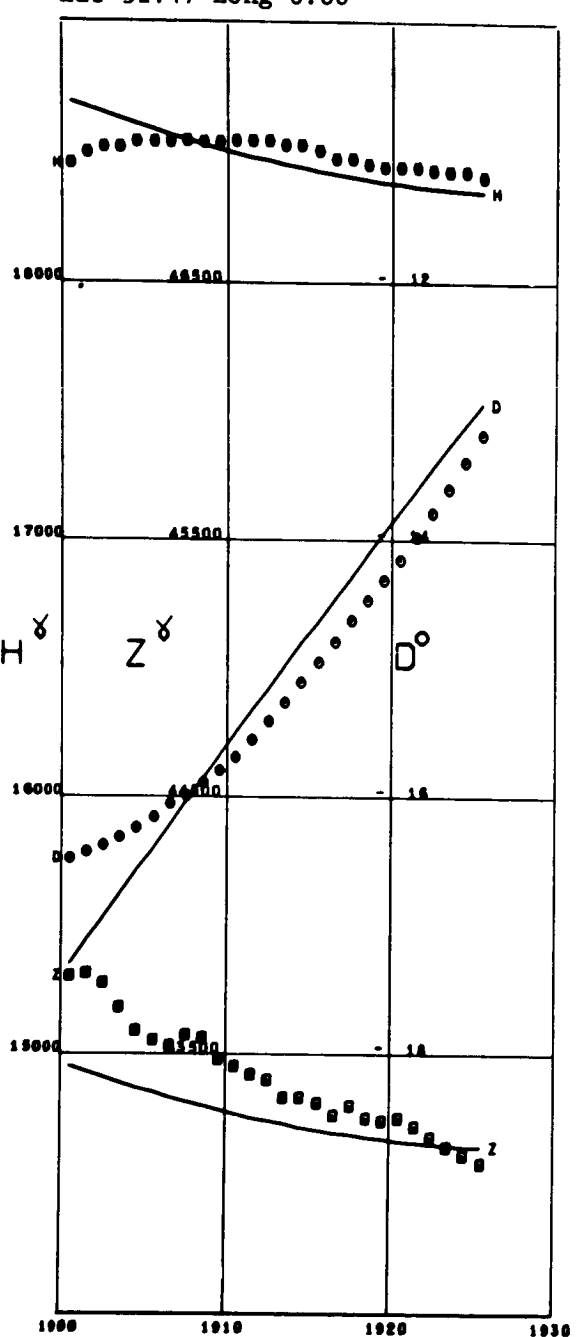
GNANGARA  
Lat -31.78 Long 115.95 Alt 0.06



GORNOTAYEZHNAЯ  
Lat 43.68 Long 132.16

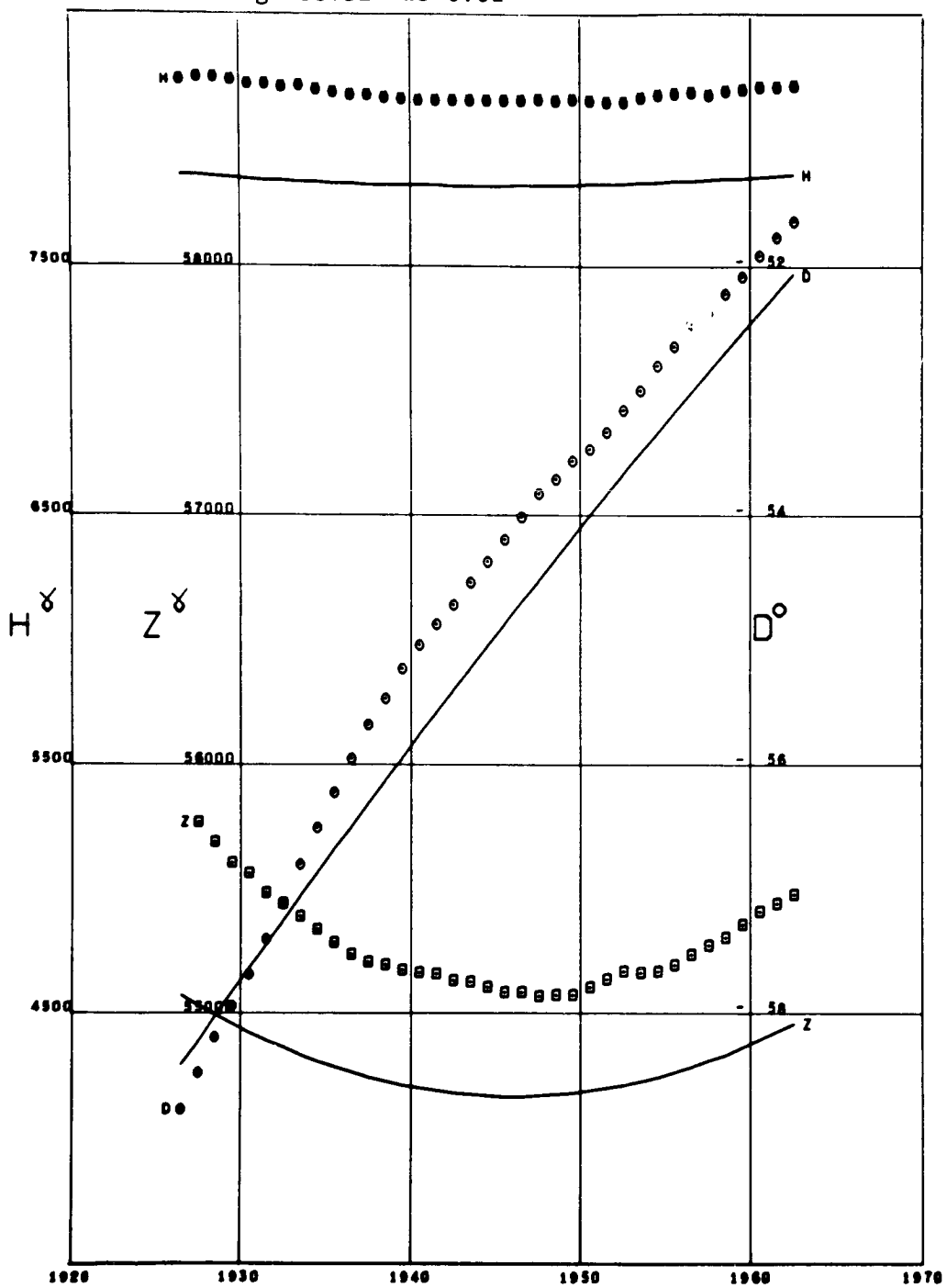


GREENWICH  
Lat 51.47 Long 0.00

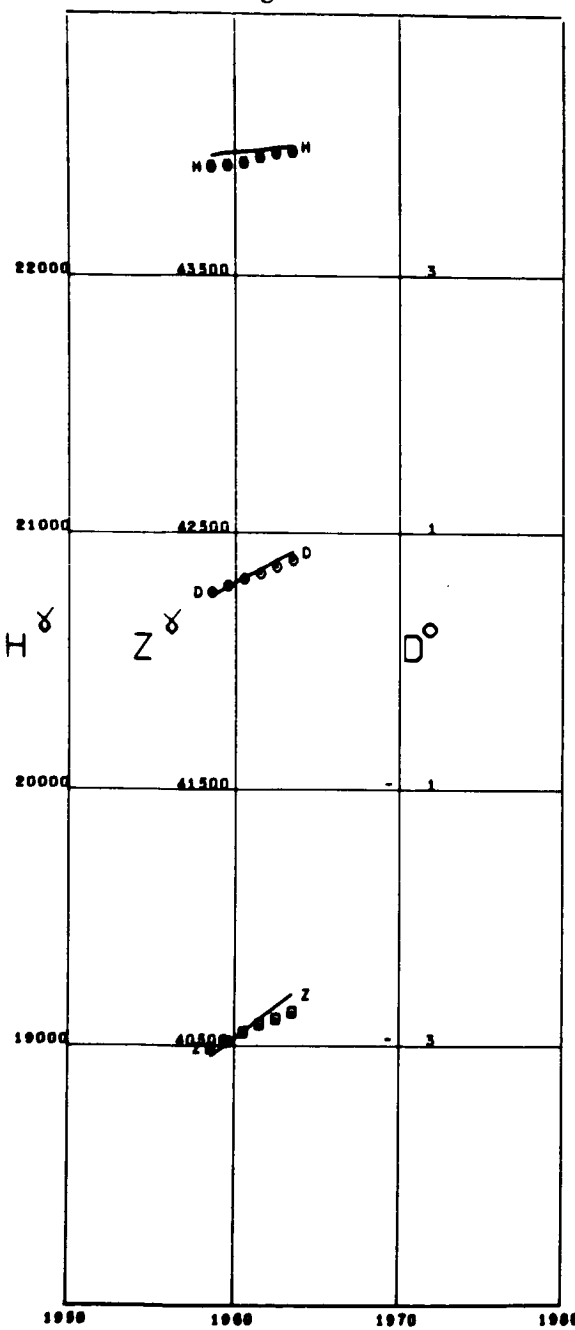


GODHAVN

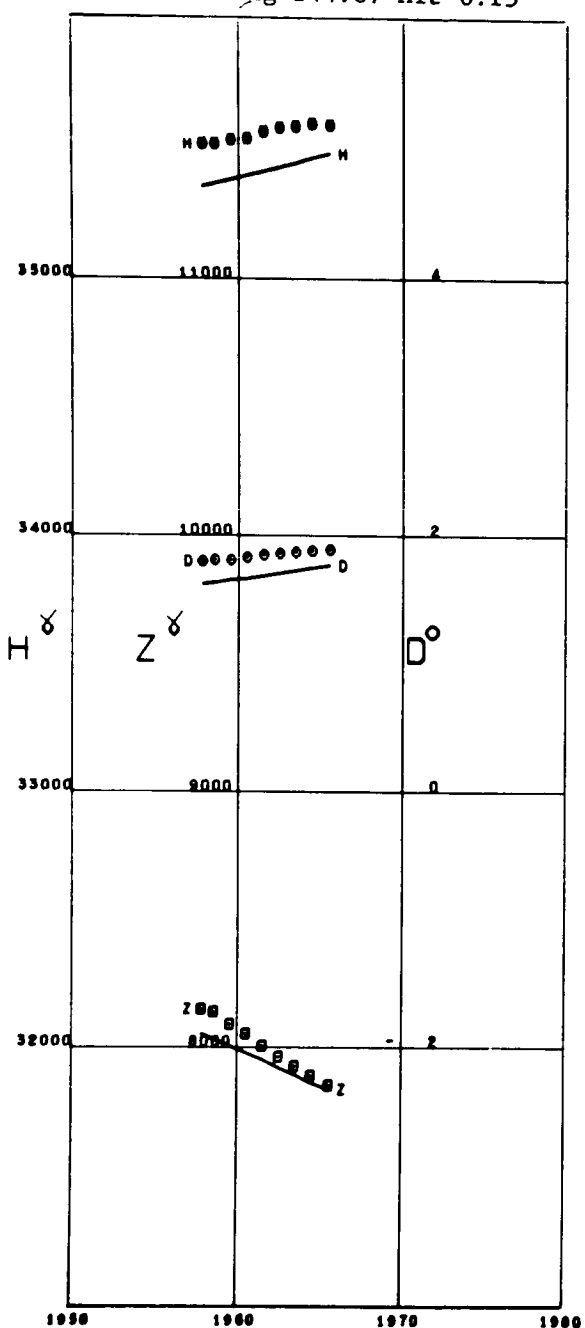
Lat 69.24 Long -53.52 Alt 0.01



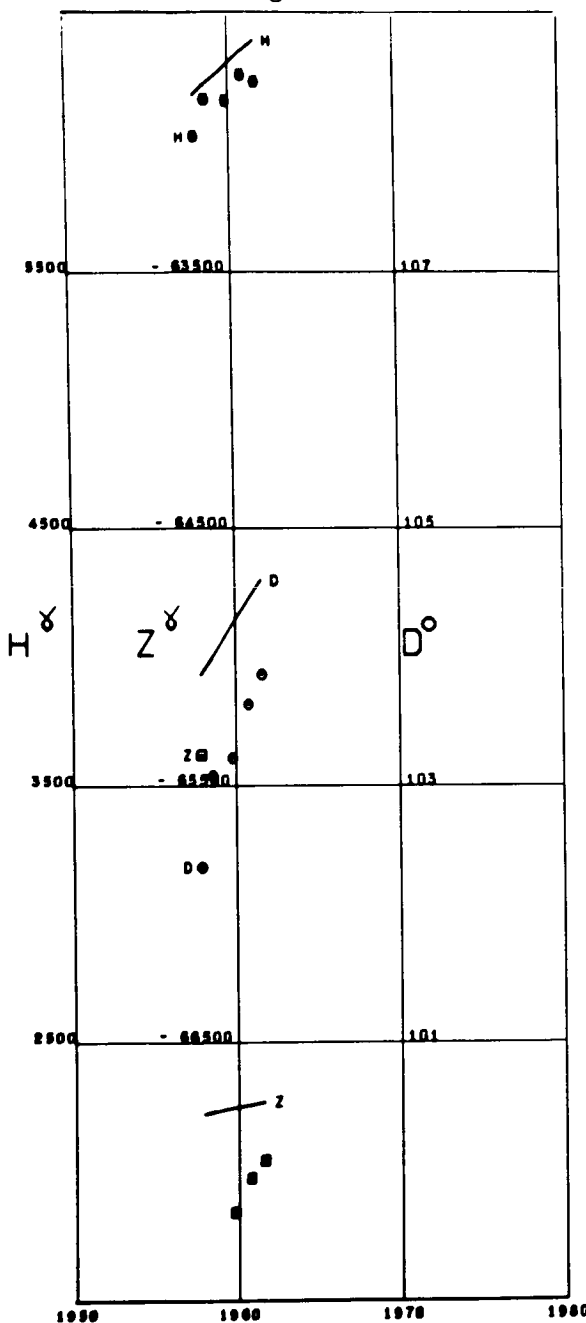
GROCKA  
Lat 44.63 Long 20.76



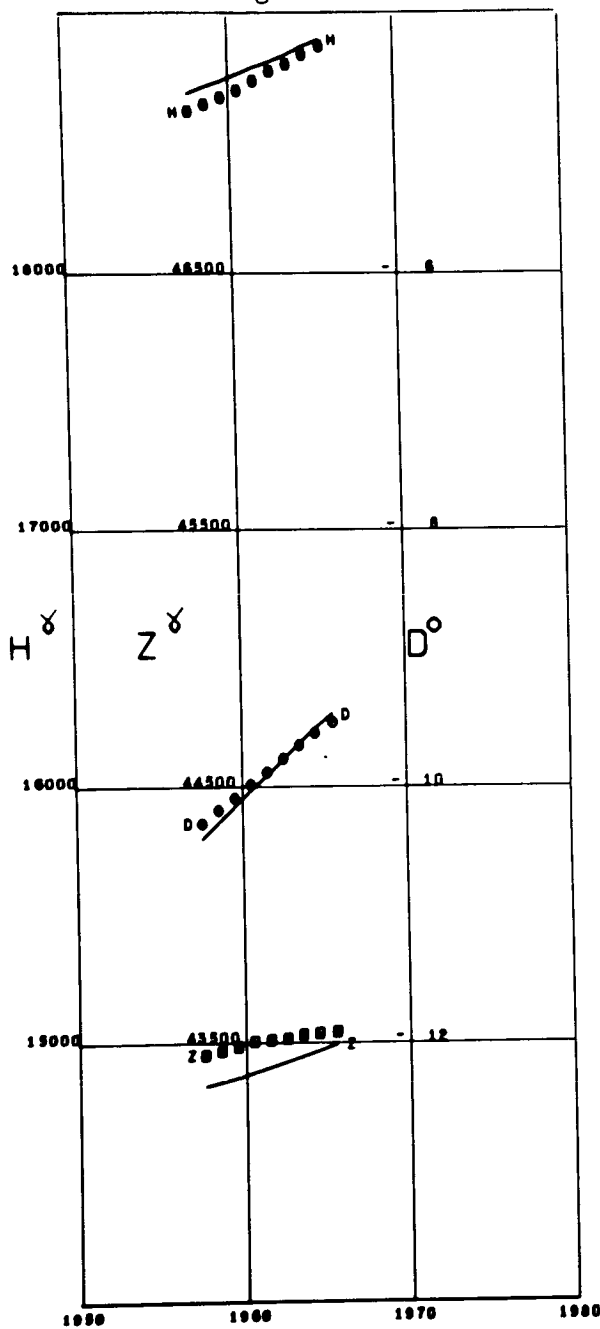
GUAM  
Lat 13.58 Long 144.87 Alt 0.15



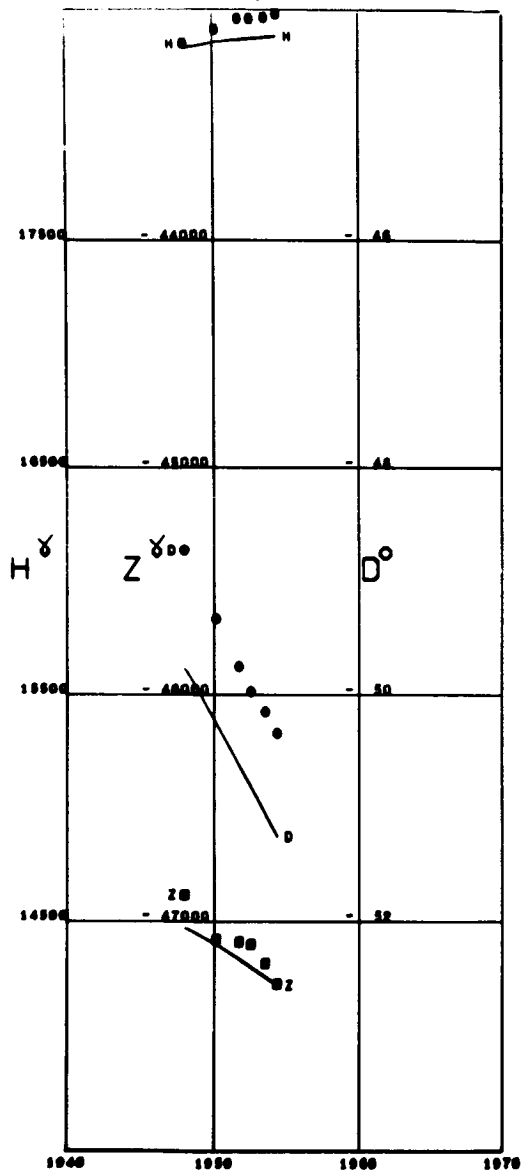
HALLETT STATION  
Lat -72.31 Long 170.21



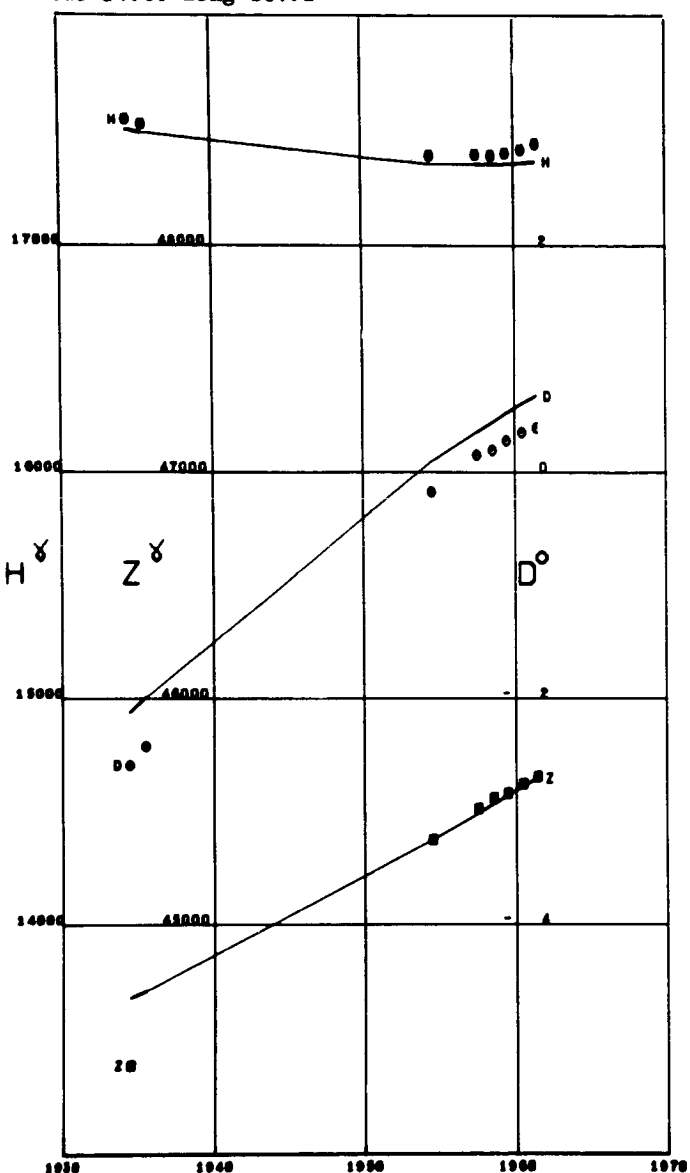
HARTLAND  
Lat 50.99 Long -4.48 Alt 0.09



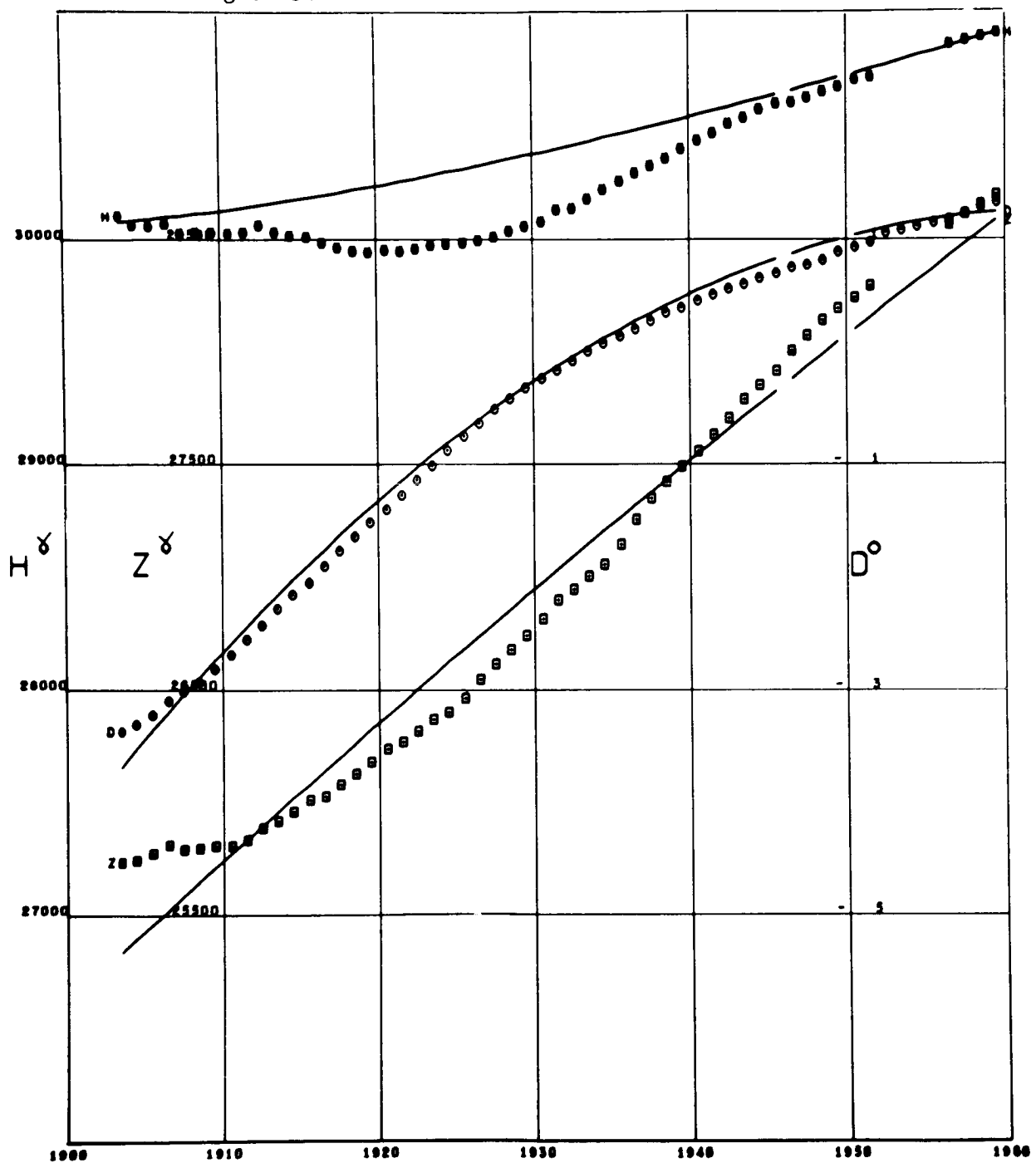
HEARD ISLAND  
Lat -53.03 Long 73.36



HEL  
Lat 54.60 Long 18.81

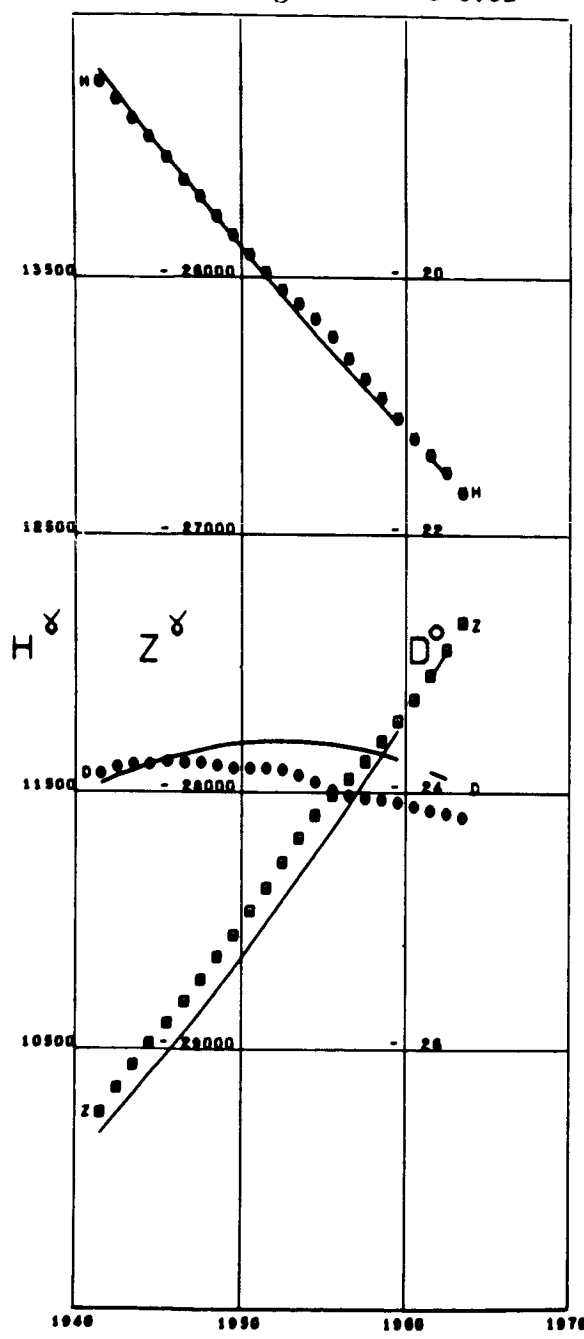


HELWAN  
Lat 29.85 Long 31.34



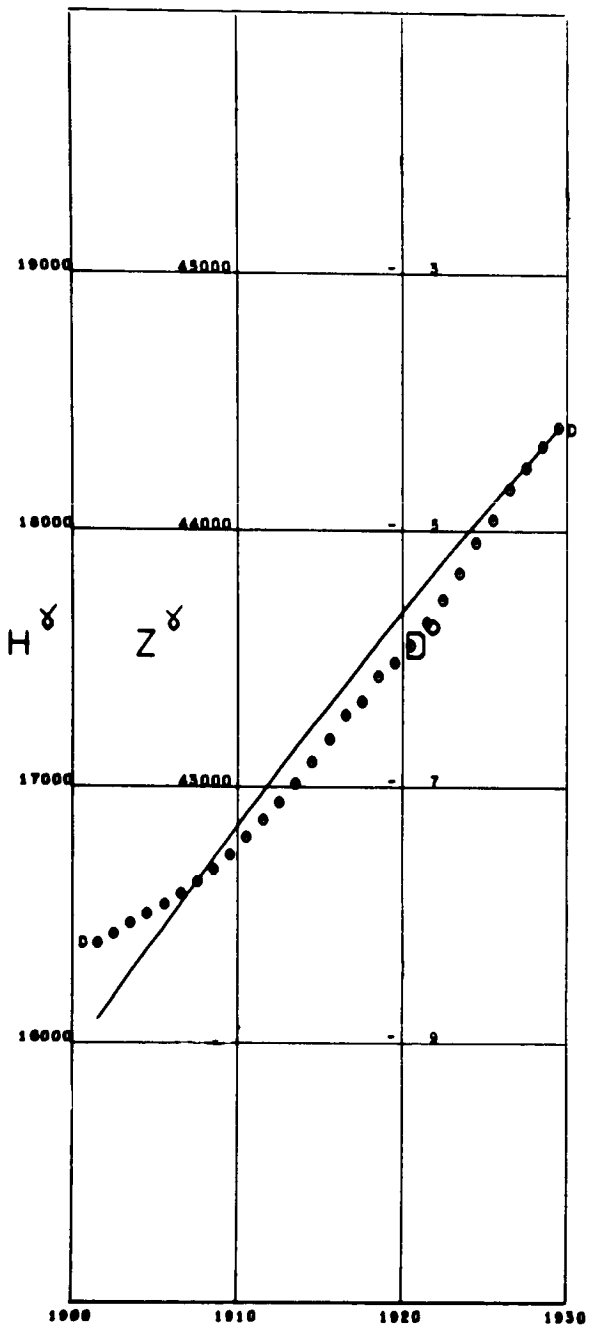
HERMANUS

Lat -34.42 Long 19.22 Alt 0.02

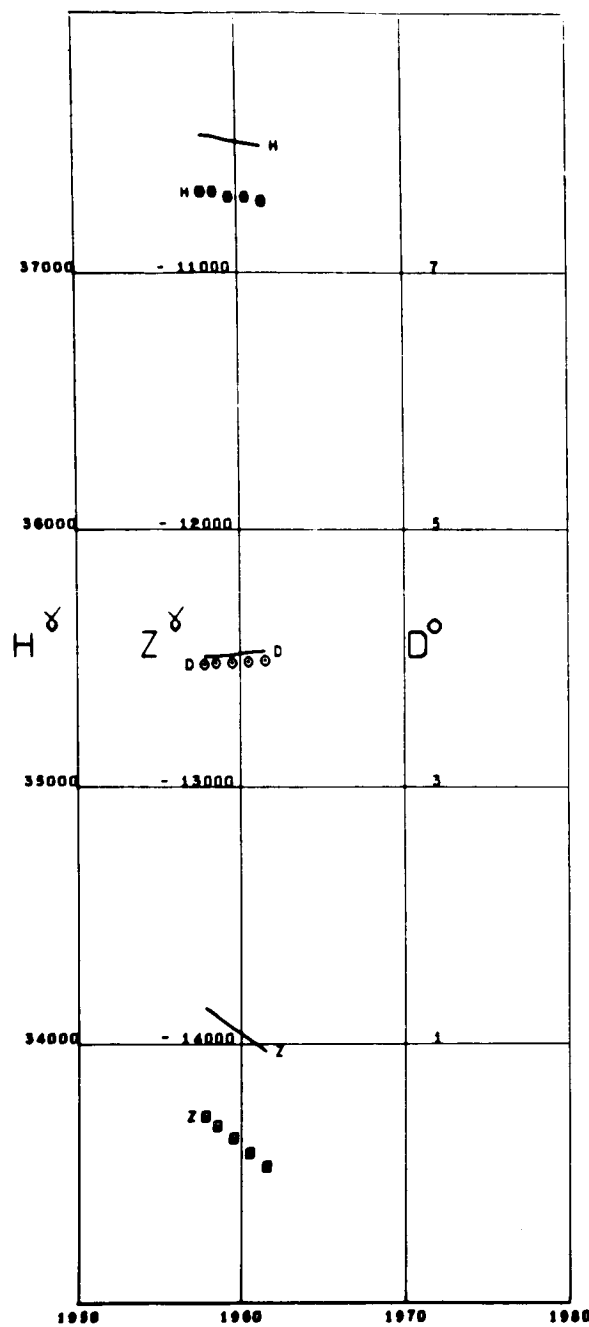


HERMSDORF

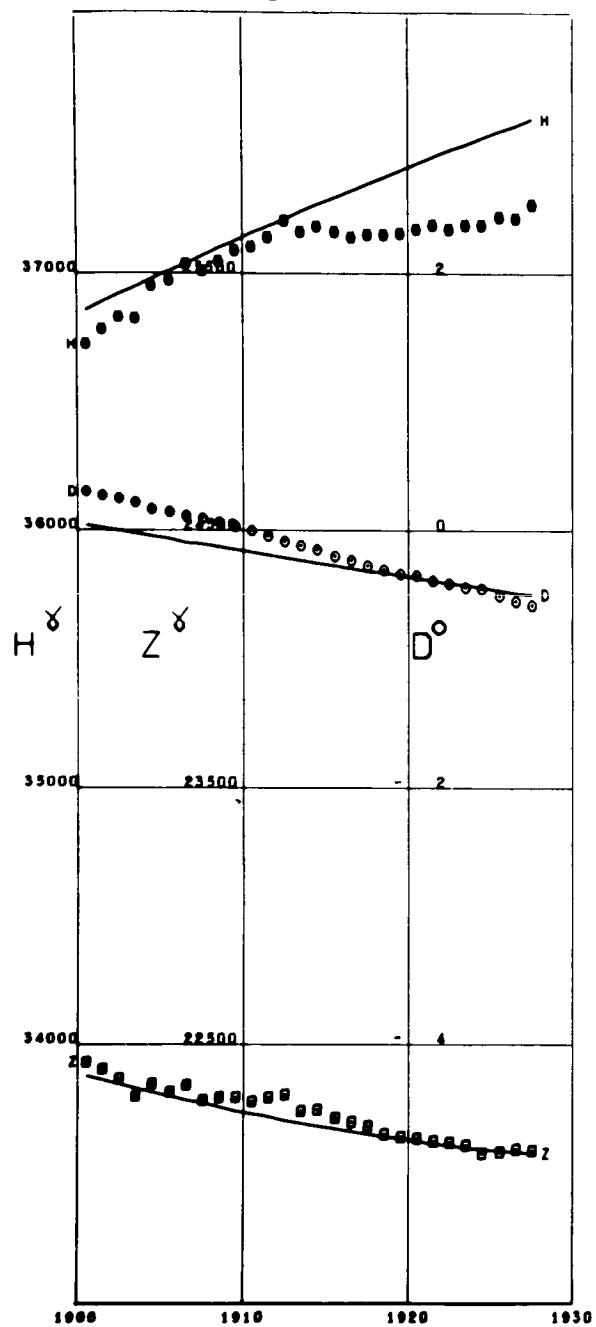
Lat 50.76 Long 16.23



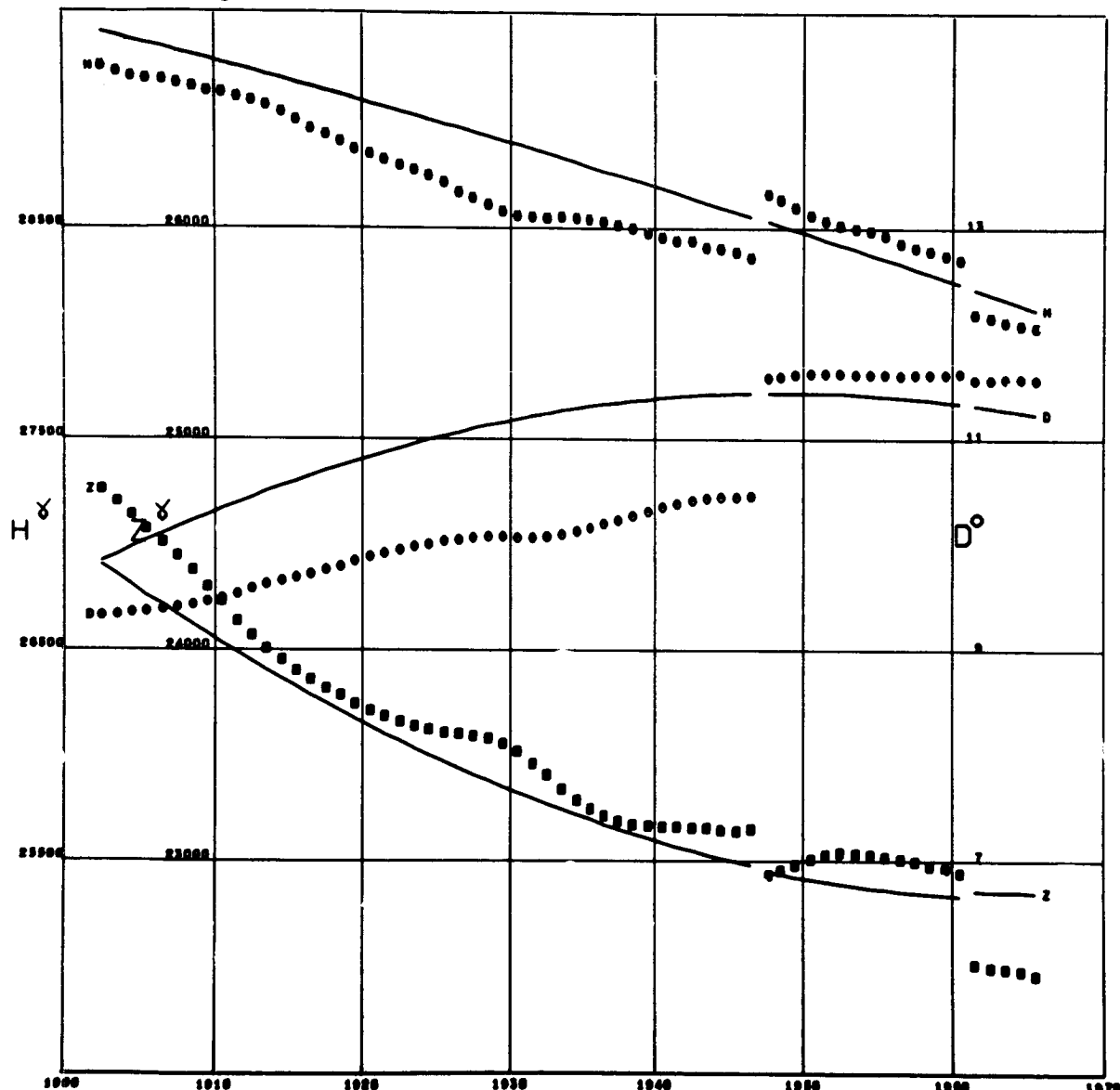
HOLLANDIA  
Lat -2.57 Long 140.51



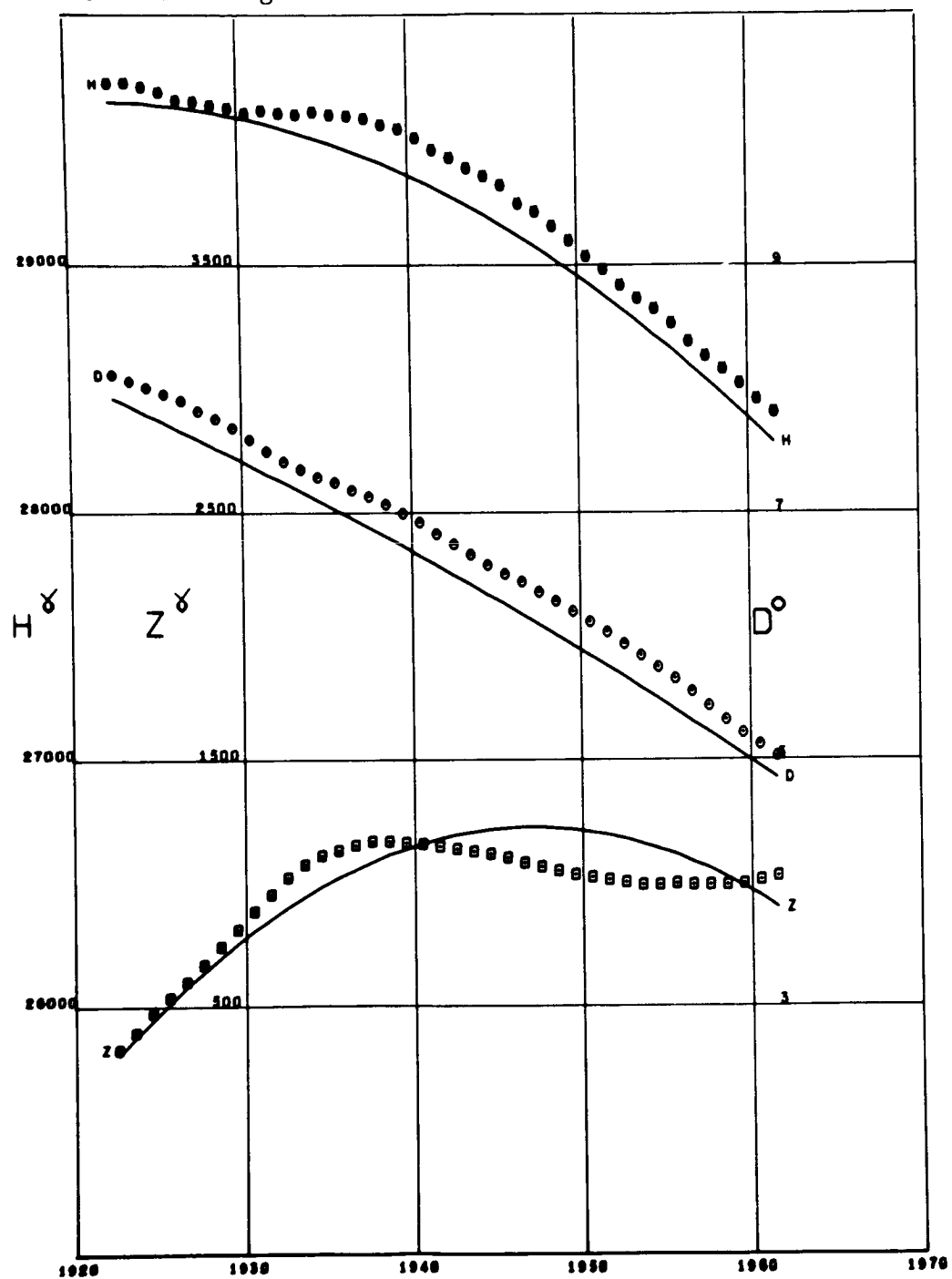
HONGKONG  
Lat 22.30 Long 114.17



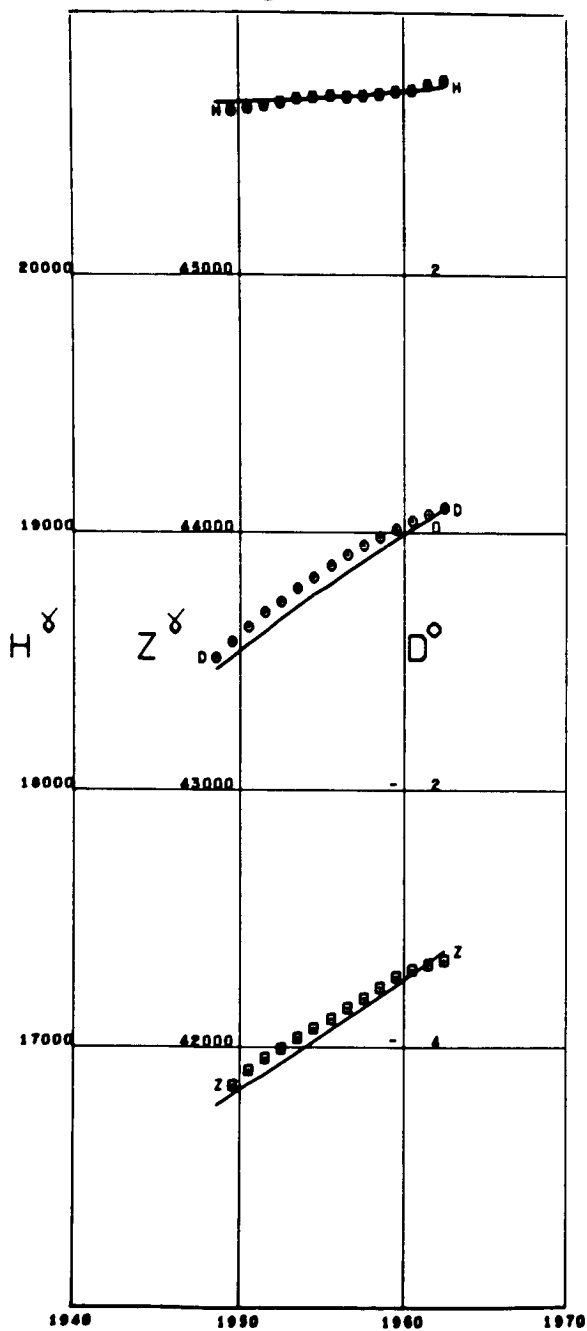
HONOLULU  
Lat 21.32 Long -158.00



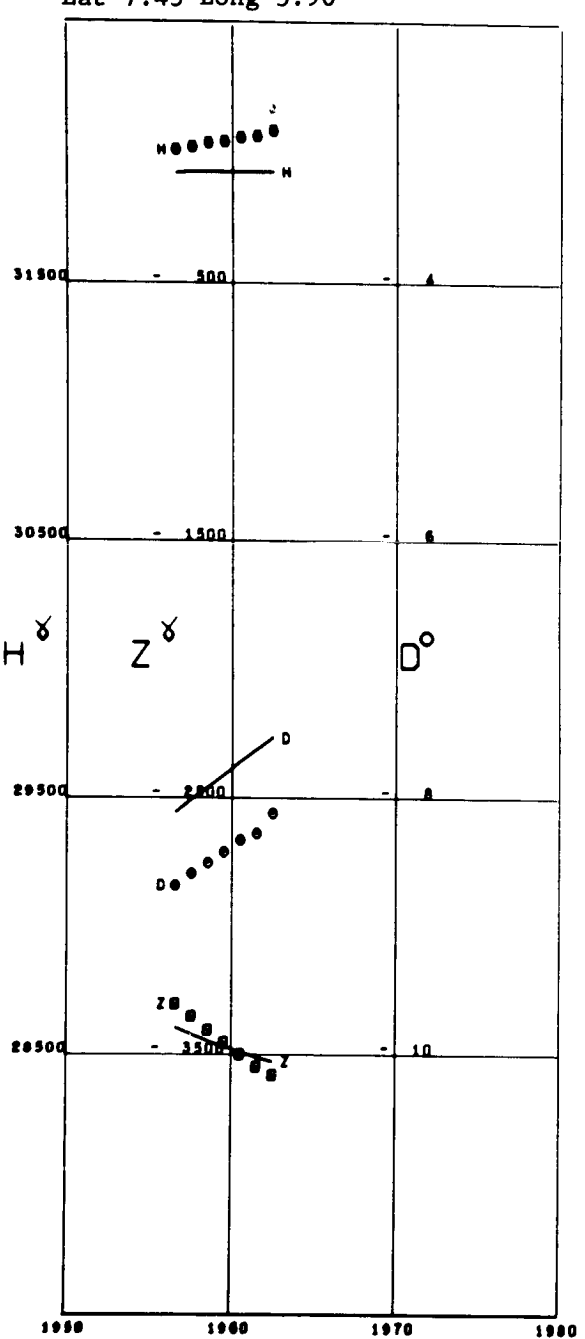
HUANCAYO  
Lat -12.04 Long -75.34 Alt 3.35



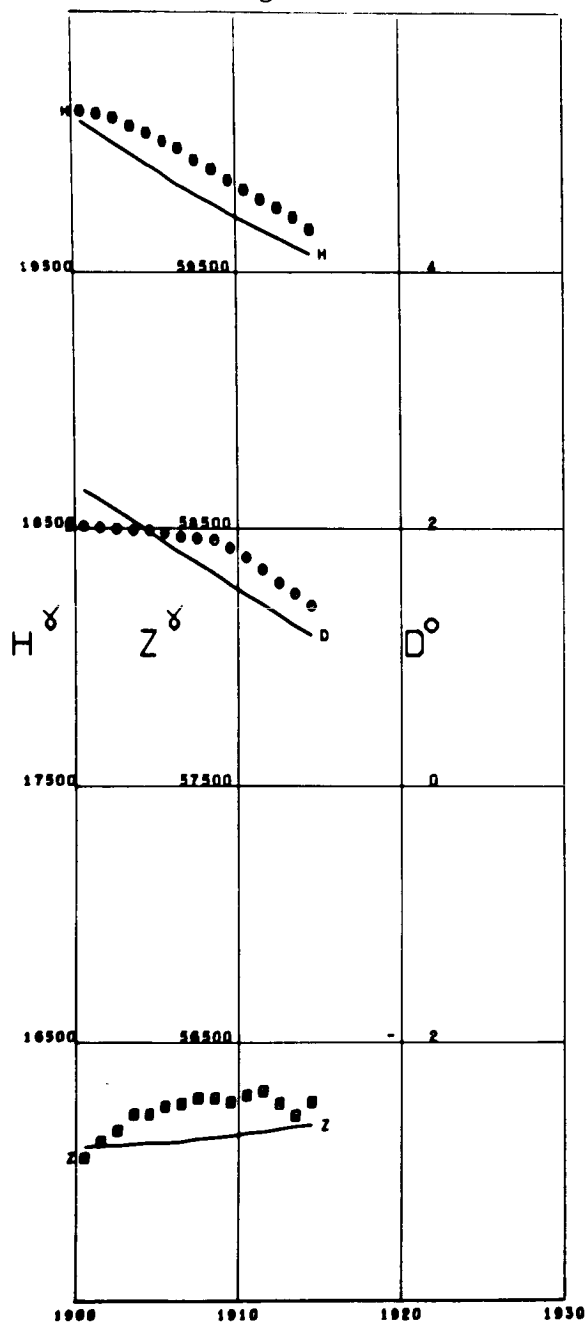
HURBANOVO  
Lat 47.87 Long 18.19



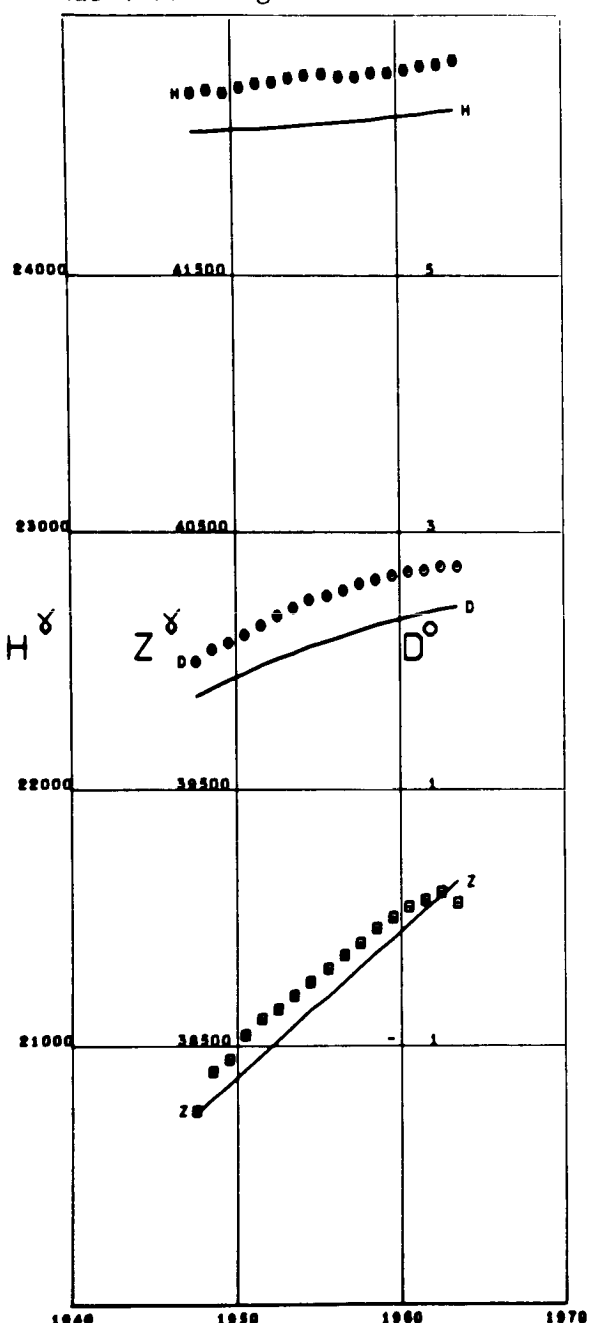
IBADAN  
Lat 7.43 Long 3.90

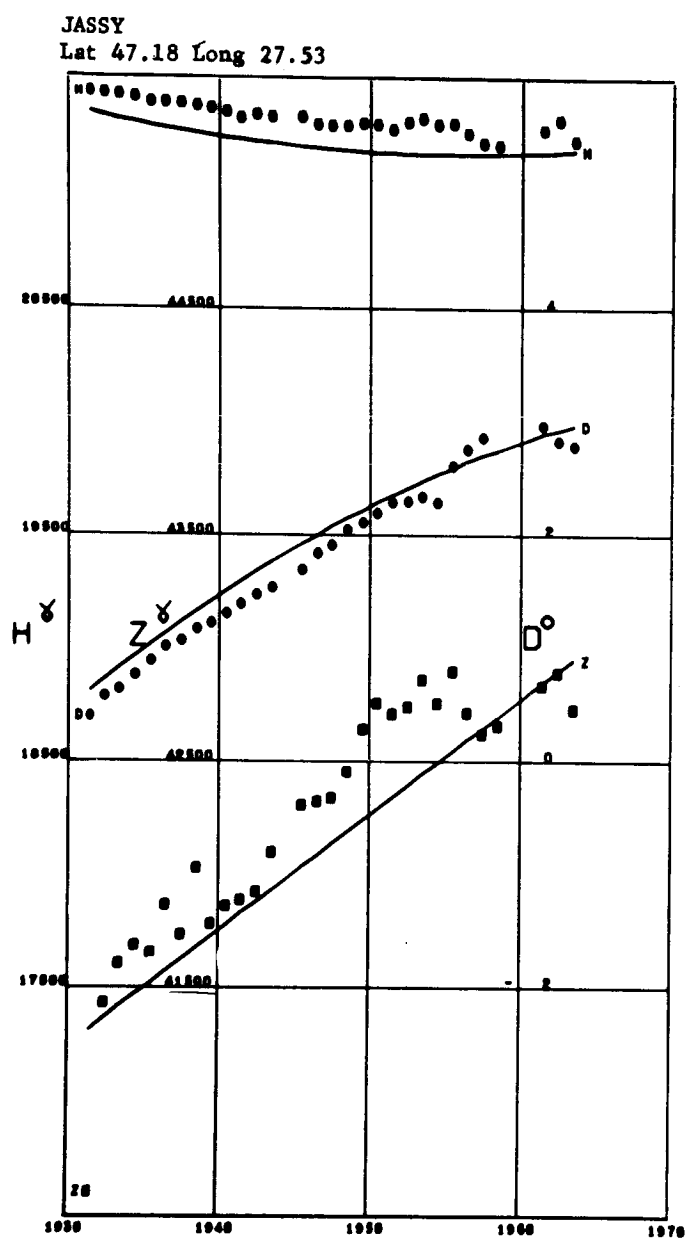
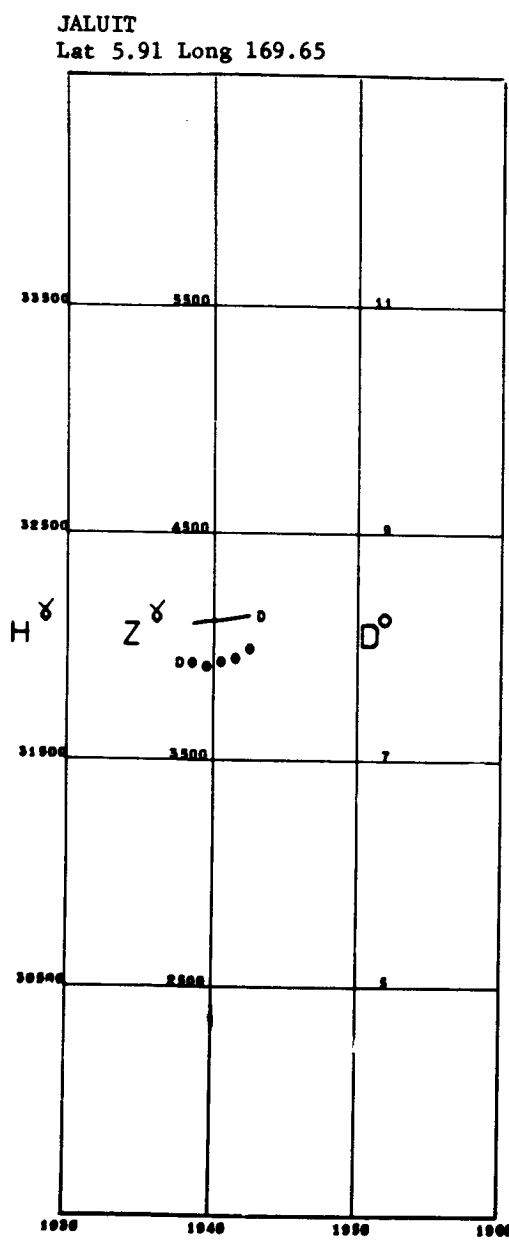


IRKUTSK  
Lat 52.26 Long 104.26



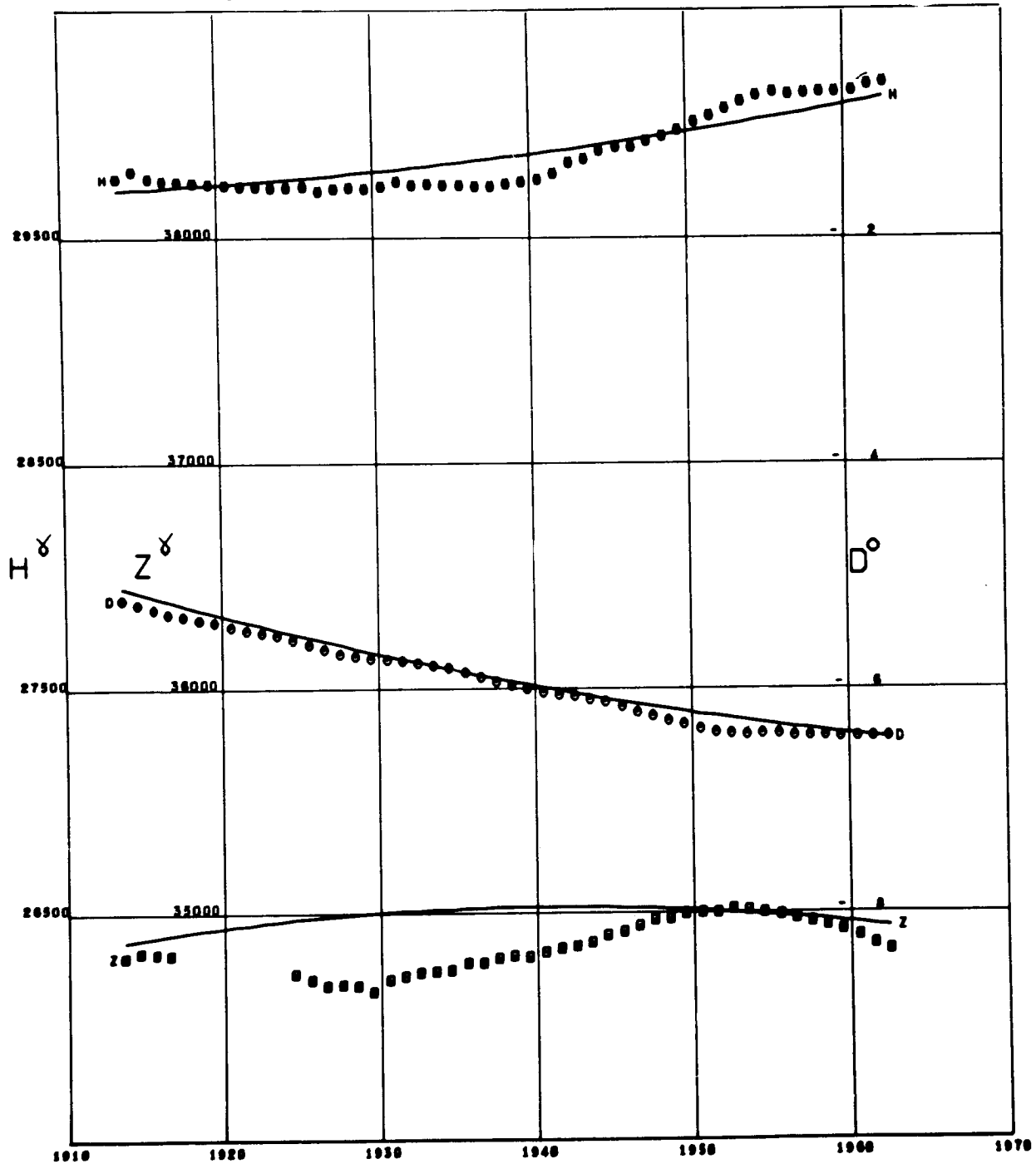
ISTANBUL KANDILLI  
Lat 41.06 Long 29.06



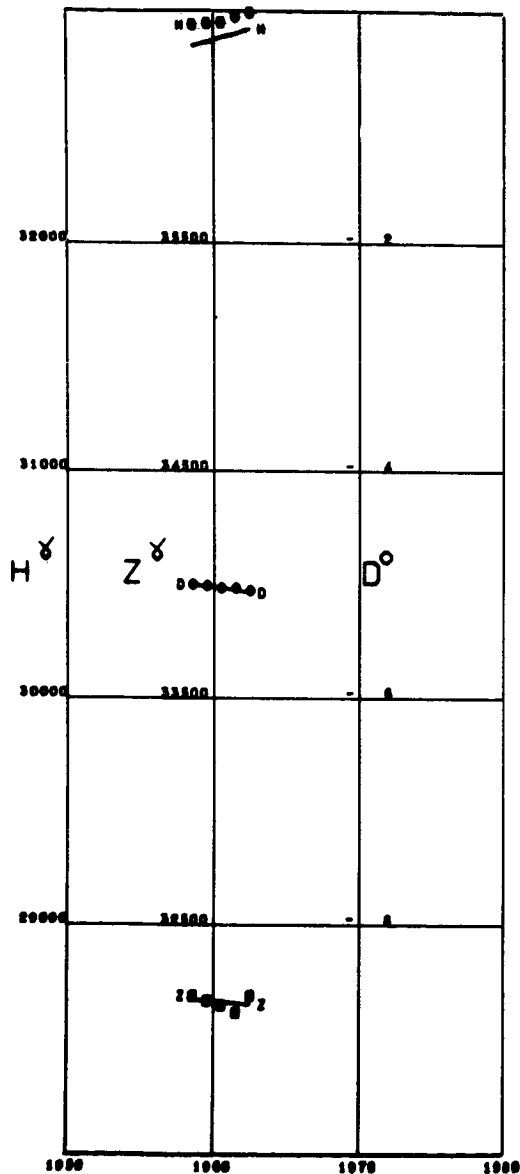


KAKIOKA

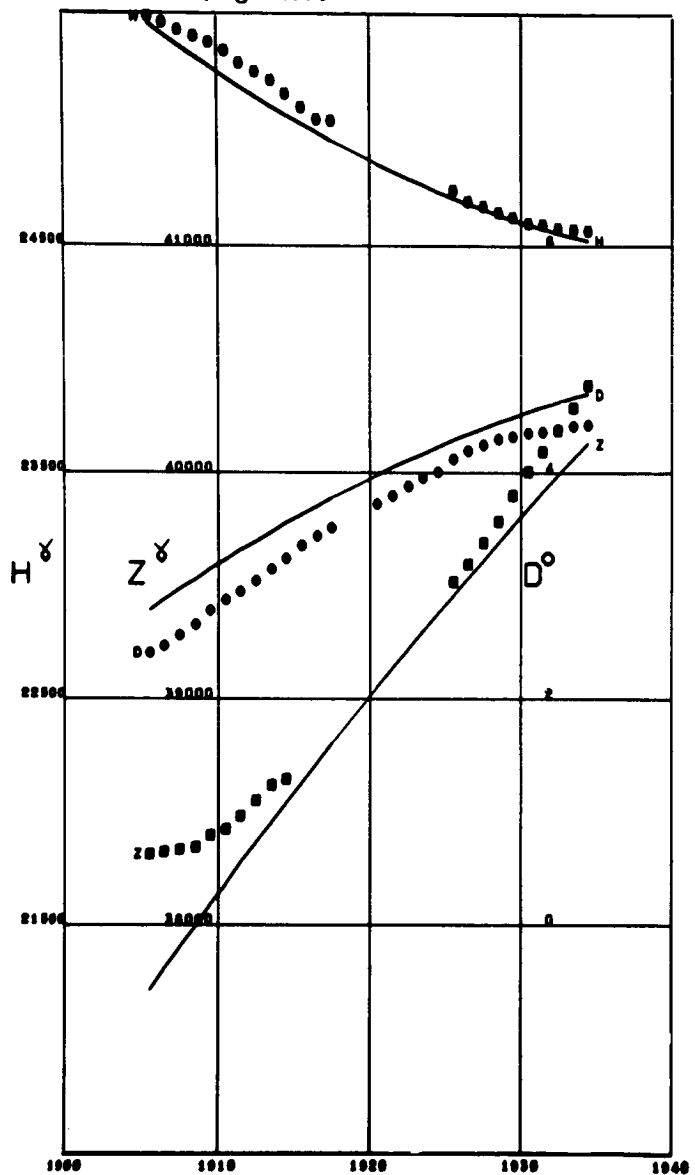
Lat 36.23 Long 140.19 Alt 0.03



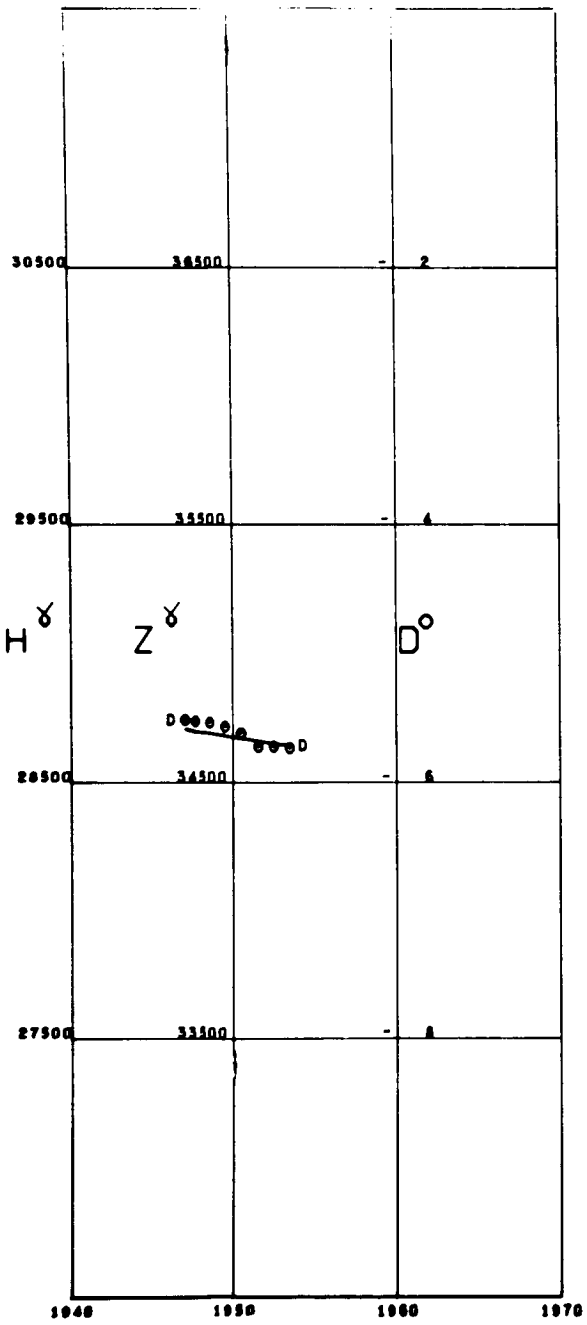
KANOYA  
Lat 31.42 Long 130.88



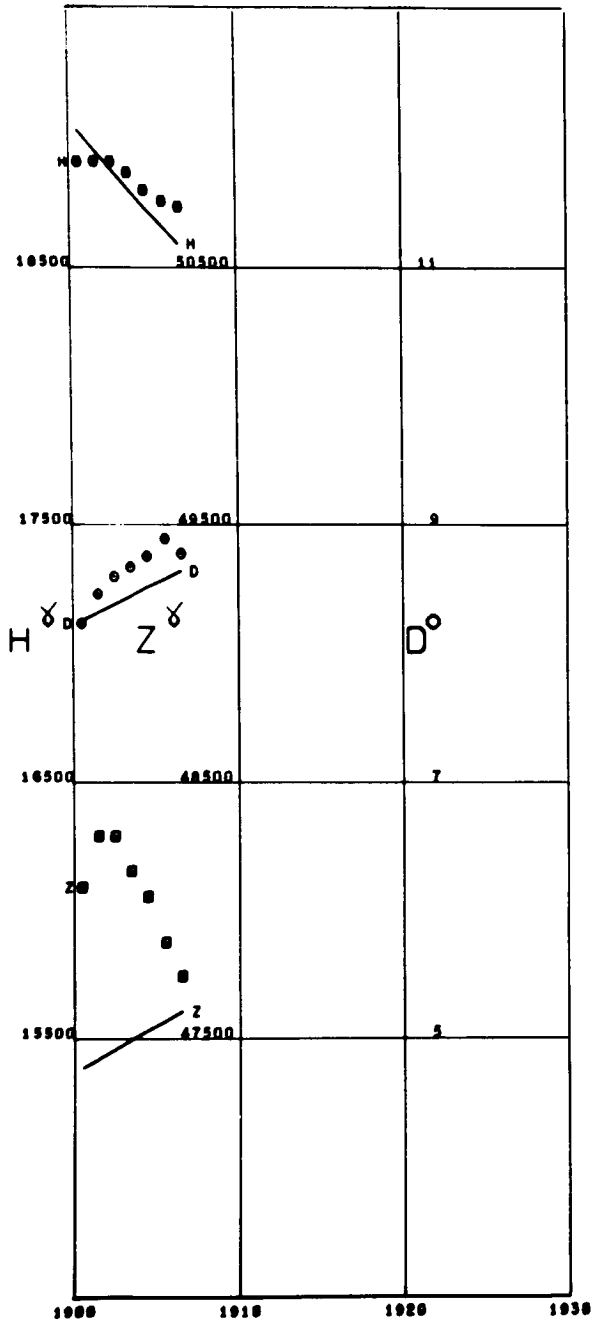
KARSANI  
Lat 41.83 Long 44.70



KATUURA  
Lat 33.63 Long 135.94

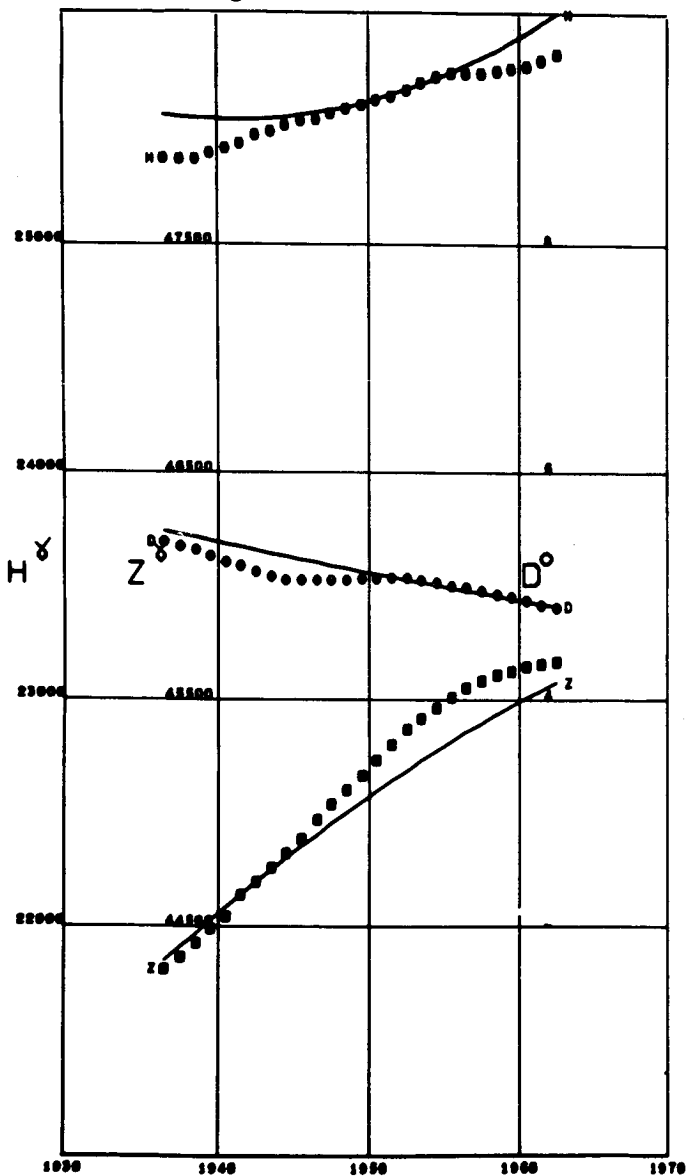


KAZAN  
Lat 55.78 Long 49.13

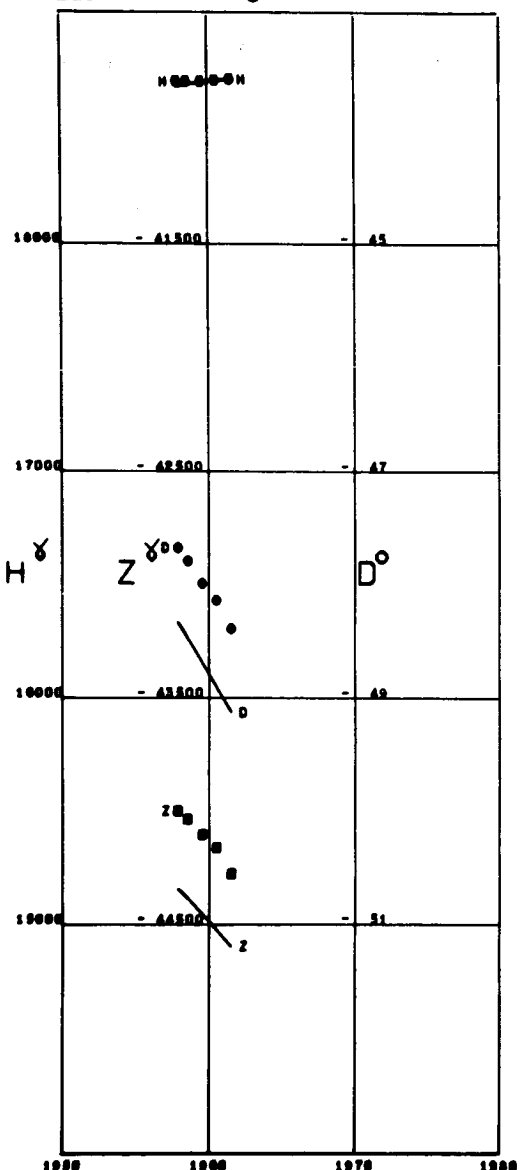


**KELES**

Lat 41.42 Long 69.20

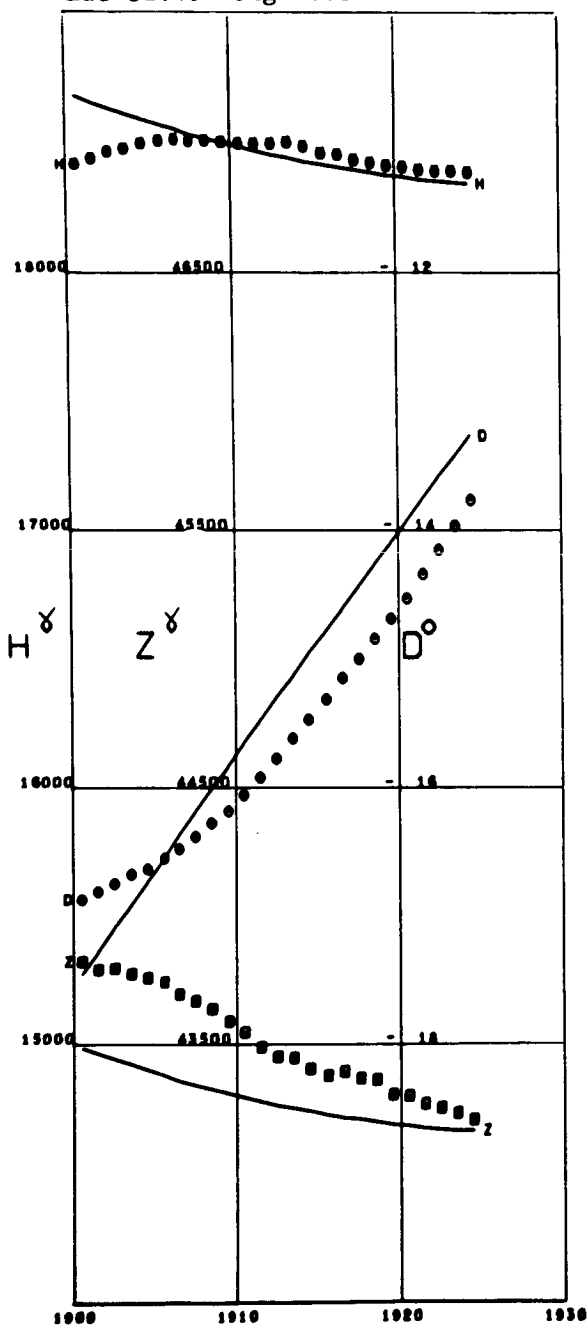
**KERGUELEN**

Lat -49.35 Long 70.20



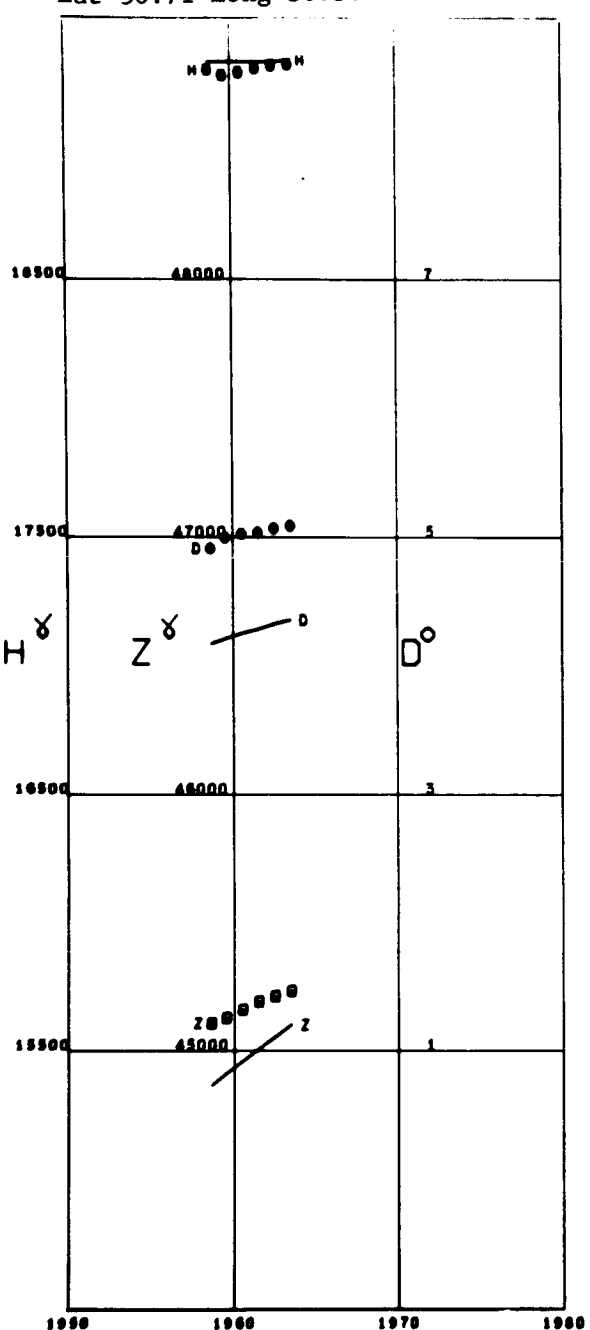
KEW

Lat 51.46 Long -0.31

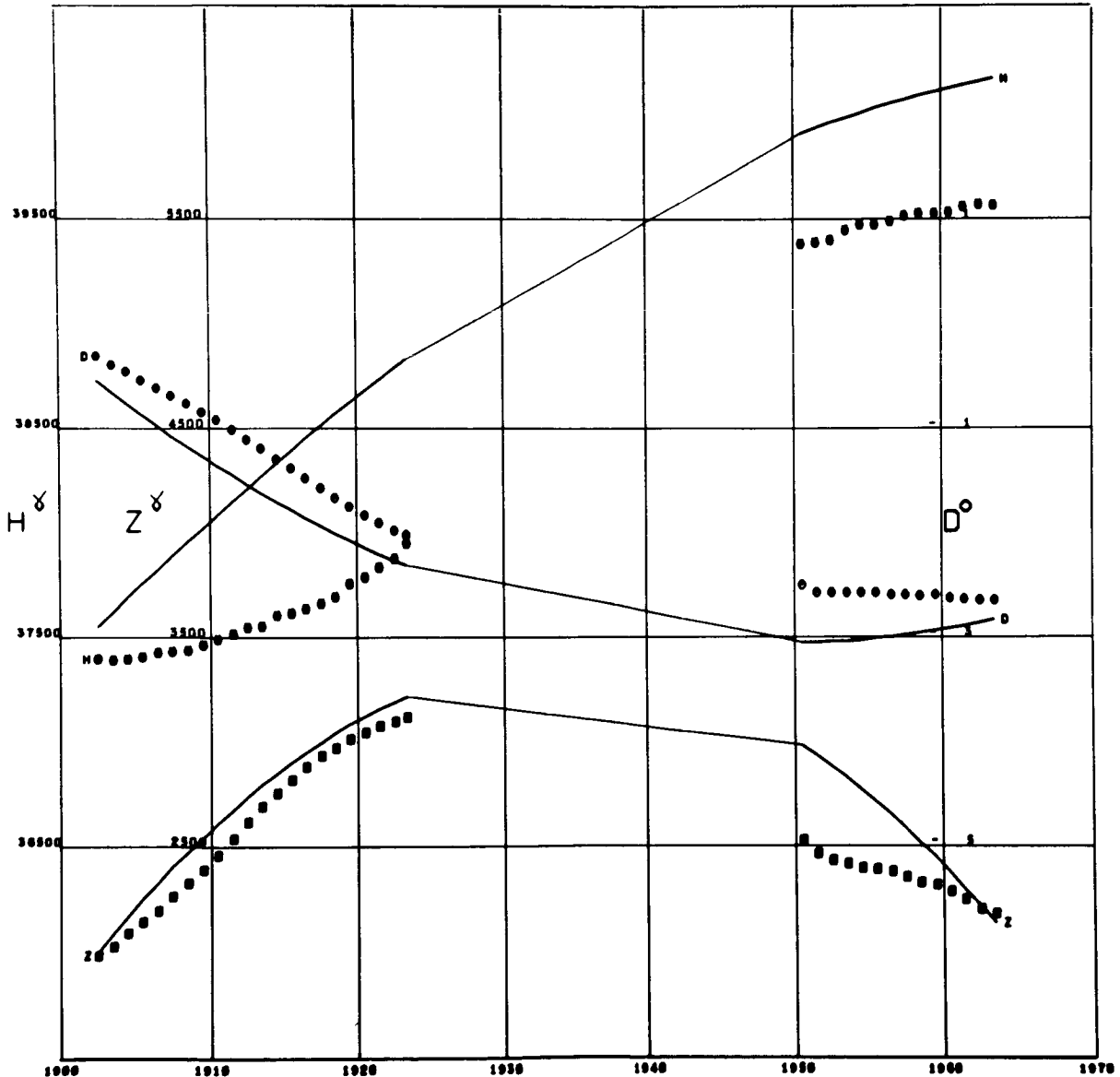


KIEV

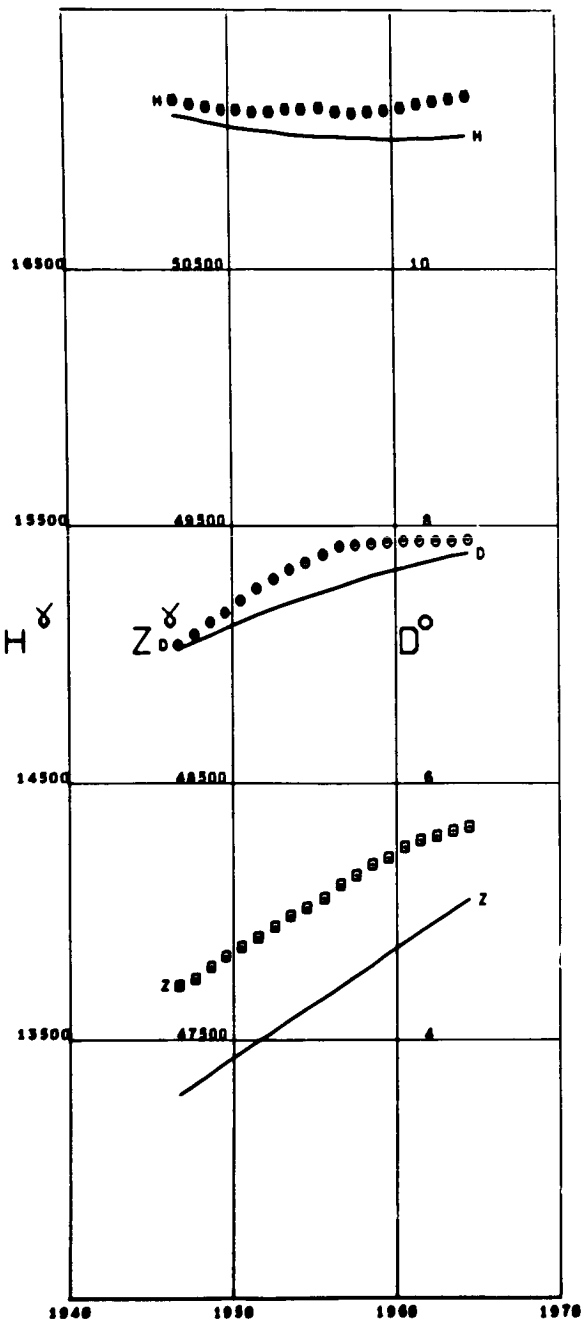
Lat 50.71 Long 30.30



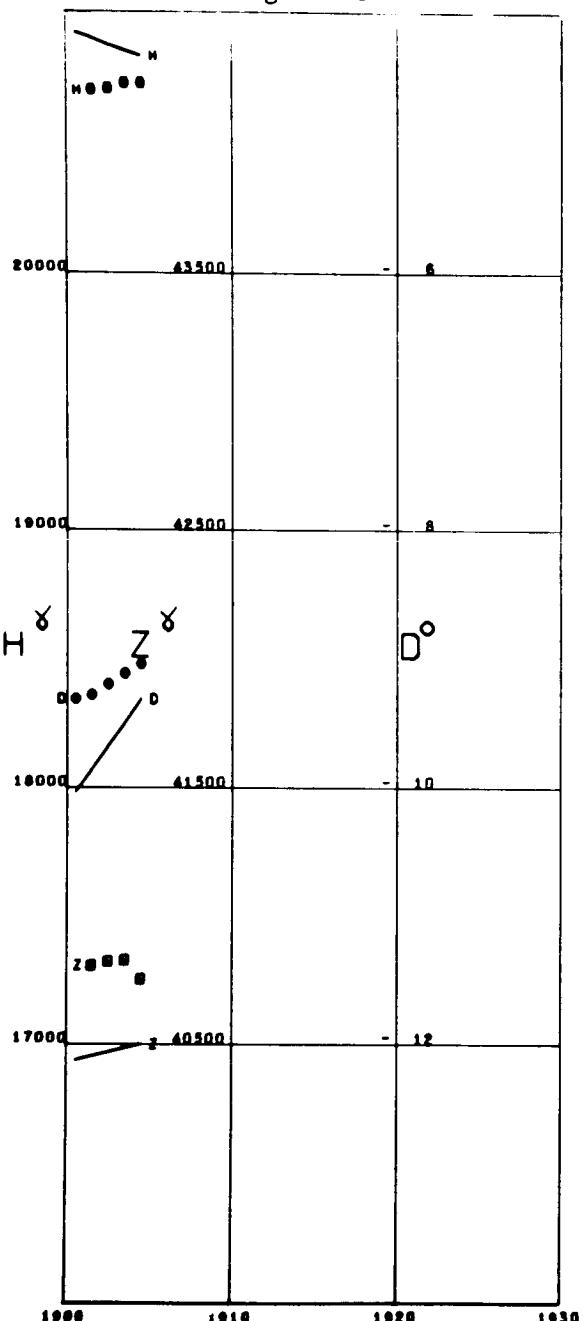
KODAIKANAL  
Lat 10.23 Long 77.46



KRASNAYA PAKHRA  
Lat 55.47 Long 37.31

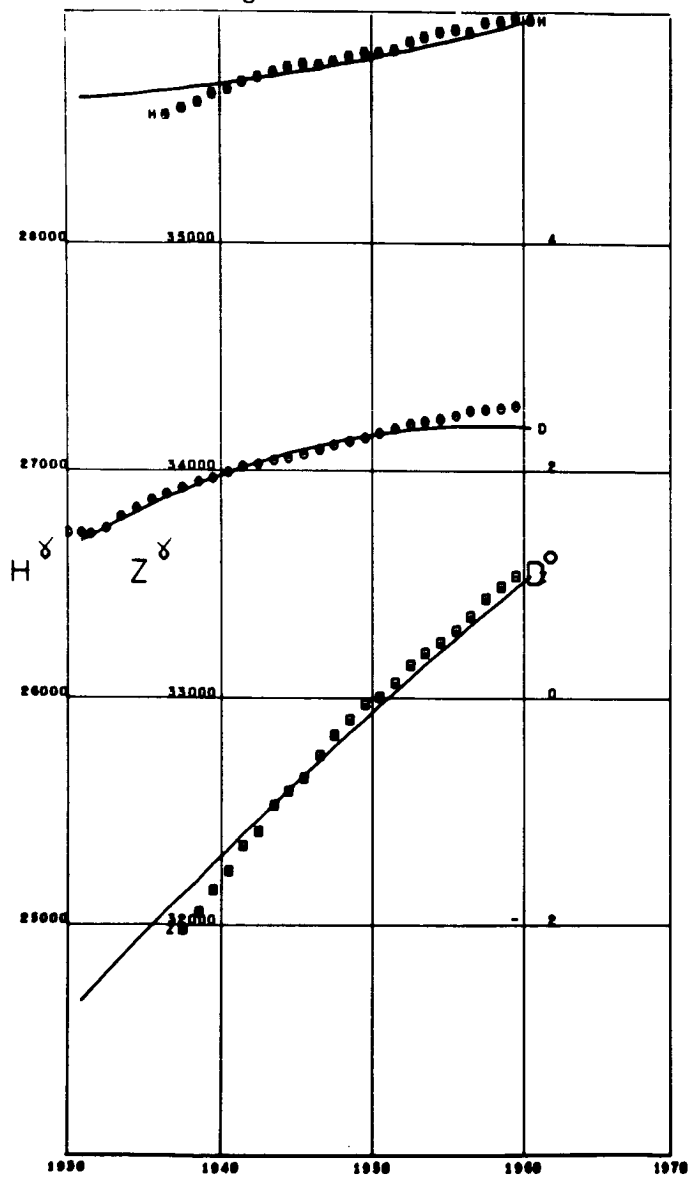


KREMSMUNSTER  
Lat 48.05 Long 14.13



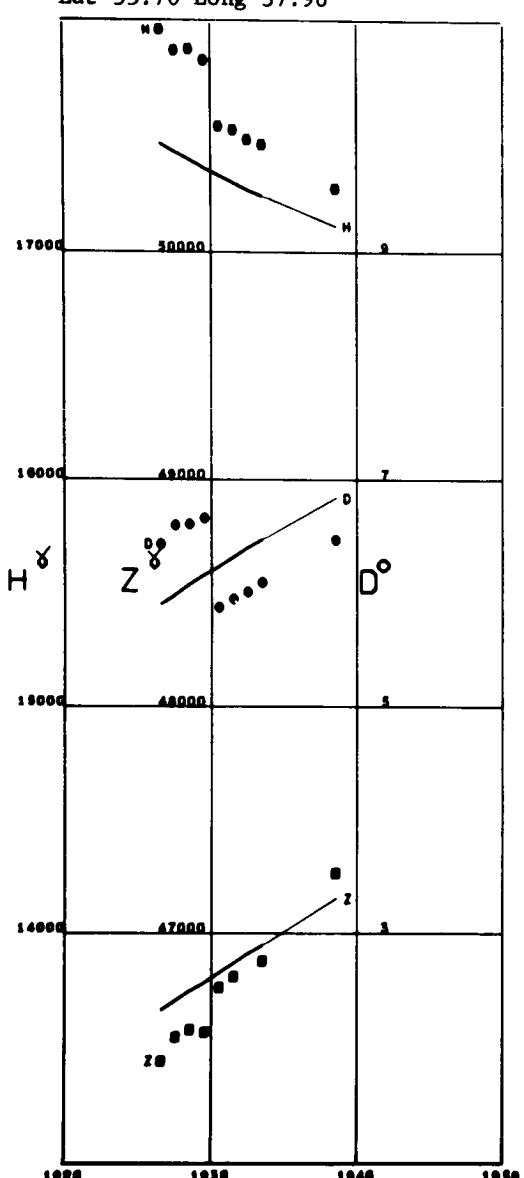
KSARA

Lat 33.82 Long 35.88

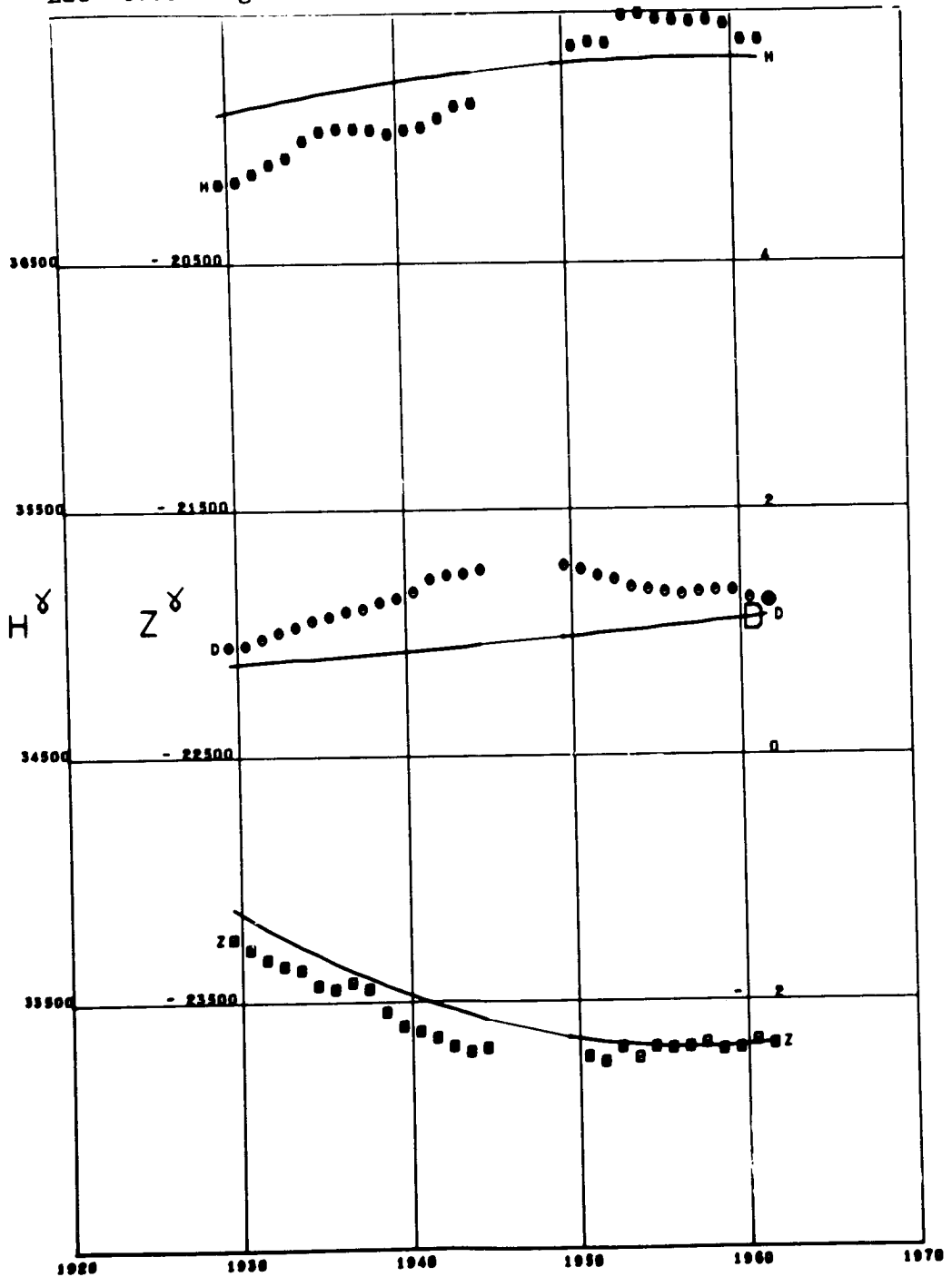


KUTSCHINO

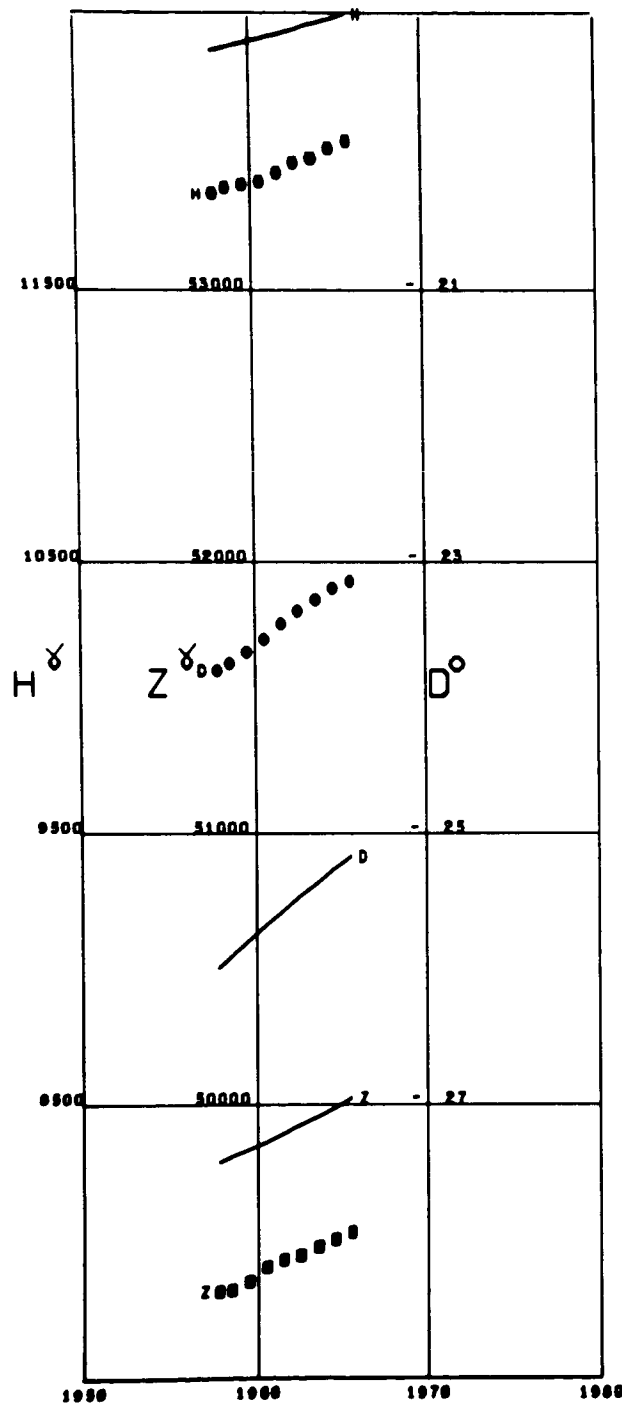
Lat 55.76 Long 37.96



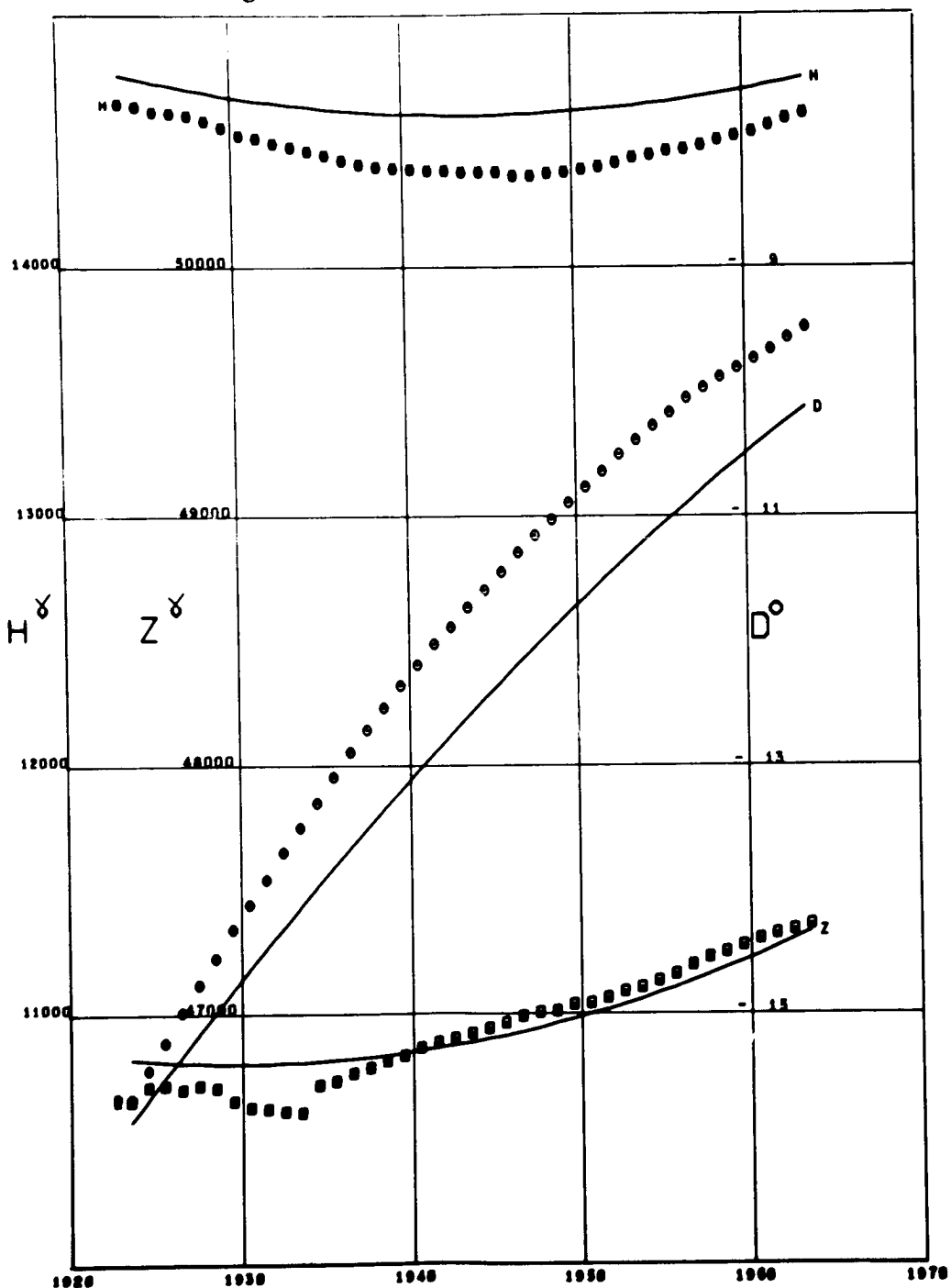
KUYPER  
Lat -6.03 Long 106.73



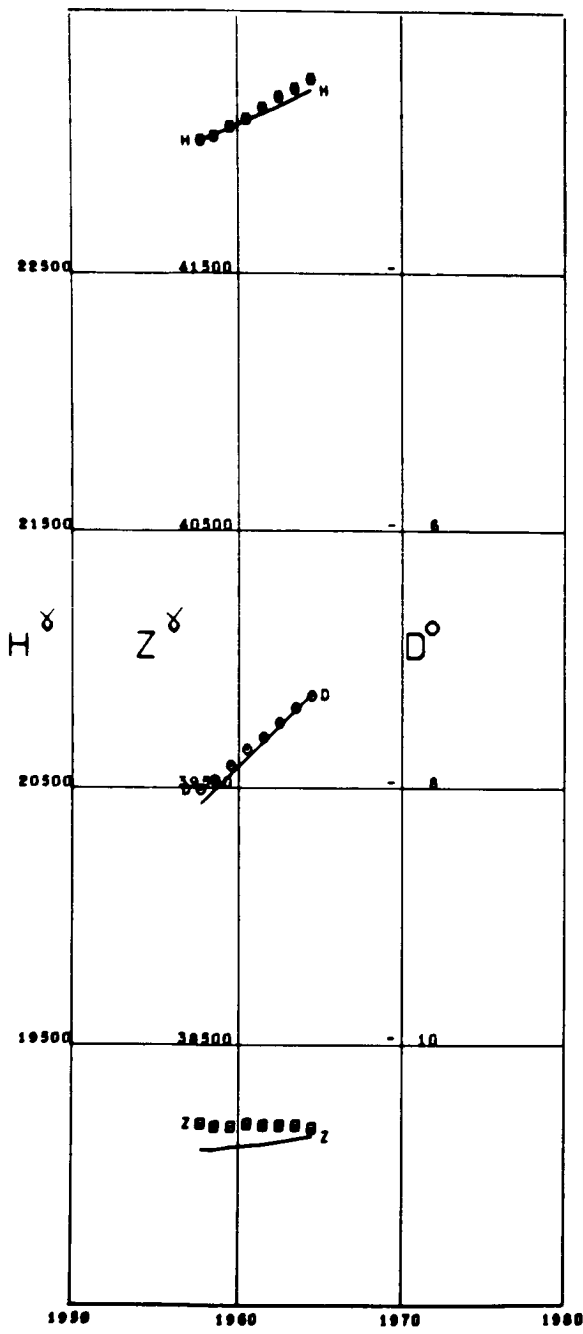
LEIRVOGUR  
Lat 64.18 Long -21.70 Alt 0.01



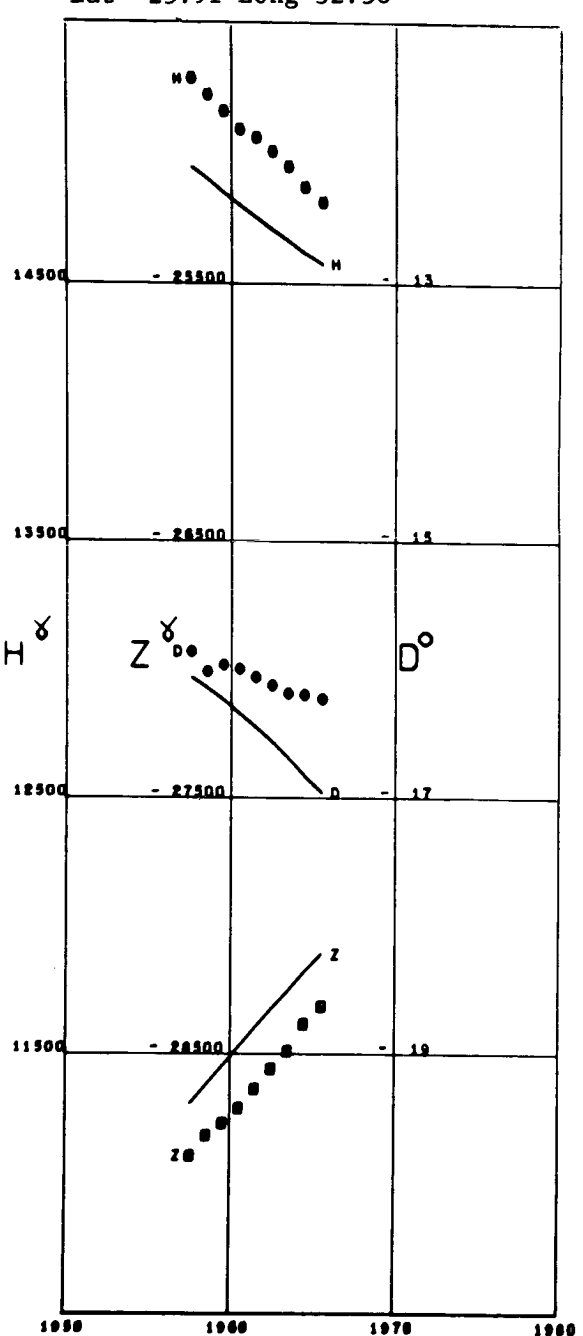
LERWICK  
Lat 60.13 Long -1.18



LOGRONO  
Lat 42.45 Long -2.50

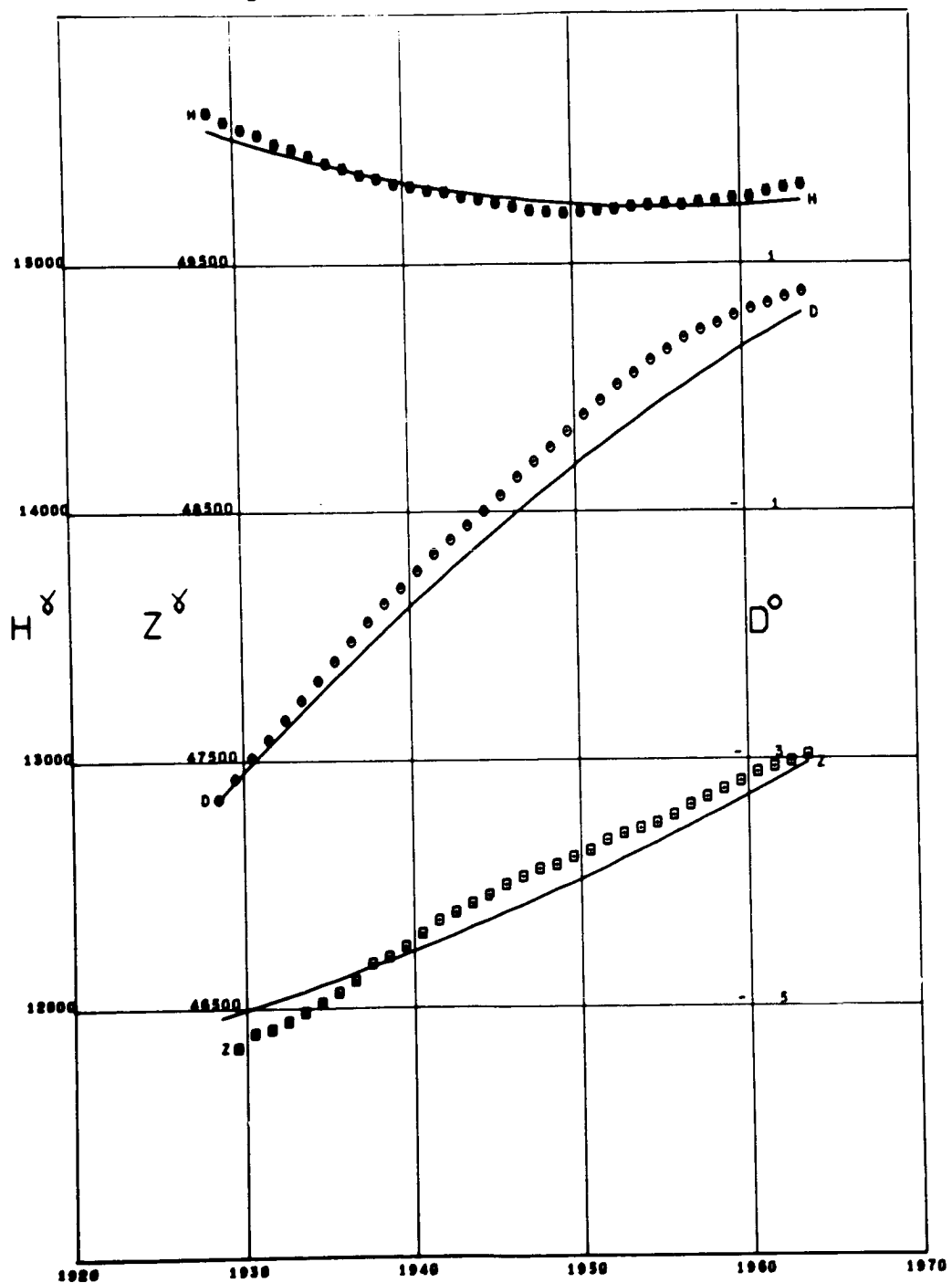


LOURENCO MARQUES  
Lat -25.91 Long 32.58

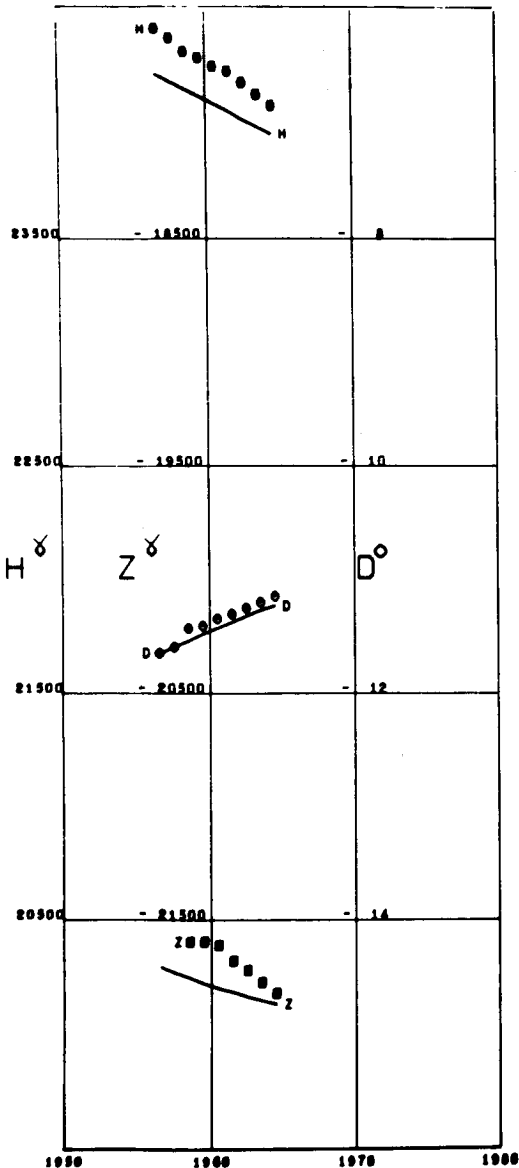


LOWO

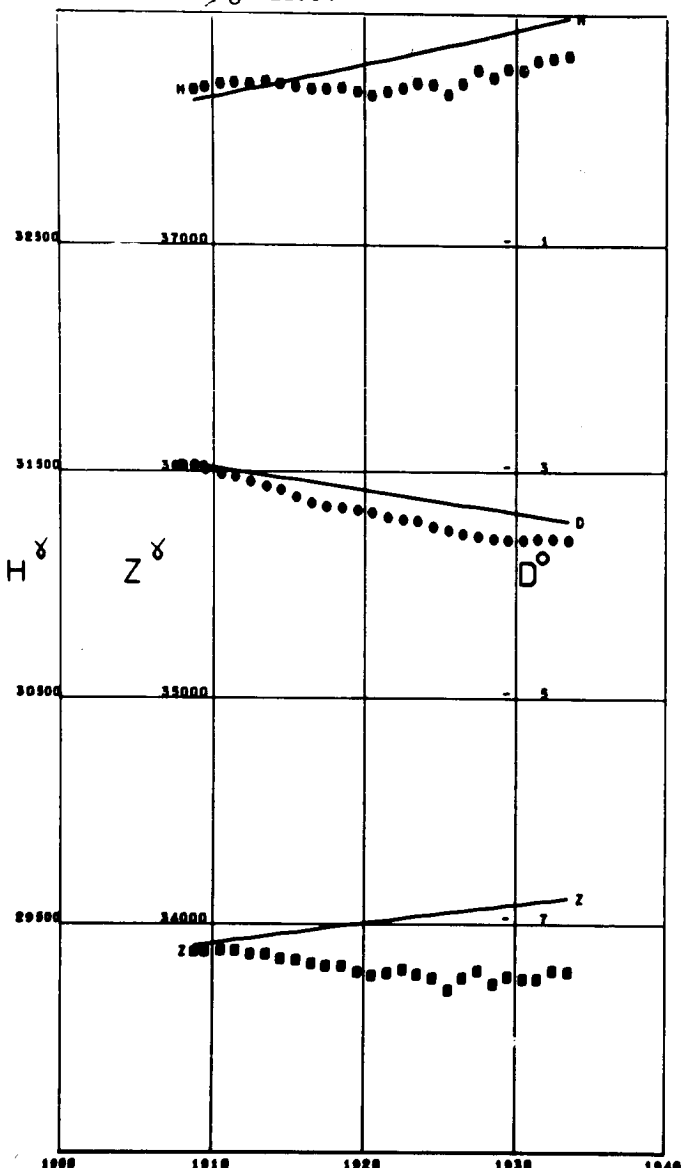
Lat 59.34 Long 17.82 Alt 0.02



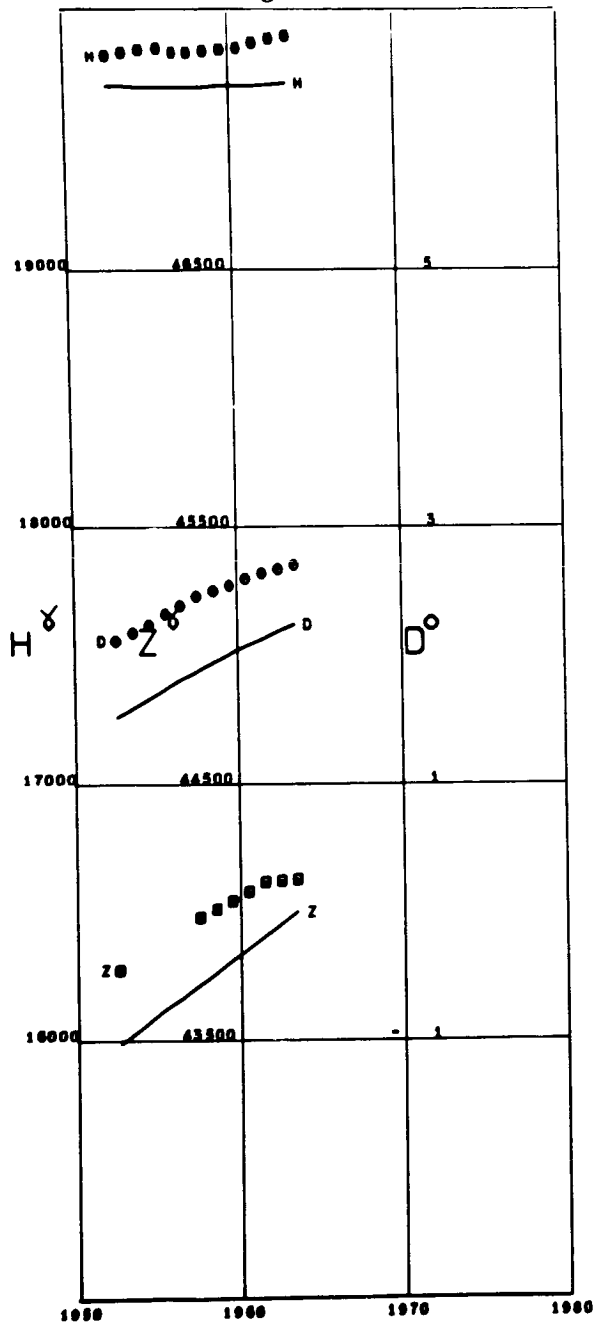
LUANDA BELAS  
Lat -8.91 Long 13.16



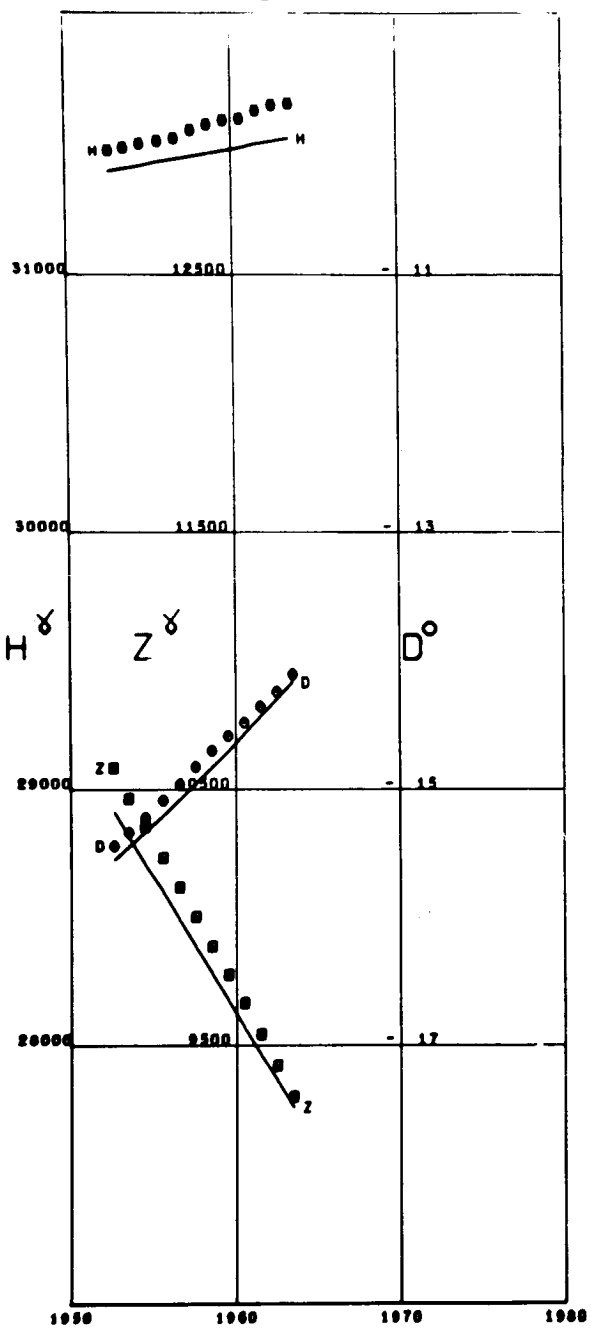
LUKIAPANG  
Lat 31.31 Long 121.04

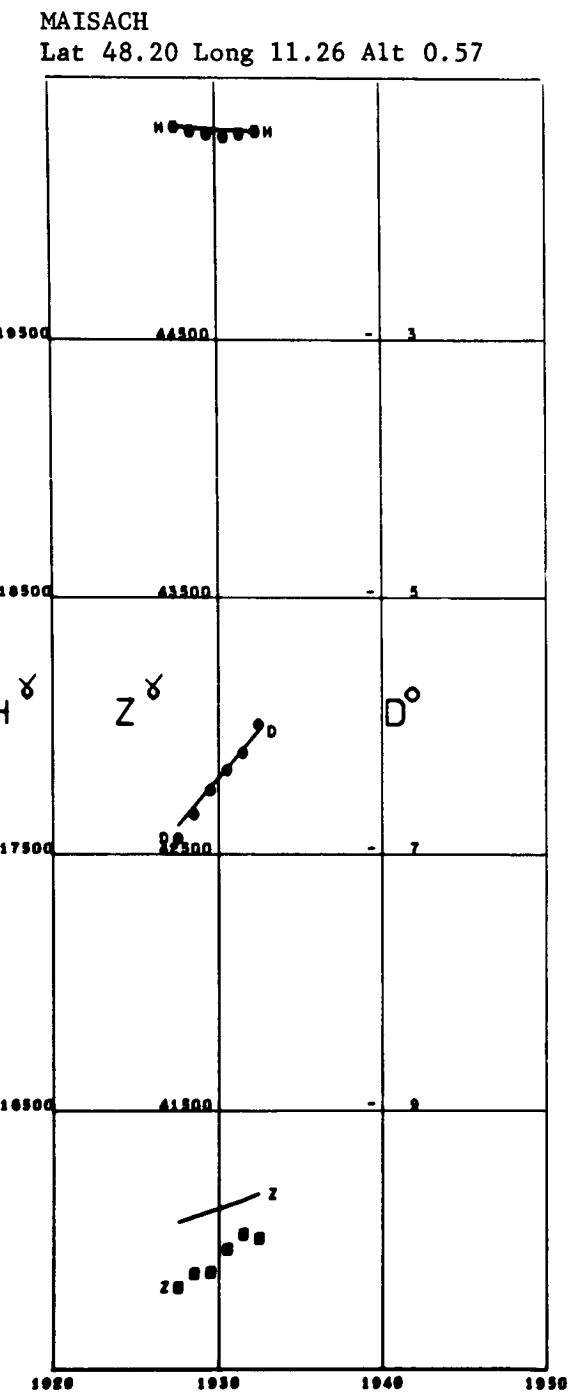
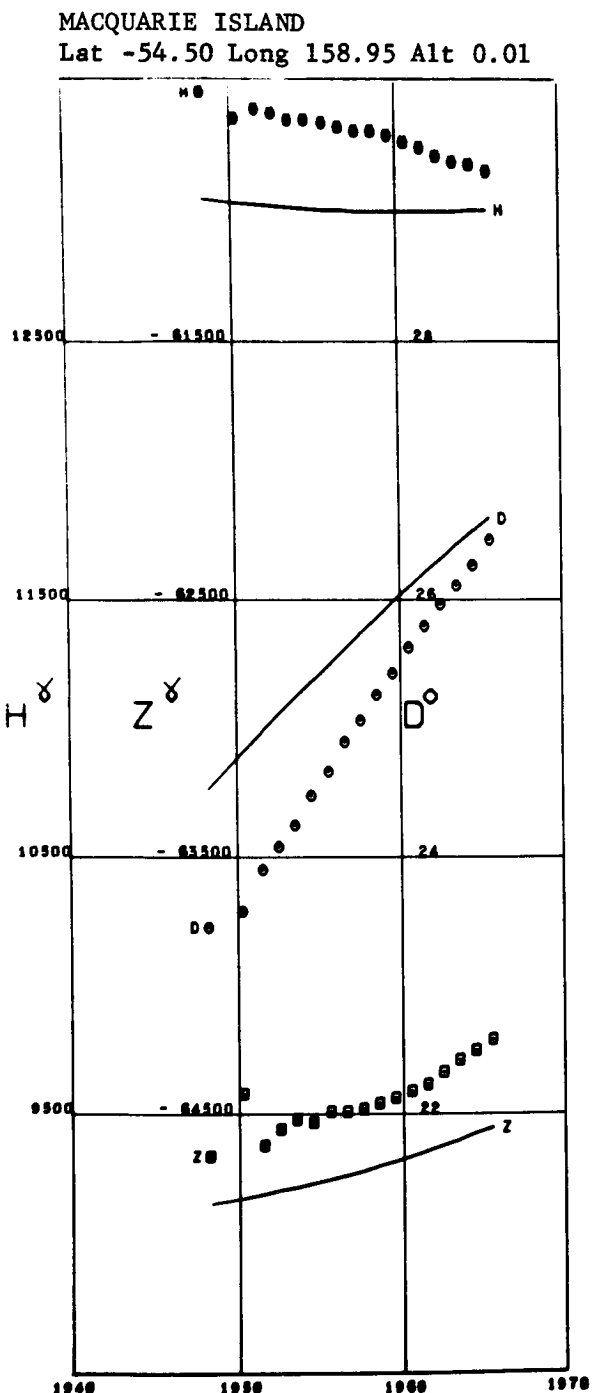


LVOV  
Lat 49.90 Long 23.75

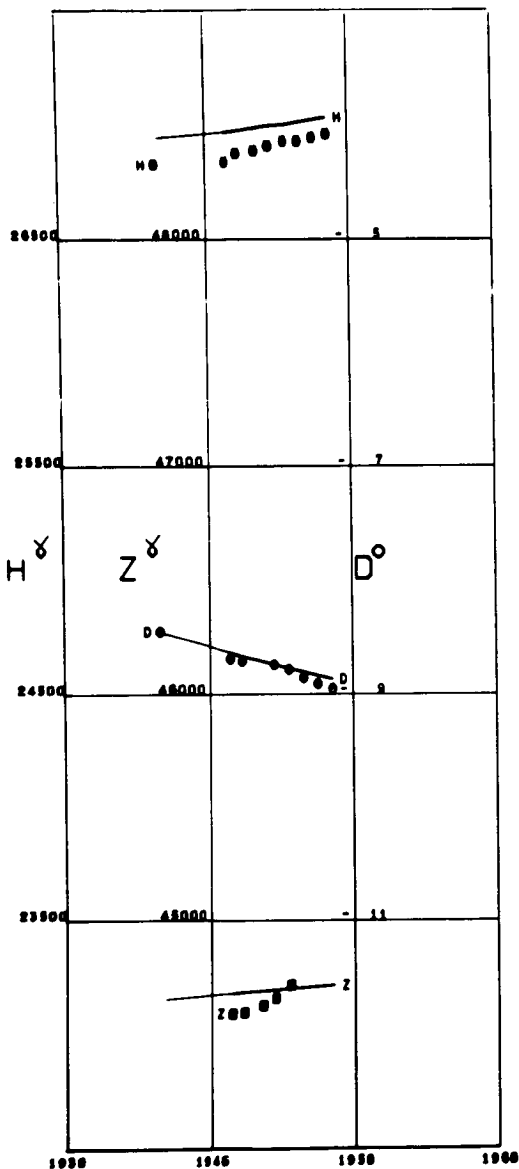


M'BOUR  
Lat 14.39 Long >16.95 Alt 0.01

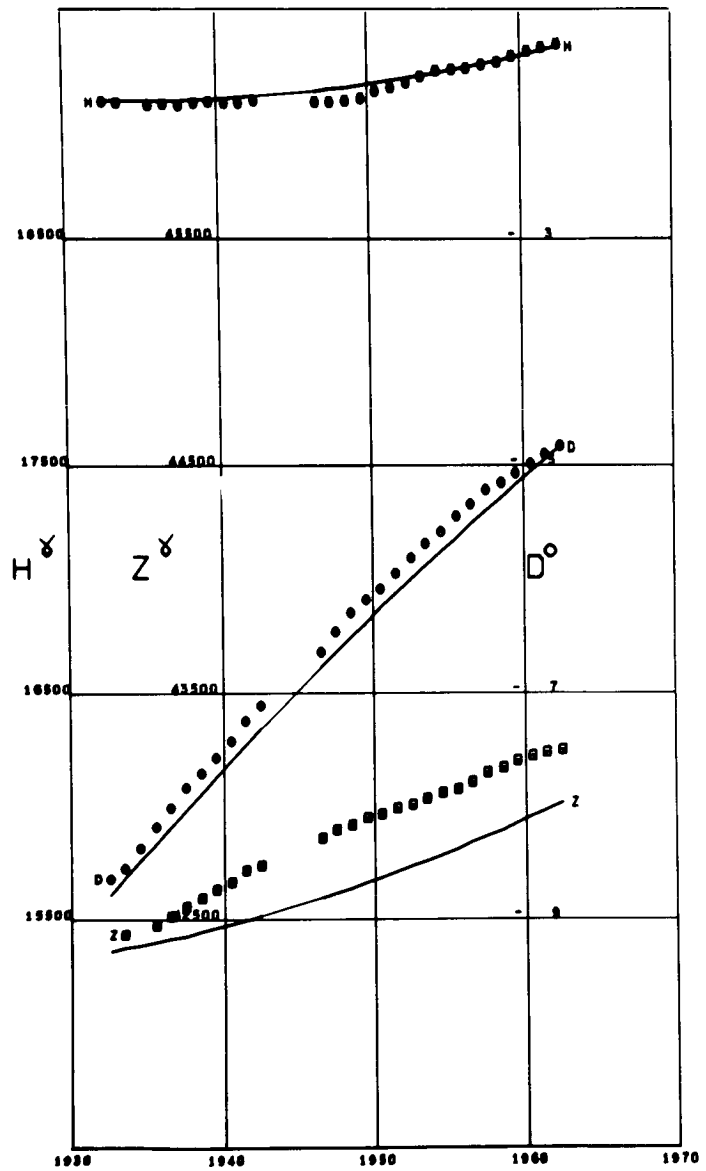




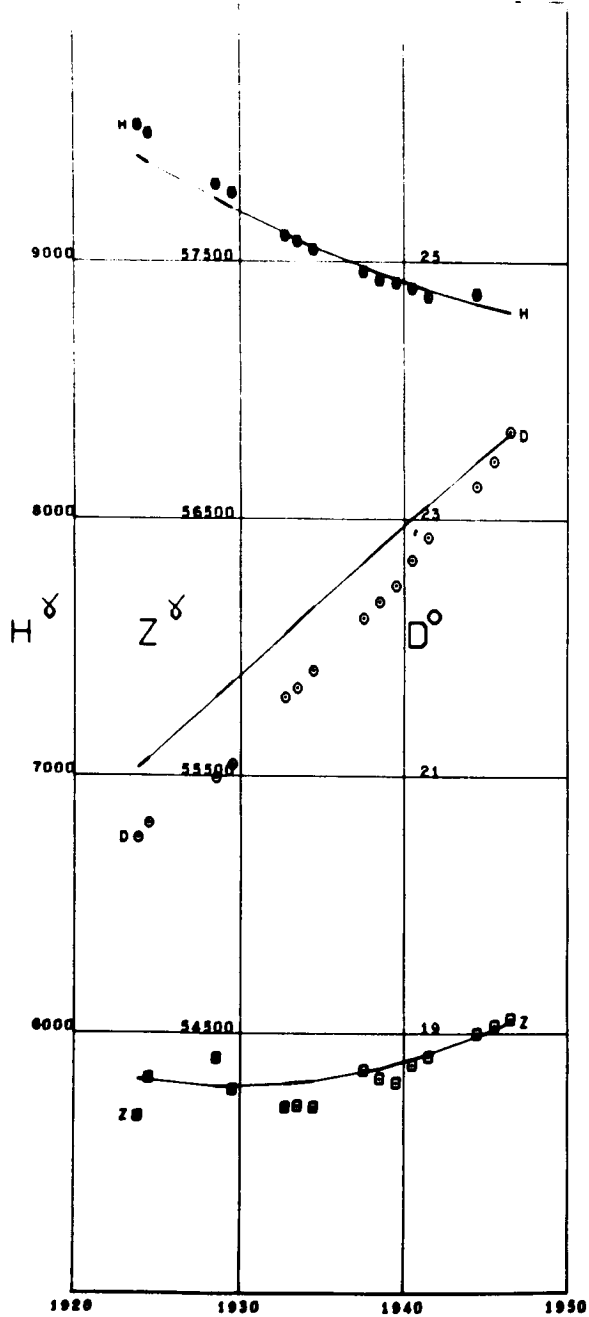
MAITUN  
Lat 43.25 Long 132.33



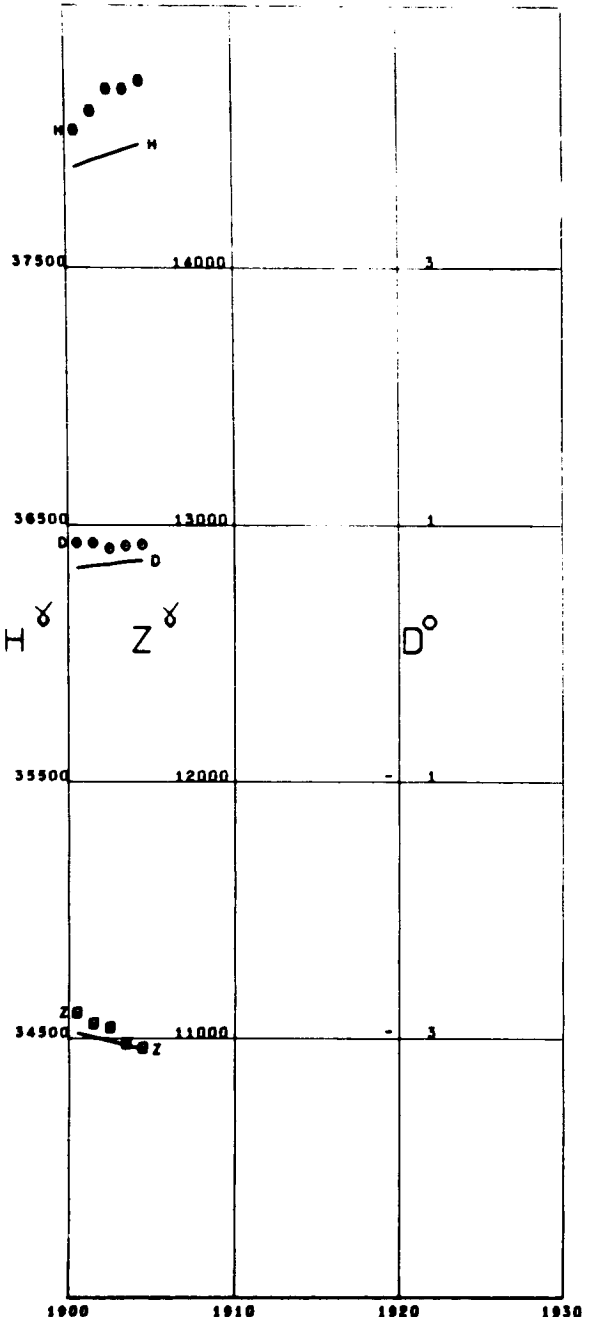
MAHNAY  
Lat 50.29 Long 5.68



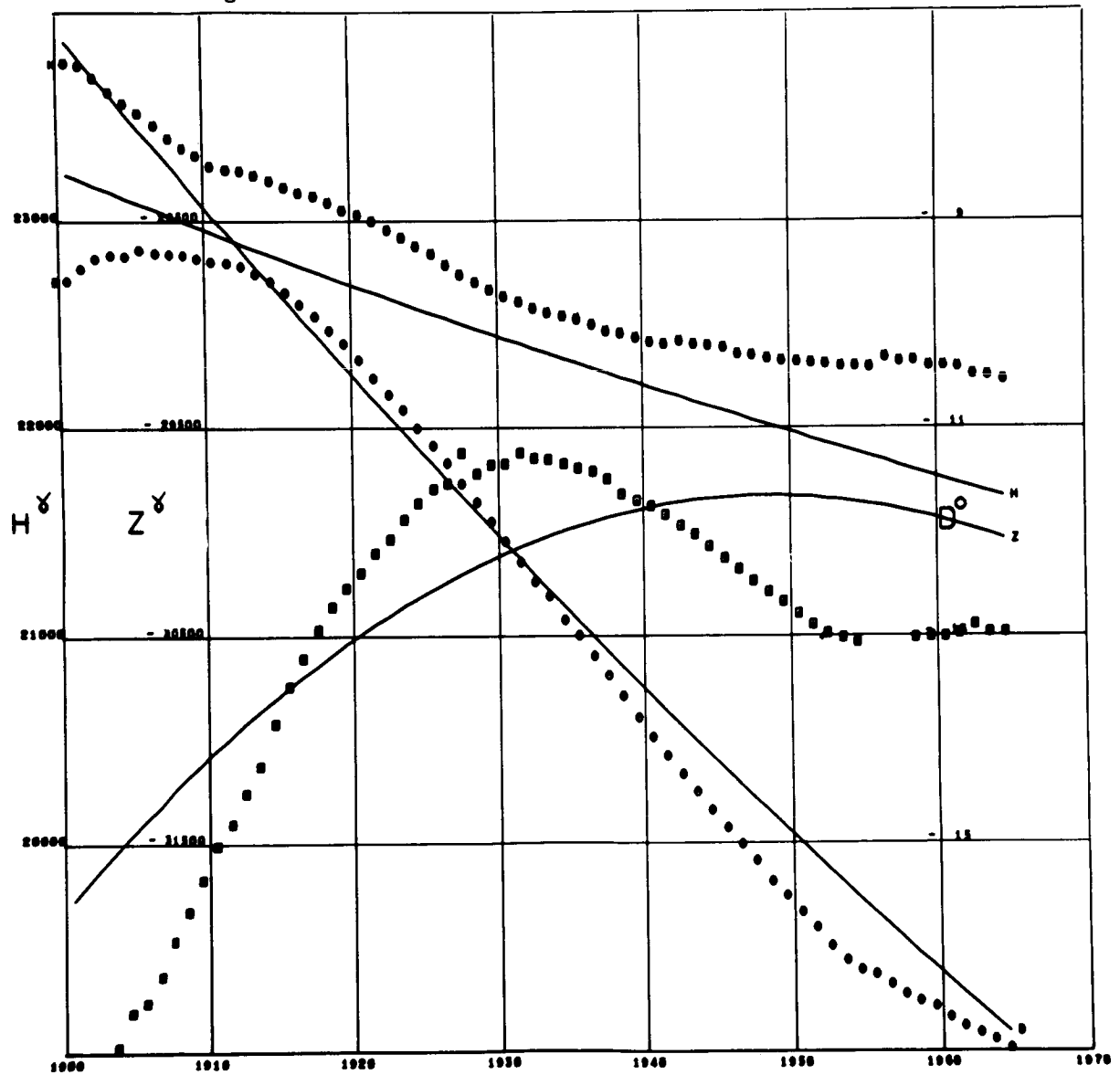
MATOCHKIN SHAR  
Lat 73.26 Long 56.39



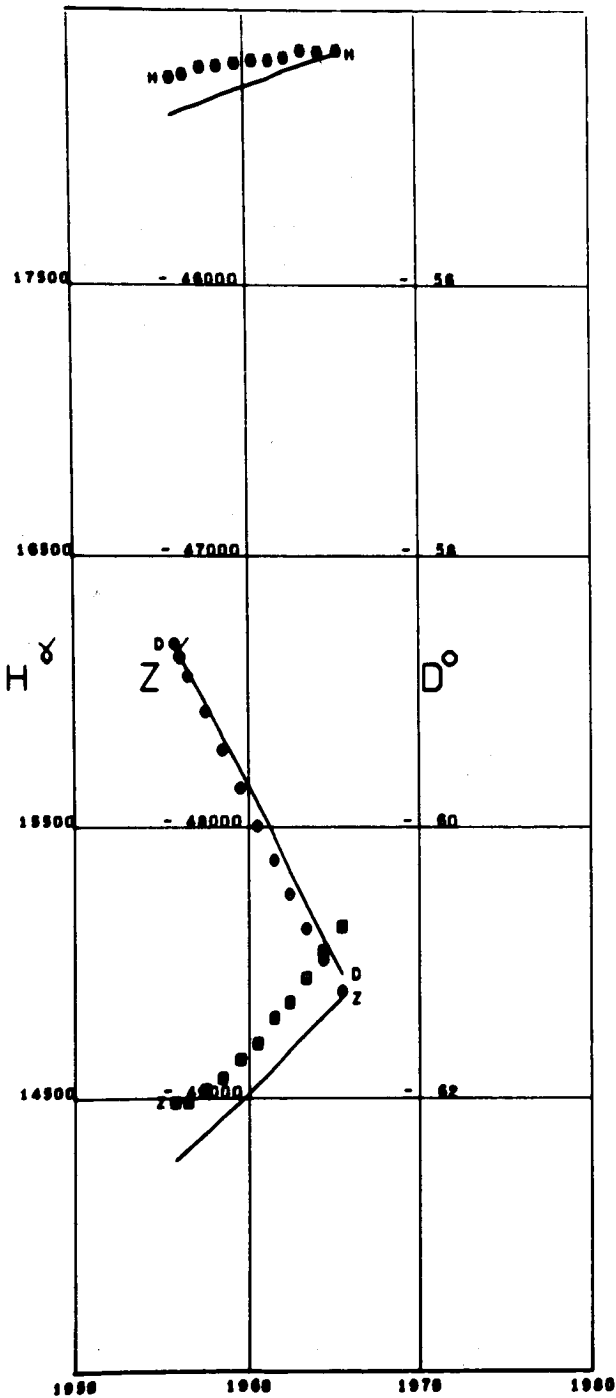
MANILA  
Lat 14.57 Long 120.97



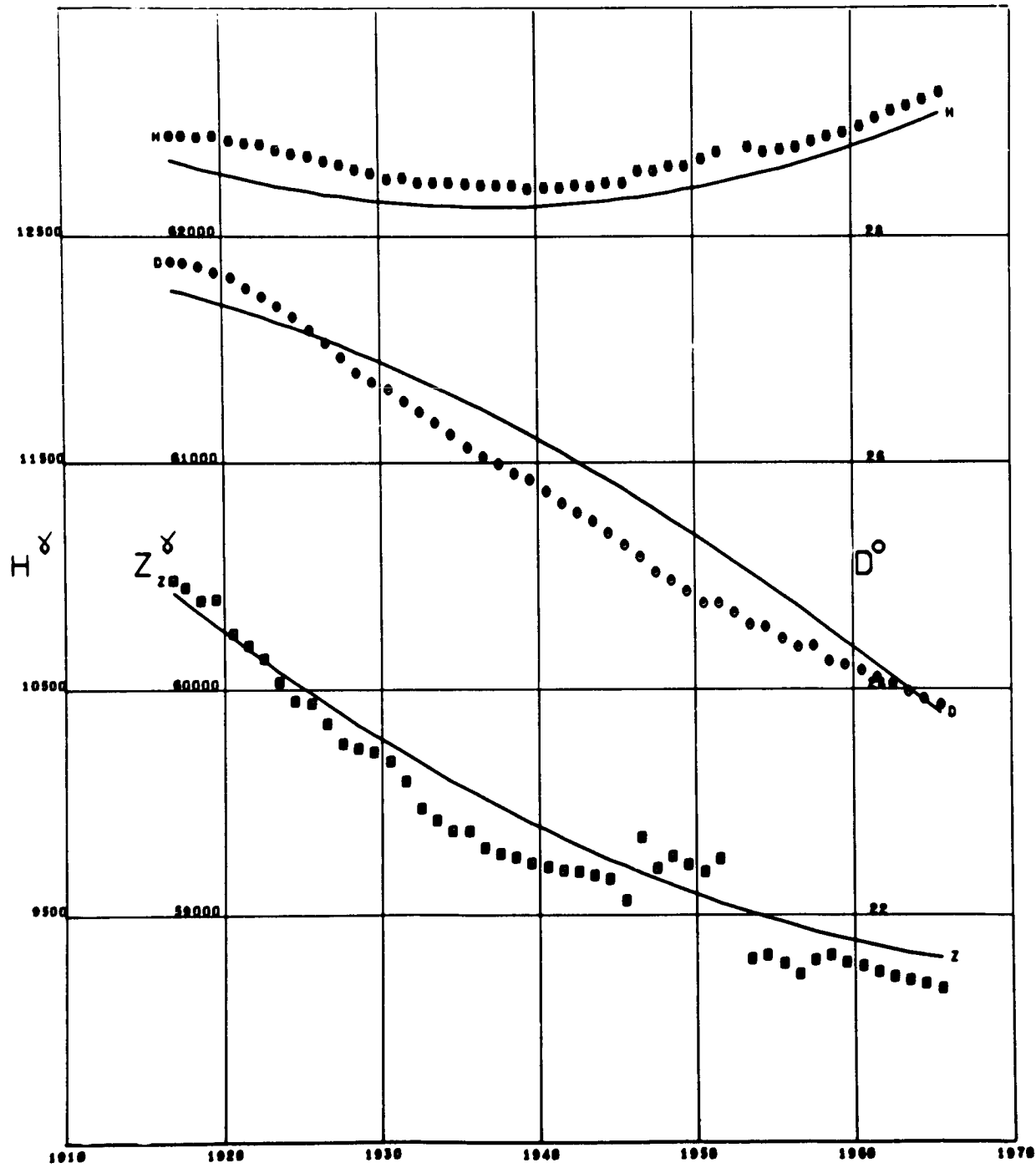
MAURITIUS  
Lat -20.09 Long 57.55



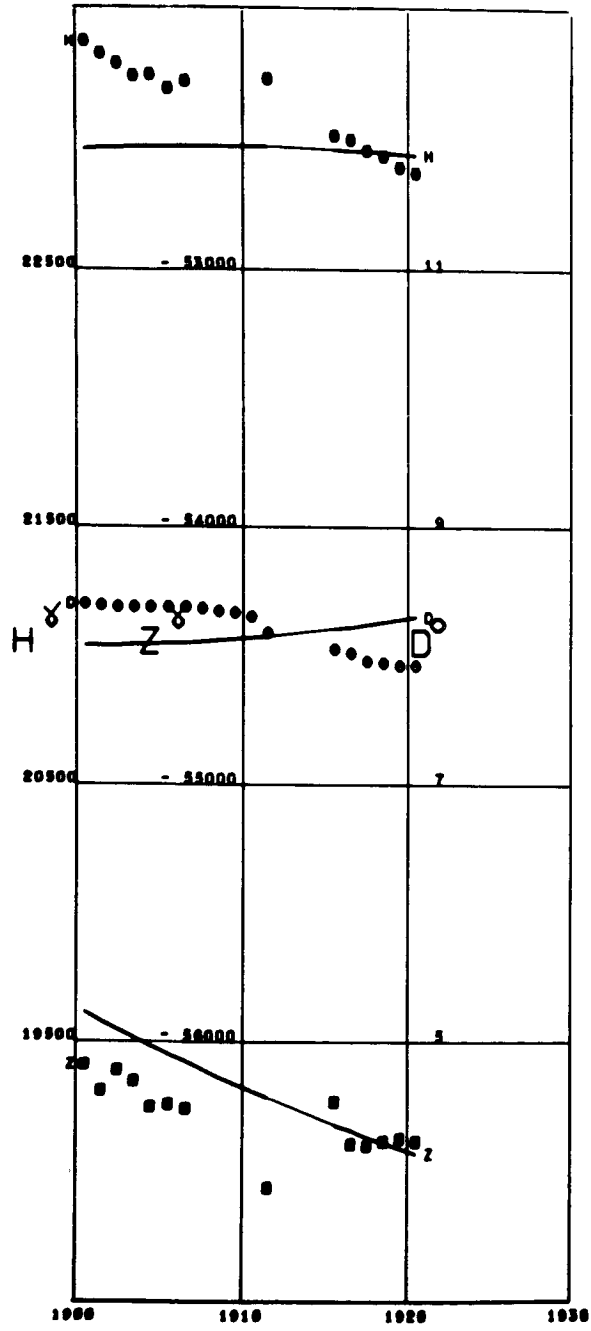
MAWSON  
Lat -67.60 Long 62.88



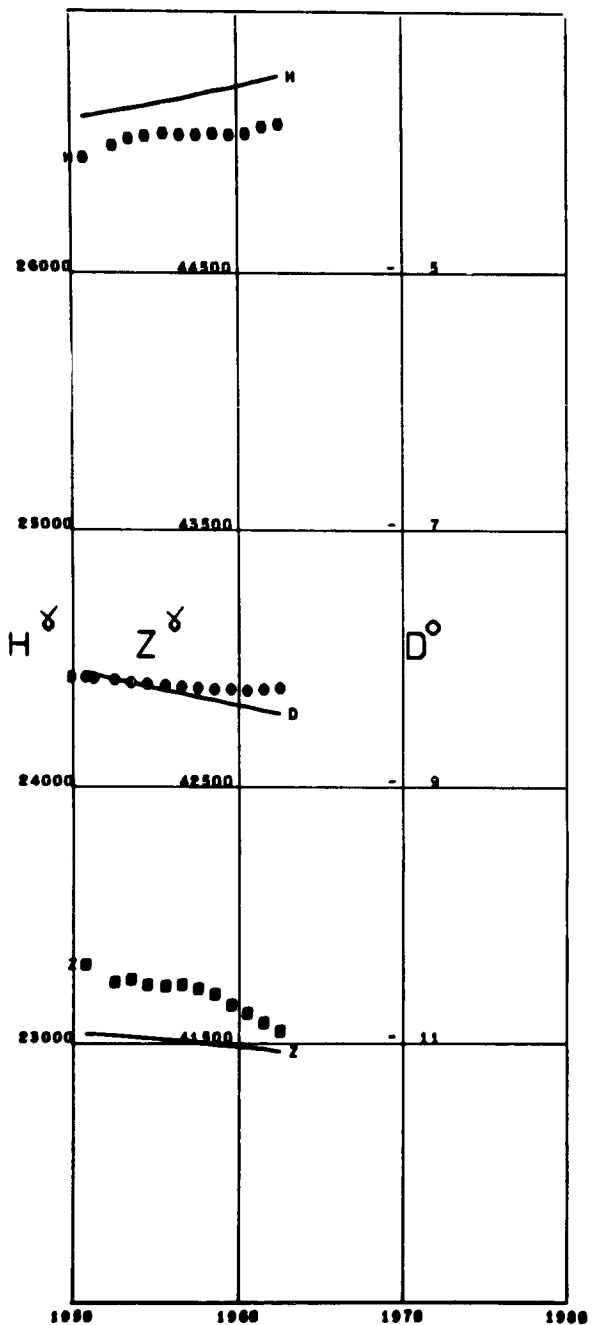
MEANOOK  
Lat 54.61 Long -113.33 Alt 0.68



MELBOURNE  
Lat -37.83 Long 144.97

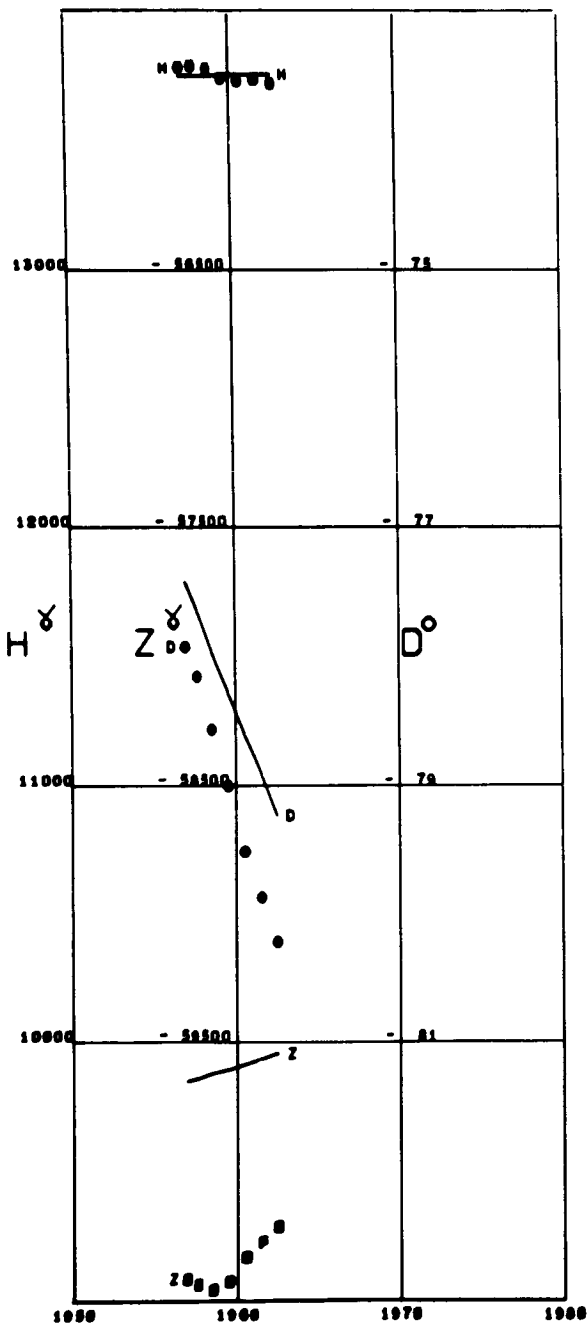


MEMAMBETSU  
Lat 43.90 Long 144.19 Alt 0.04



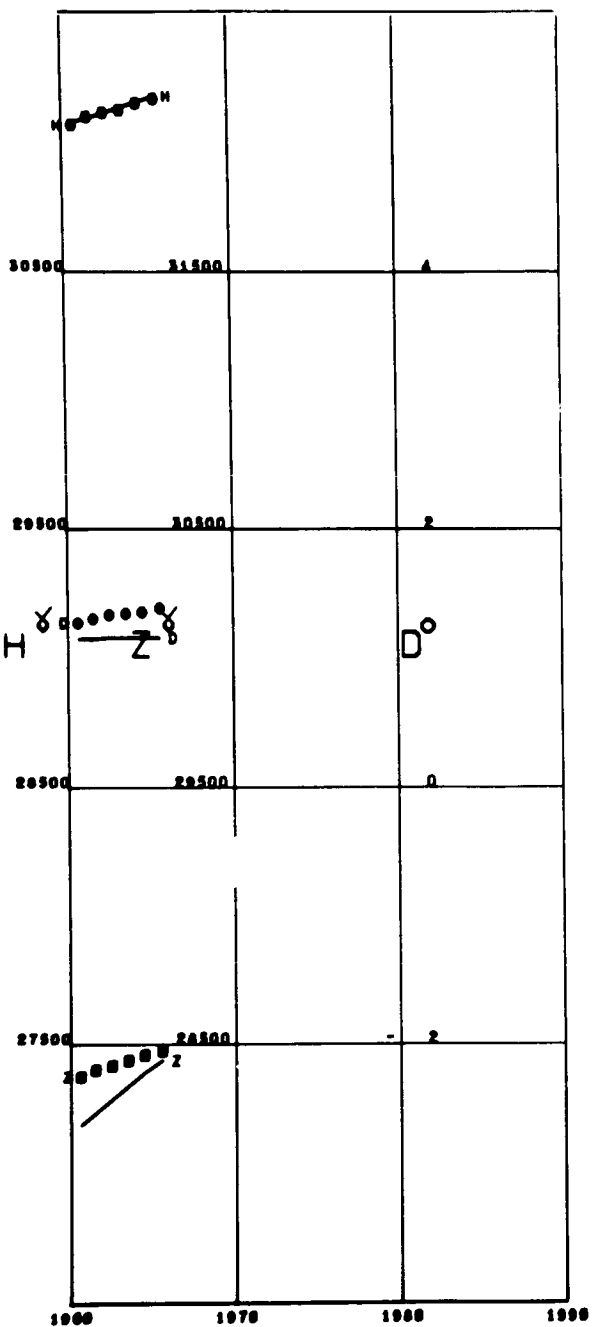
MIRNYY

Lat -66.55 Long 93.01

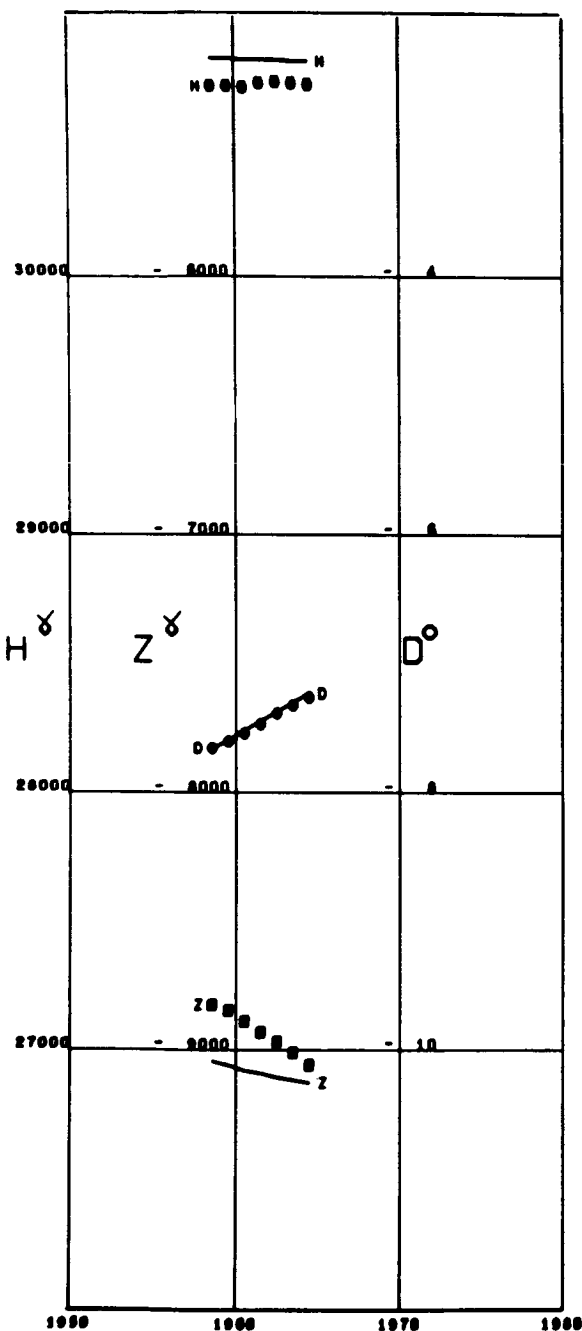


MISALLAT

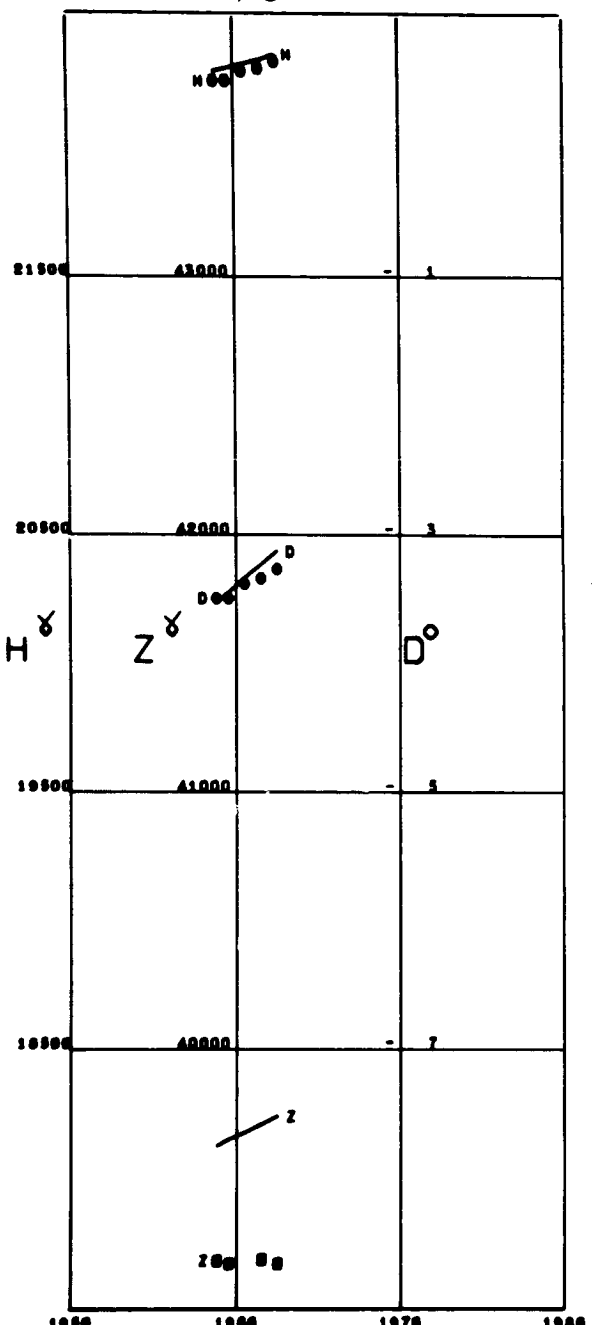
Lat 29.51 Long 30.89 Alt 0.12



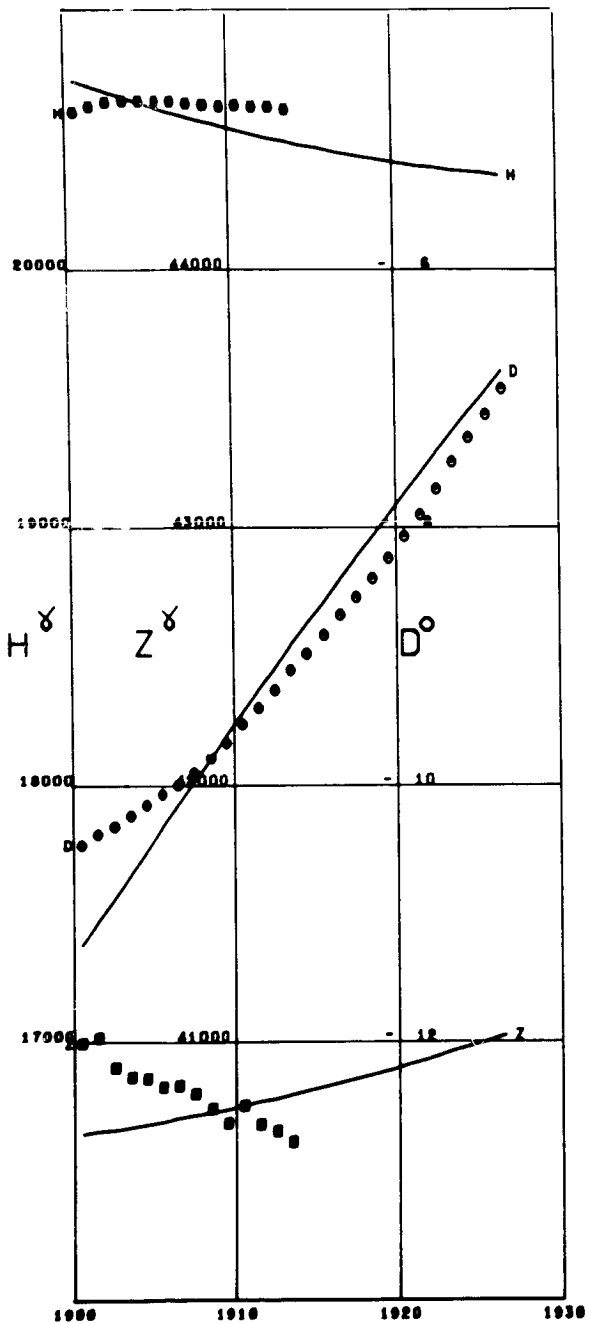
MOCA  
Lat 3.34 Long 8.66 Alt 1.35



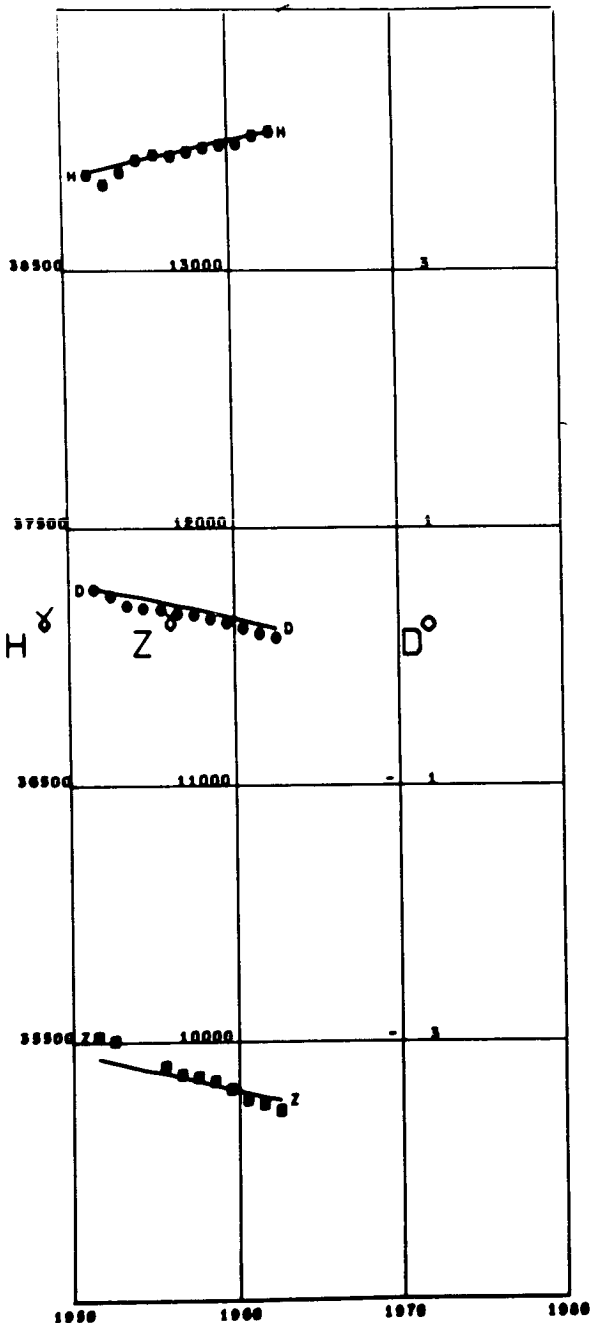
MONTE CAPPELLINO  
Lat 44.55 Long 8.95



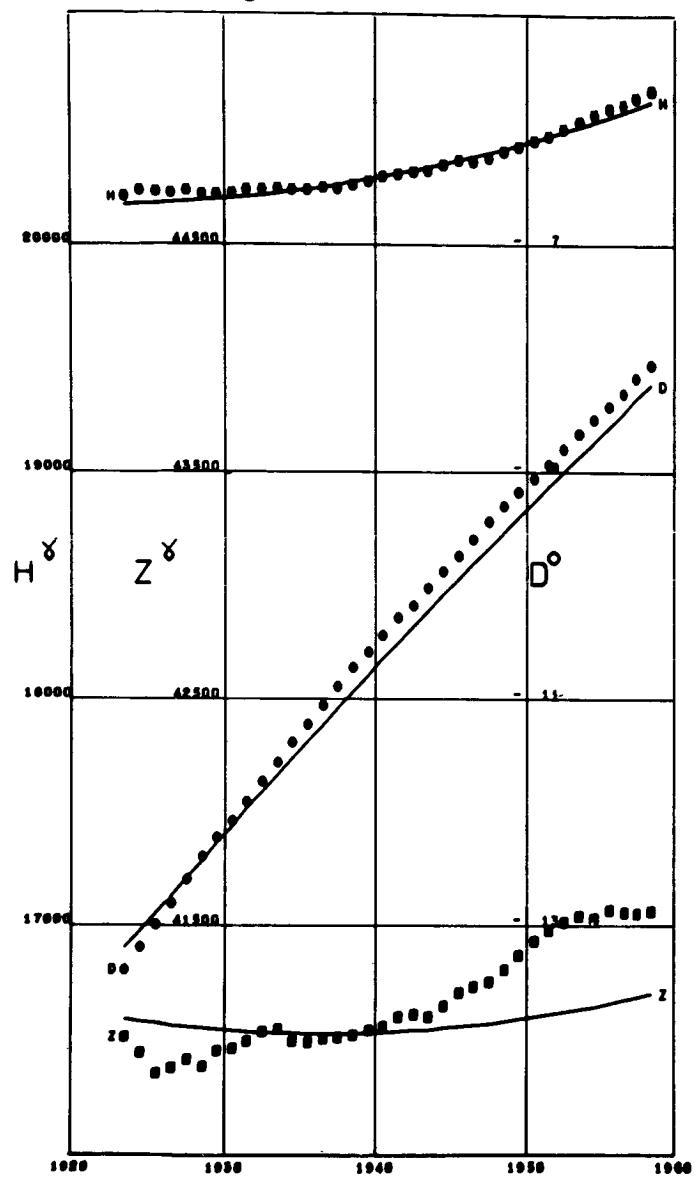
MUNICH  
Lat 48.14 Long 11.60



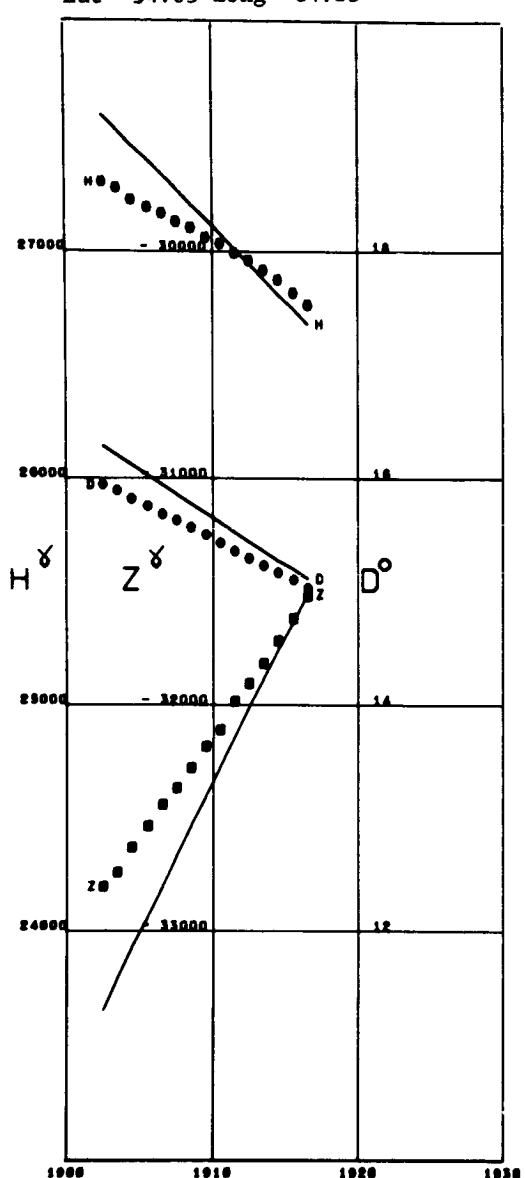
MUNTINLUPA  
Lat 14.37 Long 121.01 Alt 0.06



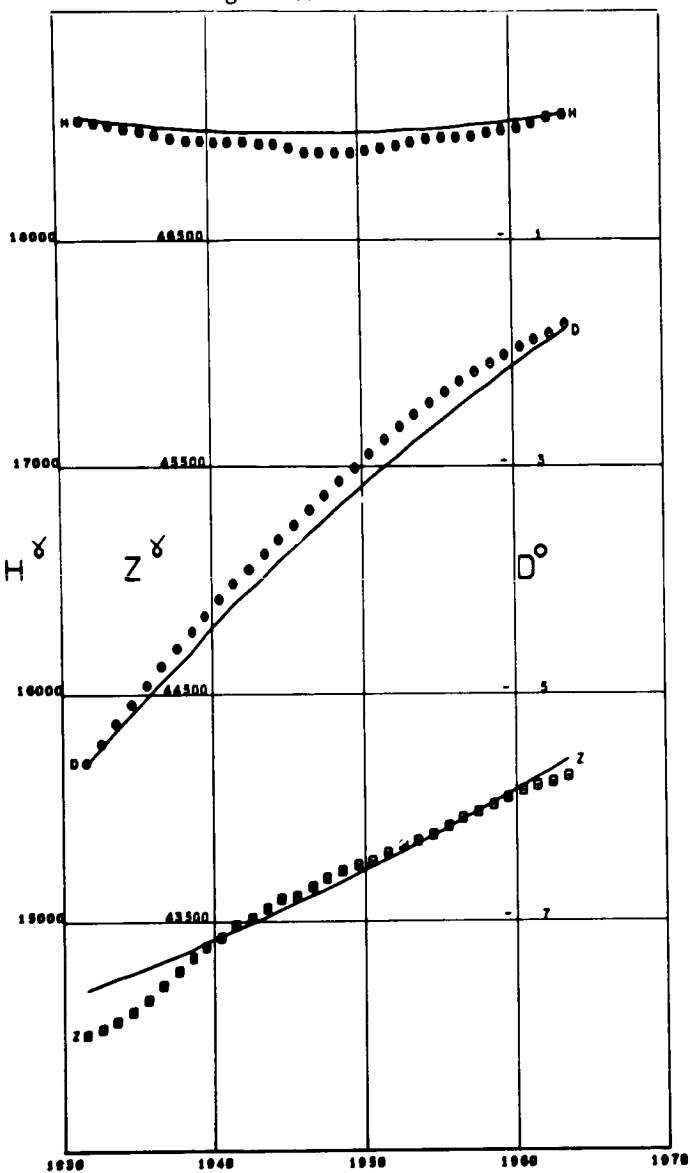
NANTES  
Lat 47.24 Long -1.56



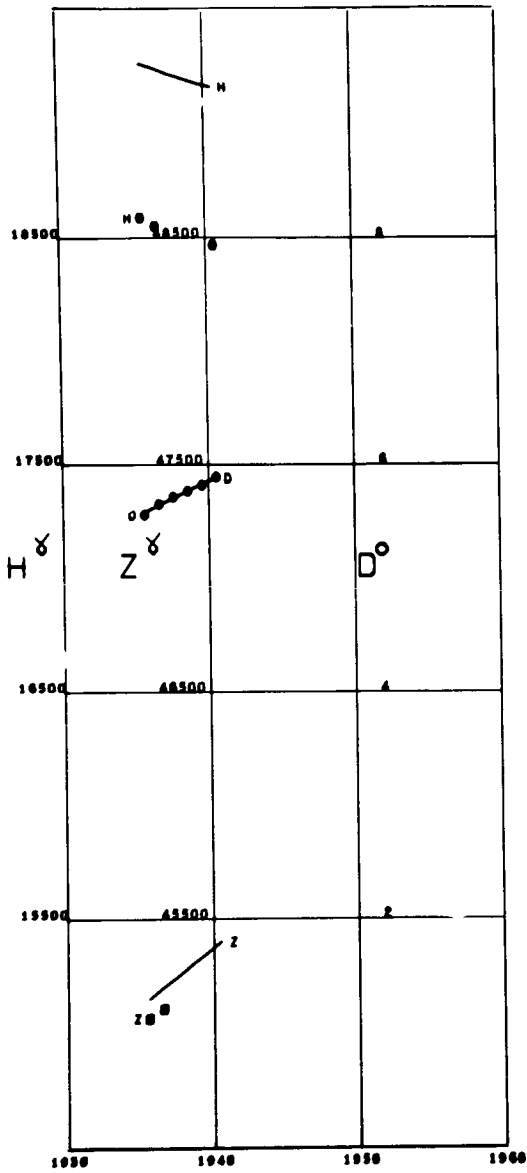
NEW YEARS ISLAND  
Lat -54.65 Long -64.15



NIEMEGK  
Lat 52.07 Long 12.67

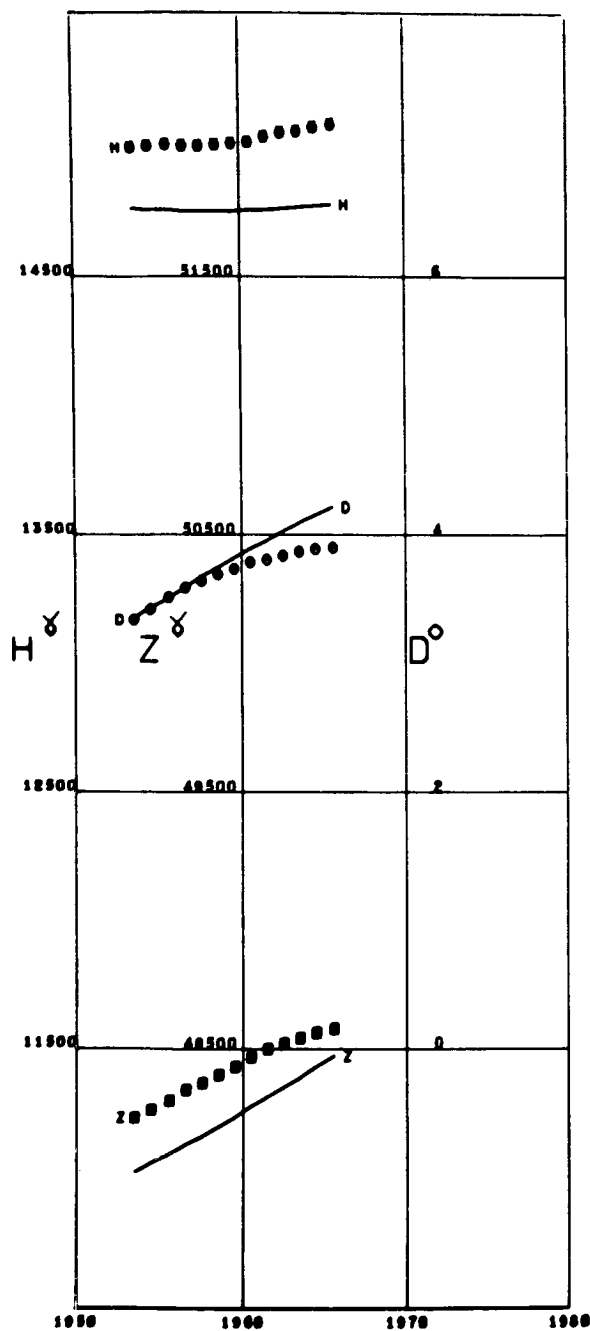


NIZHNEDEVISTSK  
Lat 51.51 Long 38.36



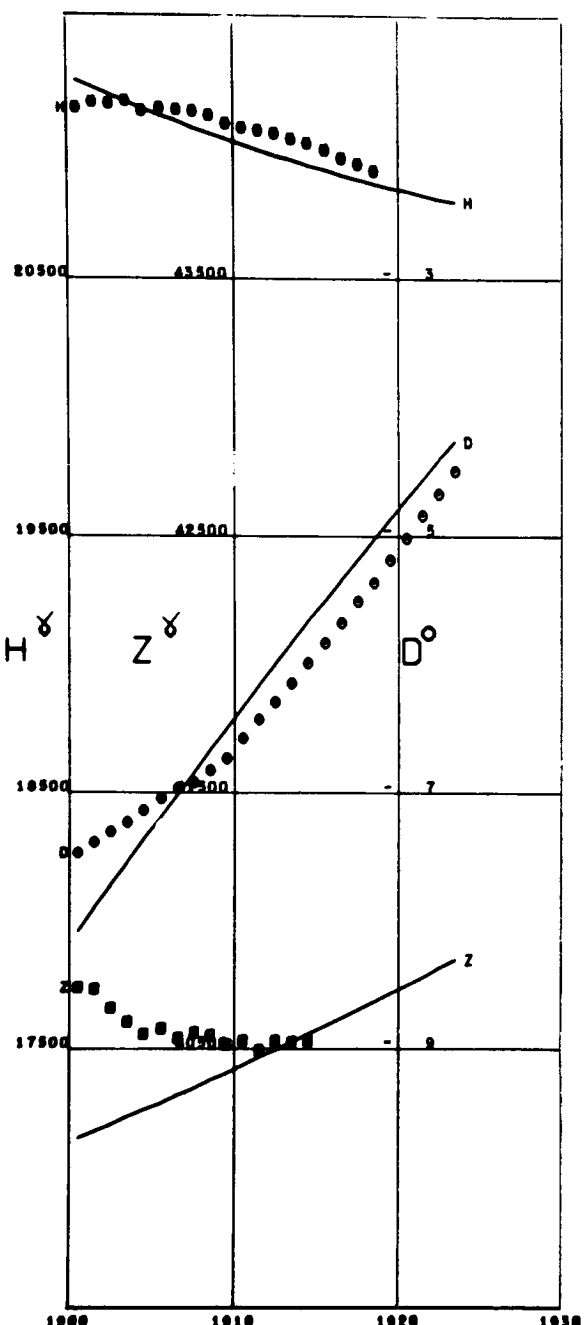
NURMIJARVI

Lat 60.50 Long 24.65 Alt 0.11

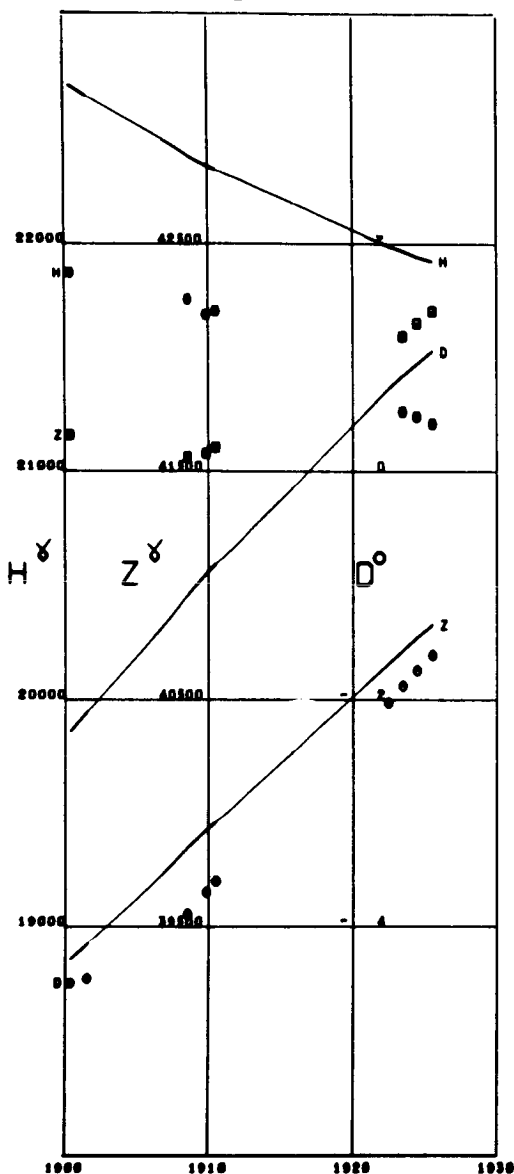


O GYALLA PESTH

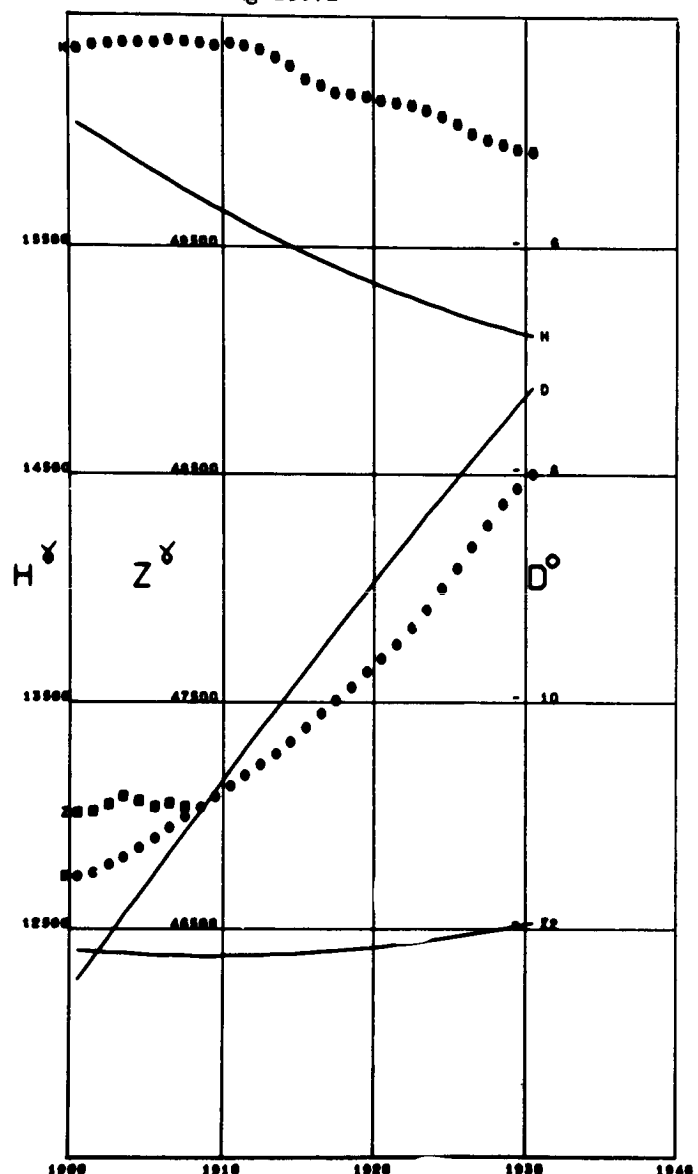
Lat 47.87 Long 18.19



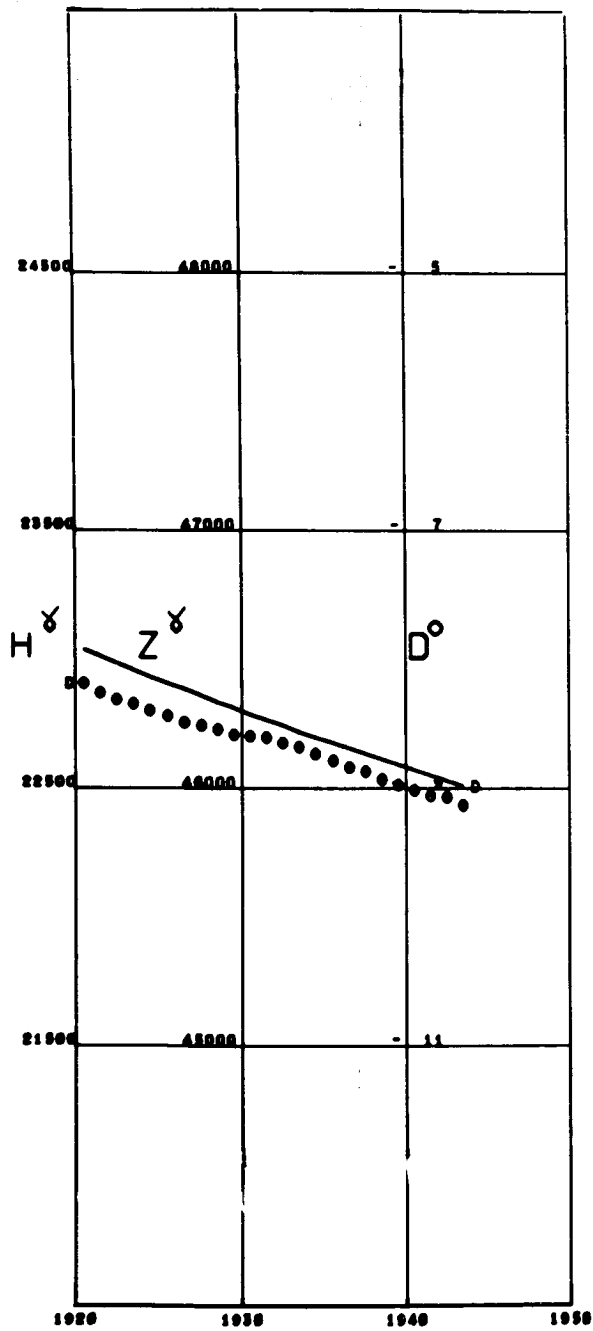
ODESSA  
Lat 46.66 Long 30.77



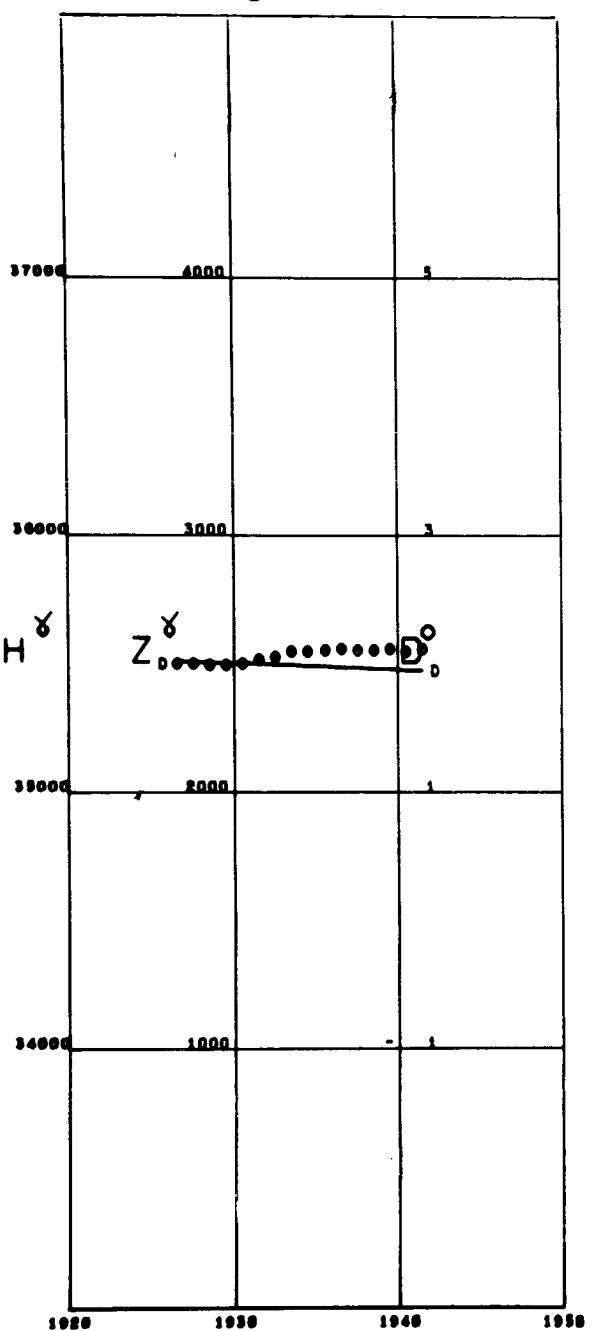
OSLO  
Lat 59.91 Long 10.72



OTOMARI  
Lat 46.65 Long 142.76

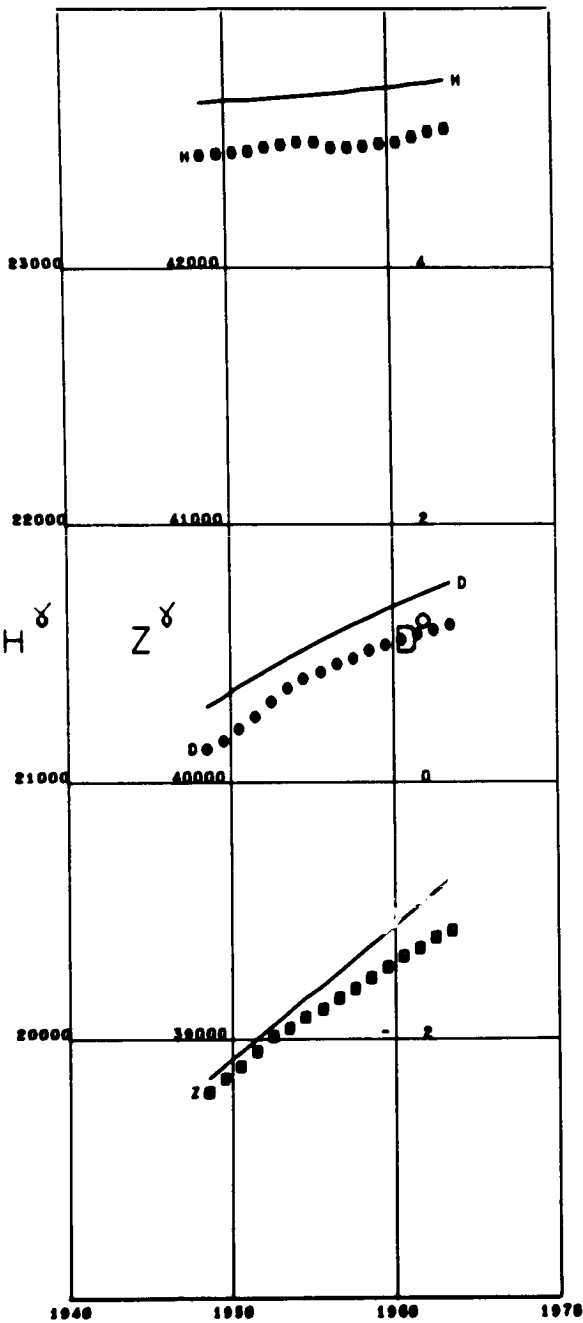


PALAU  
Lat 7.33 Long 134.48



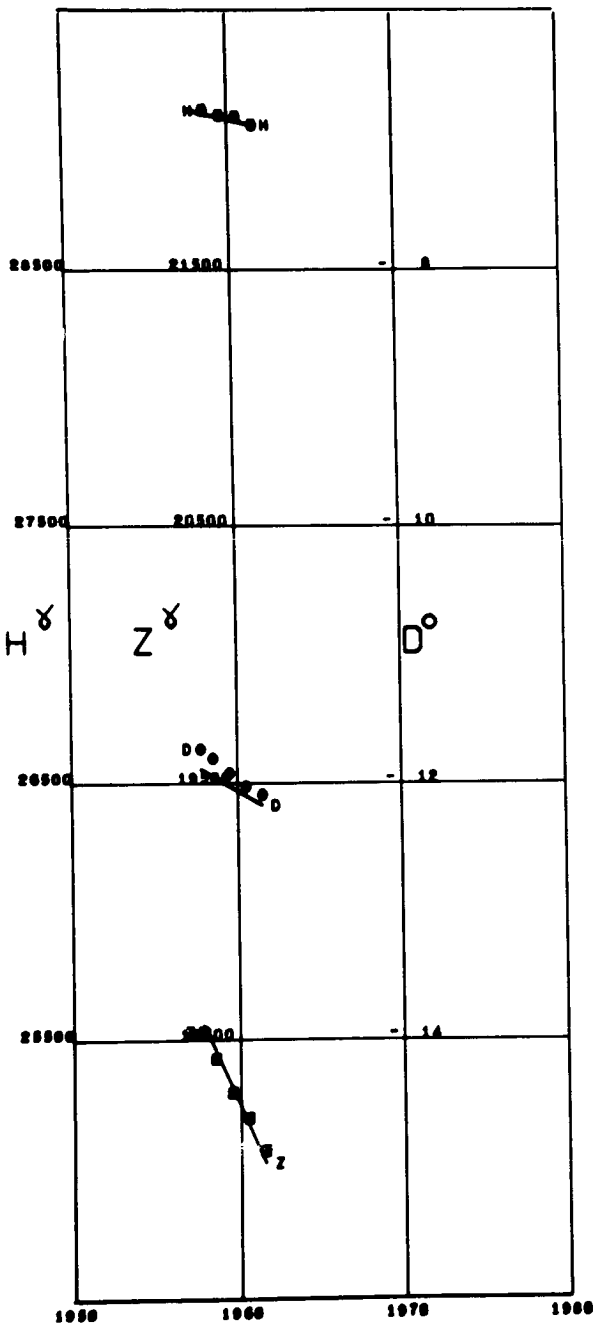
PANAGYURIShte

Lat 42.51 Long 24.18



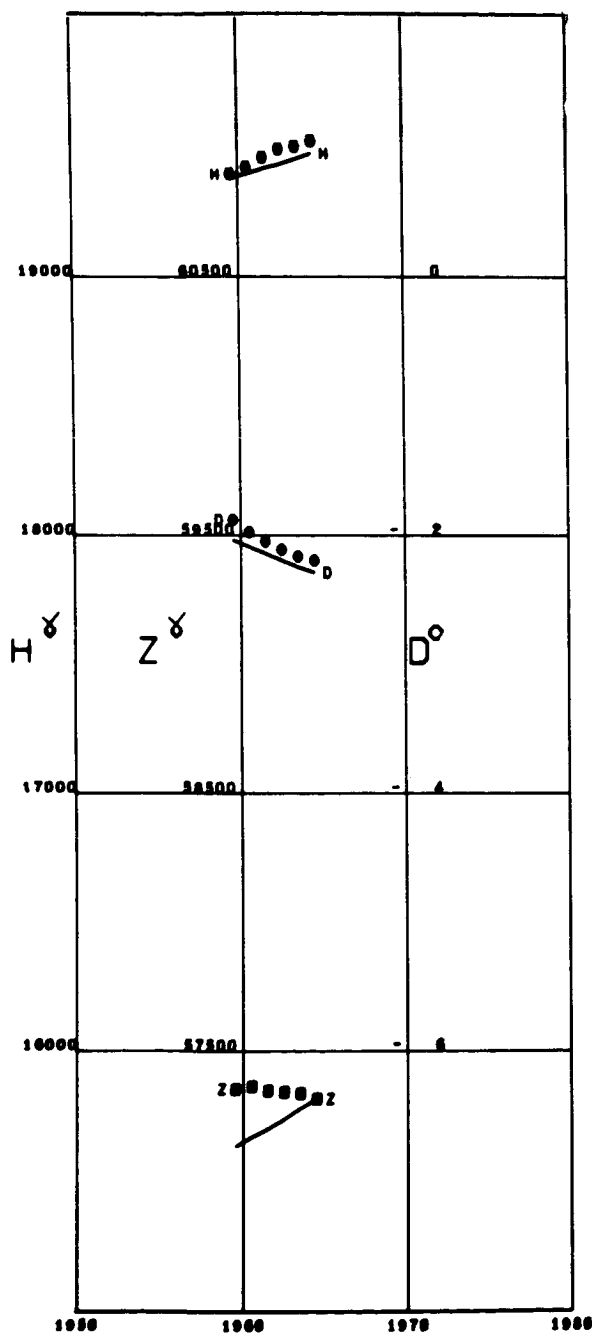
PARAMARIBO

Lat 5.81 Long -55.22 Alt 0.10



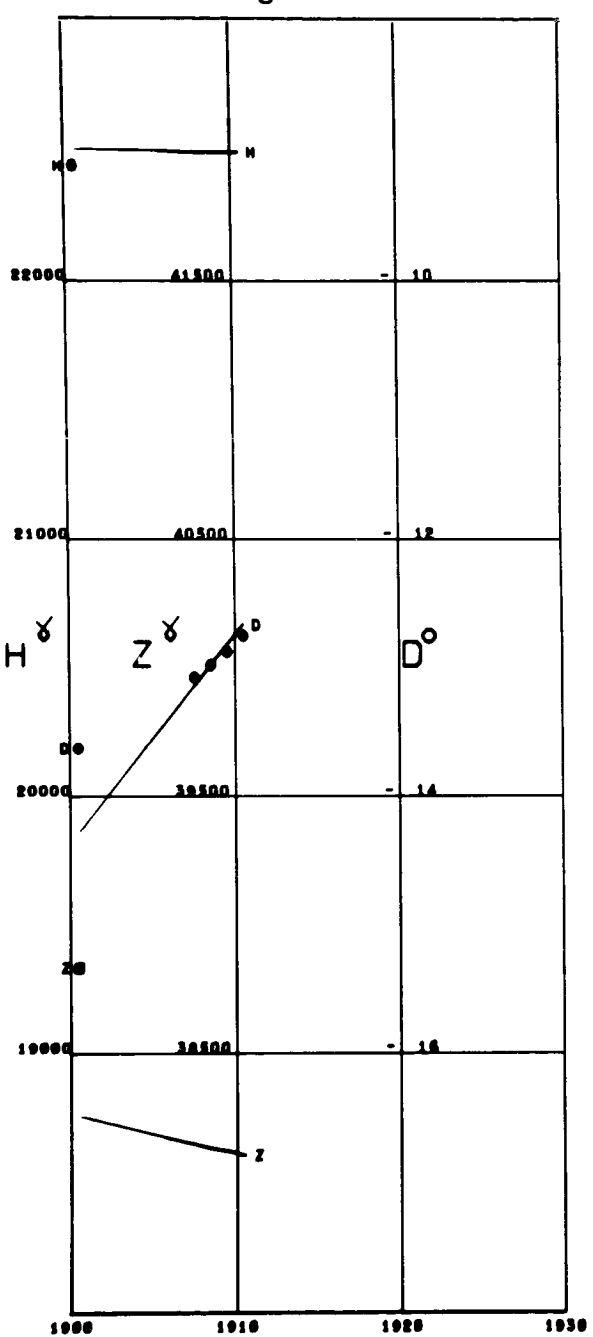
PATRONY

Lat 52.16 Long 104.45 Alt 0.76



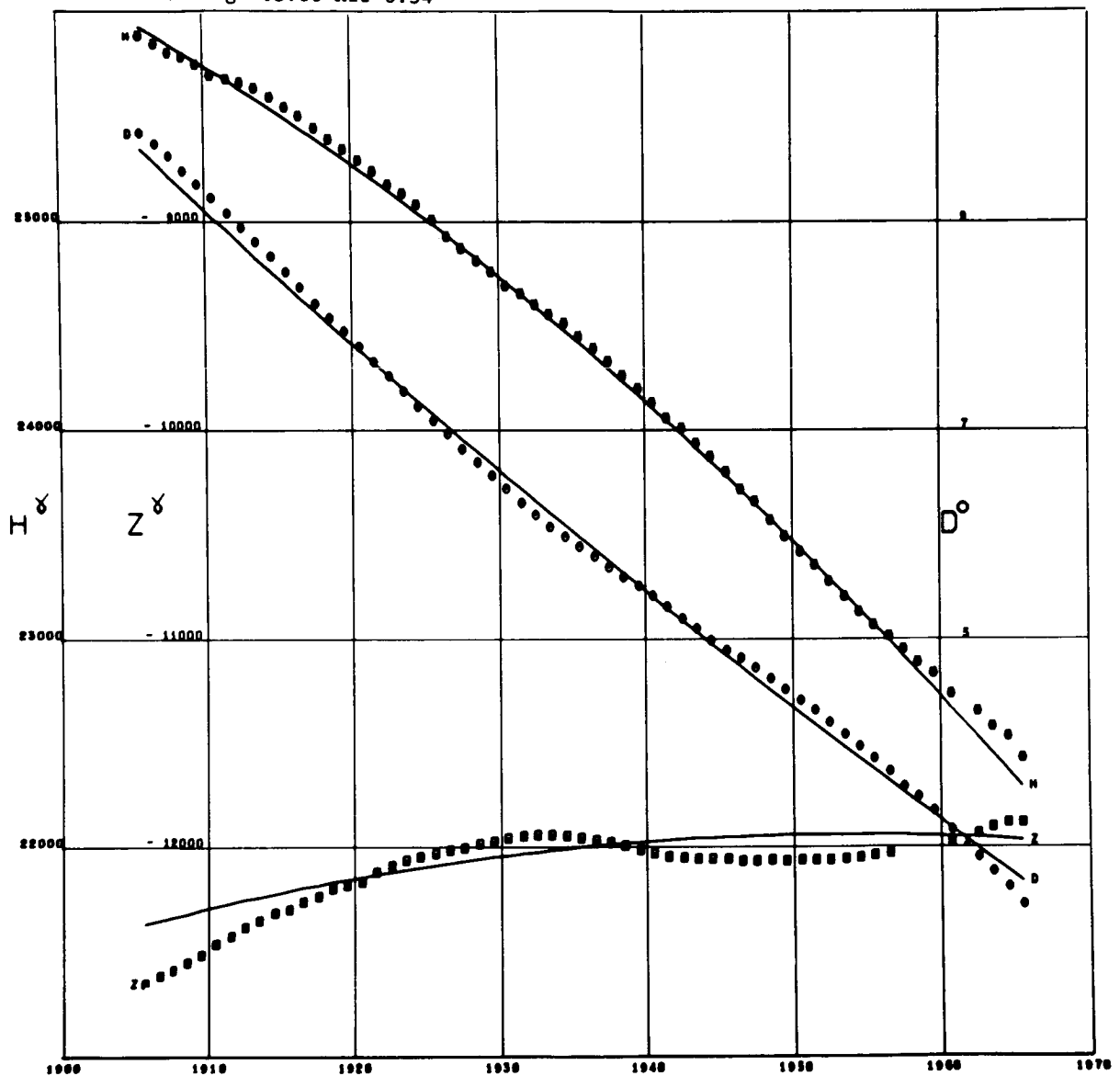
PERPIGNAN

Lat 42.70 Long 2.88

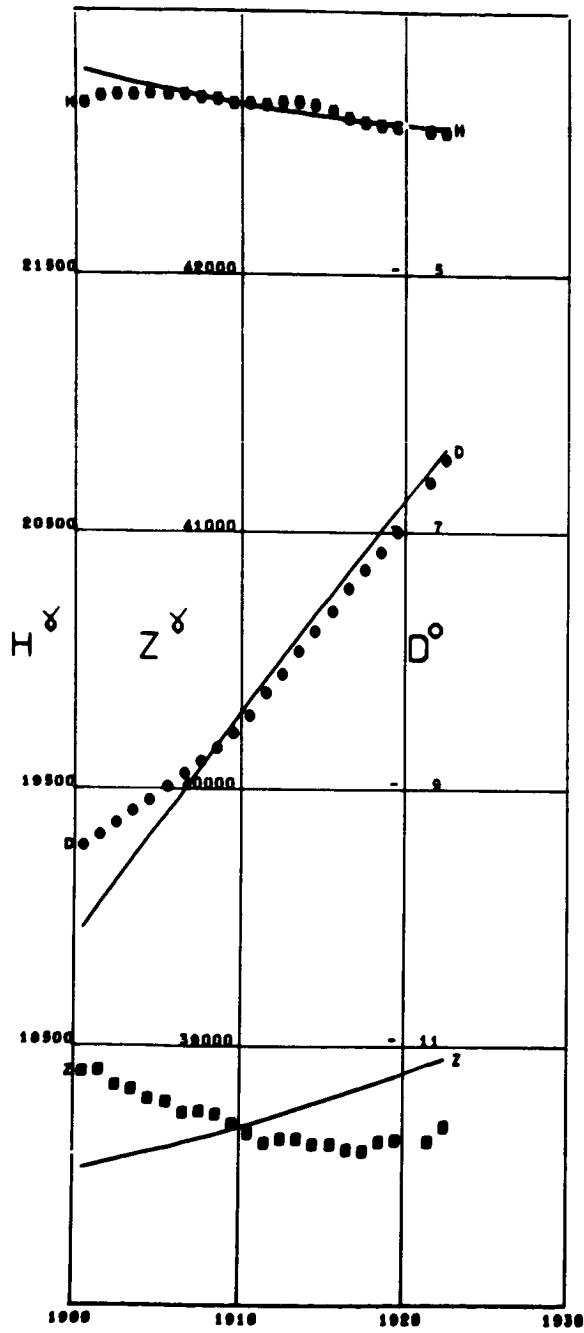


PILAR

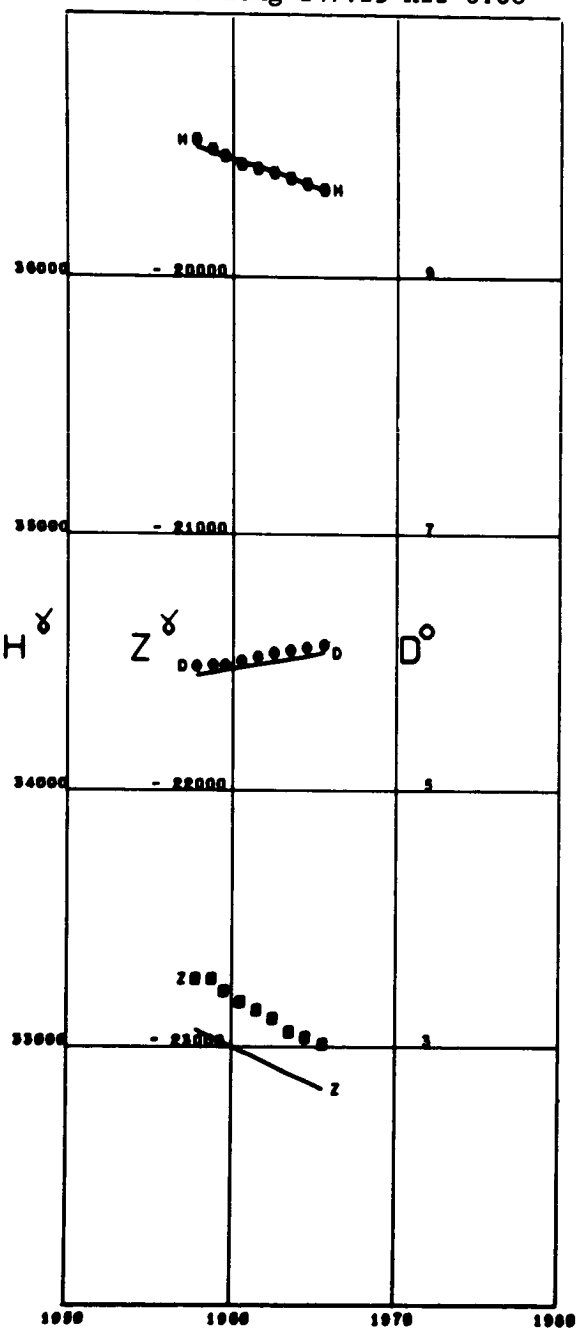
Lat -31.66 Long -63.88 Alt 0.34



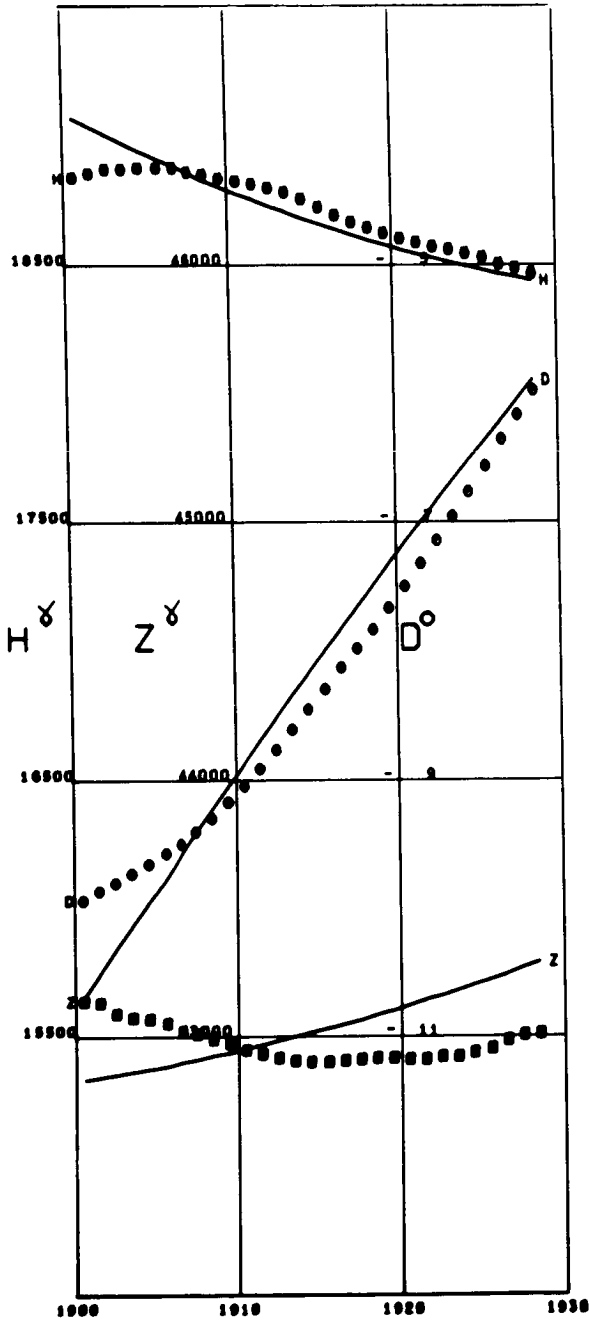
POLA  
Lat 44.86 Long 13.84



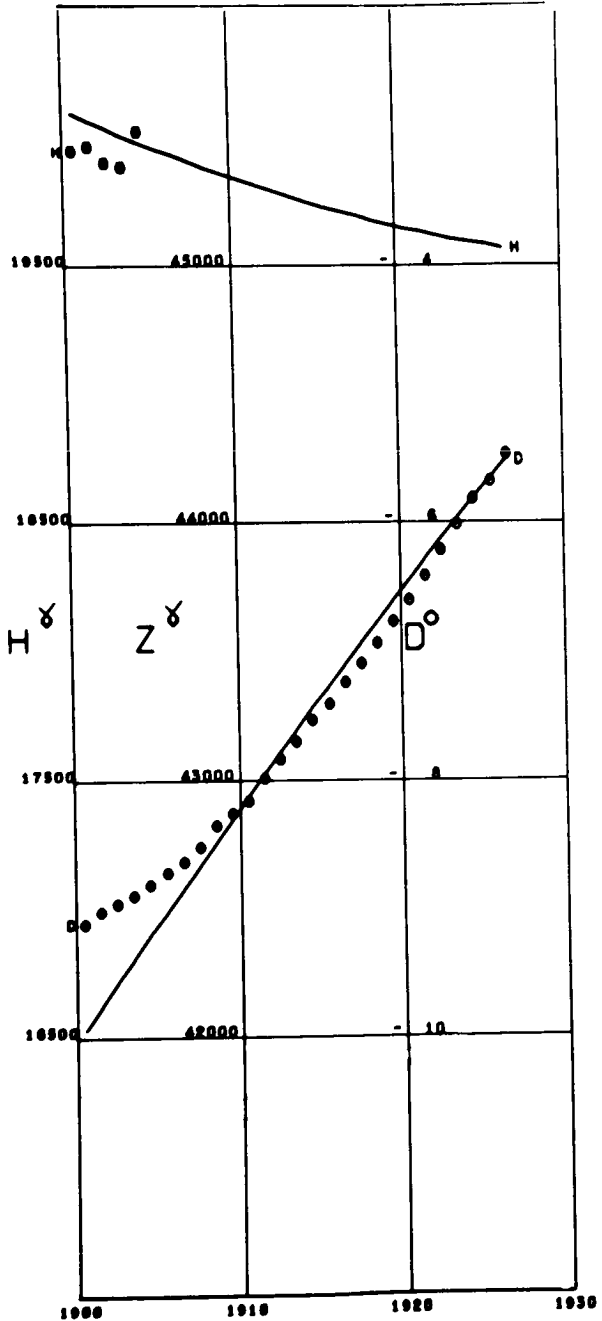
PORT MORESBY  
Lat -9.40 Long 147.15 Alt 0.08



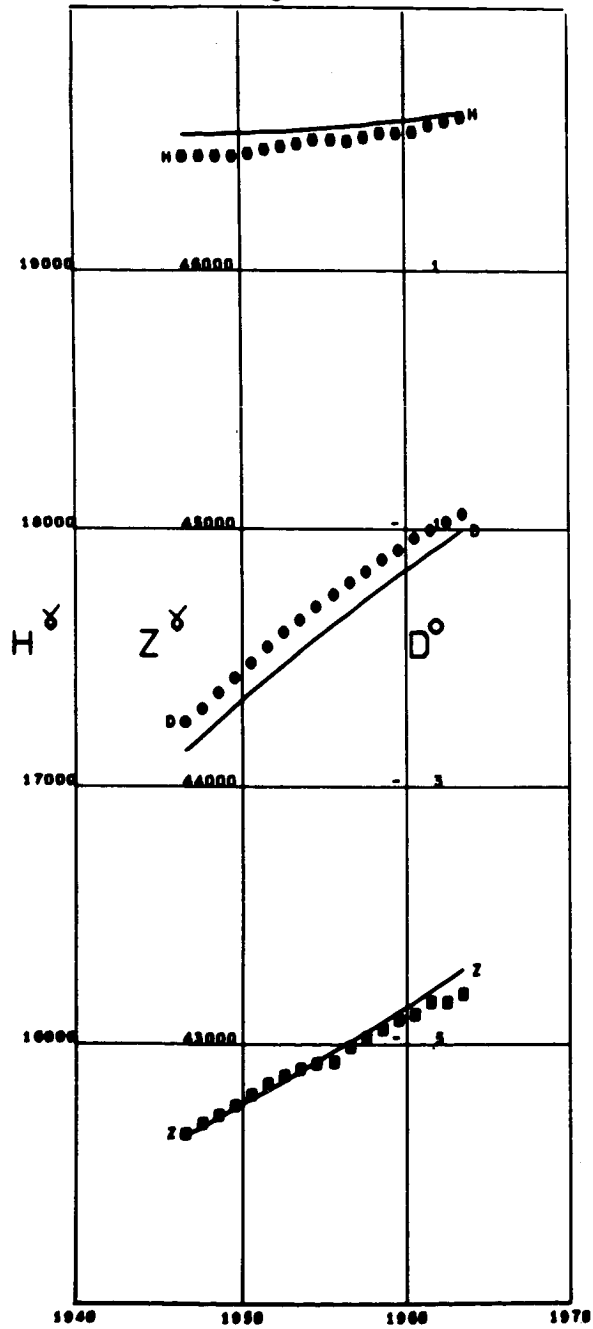
POTSDAM  
Lat 52.38 Long 13.06



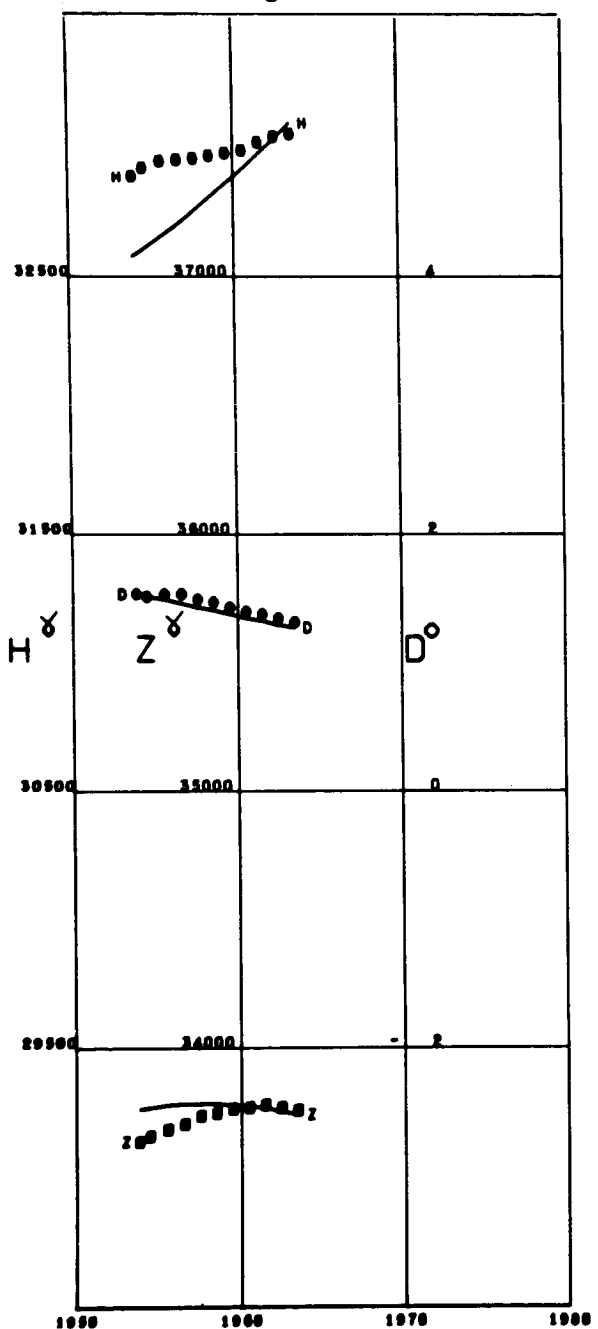
PRAGUE  
Lat 50.08 Long 14.41



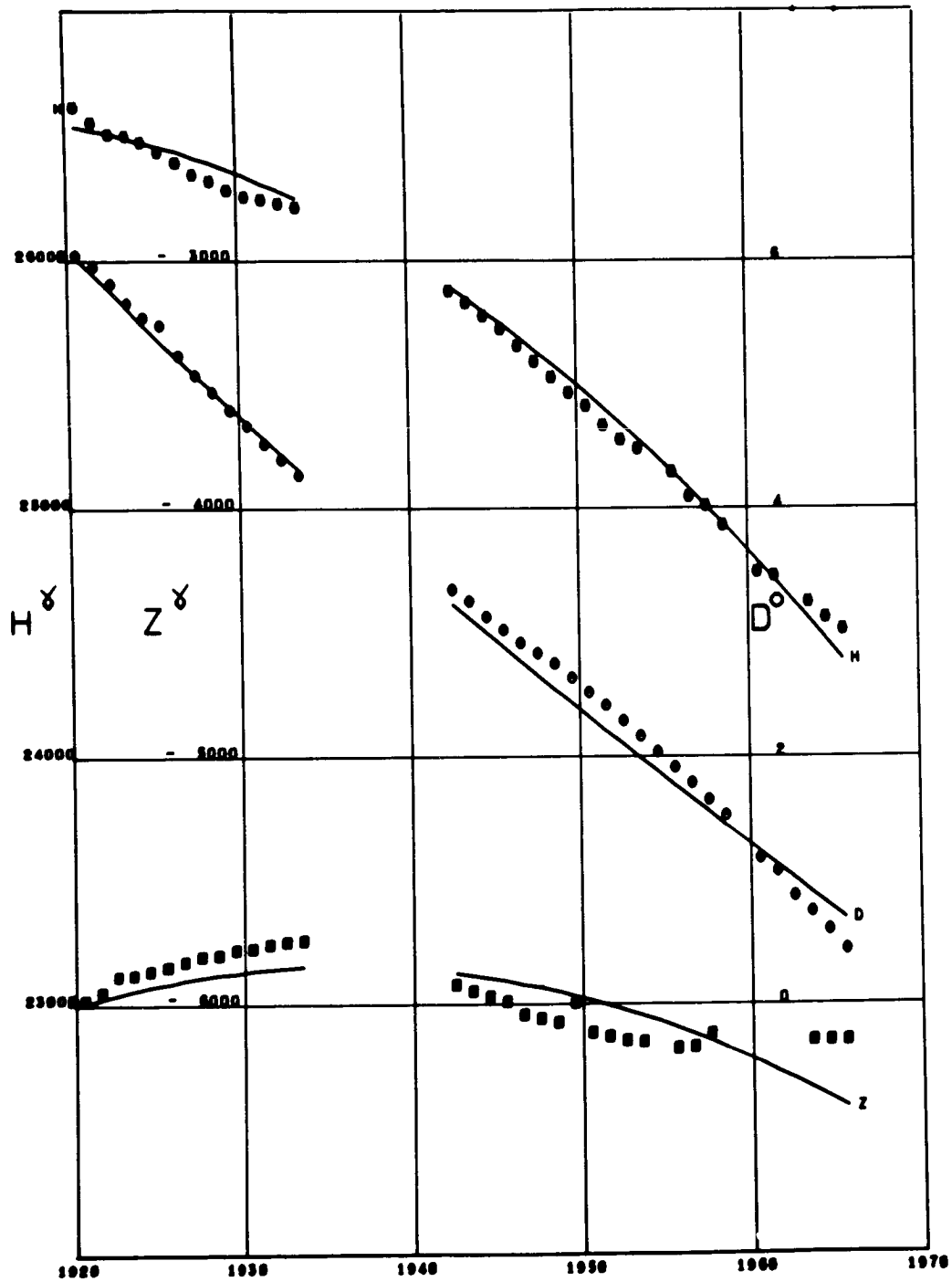
PRUHONICE  
Lat 49.99 Long 14.54



QUETTA  
Lat 30.18 Long 66.95

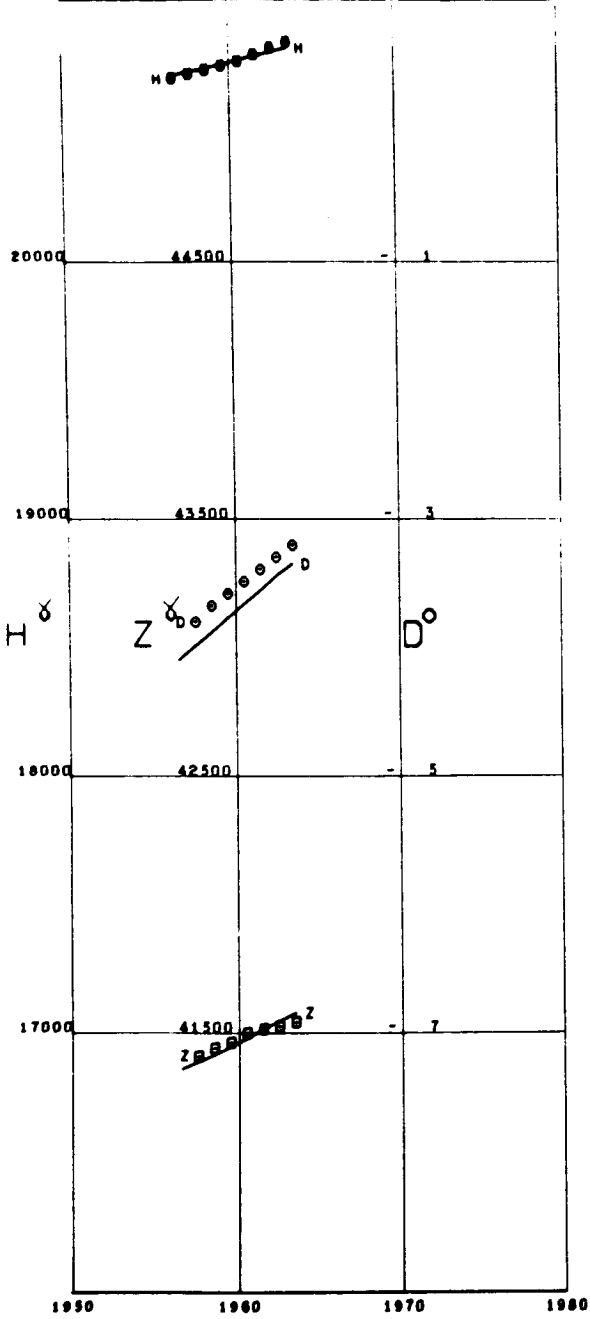


QUIACA  
Lat -22.10 Long -65.60



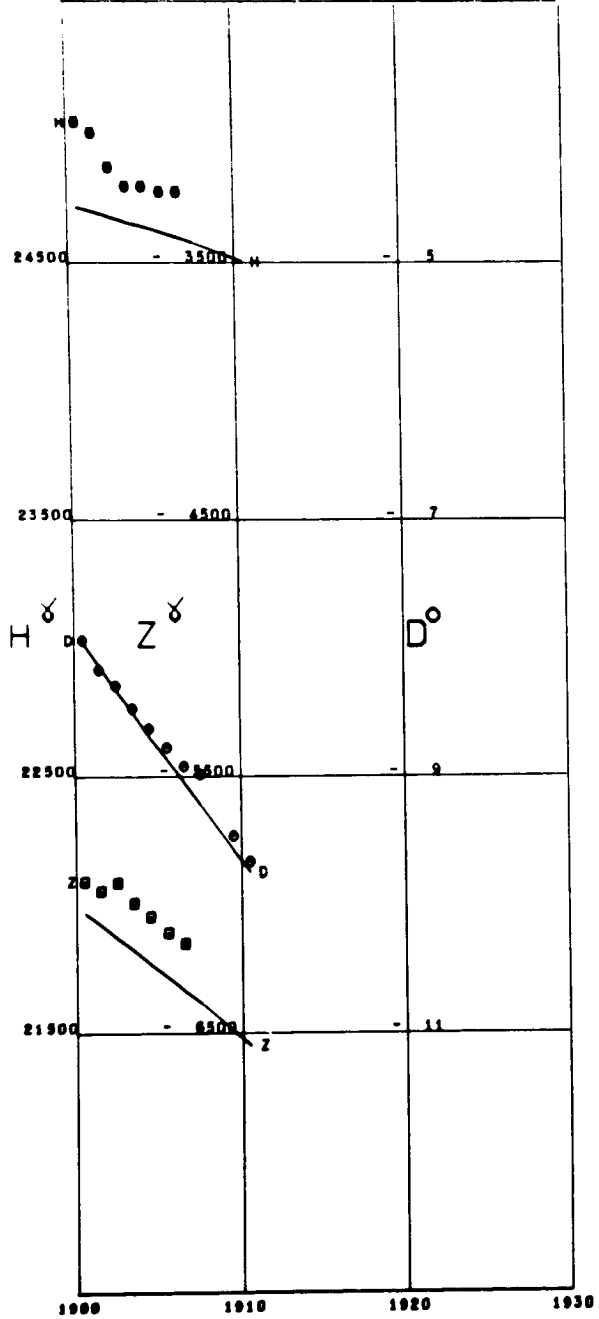
REGENSBERG

Lat 47.48 Long 8.44

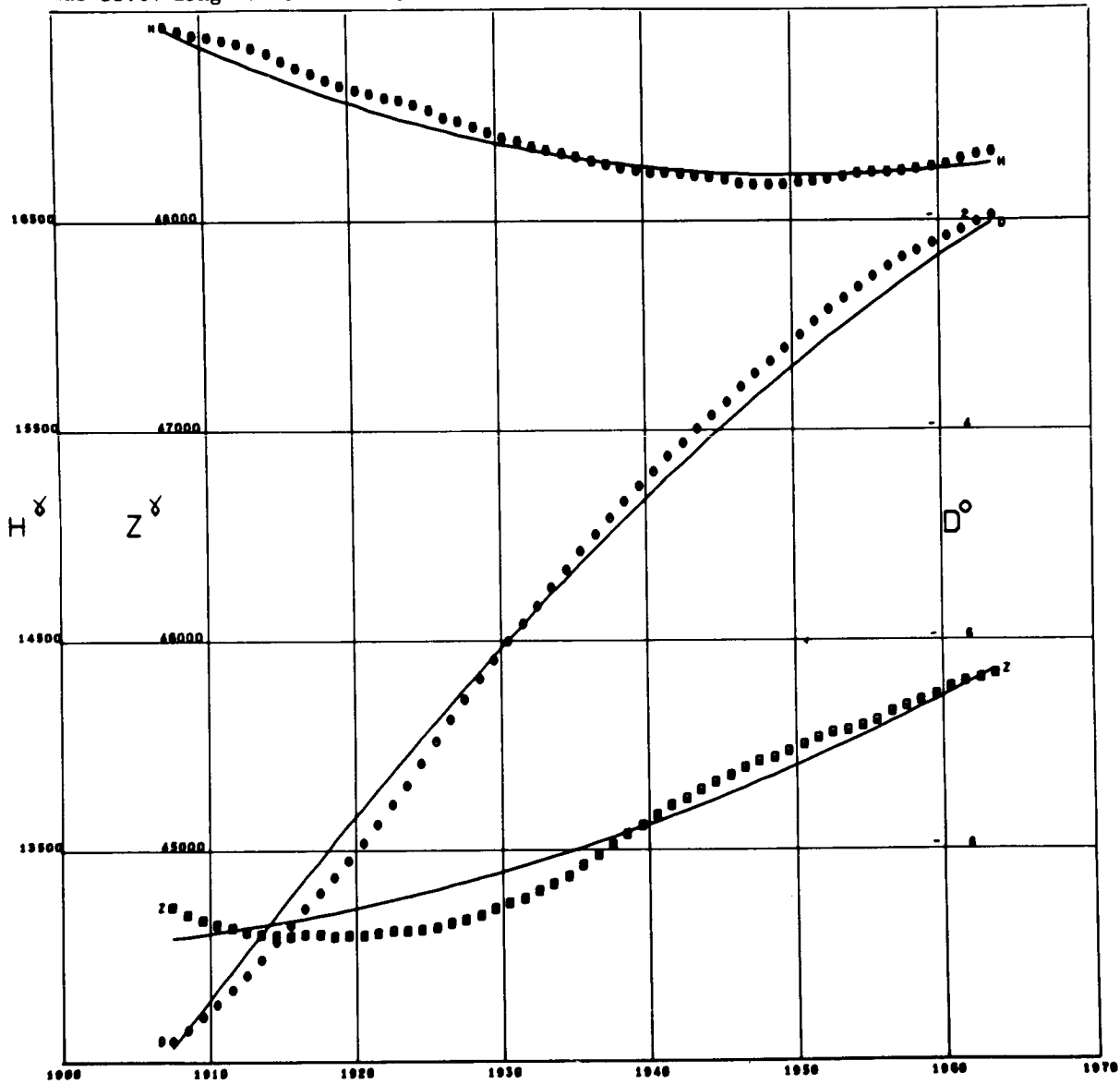


RIO DE JANEIRO

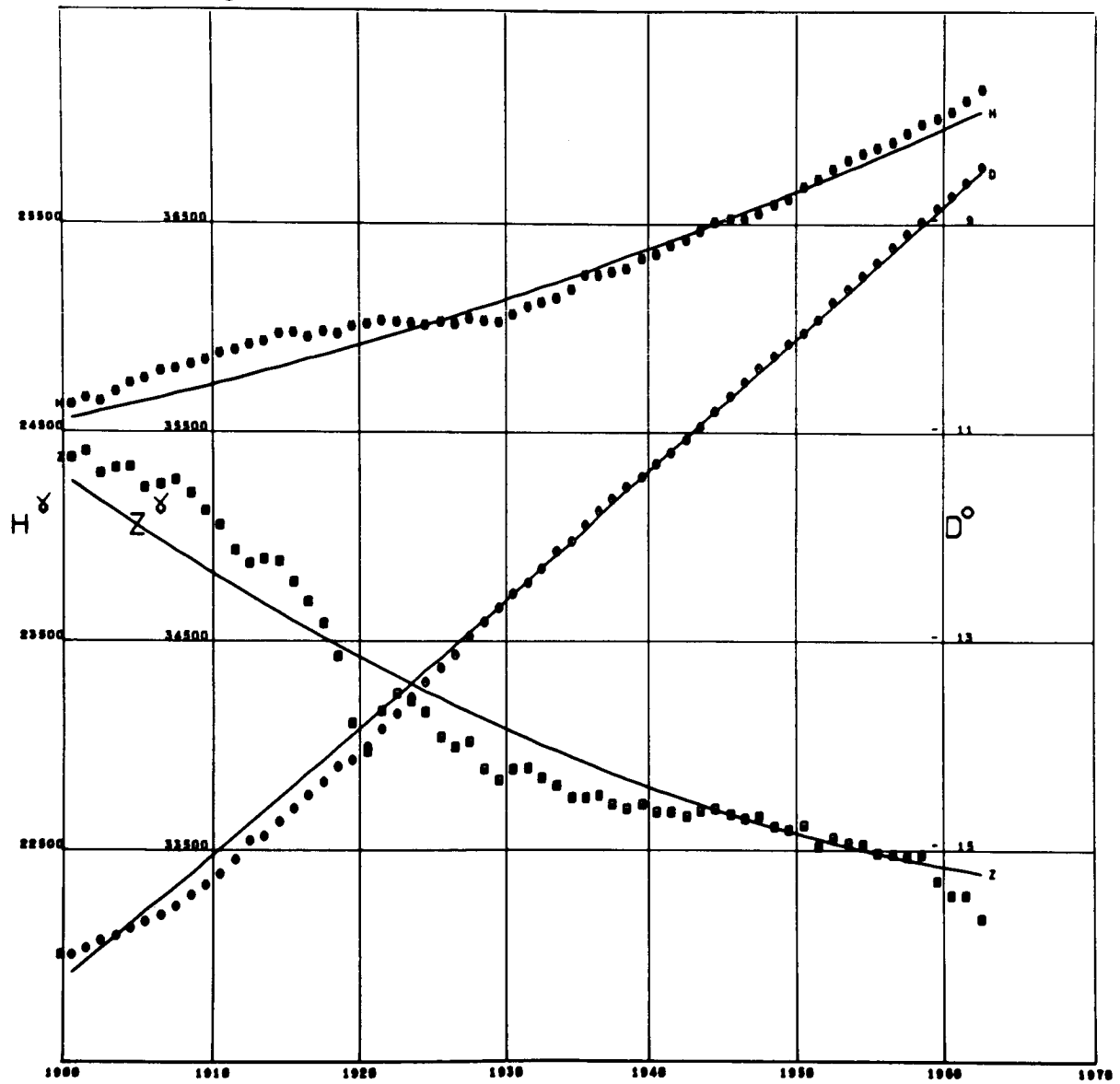
Lat -22.90 Long -43.17



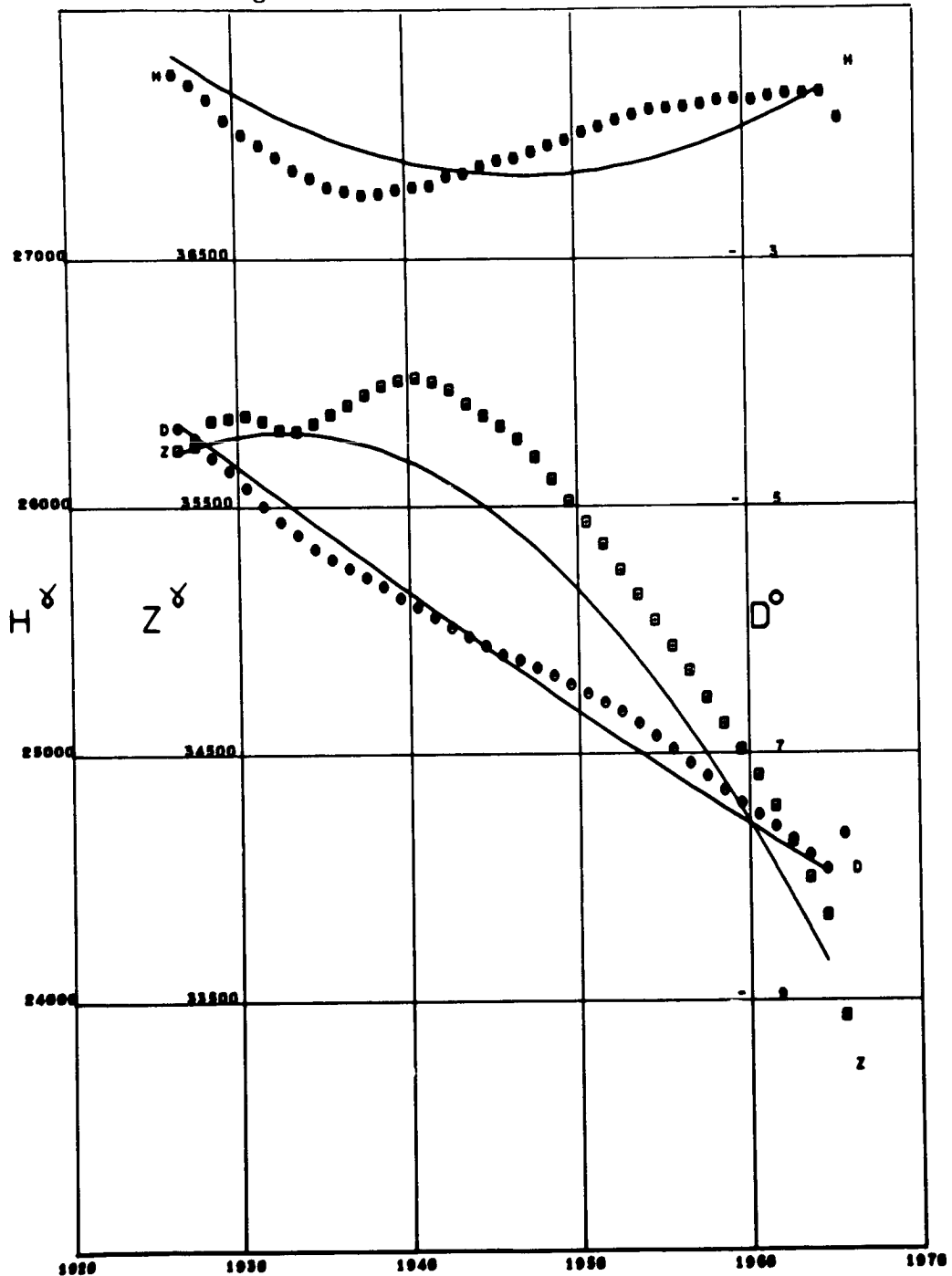
RUDE SKOV  
Lat 55.84 Long 12.45 Alt 0.05



SAN FERNANDO  
Lat 36.46 Long -6.20

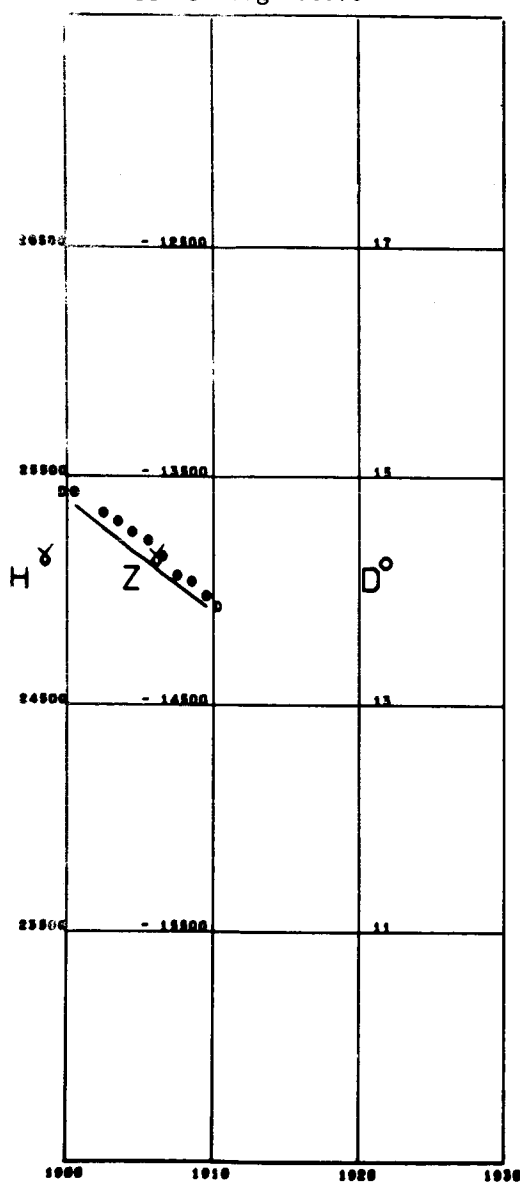


SAN JUAN  
Lat 18.11 Long -66.15 Alt 0.40



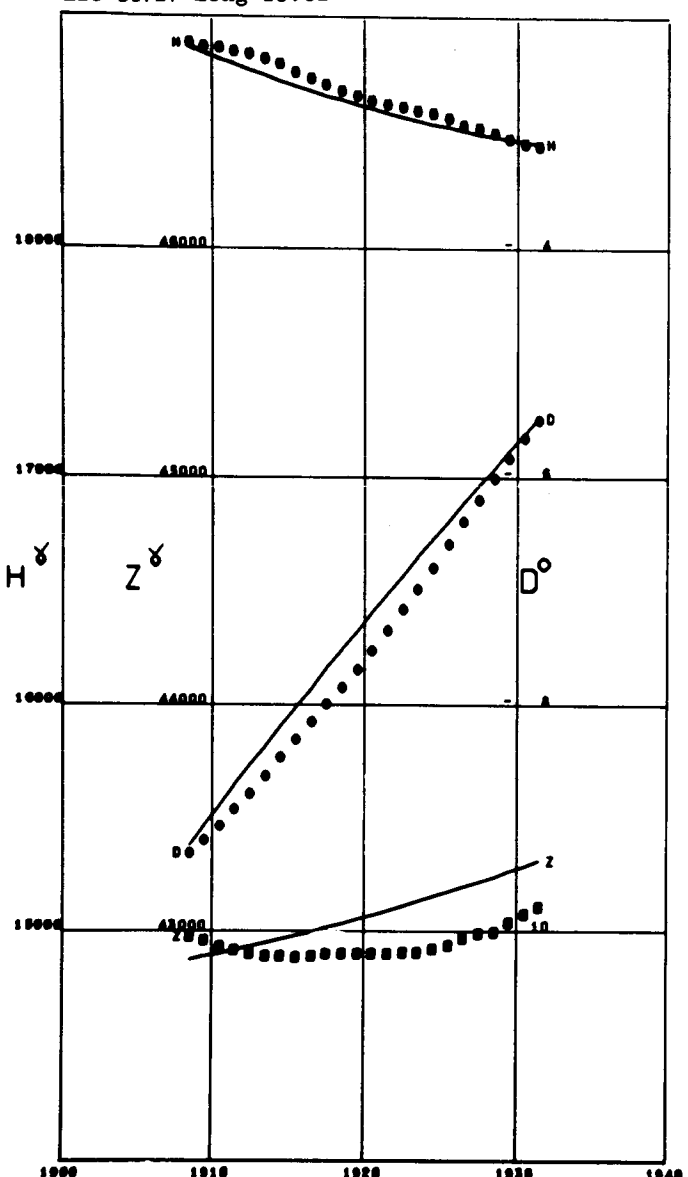
SANTIAGO

Lat -33.45 Long -70.70

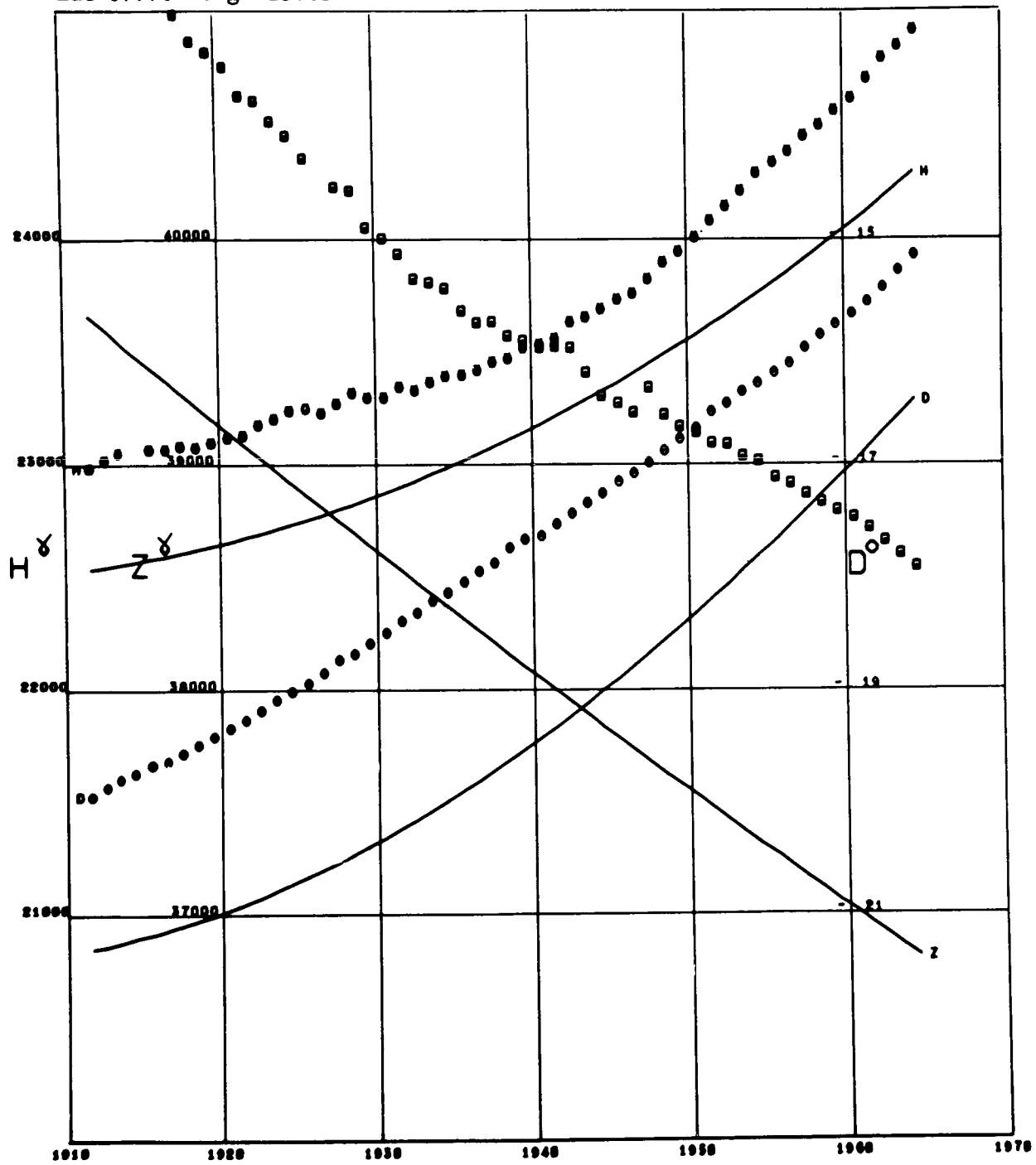


SEDDIN

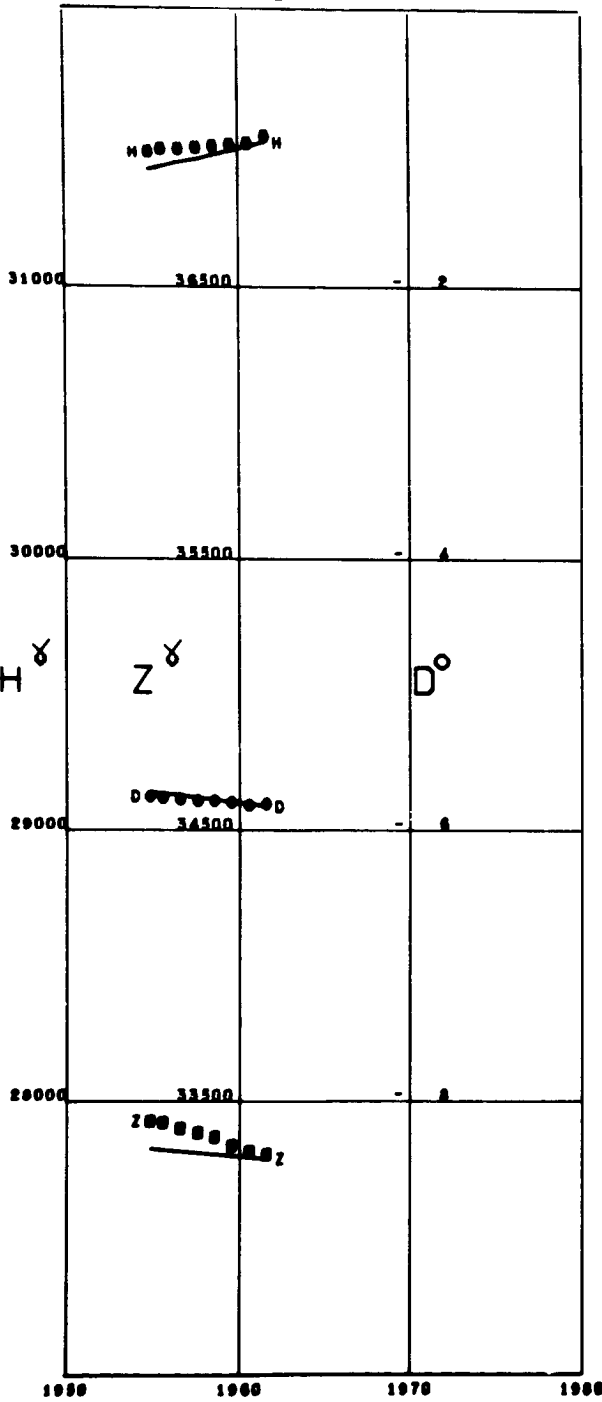
Lat 52.27 Long 13.01



SAN MIGUEL  
Lat 37.76 Long -25.65

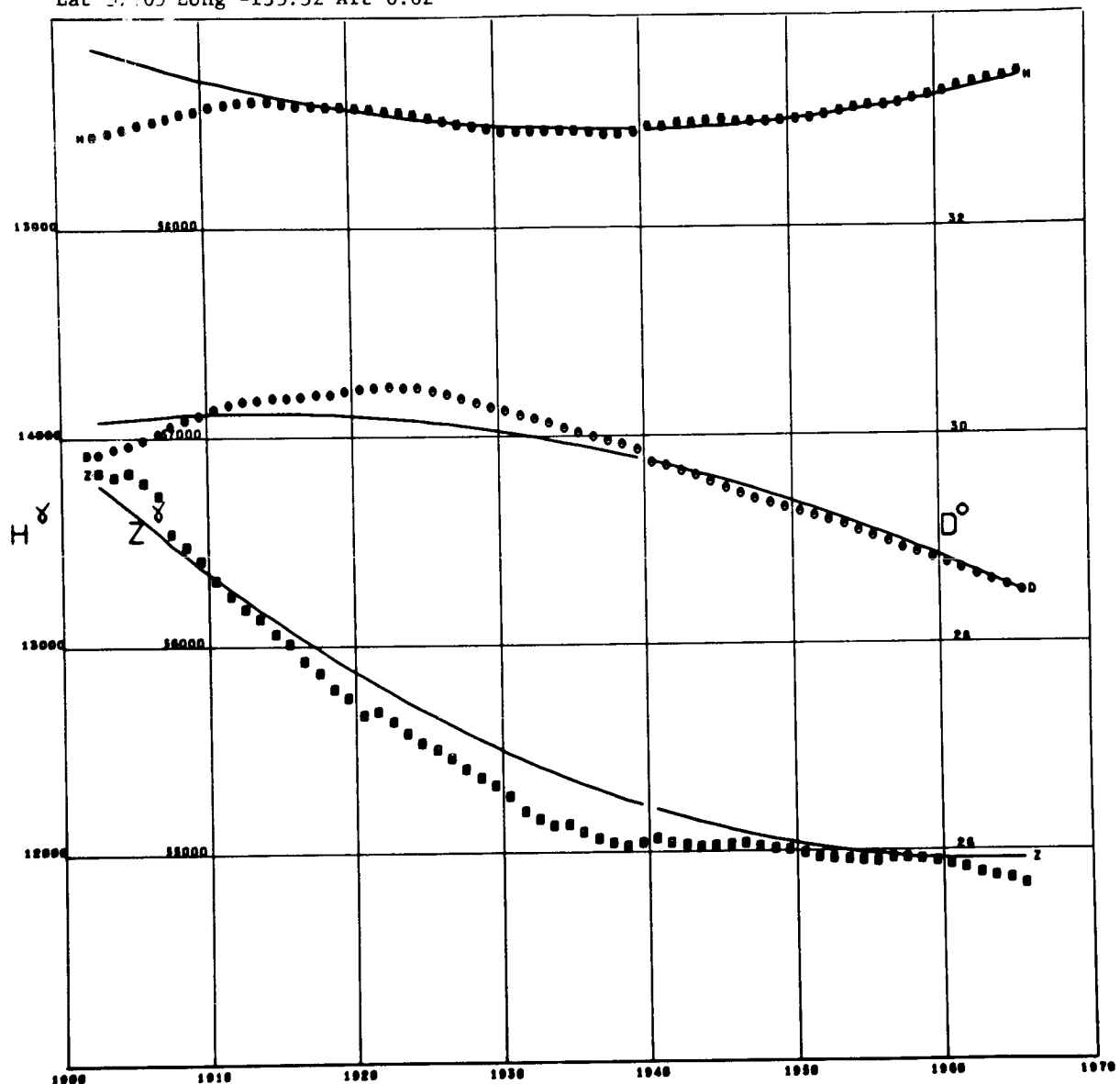


SIMOSATO  
Lat 33.57 Long 135.94

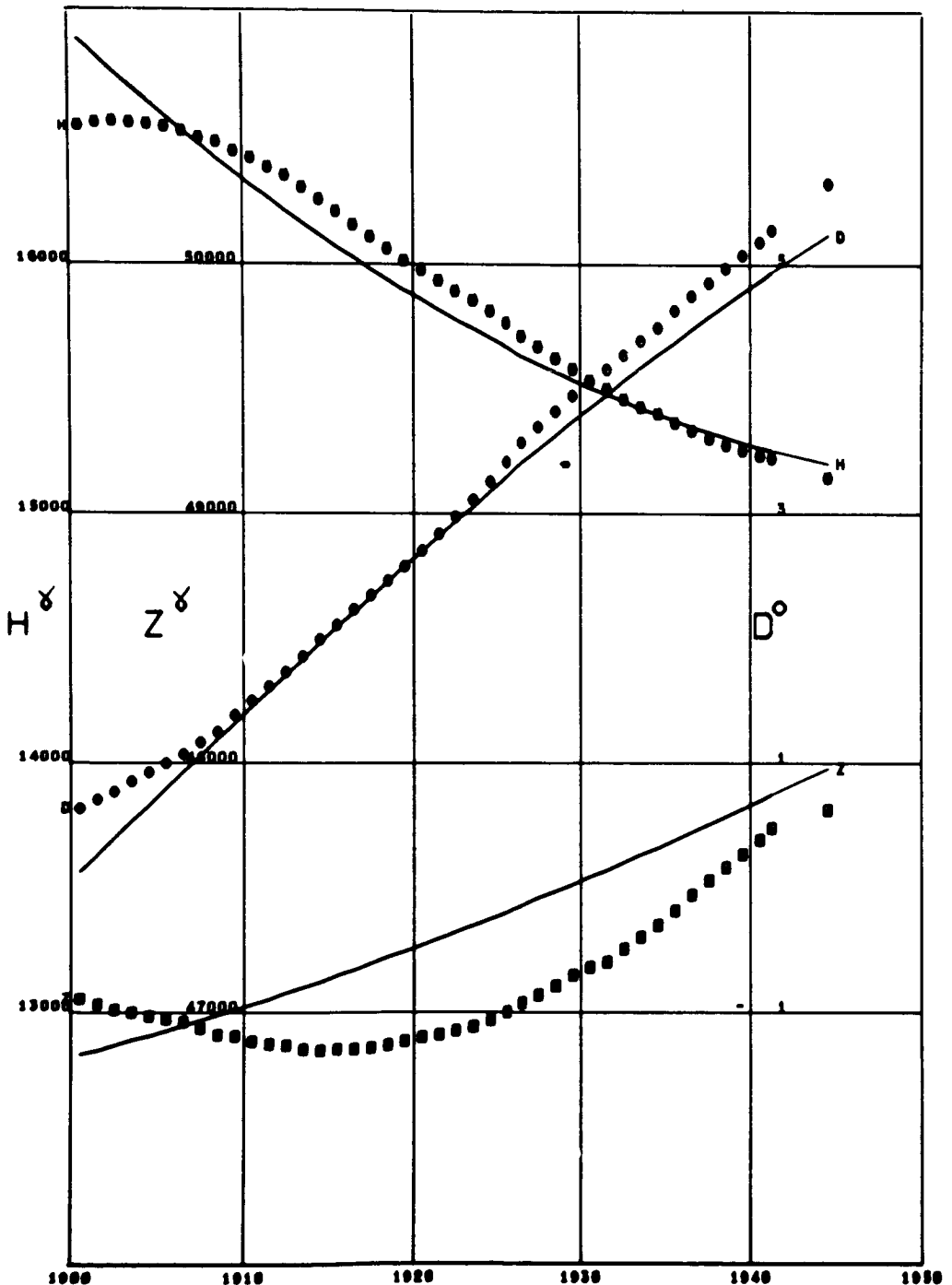


SITKA

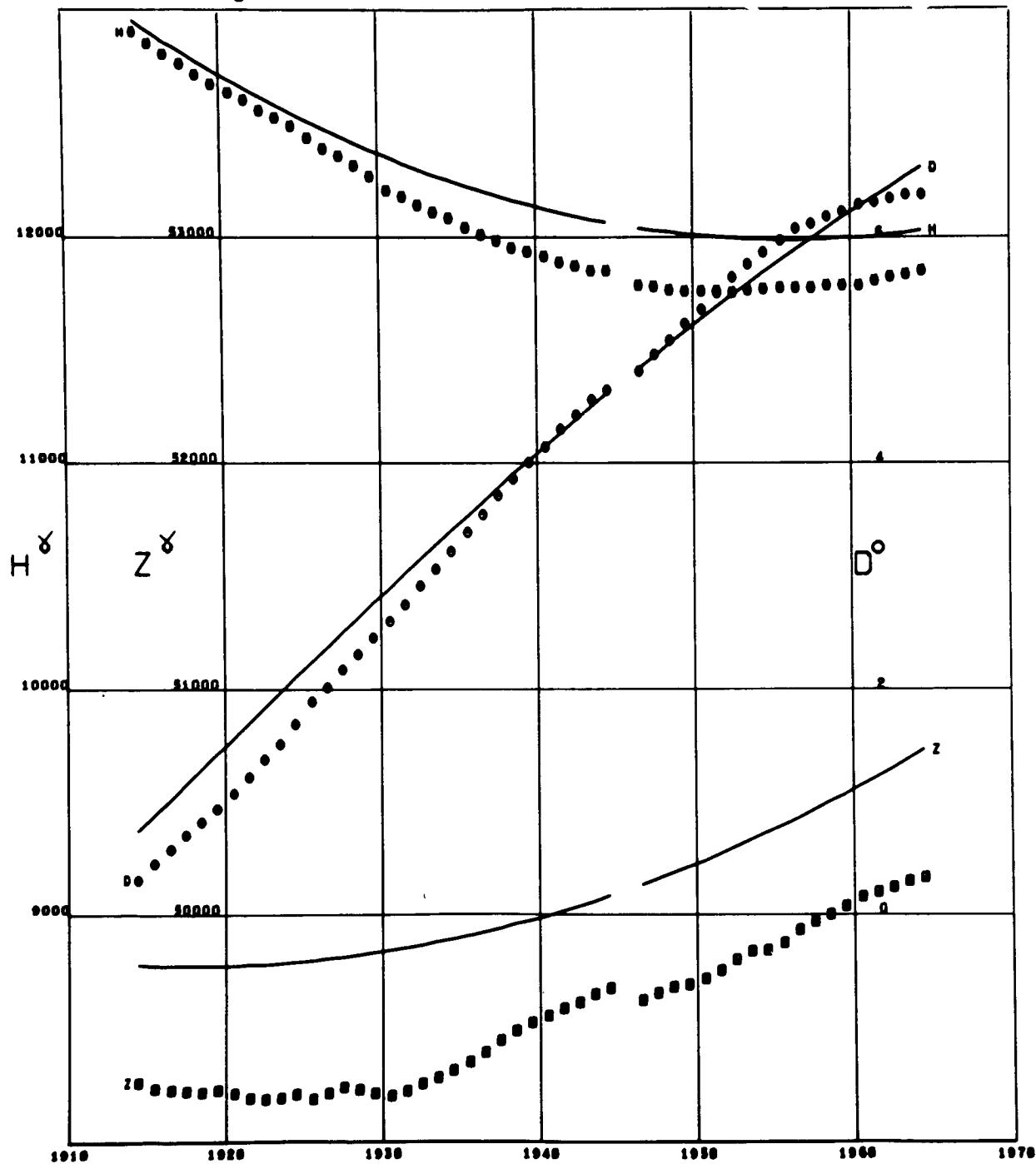
Lat 51.05 Long -135.32 Alt 0.02



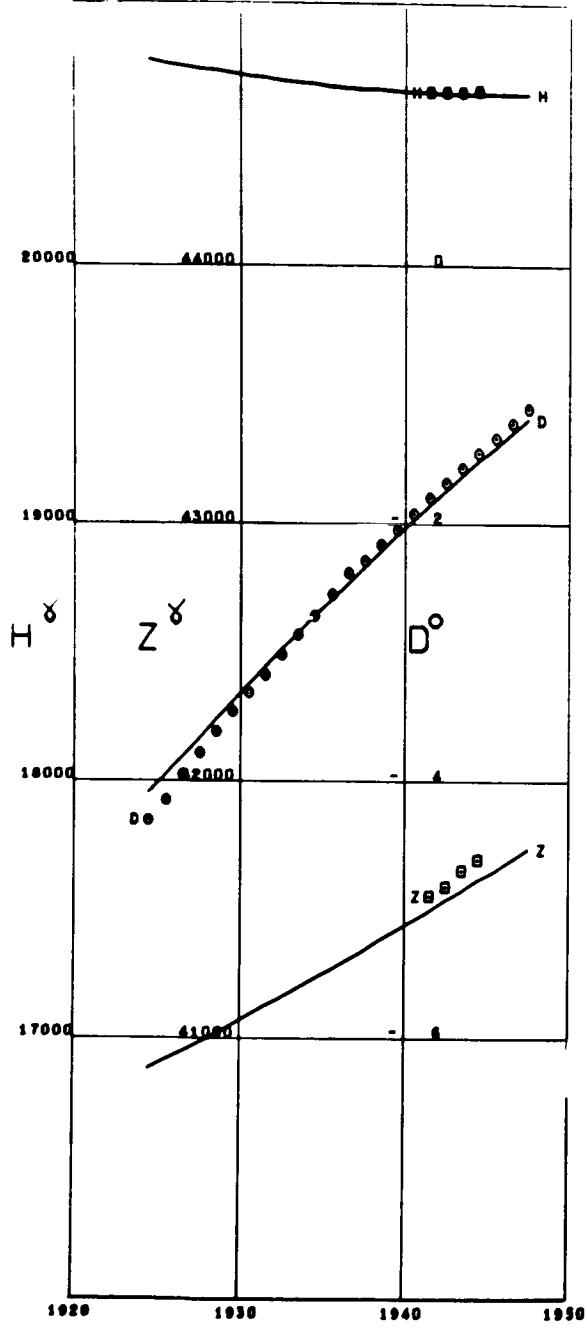
SLUTZK  
Lat 59.68 Long 30.48



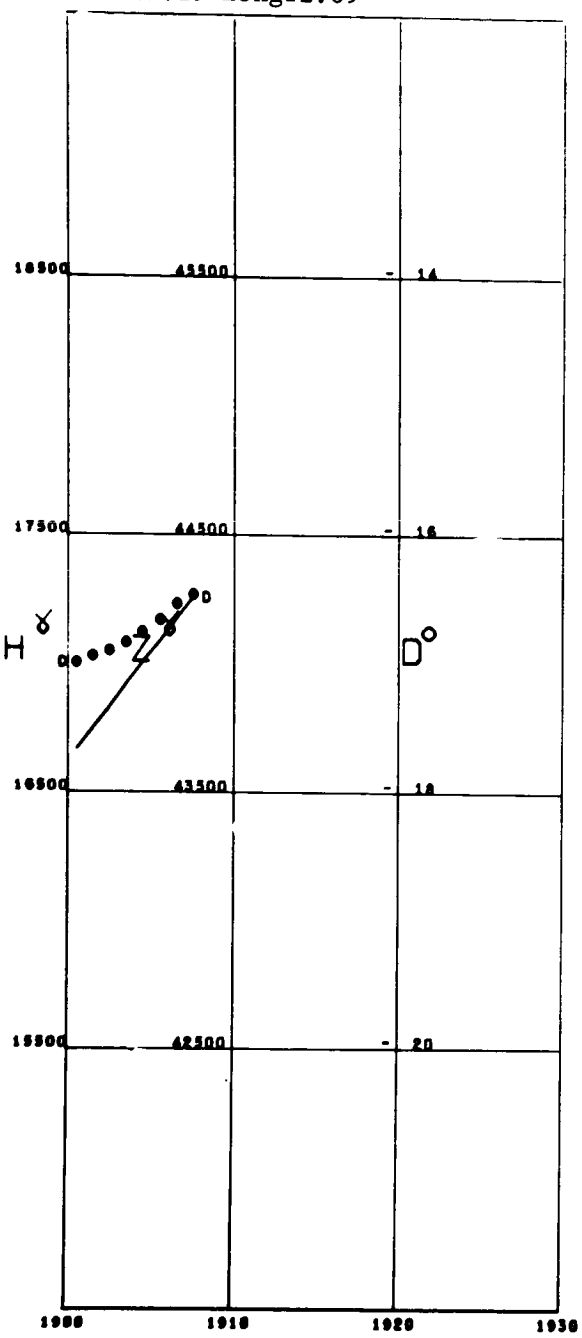
SODANKYLA  
Lat 67.36 Long 26.63



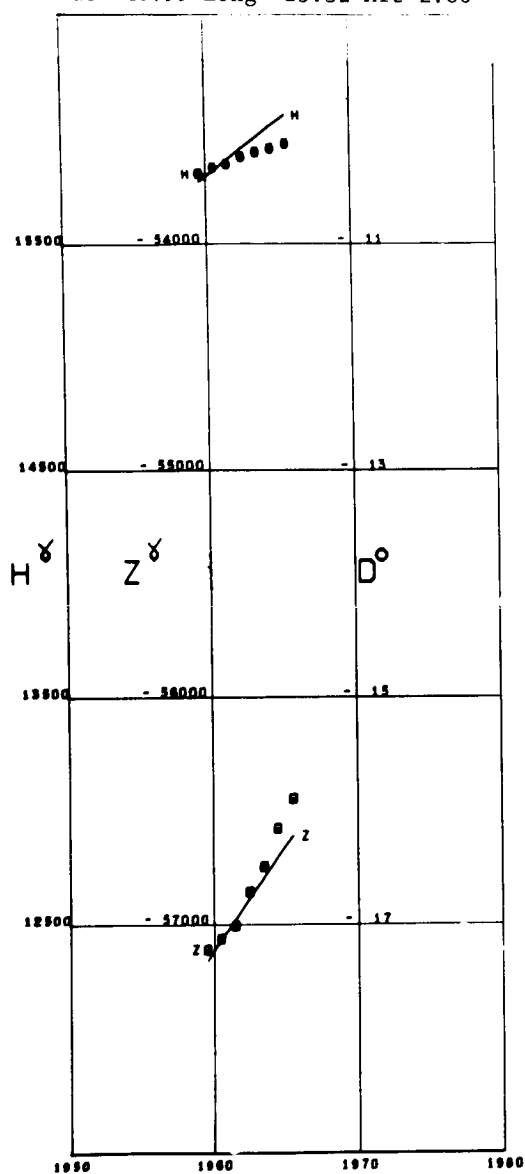
STARA DALA  
Lat 47.87 Long 18.19



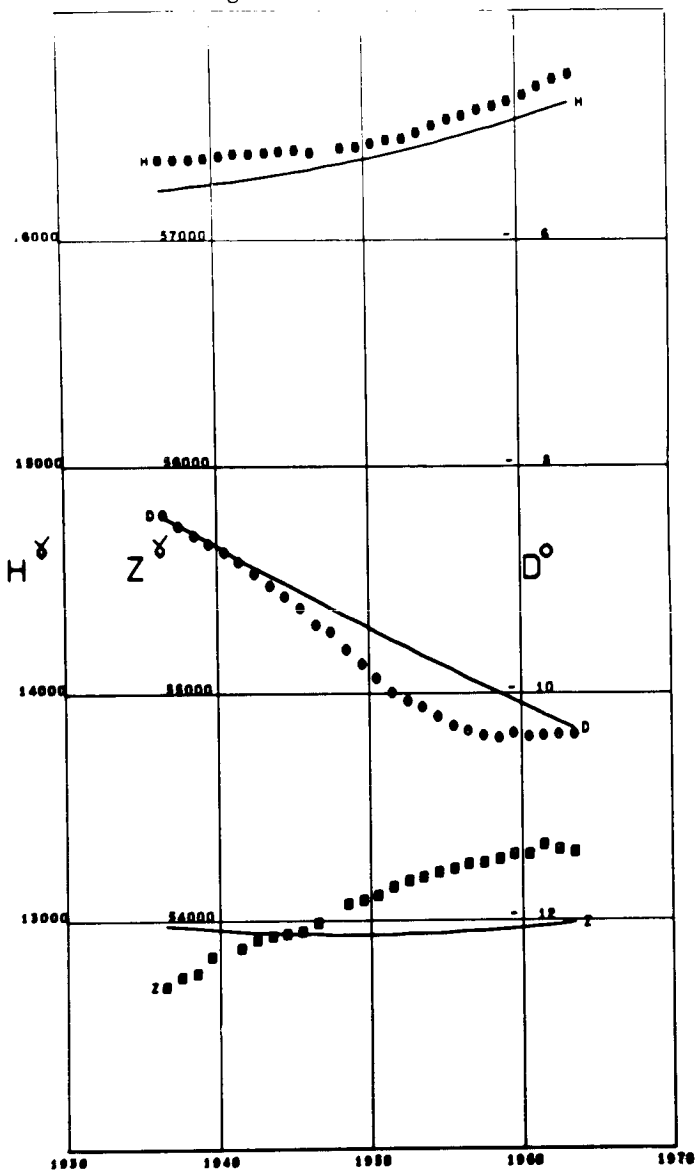
ST. HELIER  
Lat 49.19 Long -2.09



SOUTH POLE  
Lat -89.99 Long -13.32 Alt 2.80

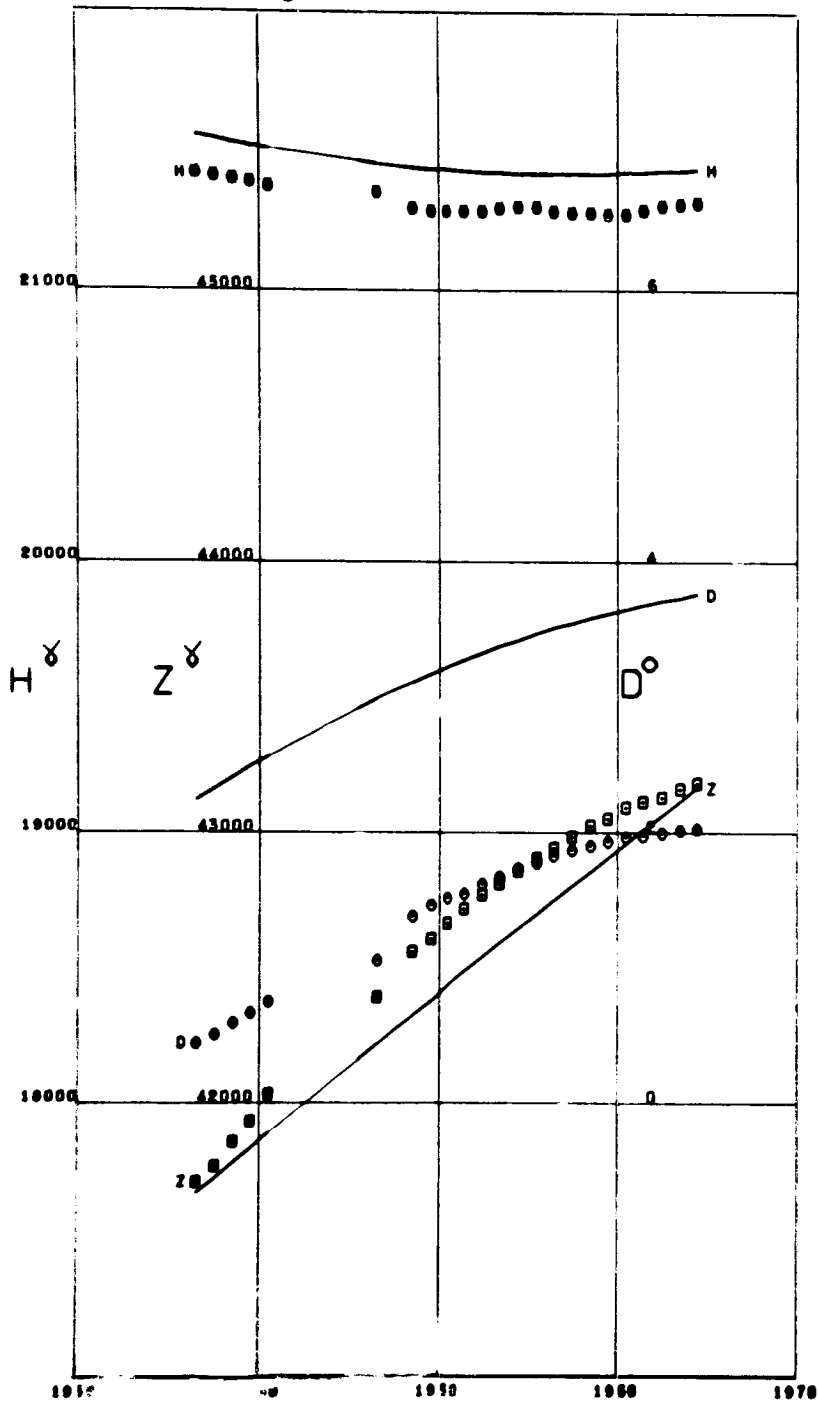


SREDNIKAN  
Lat 62.44 Long 152.31



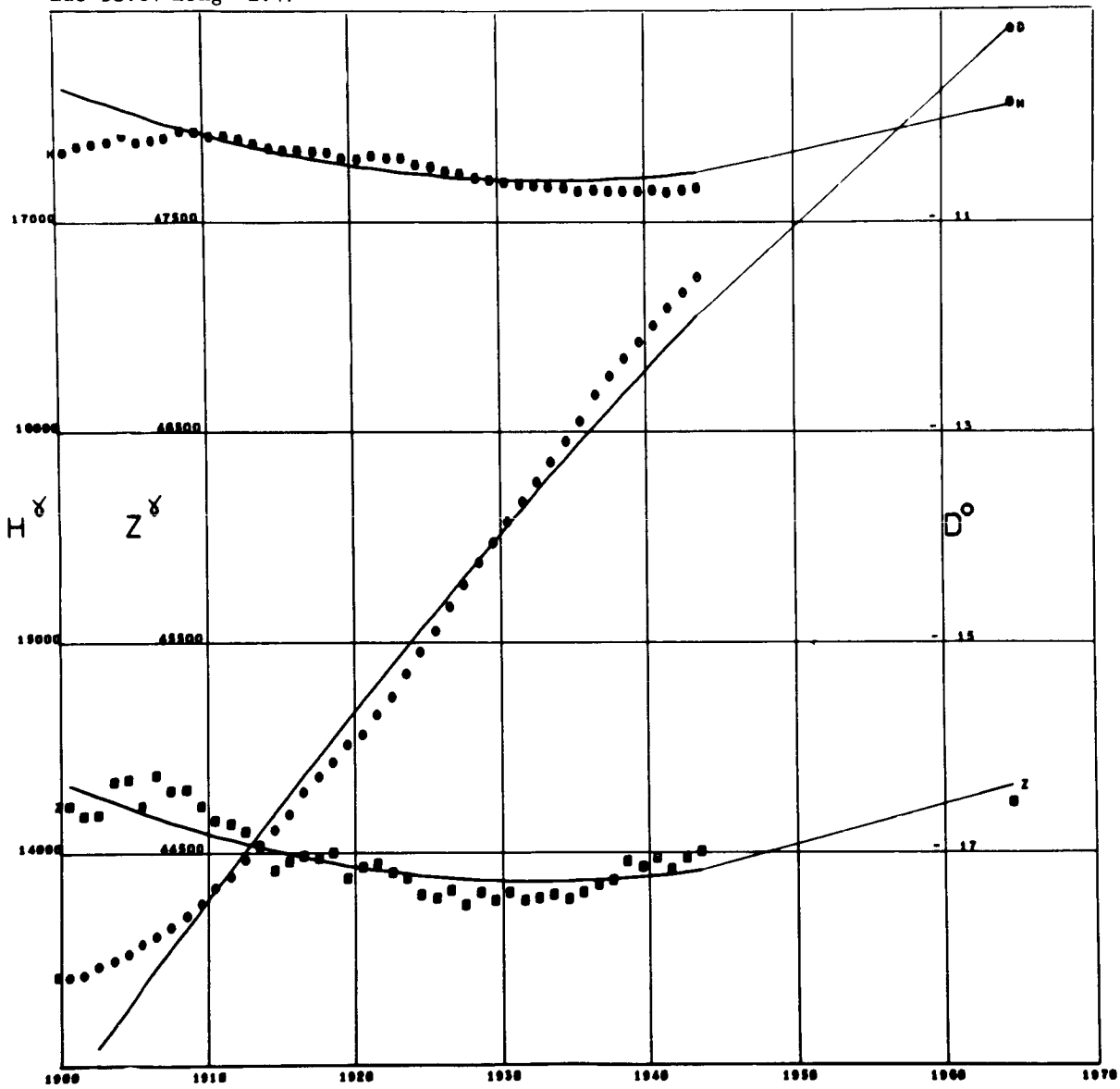
STEPANOVKA

Lat 46.78 Long 30.88 Alt 0.14



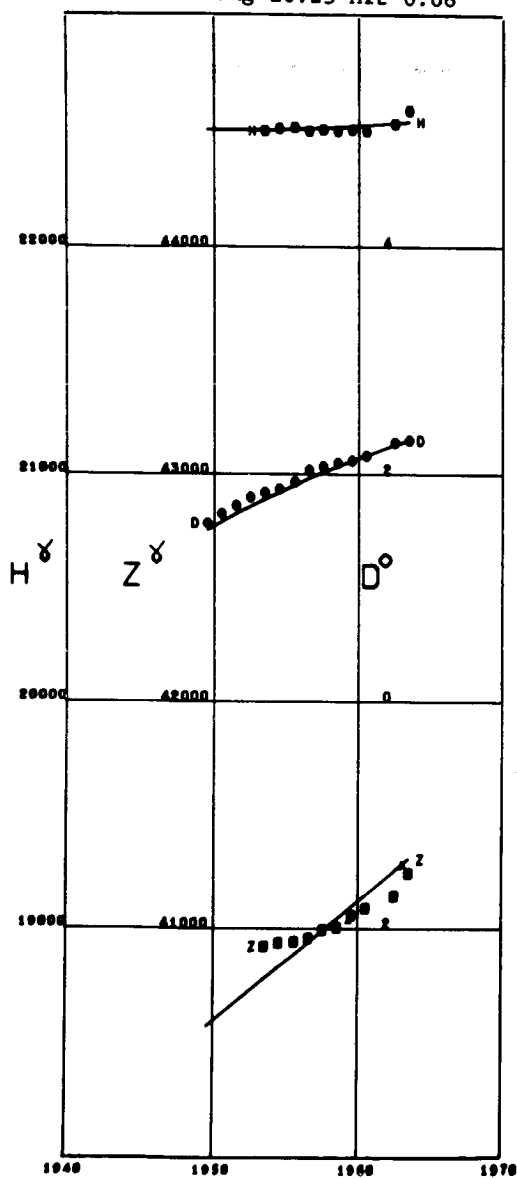
STONYHURST

Lat 53.84 Long -2.47



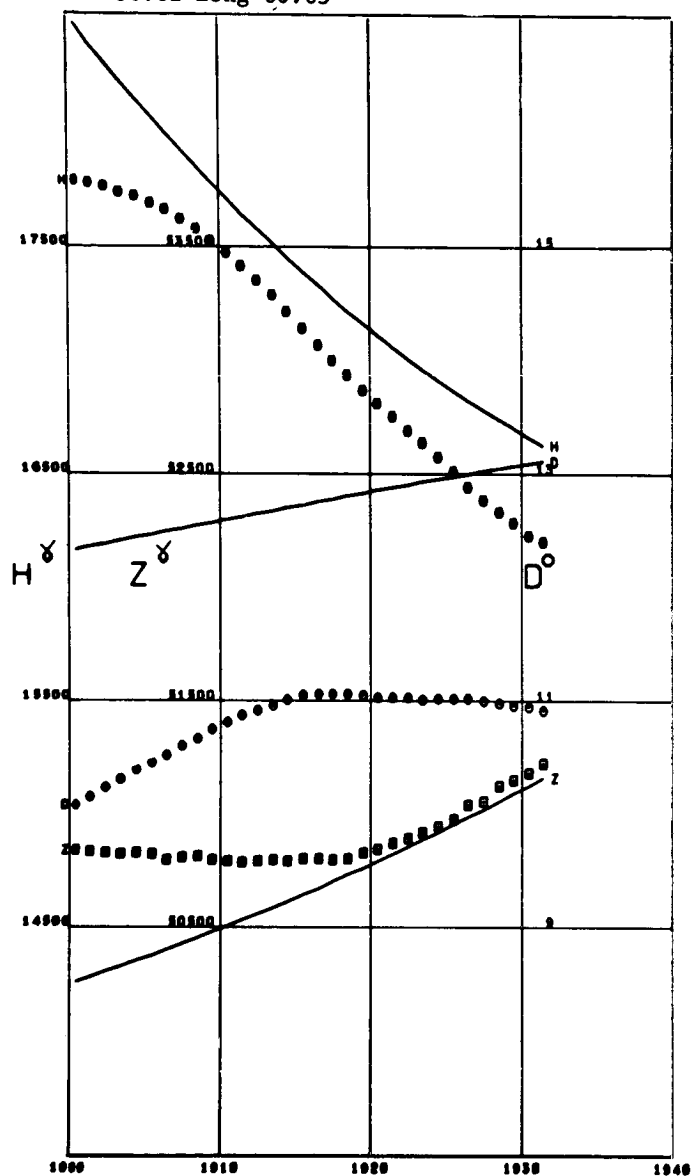
SURLARI

Lat 44.68 Long 26.25 Alt 0.08

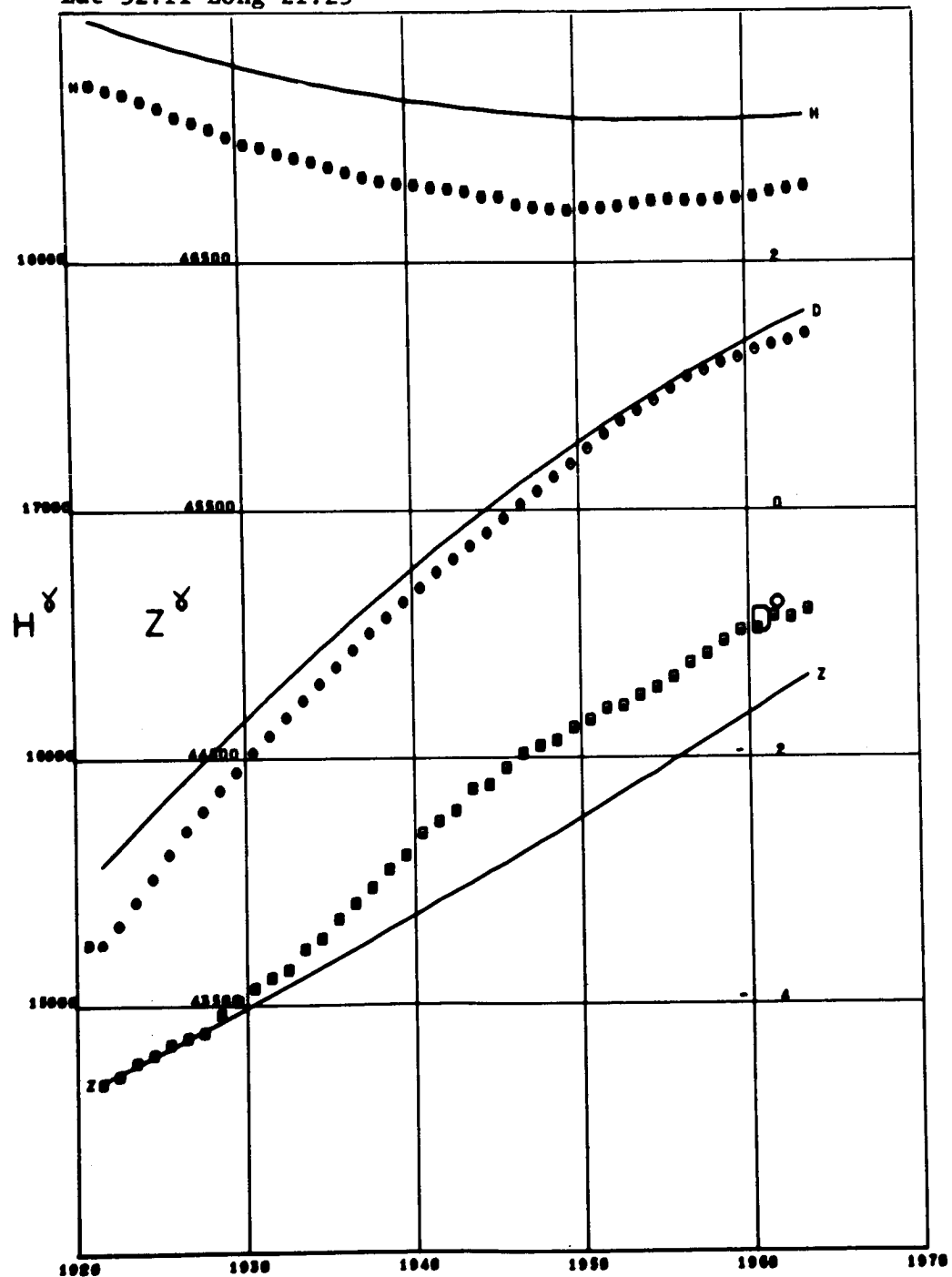


SVERDLOVSK

Lat 56.82 Long 60.63

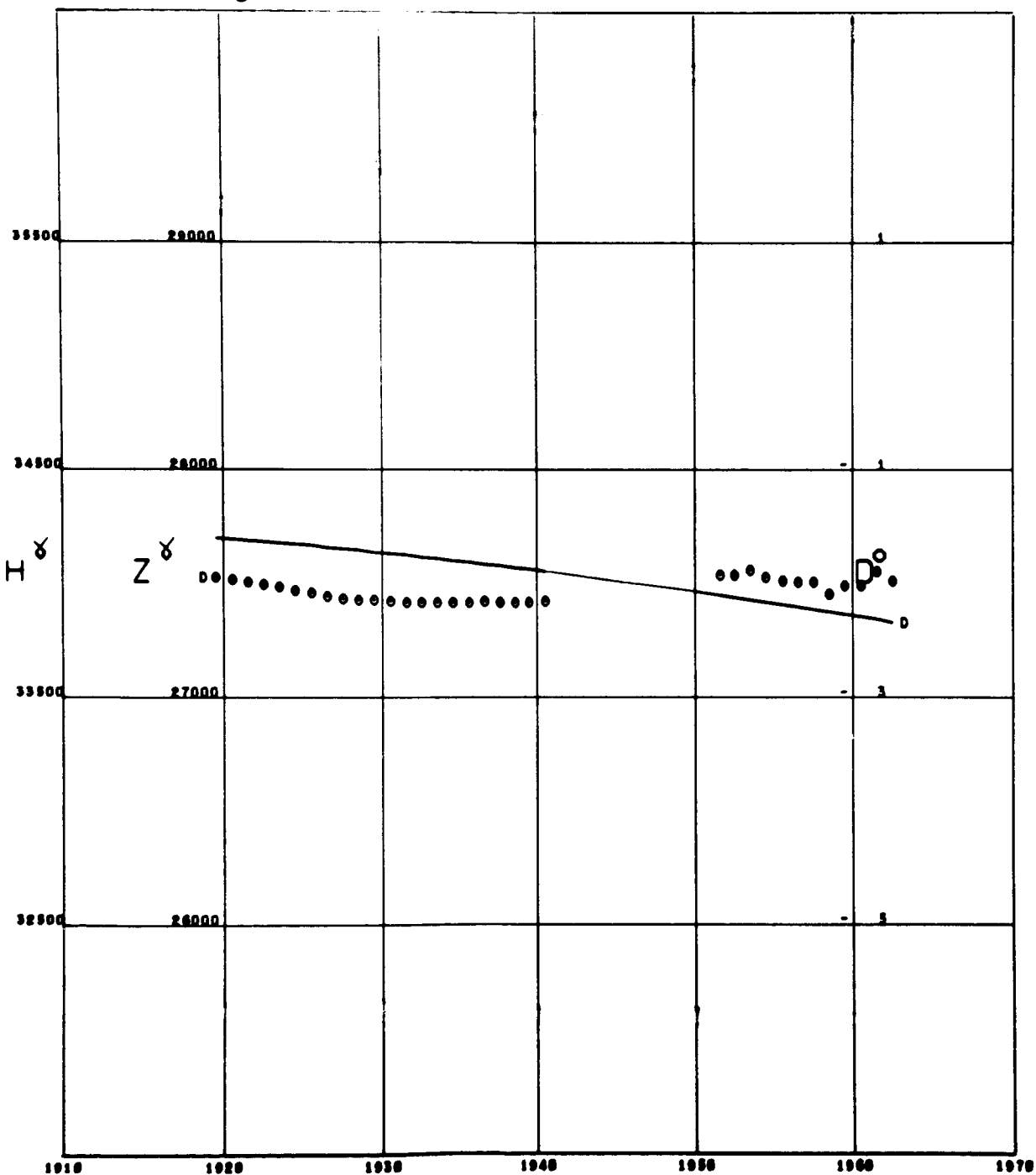


**SWIDER**  
Lat 52.11 Long 21.25

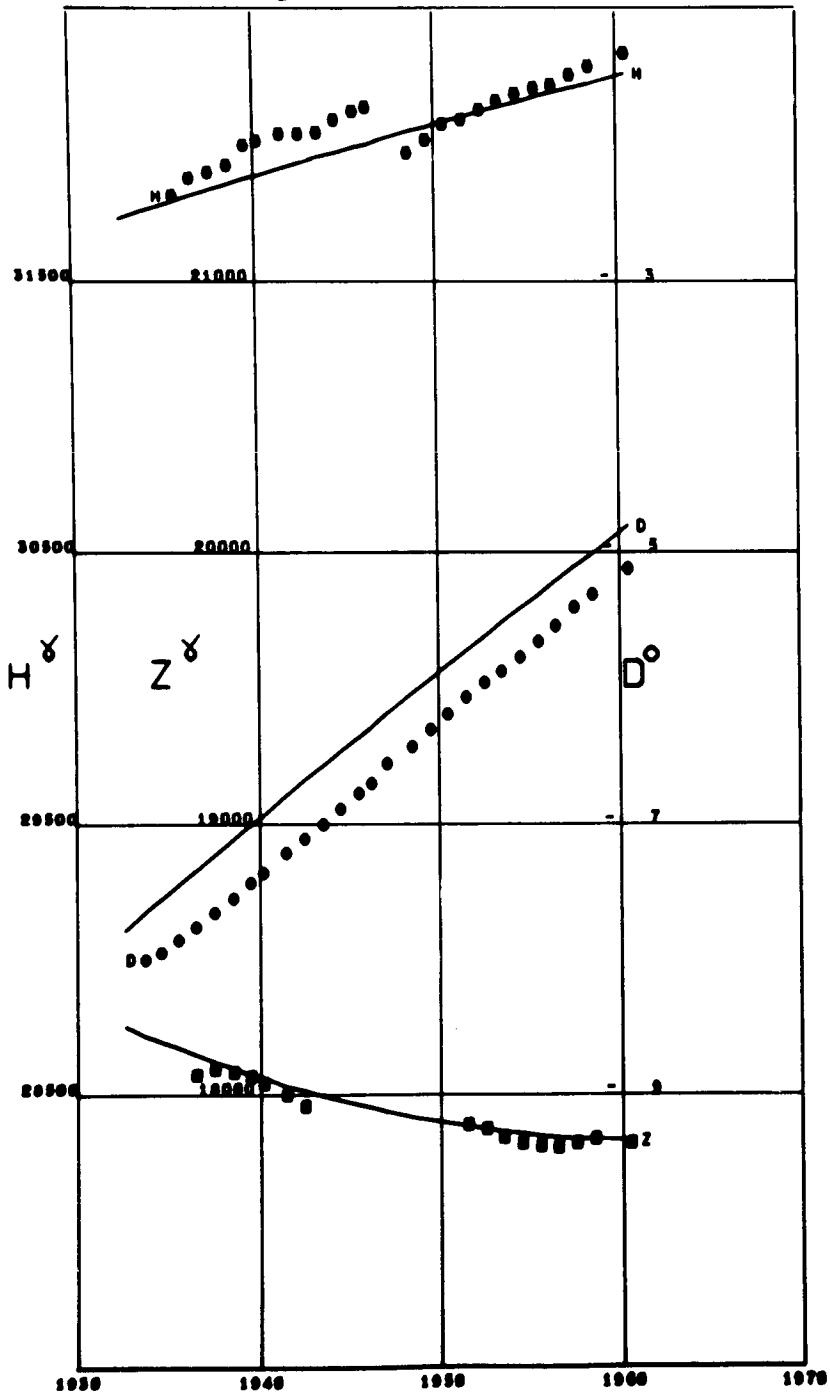


TAIPEI

Lat 25.03 Long 121.51

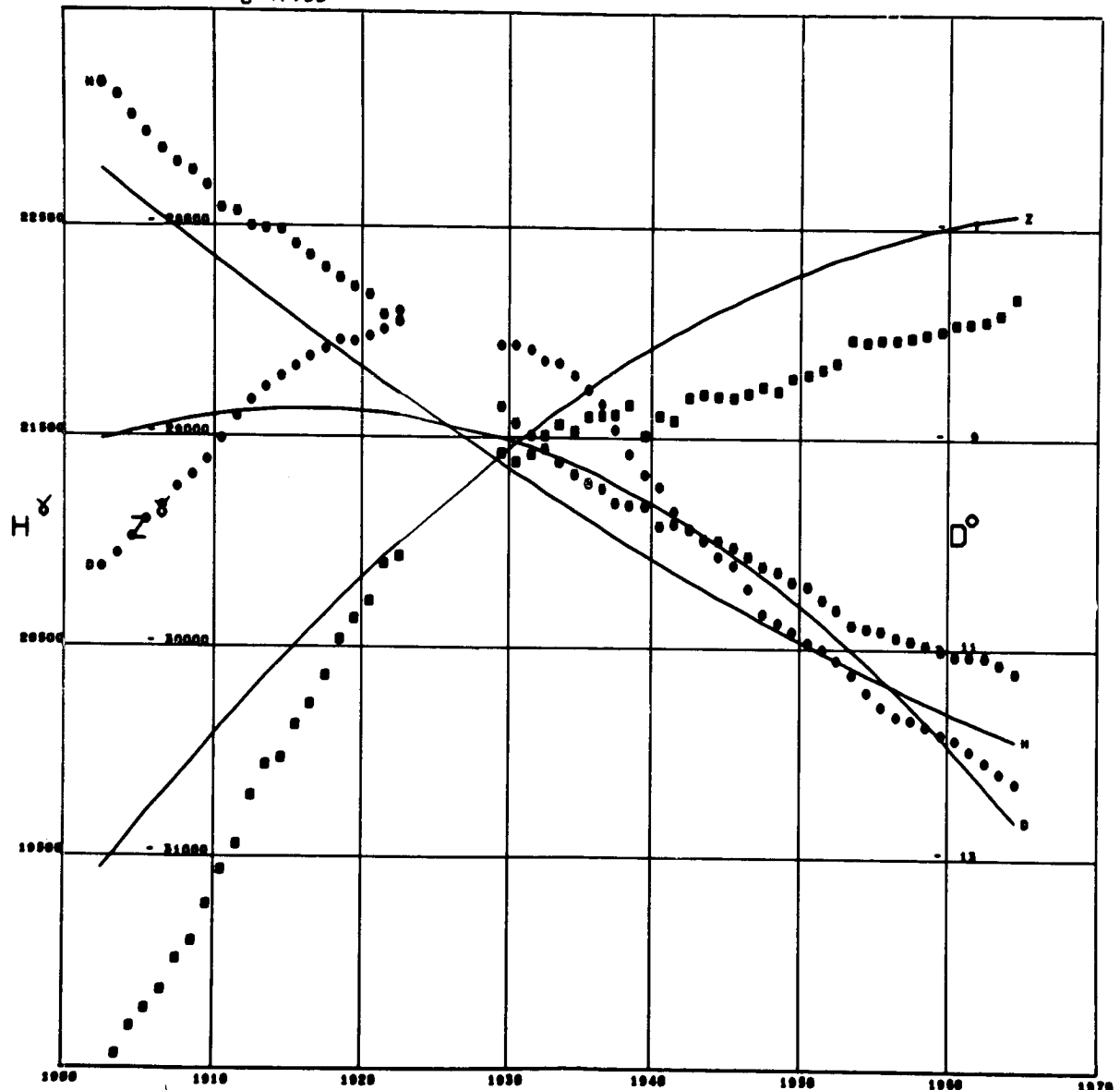


TAMANRASSET  
Lat 22.79 Long 5.52

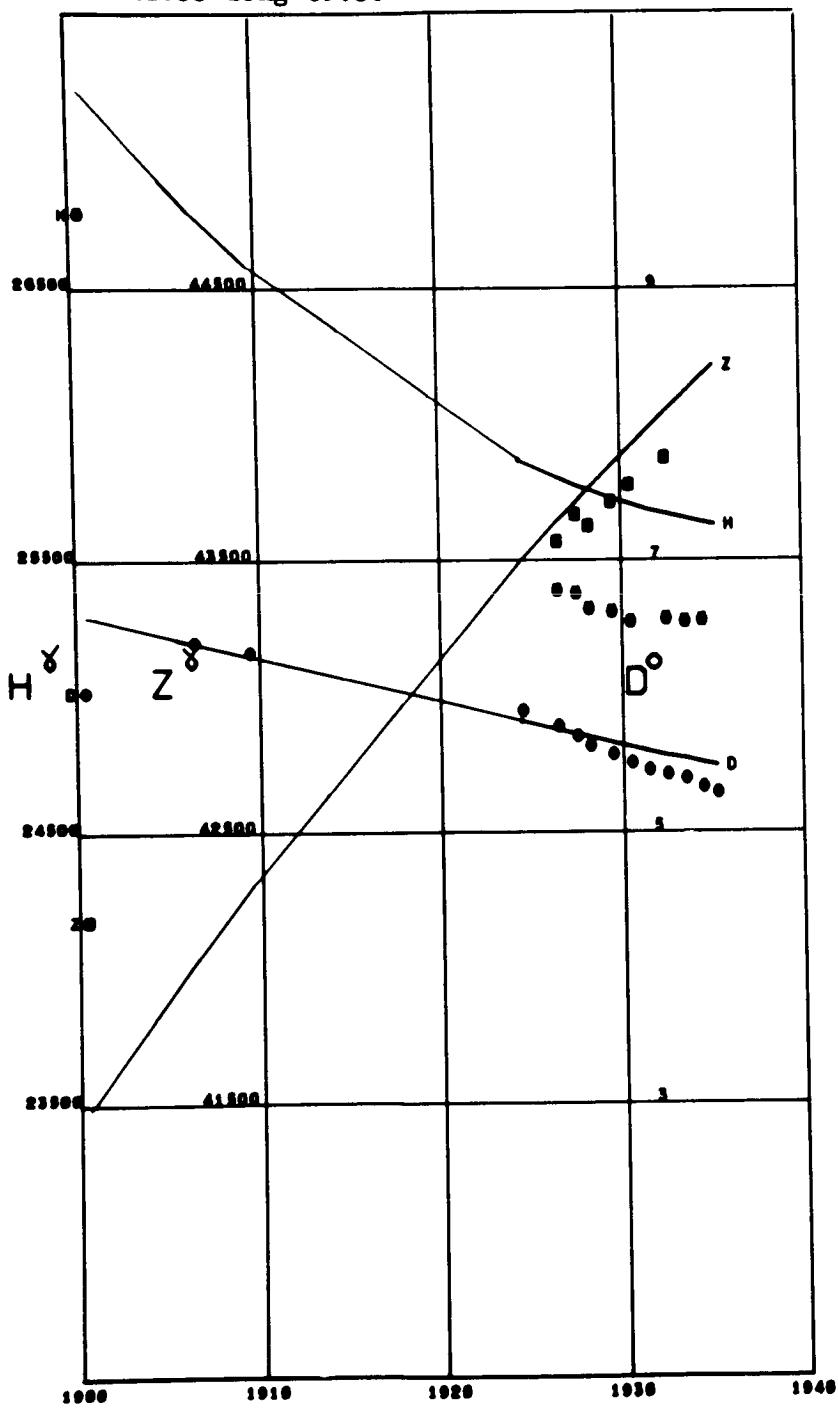


TANANARIVE

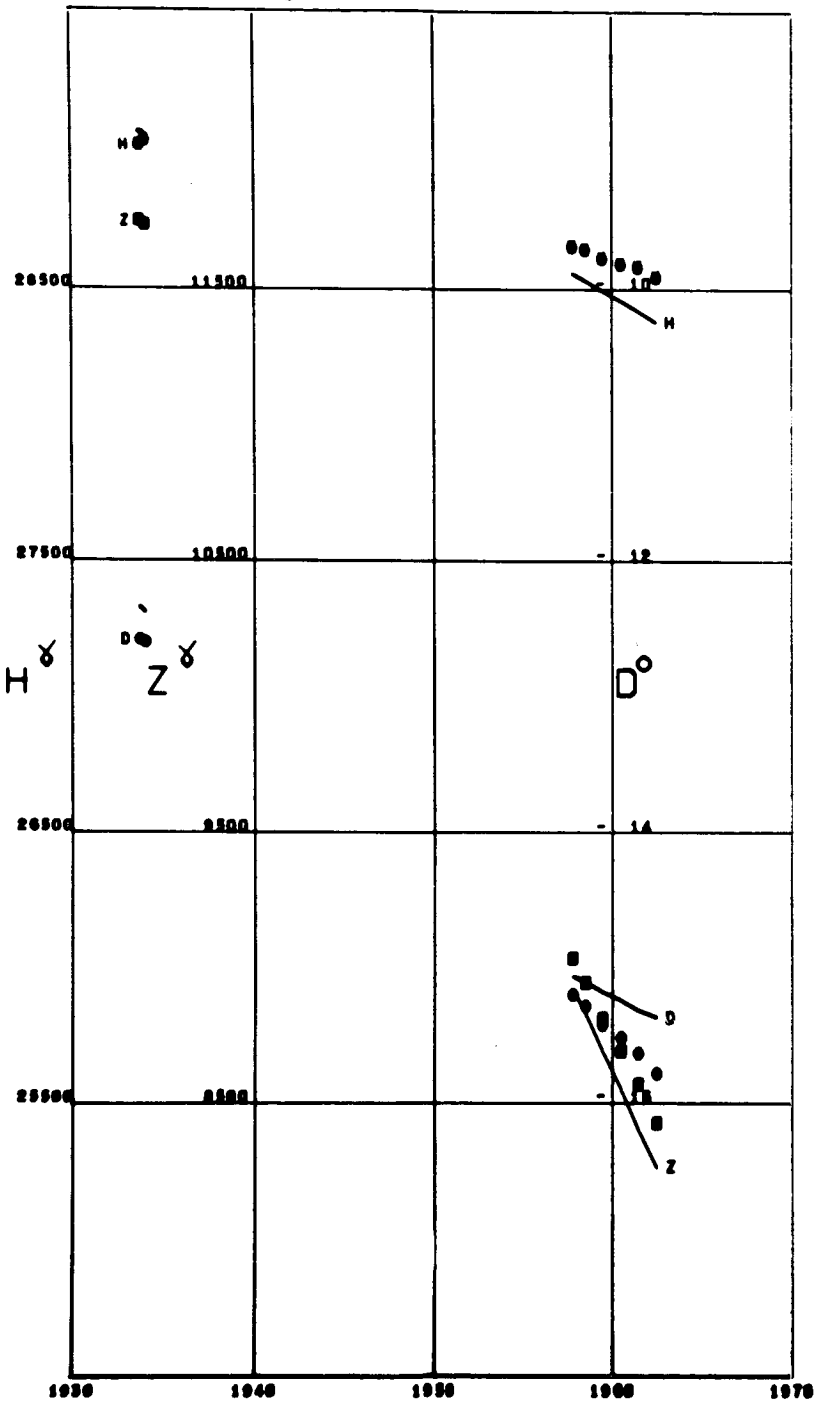
Lat -18.91 Long 47.55



TASHKENT  
Lat 41.33 Long 69.30

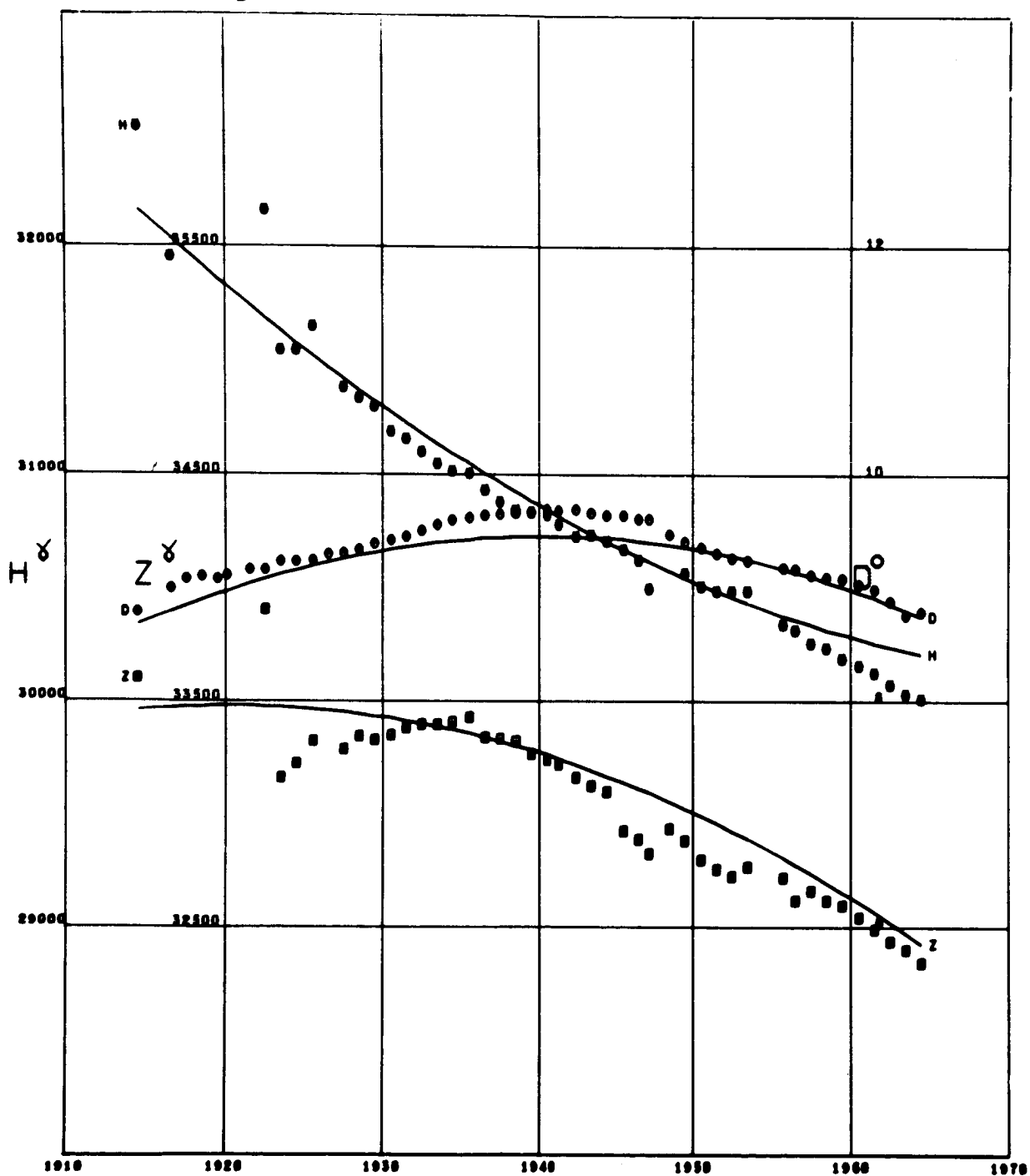


TATUOCA  
Lat -1.2° Long -48.51

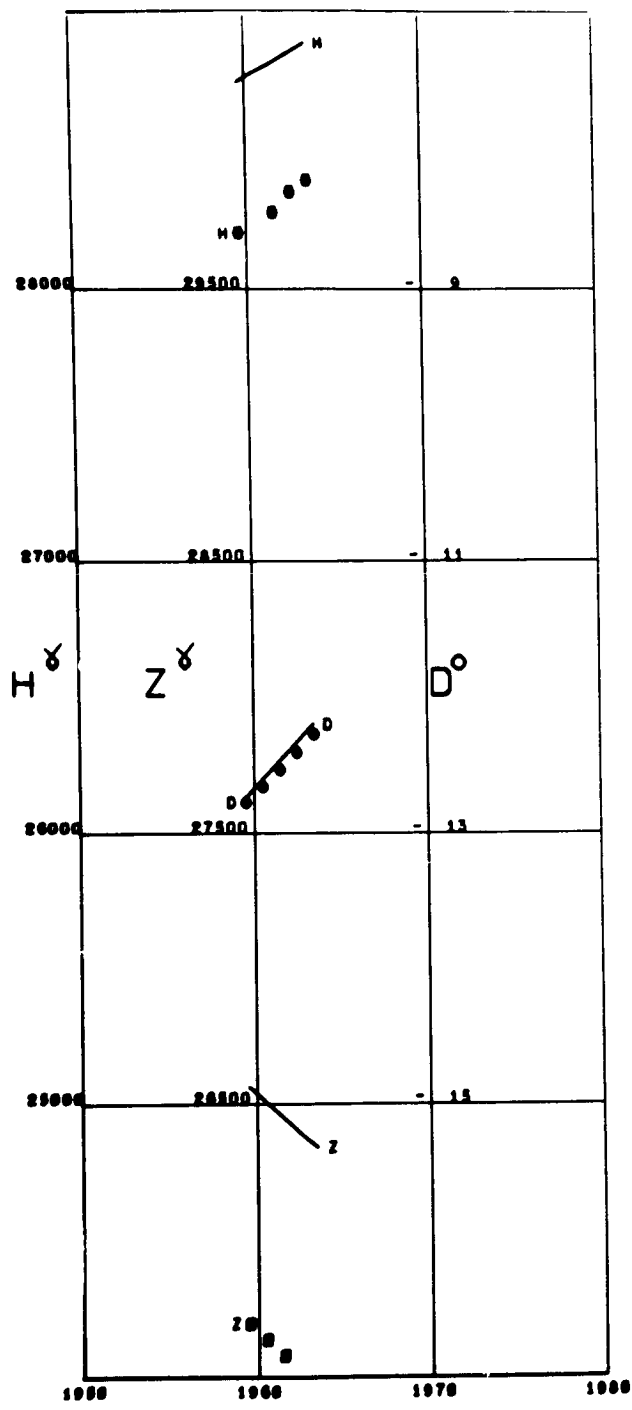


TEOLOYUCAN

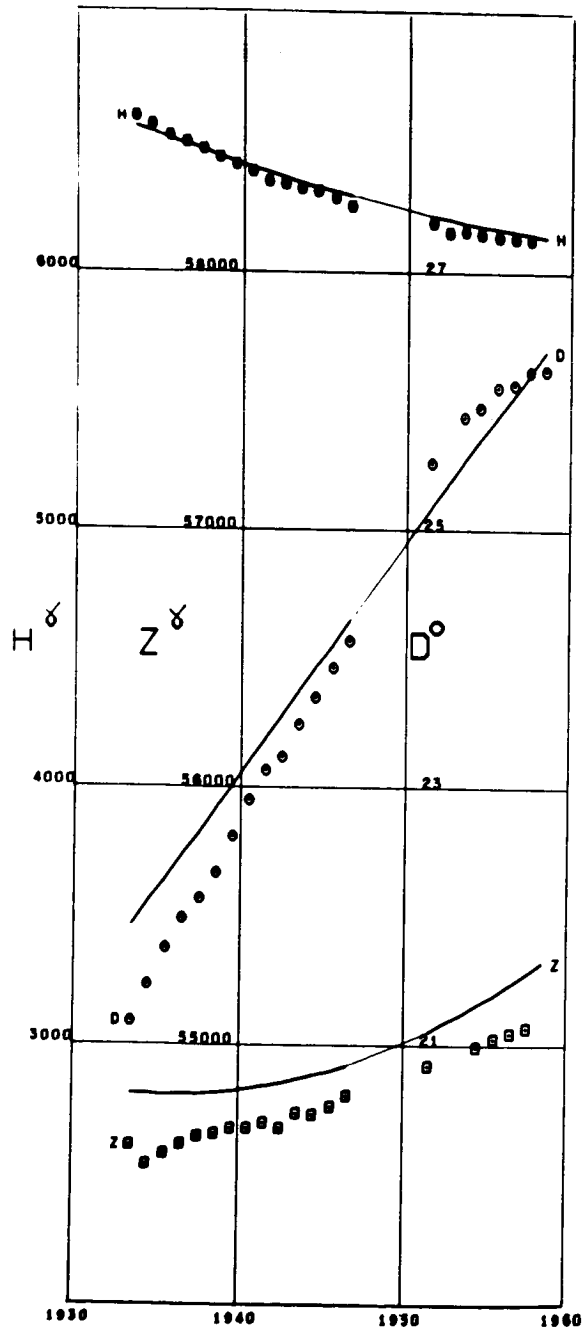
Lat 19.74 Long -99.18



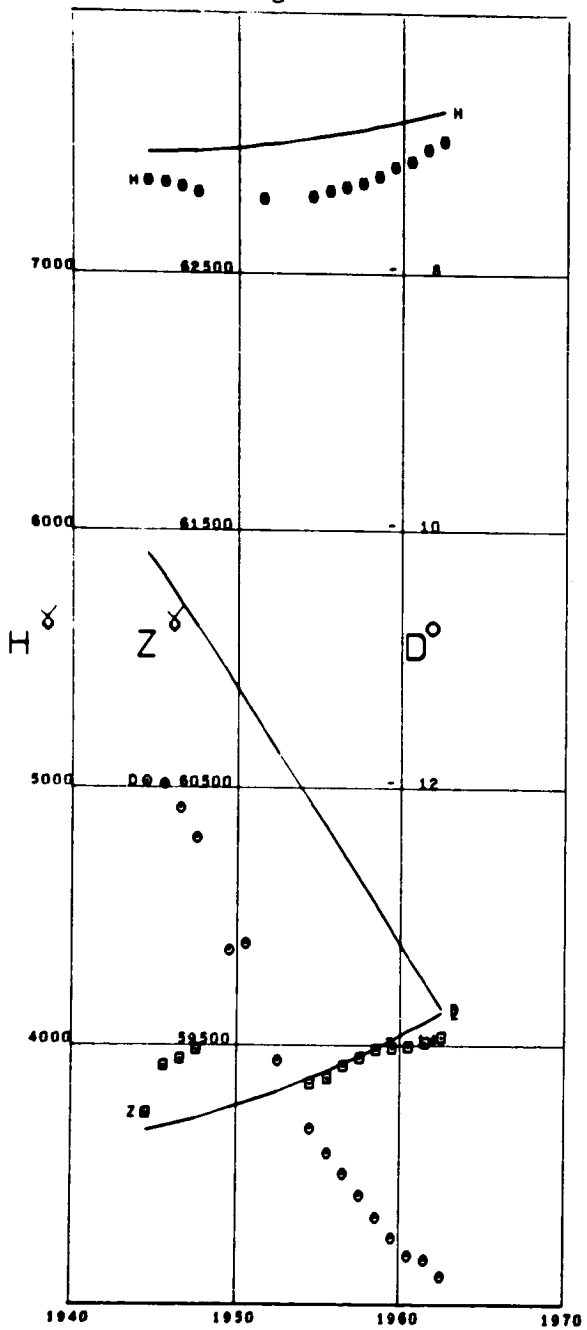
TENERIFE  
Lat 28.47 Long -16.27 Alt 0.40



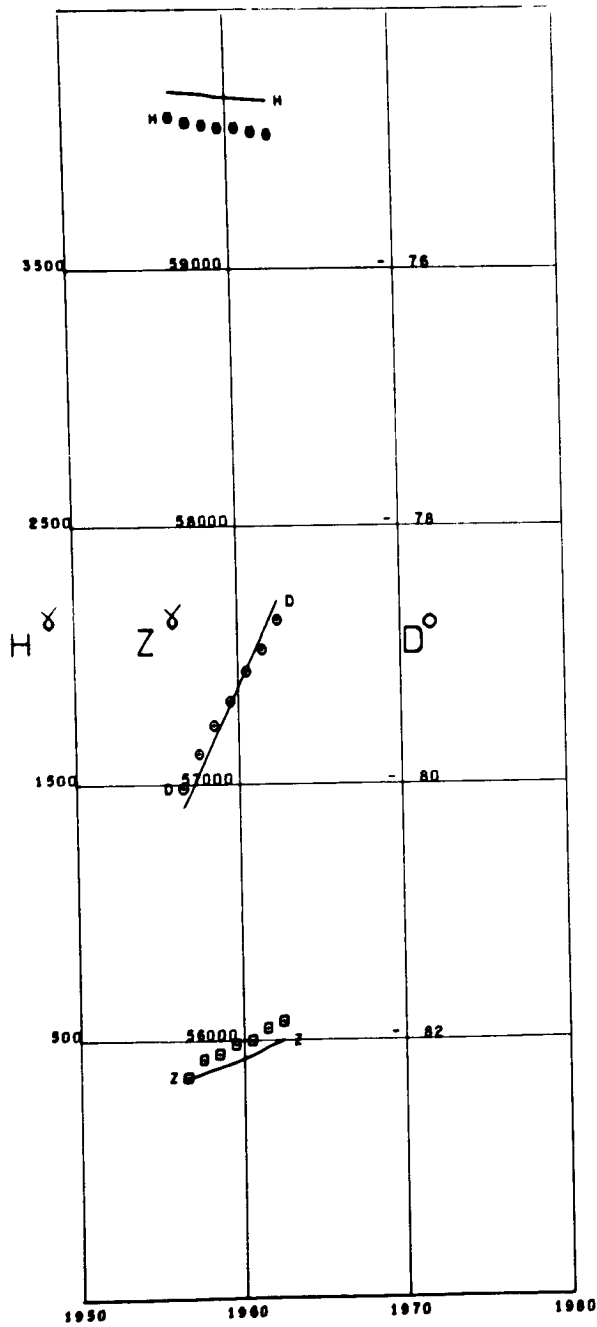
TIKHAYA BAY  
Lat 80.33 Long 52.80



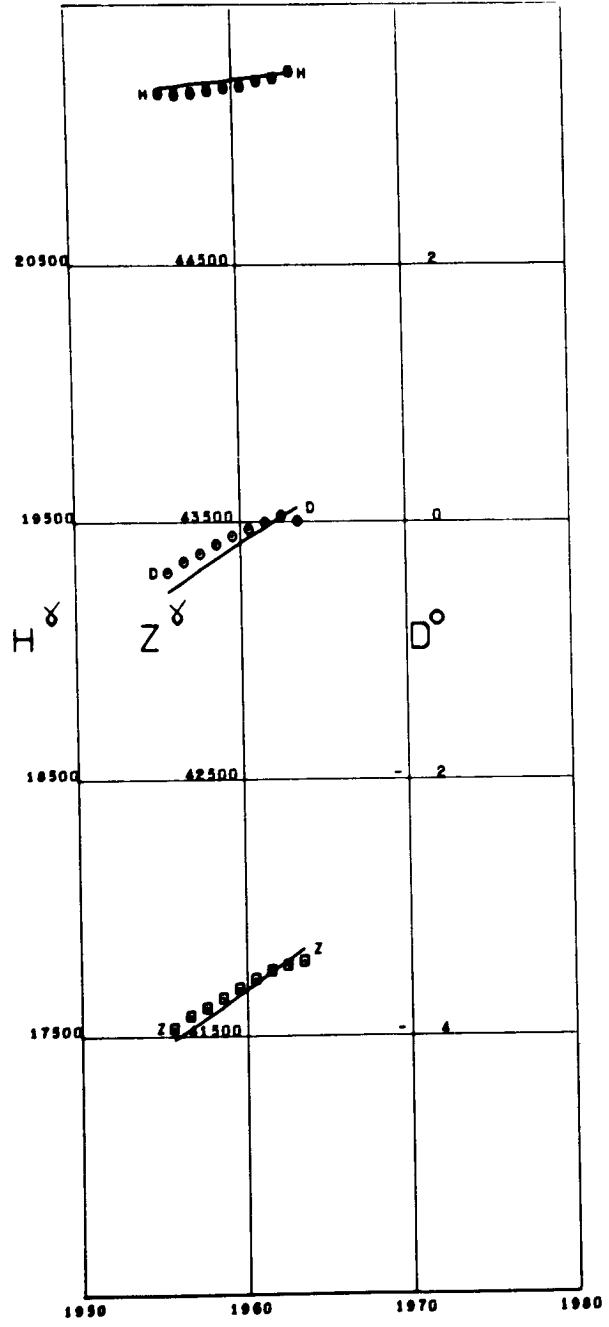
TIKSI  
Lat 71.58 Long 129.00



THULE II  
Lat 77.48 Long -69.16

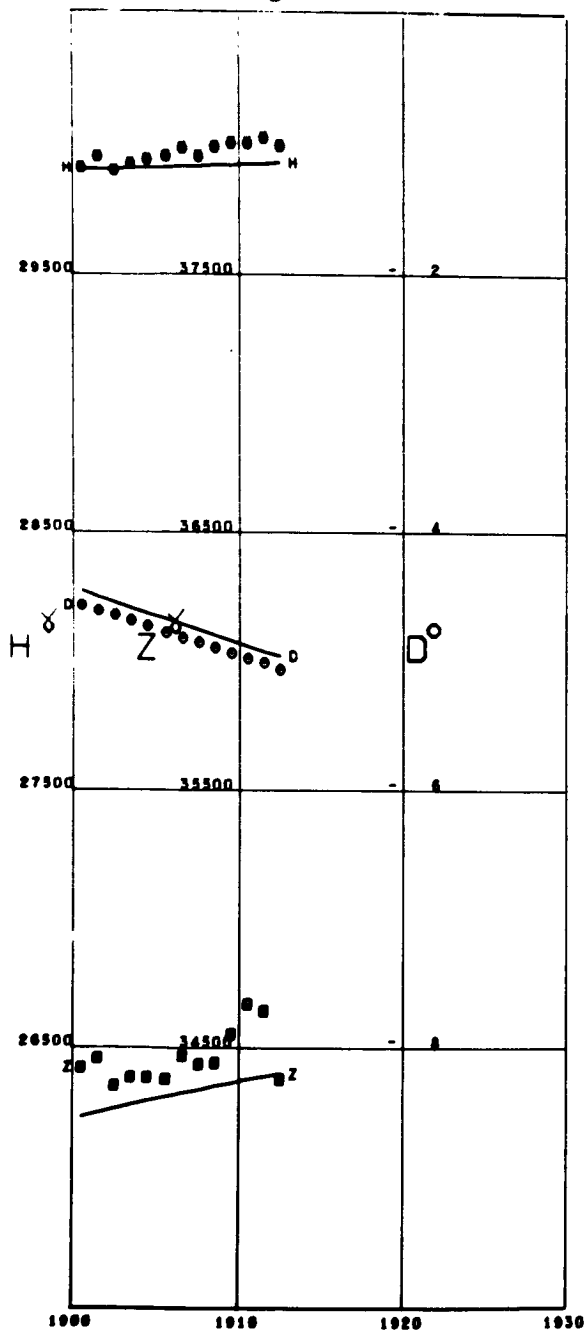


TIHANY  
Lat 46.90 Long 17.89



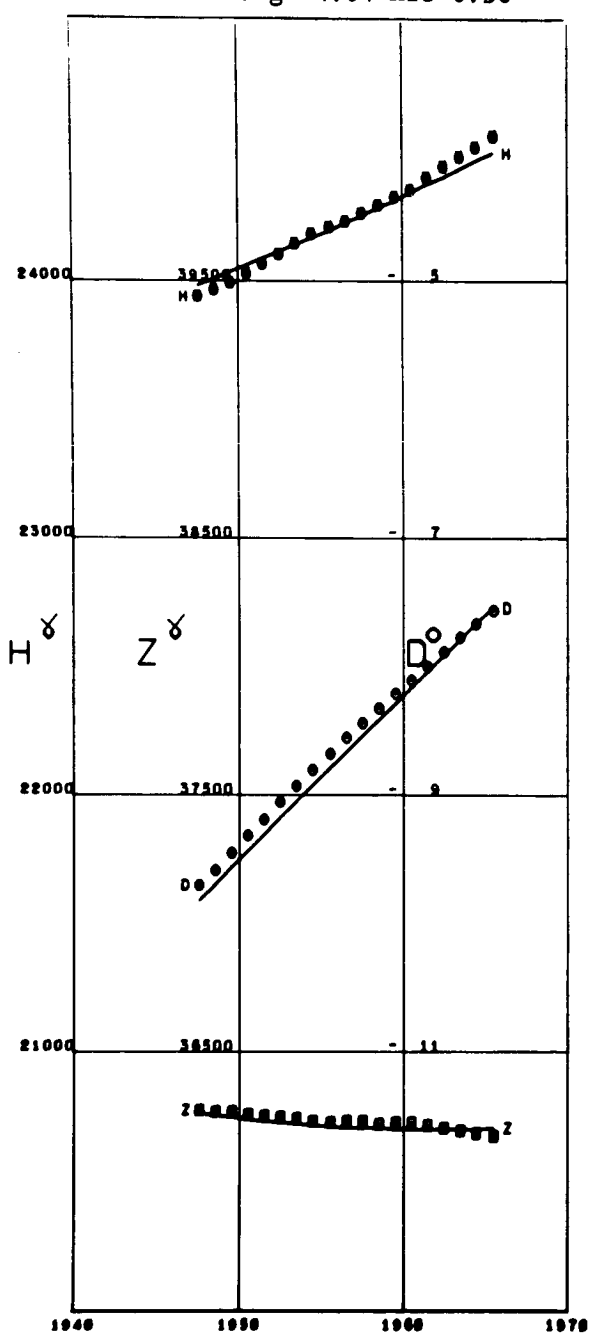
TOKYO

Lat 35.68 Long 139.75



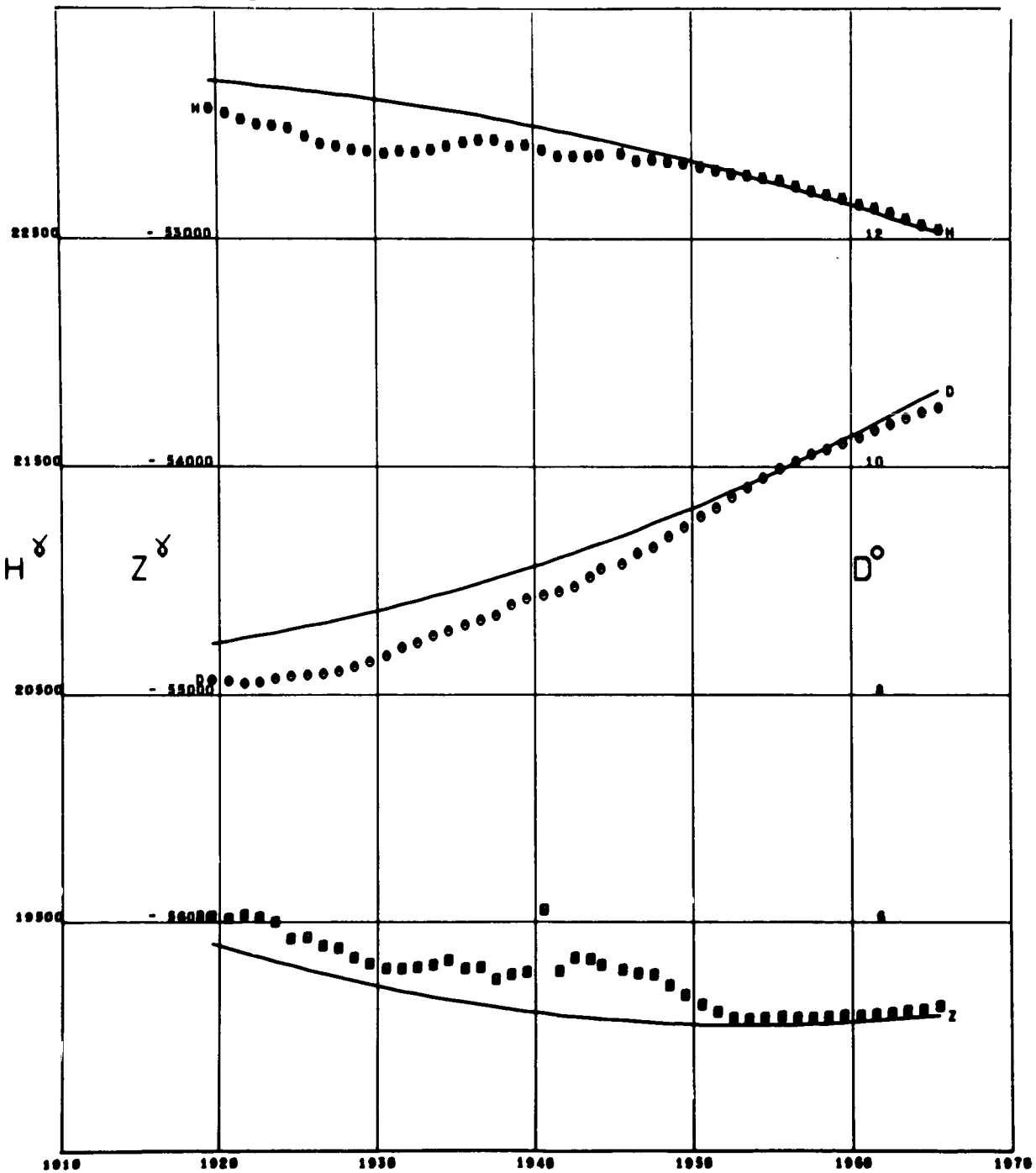
TOLEDO

Lat 39.88 Long -4.04 Alt 0.50

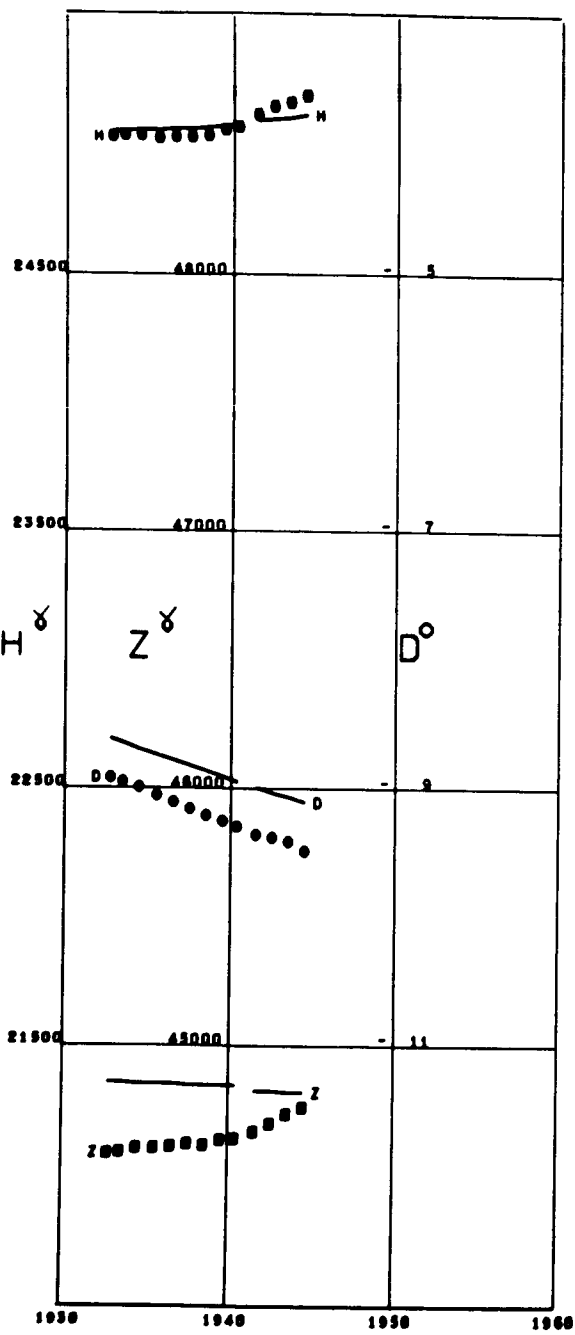


TOOLANGI

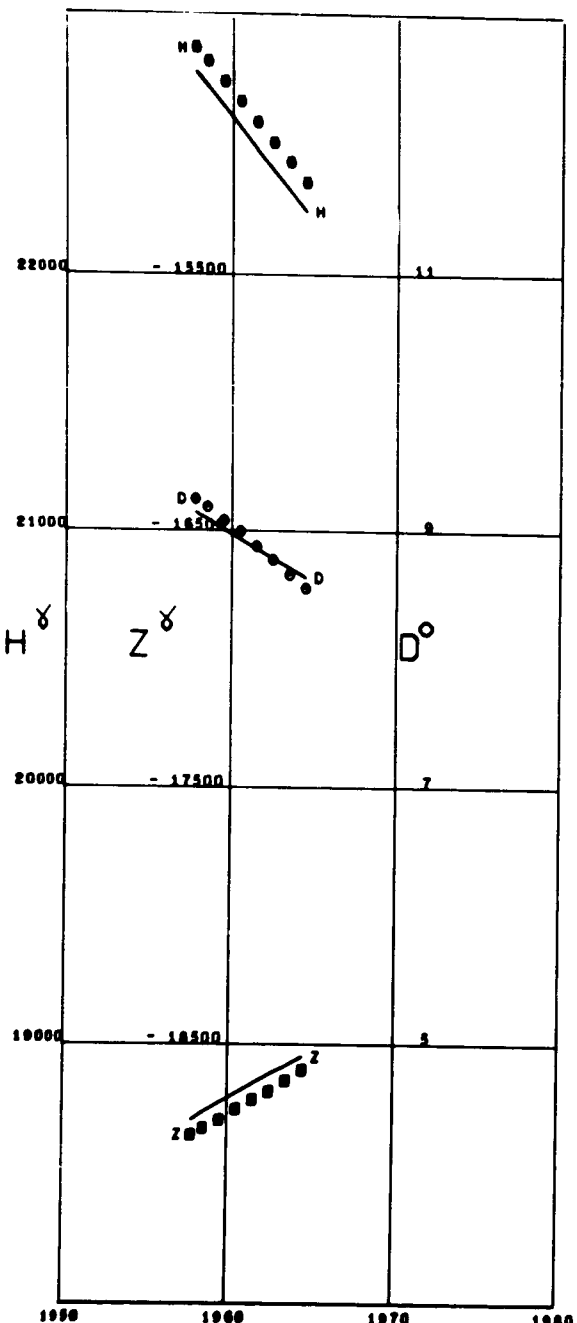
Lat -37.53 Long 145.46 Alt 0.48



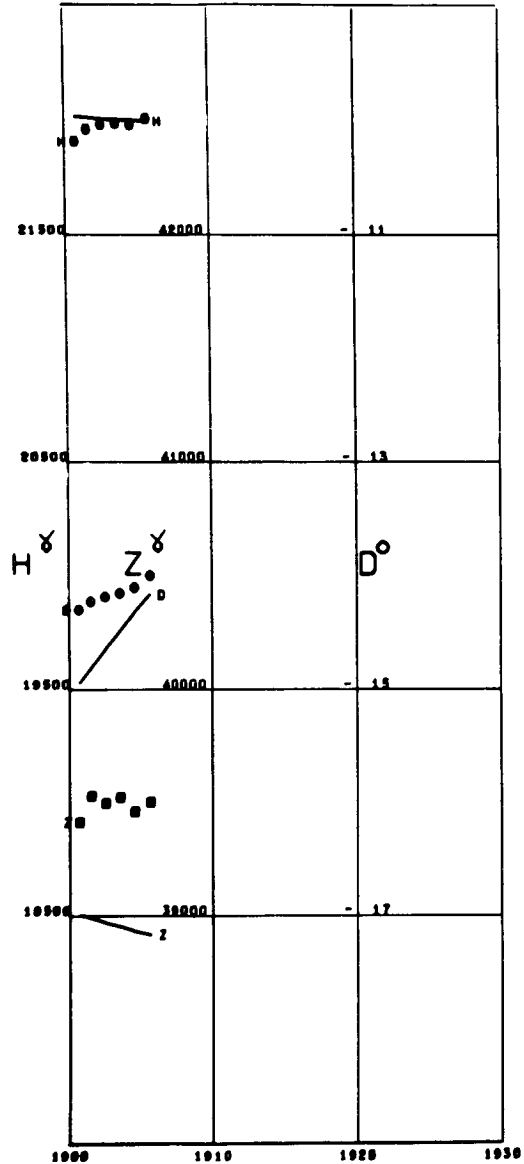
TOYOHARA  
Lat 46.94 Long 142.74



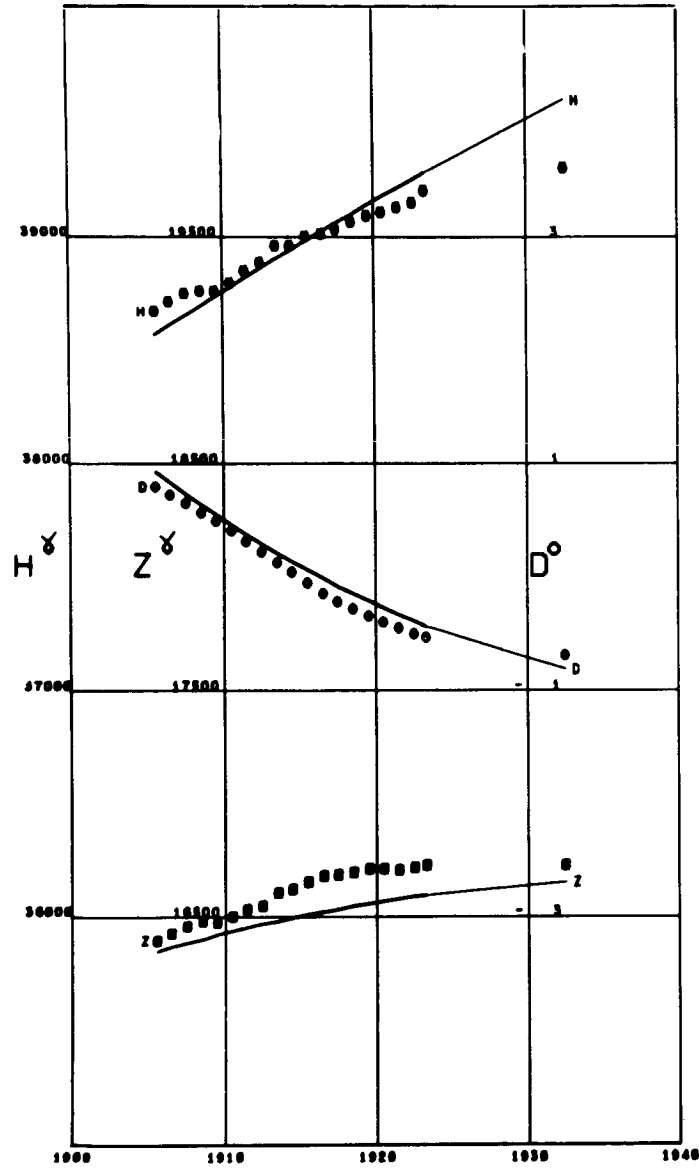
TRELEW  
Lat -43.24 Long -65.31 Alt 0.03



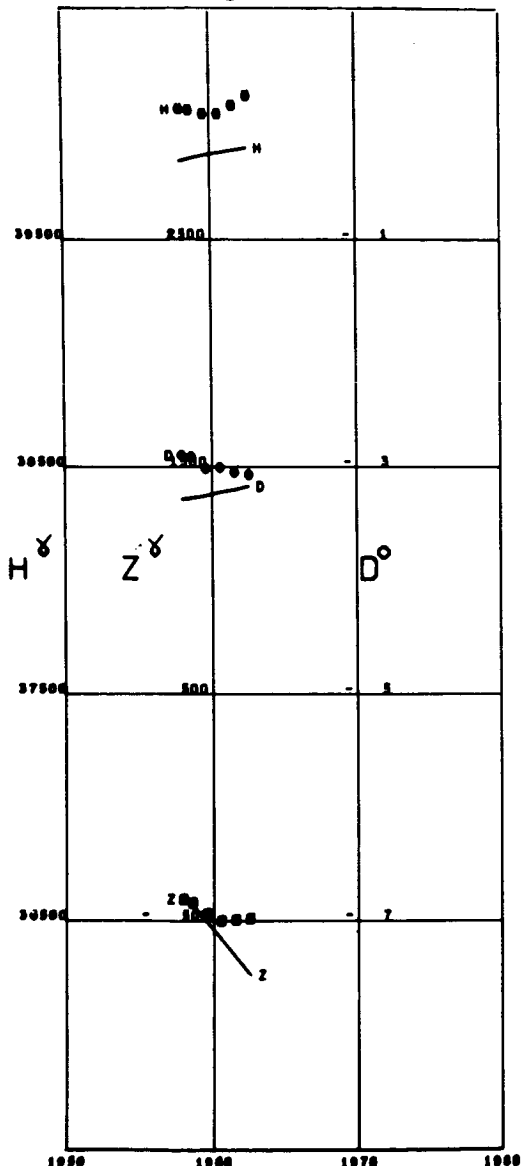
TOULOUSE  
Lat 43.61 Long 1.45



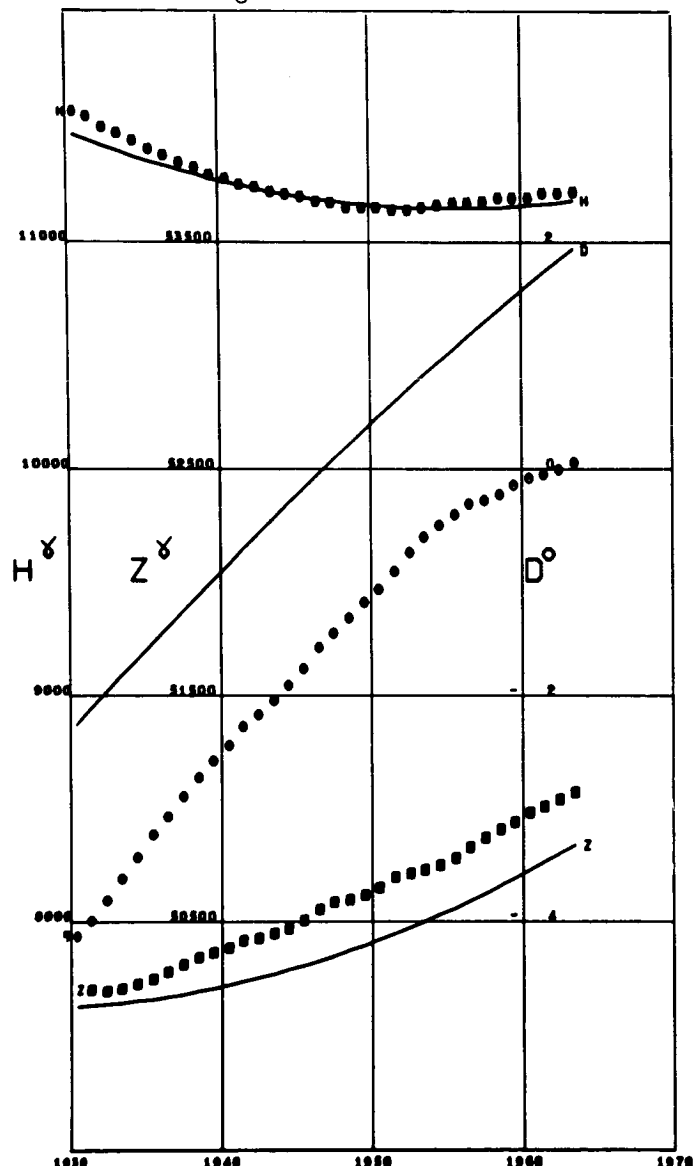
TOUNGOO  
Lat 18.93 Long 96.45



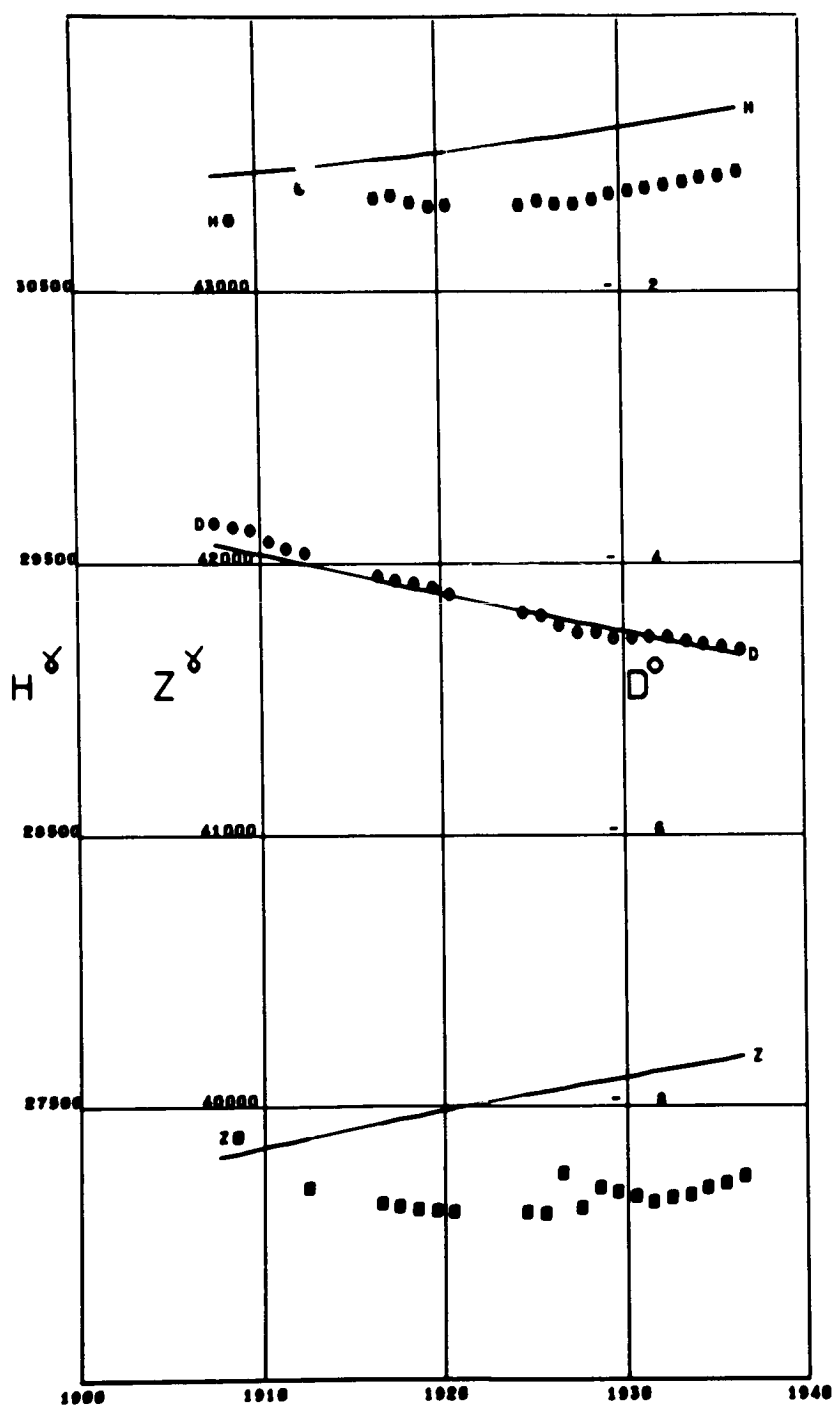
TRIVANDRUM  
Lat 8.48 Long 76.95



TROMSO  
Lat 69.66 Long 18.94

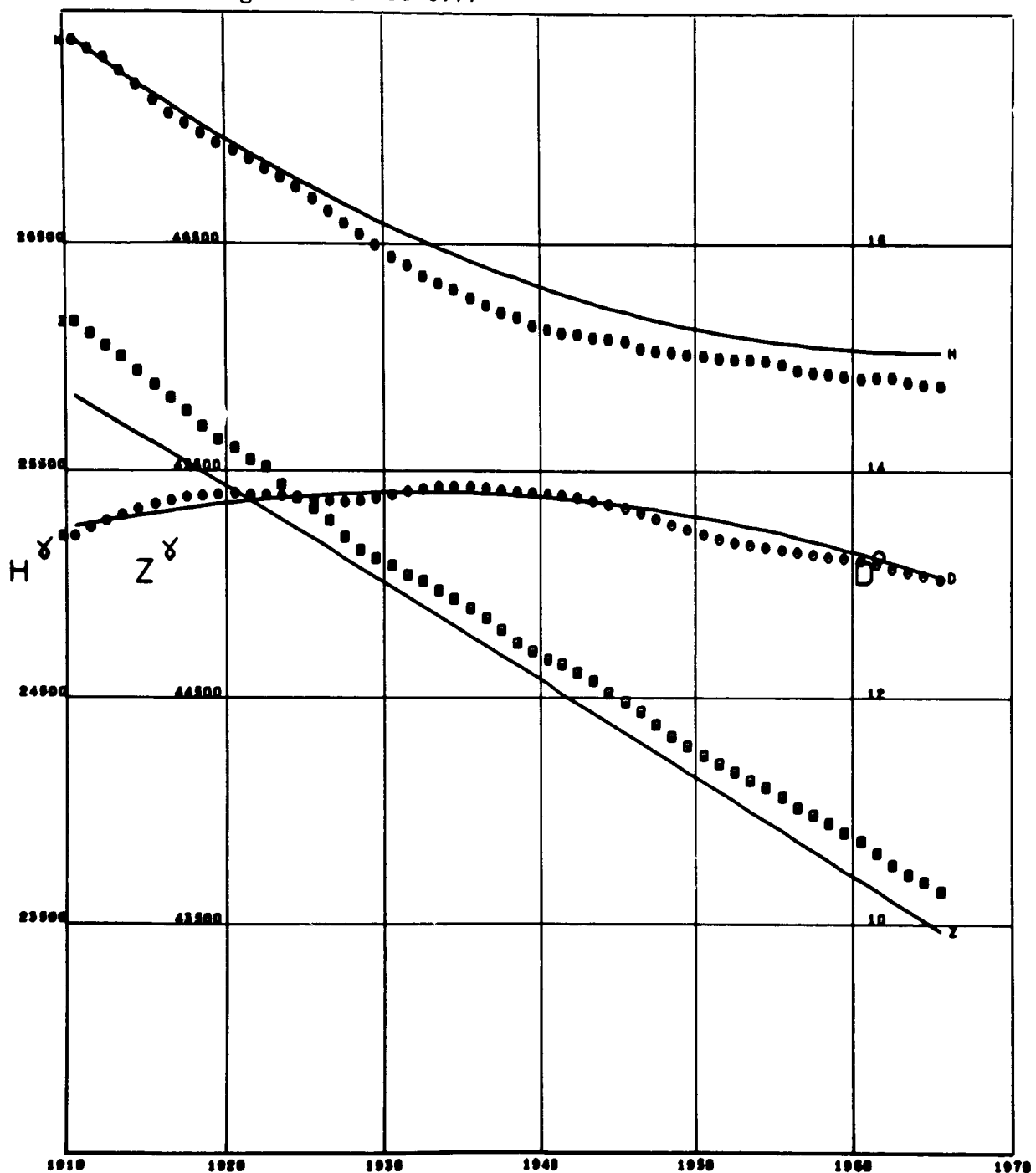


TSINGTAO  
Lat 36.07 Long 120.32



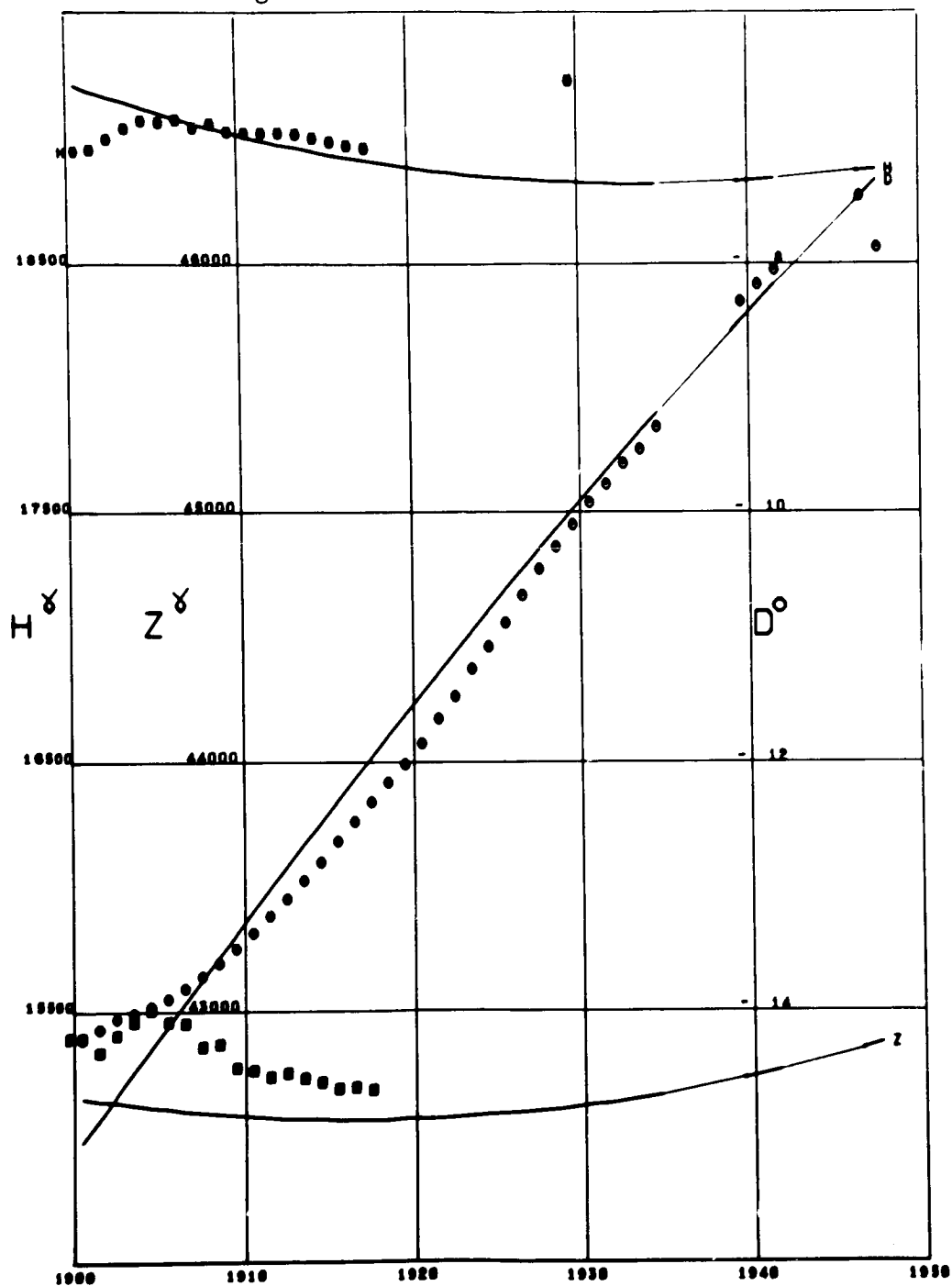
TUCSON

Lat 32.24 Long -110.83 Alt 0.77



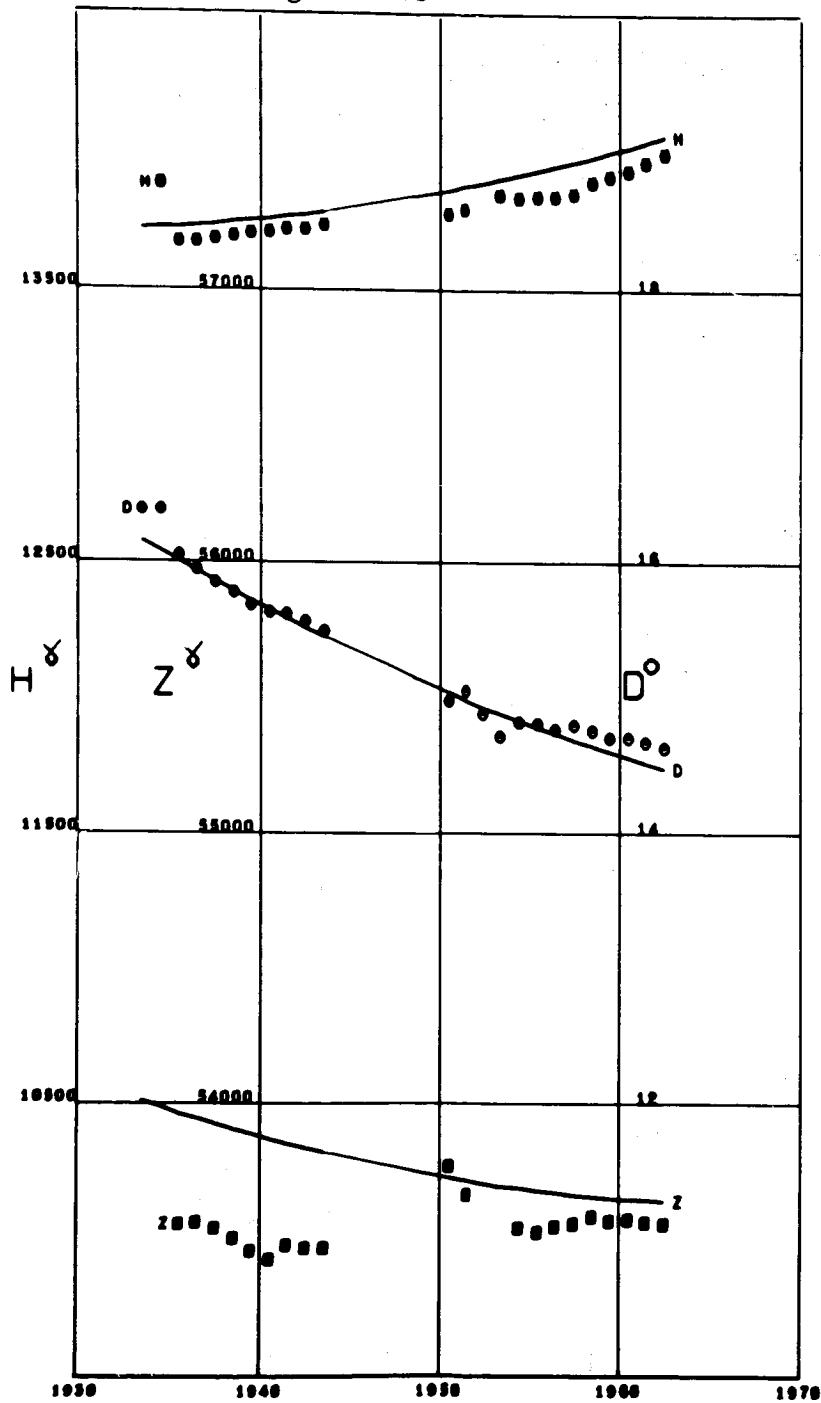
UCCLE

Lat 50.79 Long 4.36

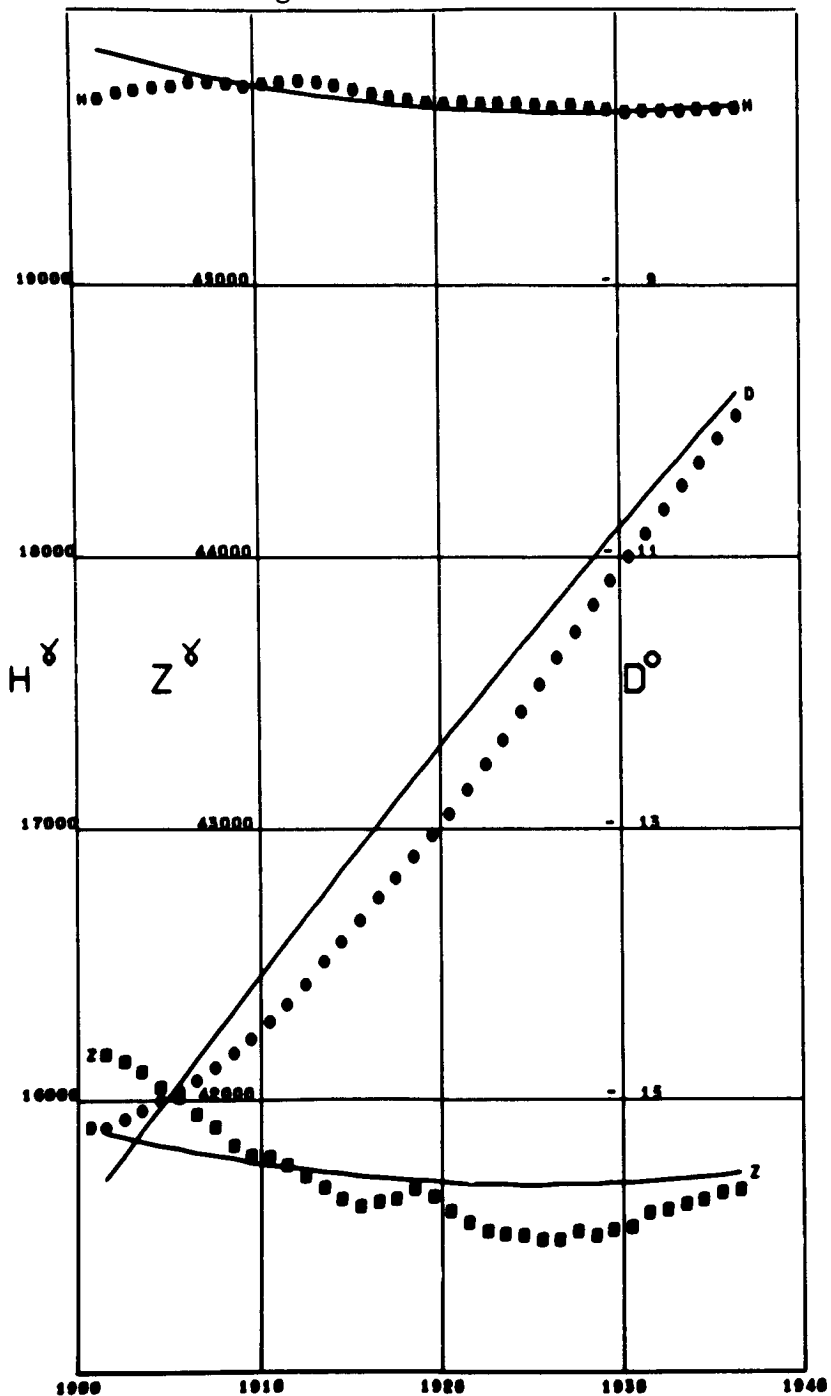


UELEN

Lat 66.16 Long -169.83

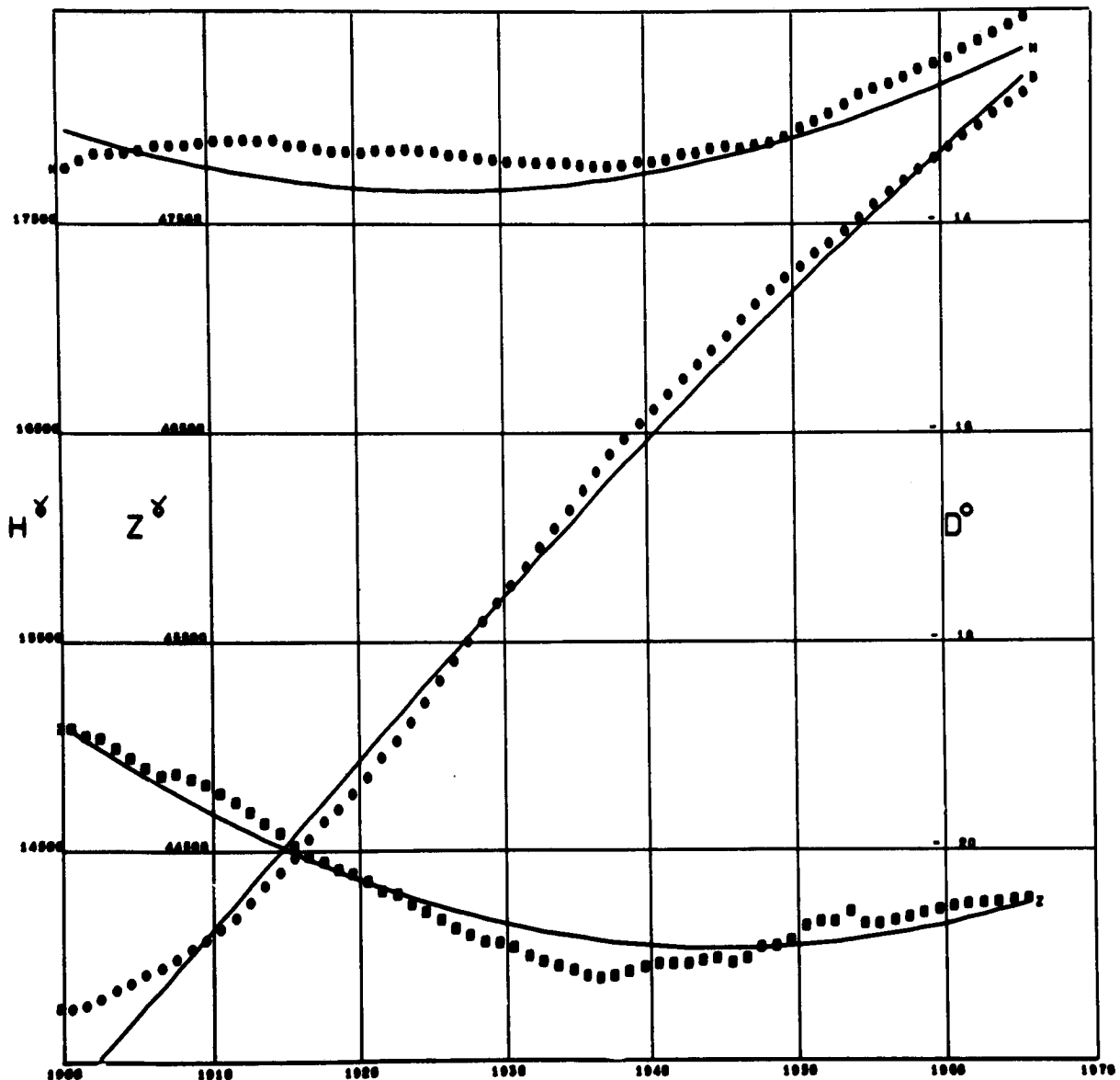


VAL JOYEUX  
Lat 48.82 Long 2.01



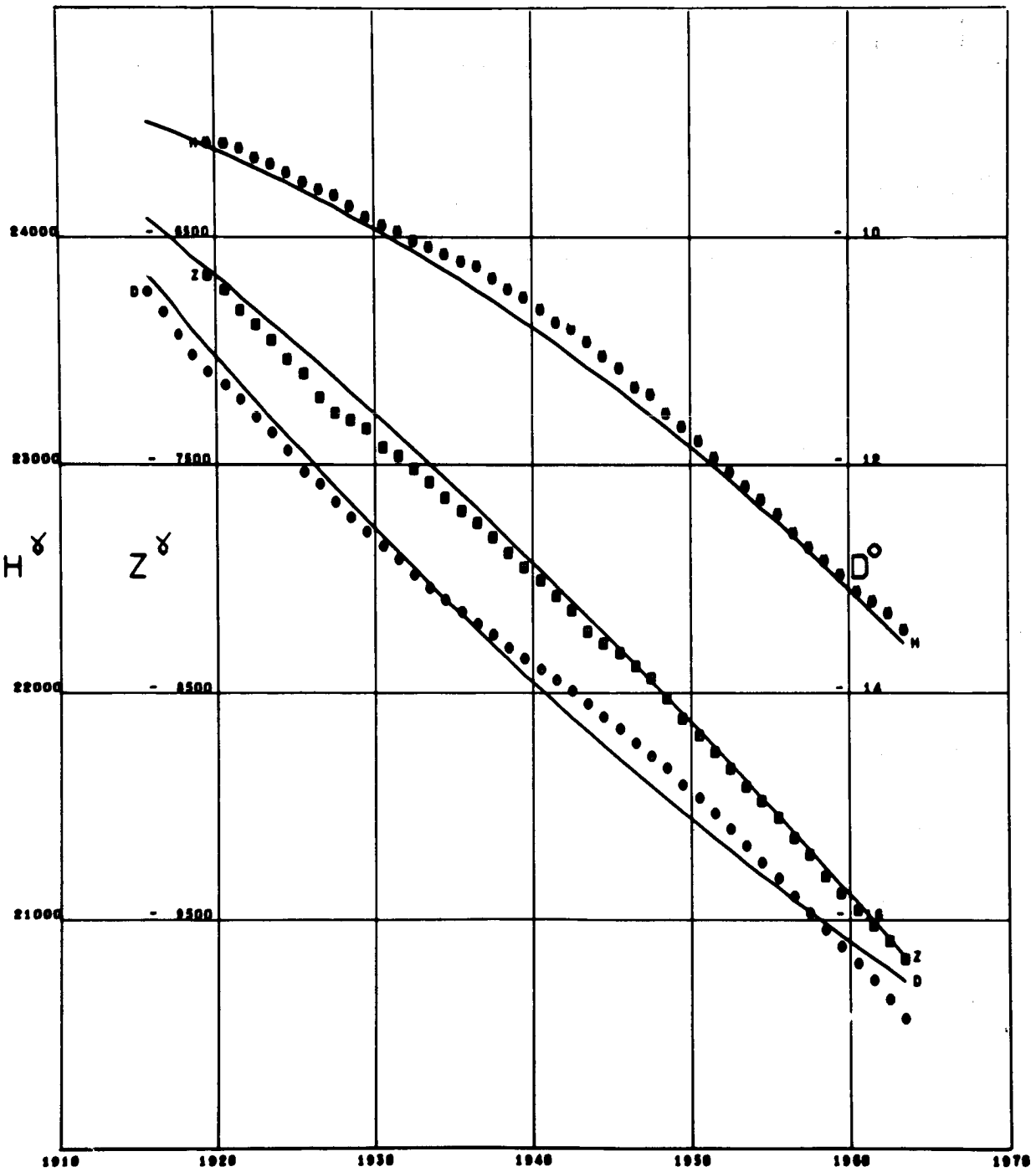
**VALENTIA**

Lat 51.93 Long -10.25

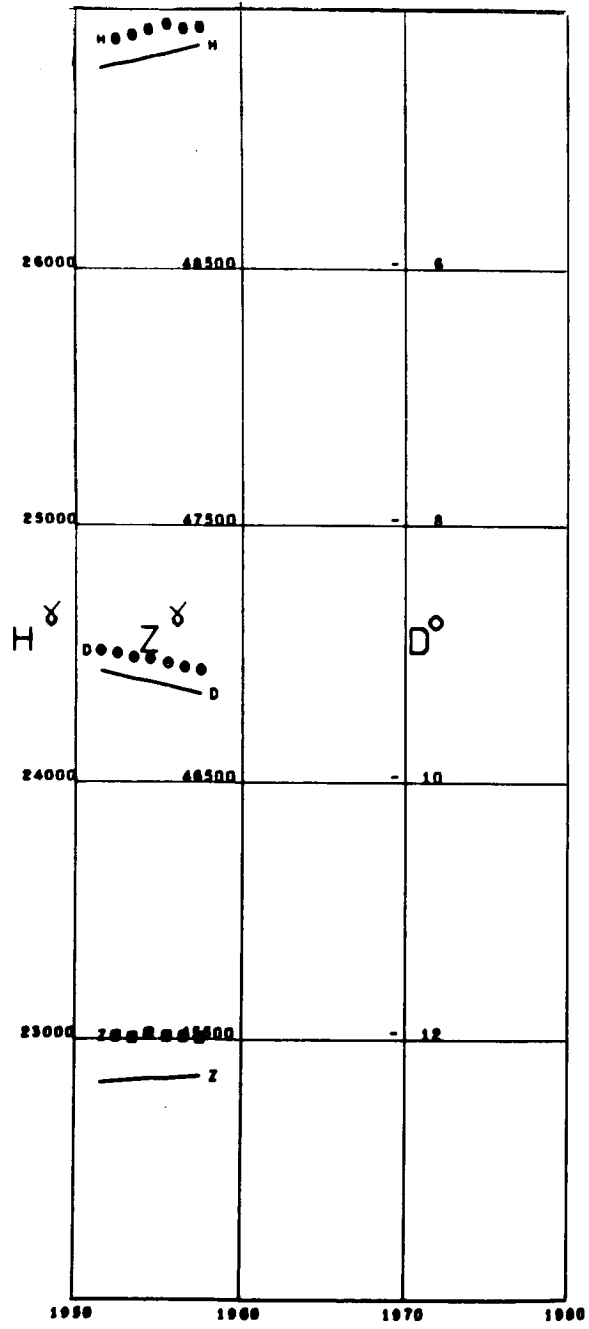


VASSOURAS

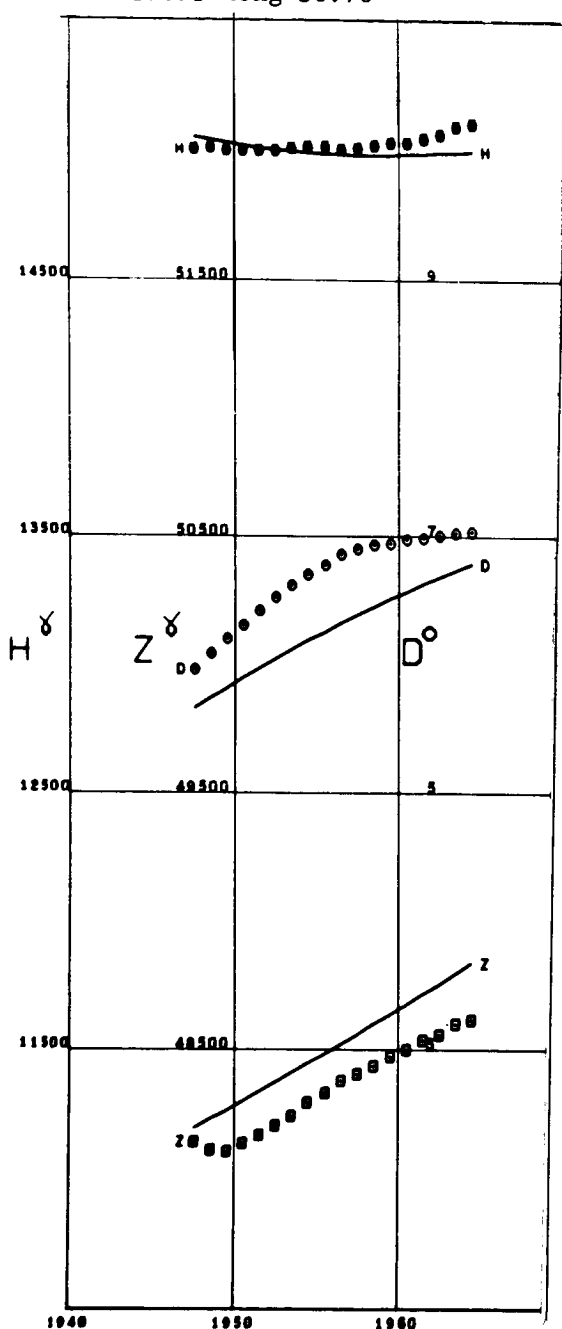
Lat -22.40 Long -43.65 Alt 0.46



VOROSHILOV  
Lat 43.78 Long 132.03

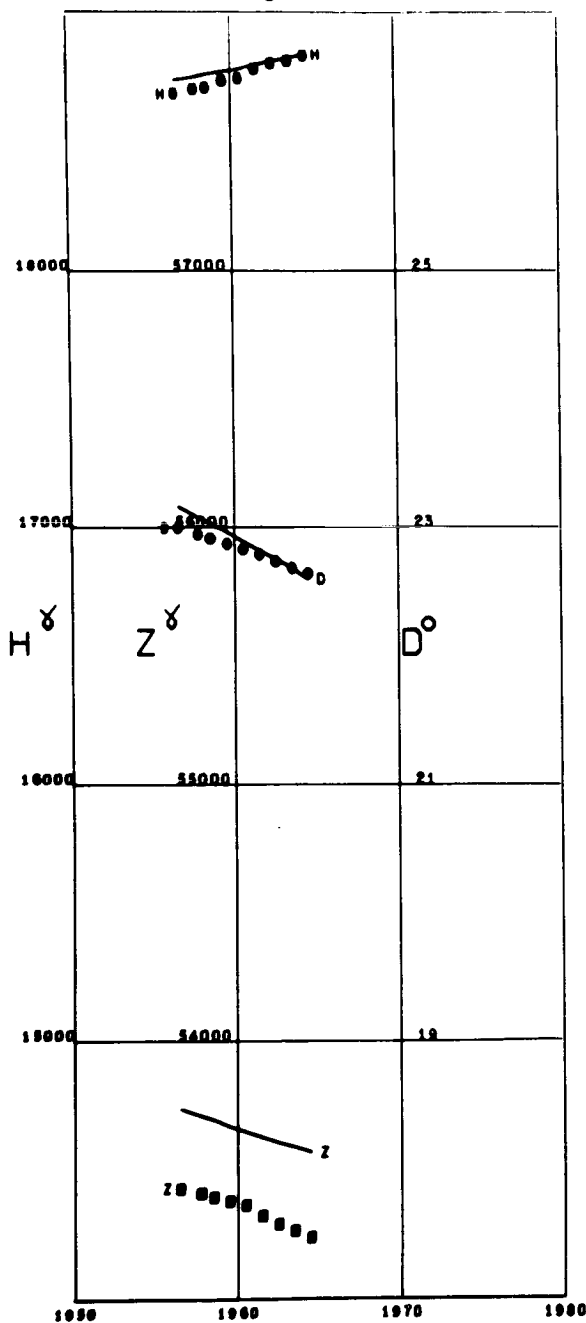


VOYEKHOVO  
Lat 59.95 Long 30.70



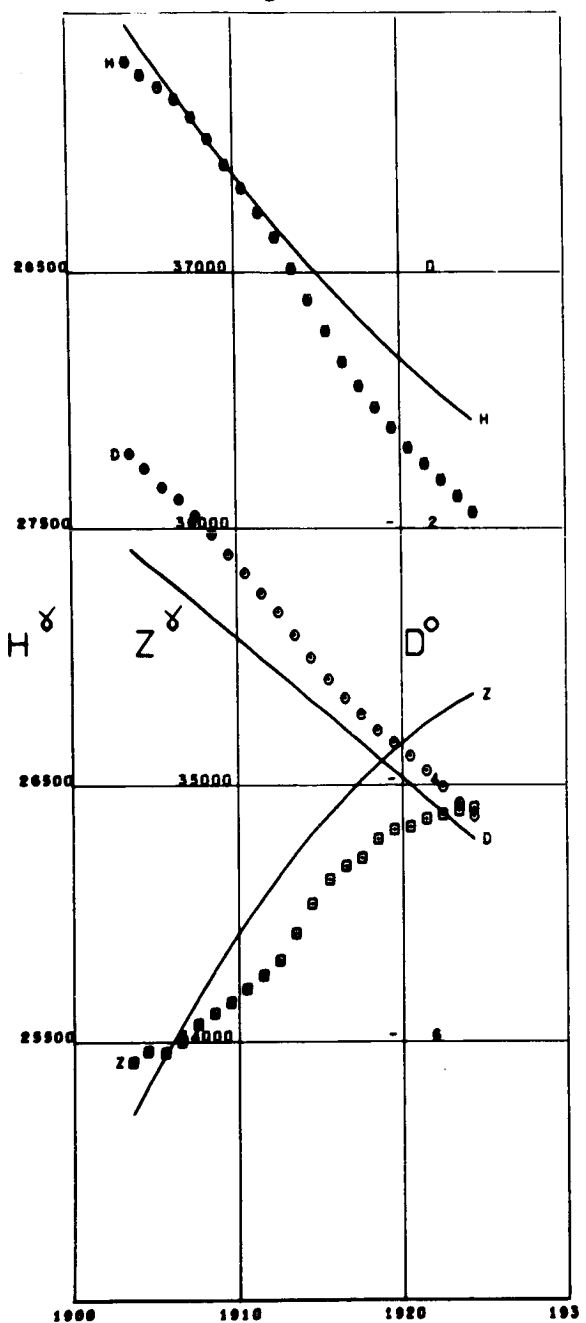
VICTORIA

Lat 48.51 Long -123.41 Alt 0.03

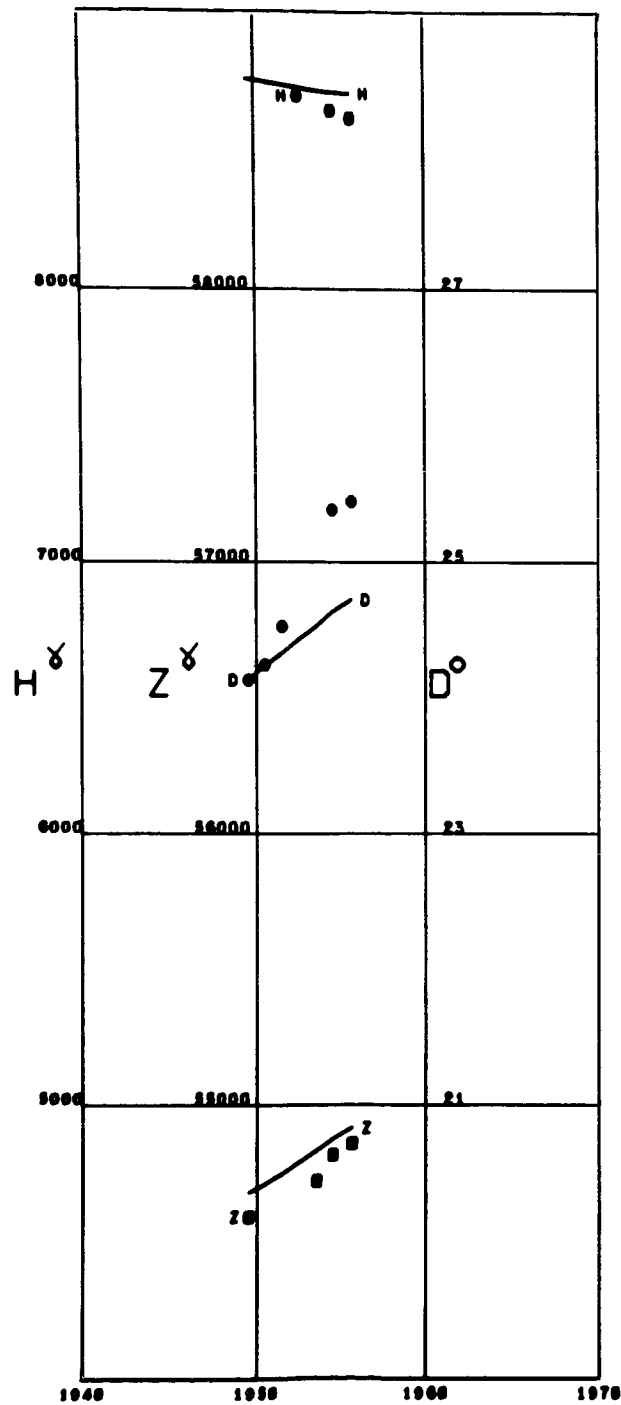


VIEQUES

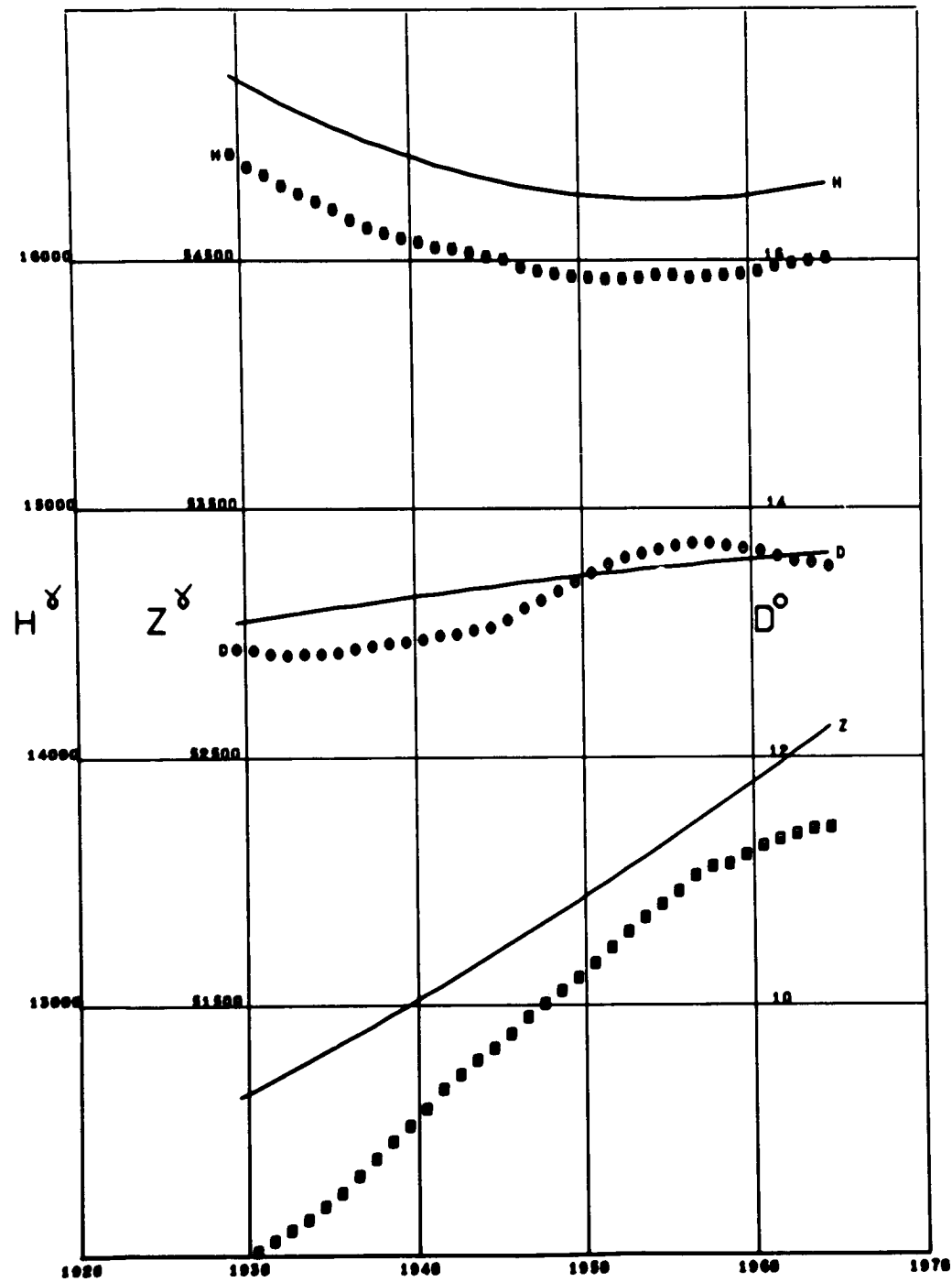
Lat 18.14 Long -65.44



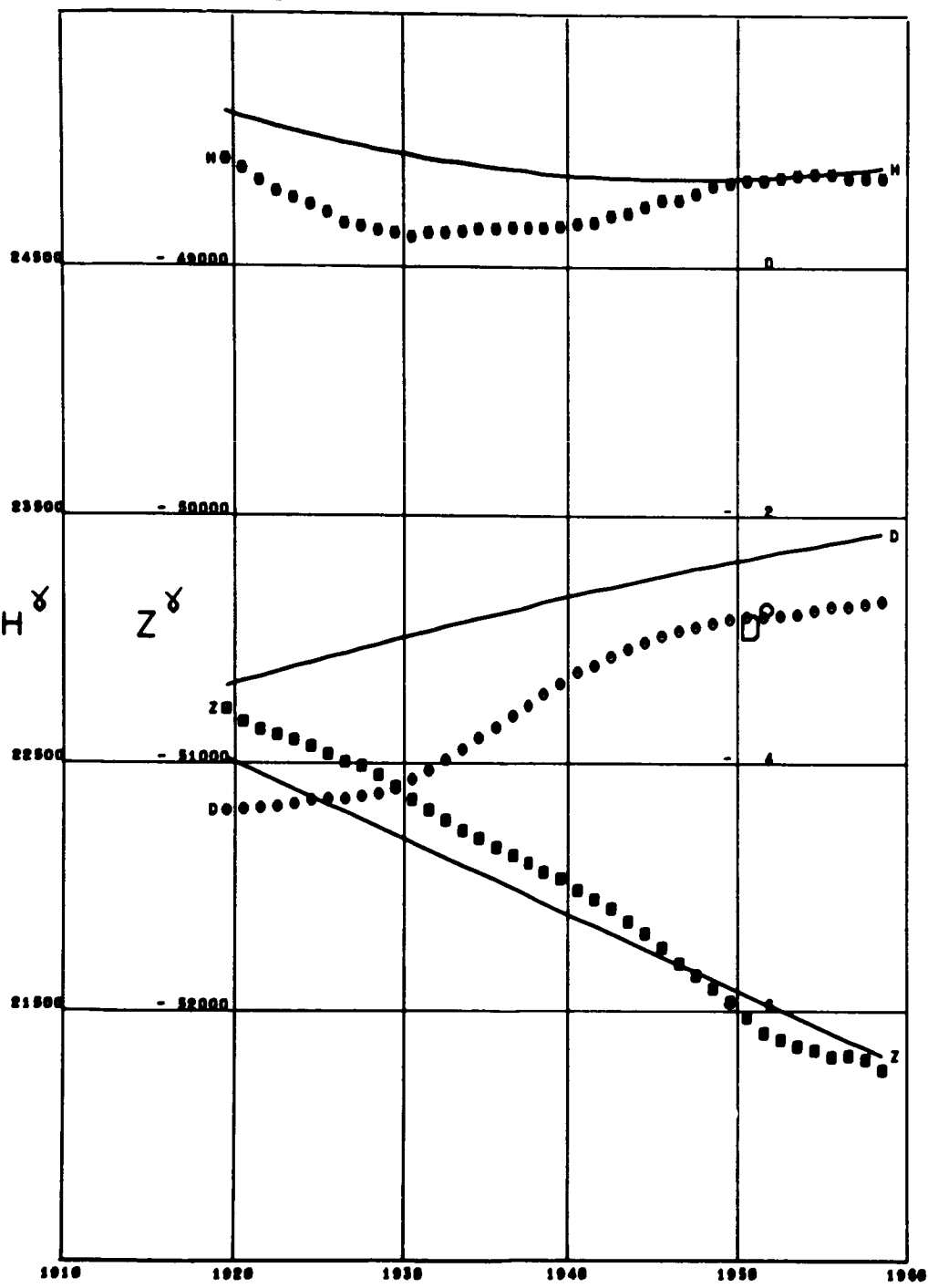
VYKHODNOY  
Lat 73.23 Long 56.73



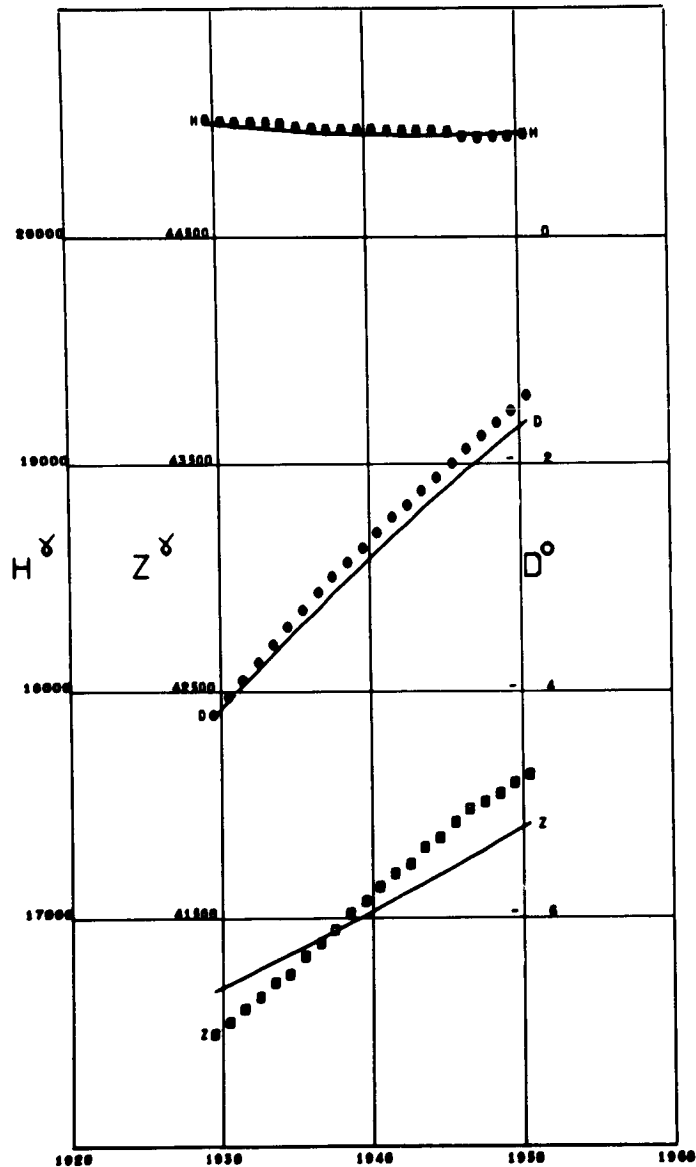
VYSOKAYA DUBRAVA  
Lat 56.73 Long 61.06 Alt 0.29



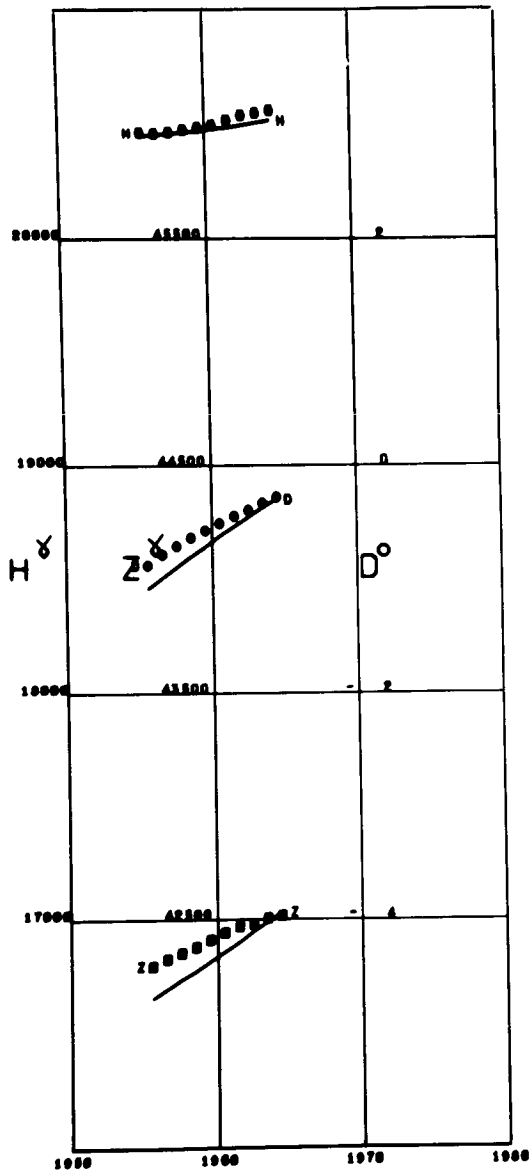
WATHEROO  
Lat -30.31 Long 115.87



WIEN AUHOF  
Lat 48.20 Long 16.23

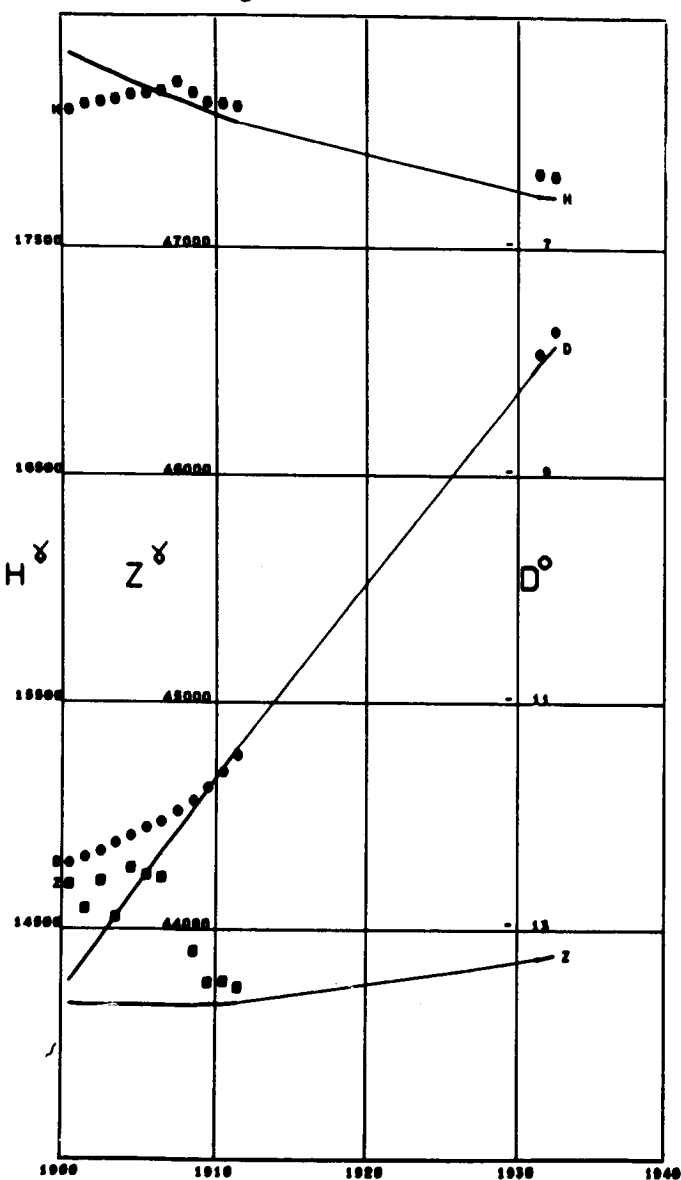


WIEN KOBENZL  
Lat 48.26 Long 16.31



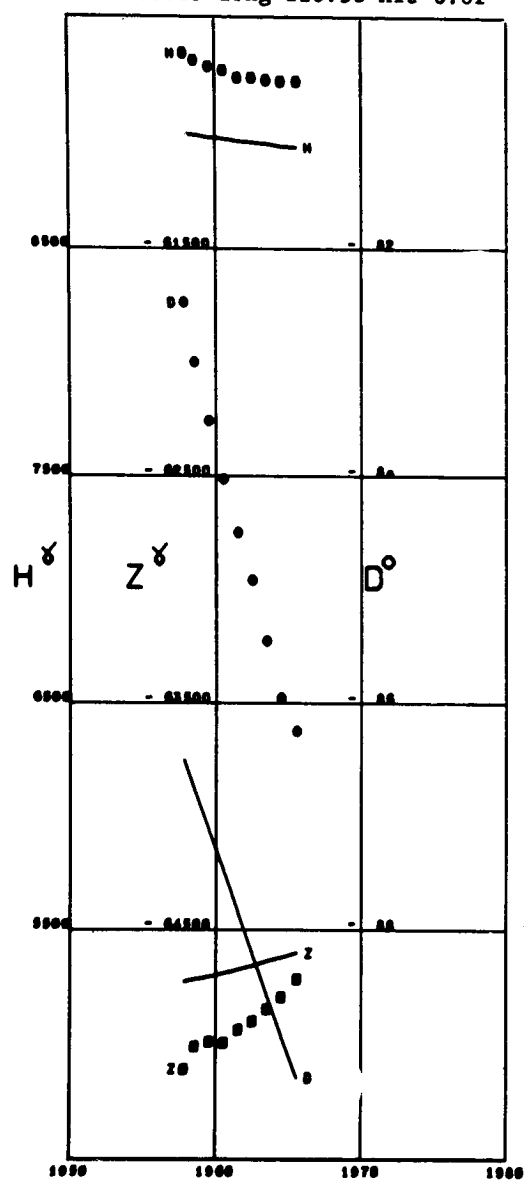
WILHELMSHAVEN

Lat 53.53 Long 8.14

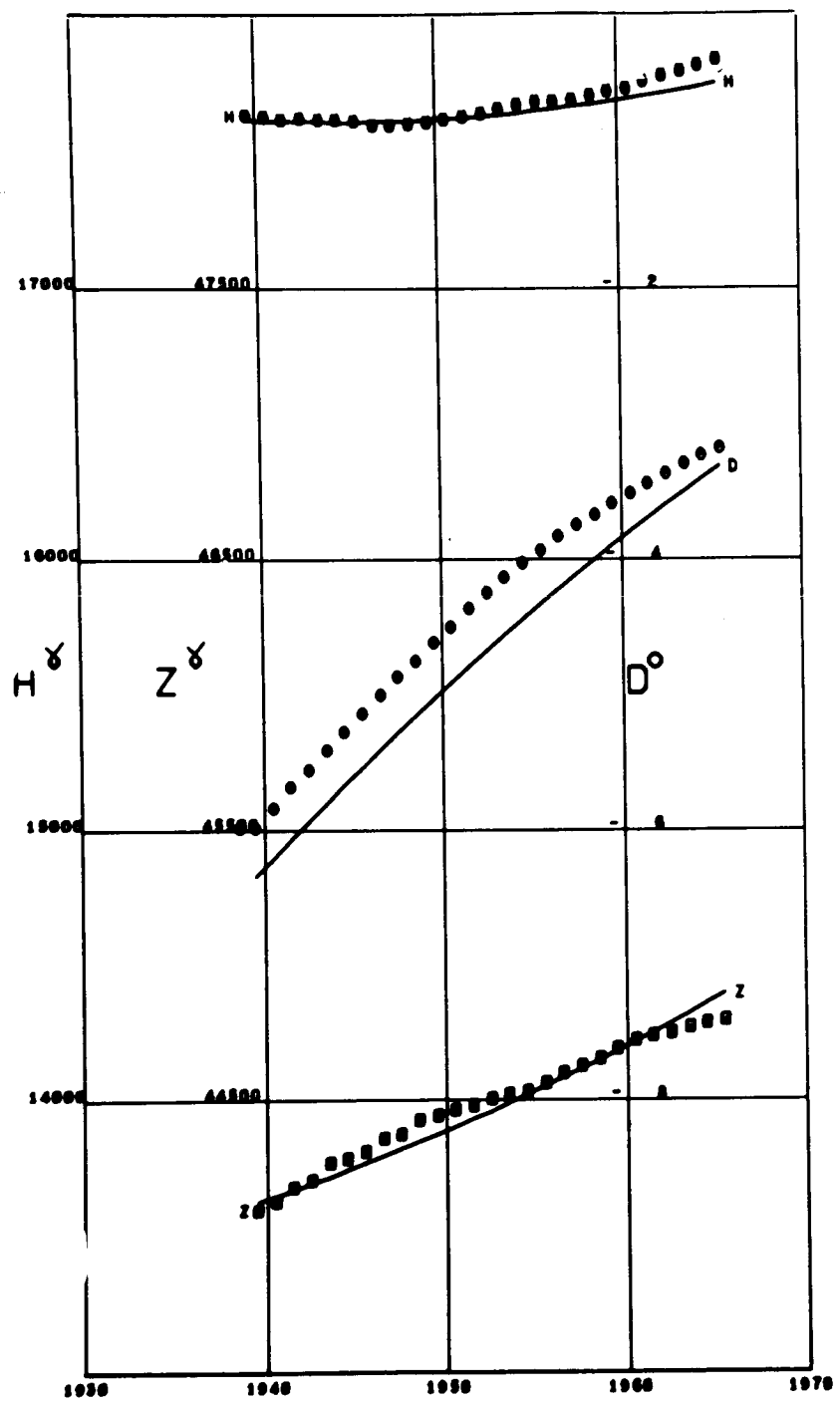


WILKES

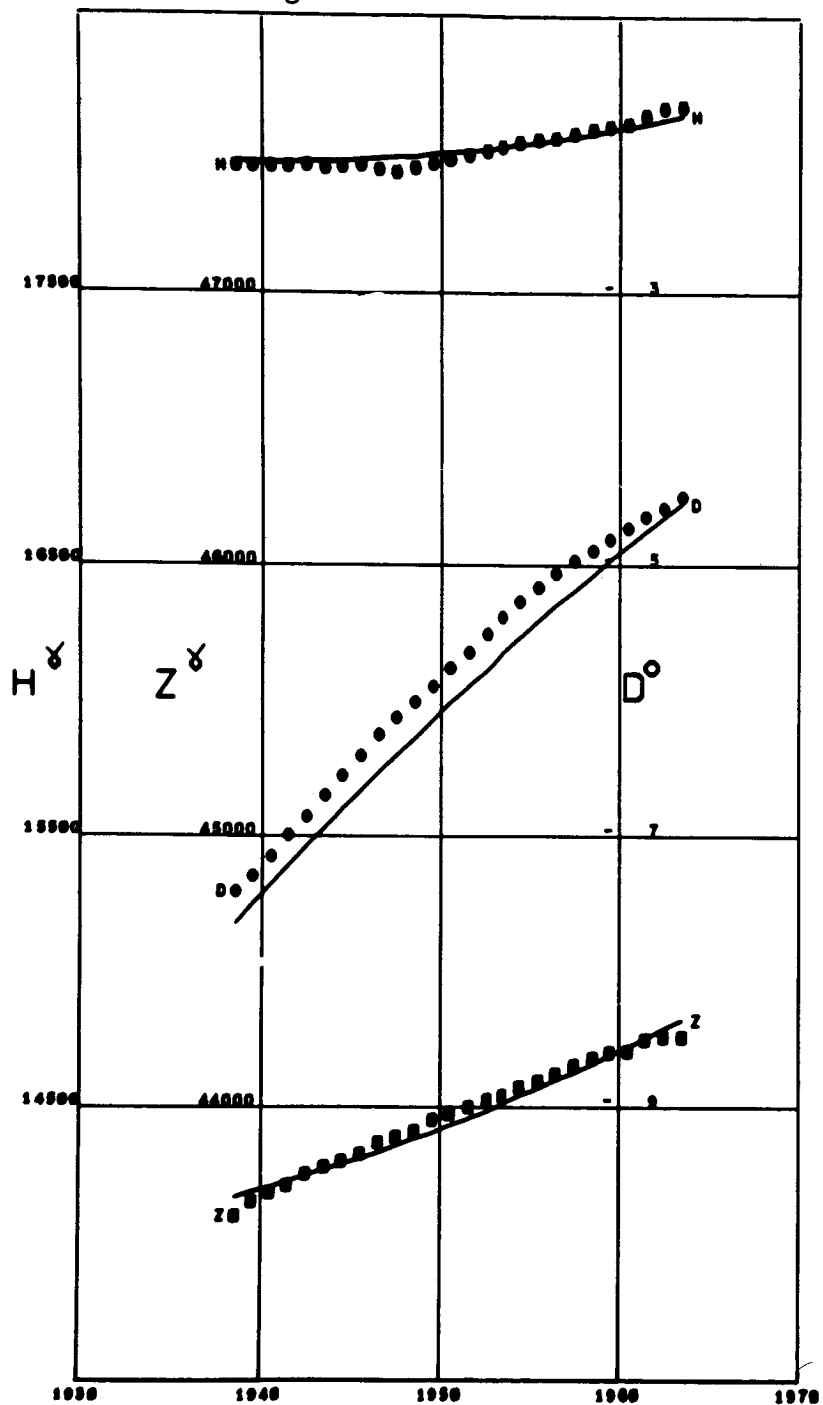
Lat -66.25 Long 110.58 Alt 0.01



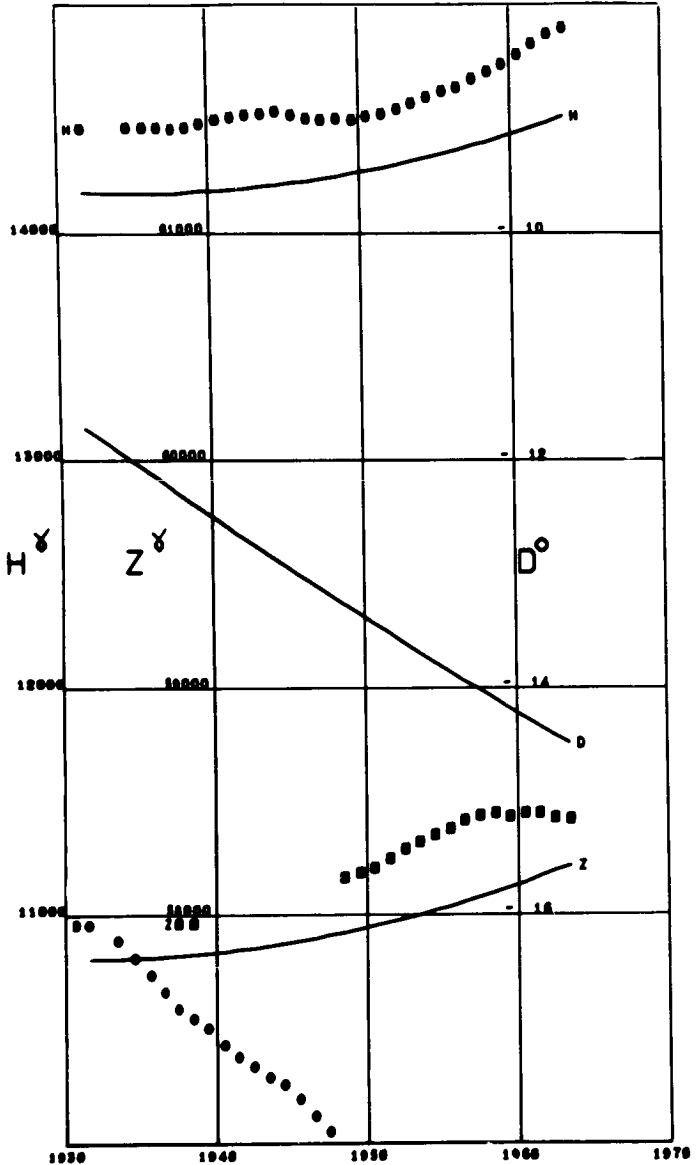
WINGST  
Lat 53.74 Long 9.07



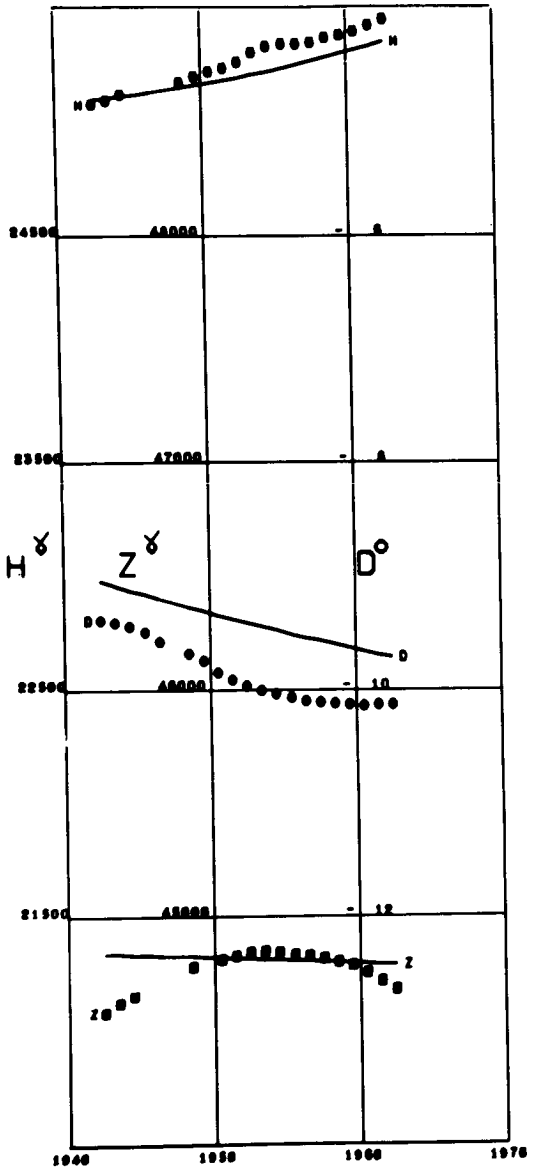
WITTEVEEN  
Lat 52.81 Long 6.66



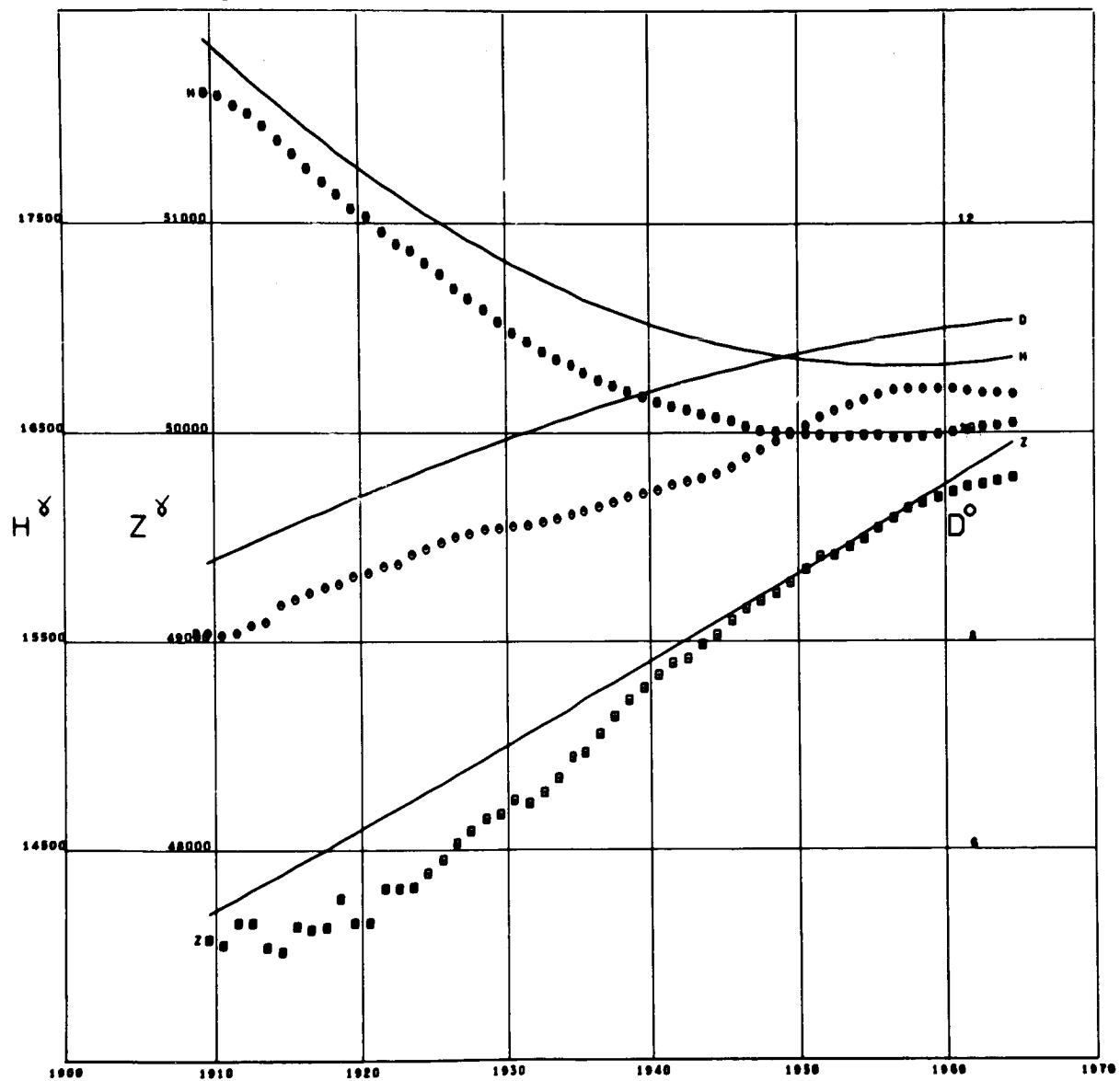
YAKUTSK  
Lat 62.01 Long 129.71 Alt 0.10



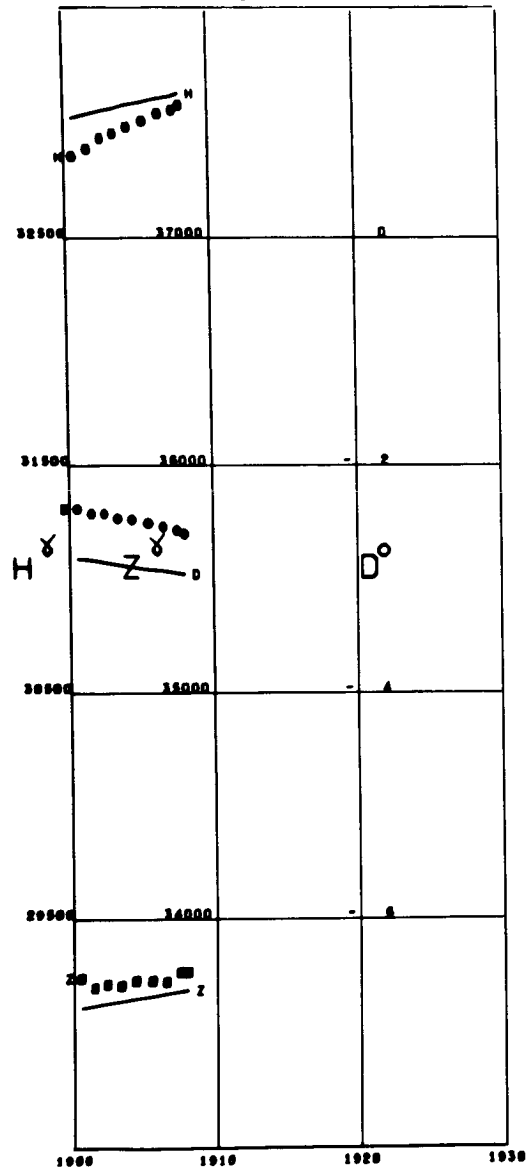
YUZHNO SAKHALINSK  
Lat 46.95 Long 142.71



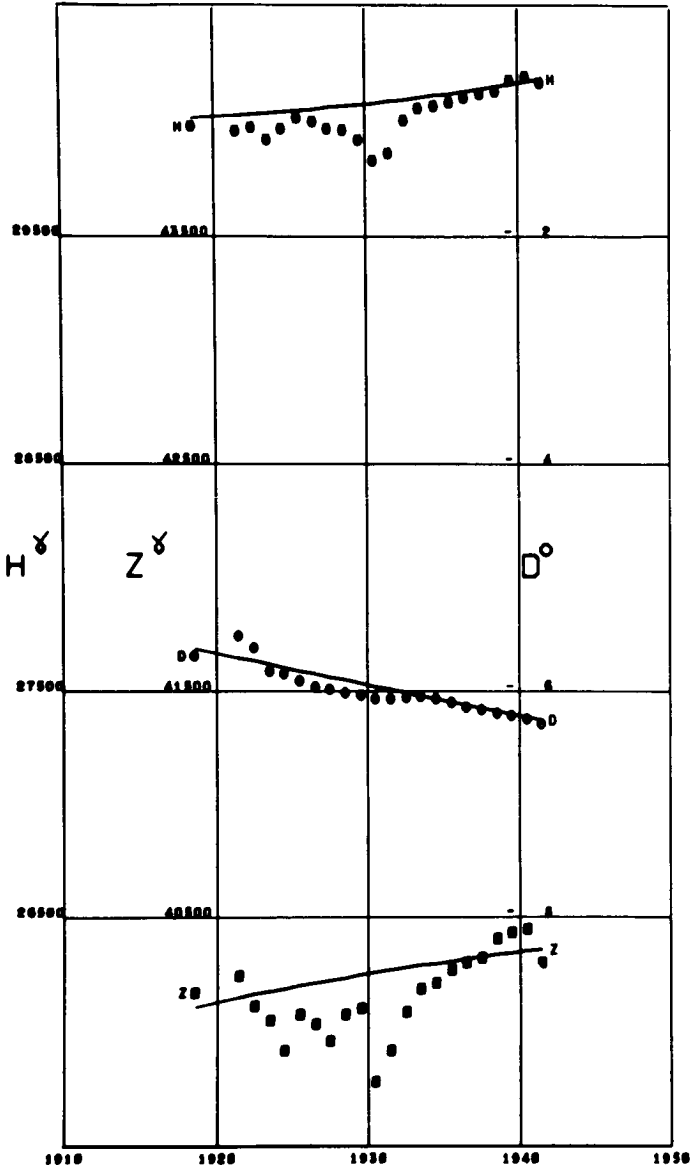
ZAYMISHCHE  
Lat 55.83 Long 48.85



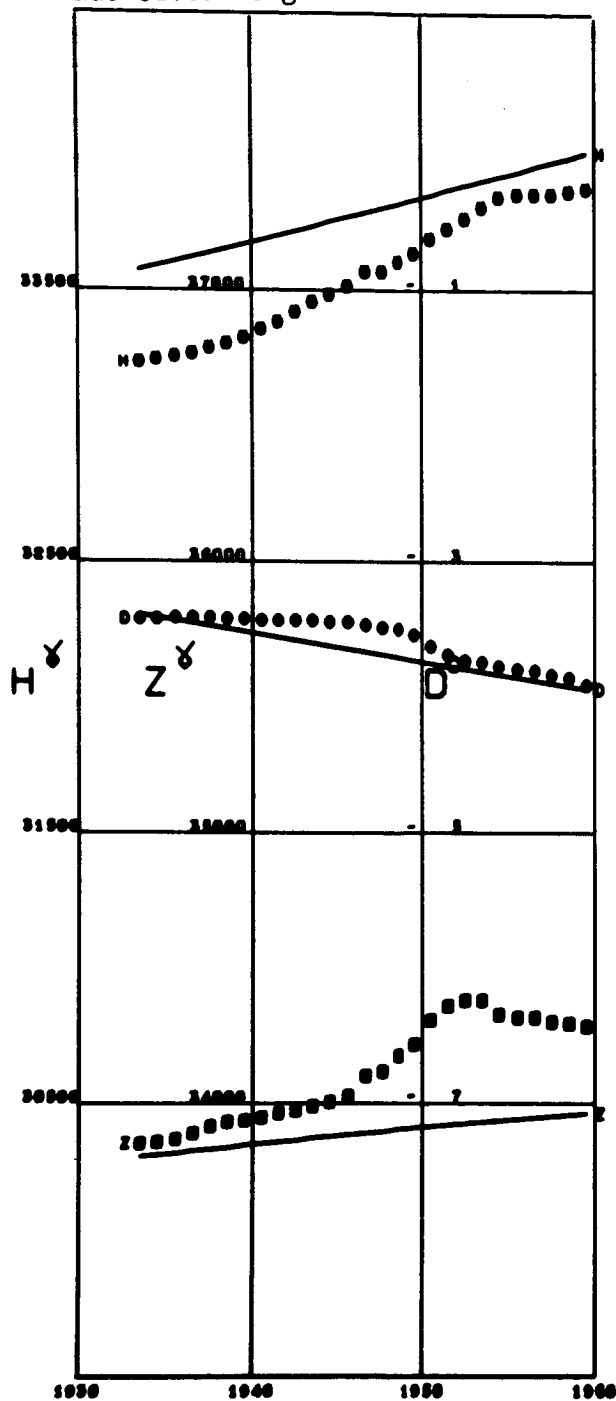
ZIKWEI  
Lat 31.20 Long 121.43



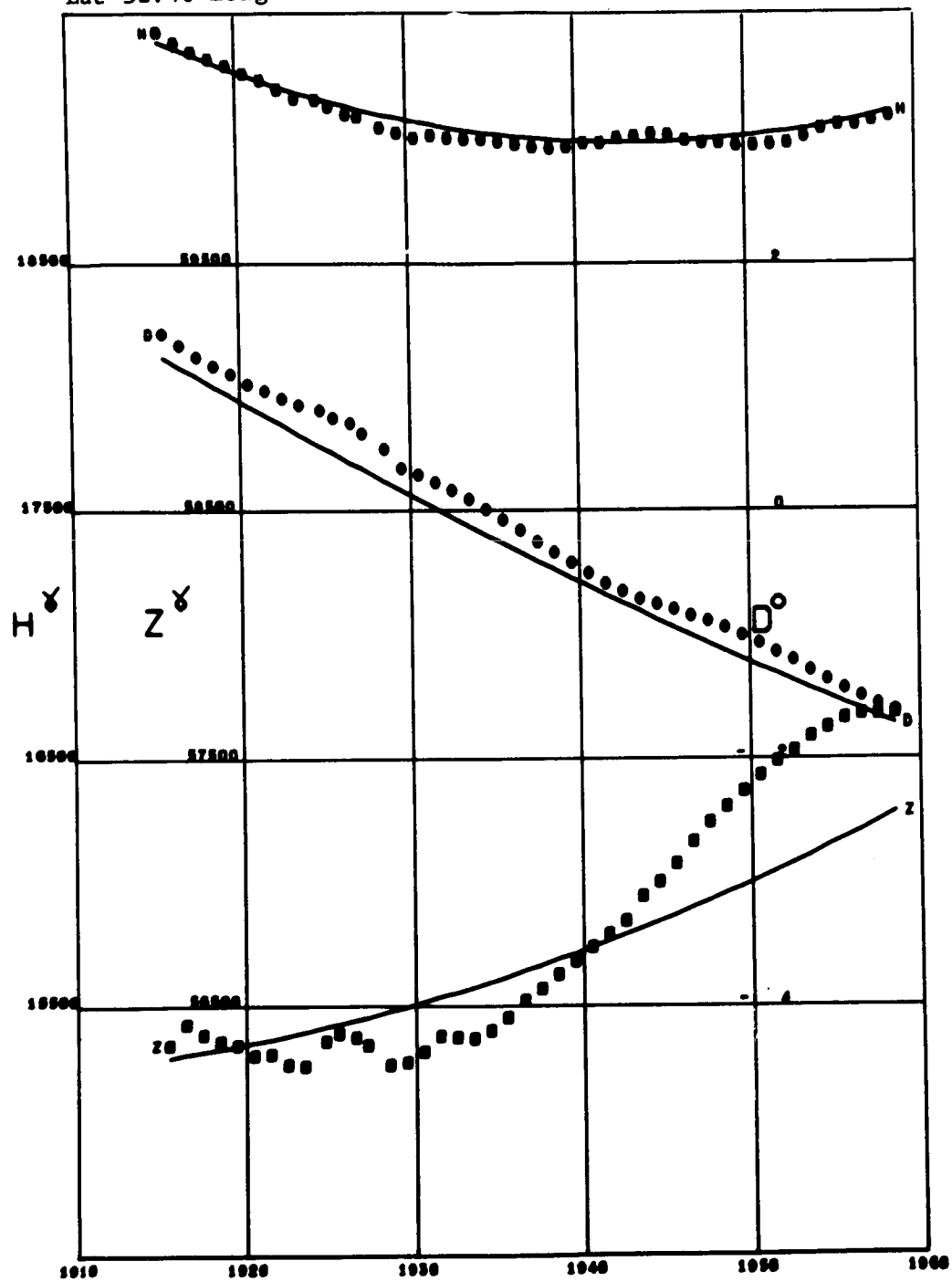
ZINSEN  
Lat 37.47 Long 126.62



ZO SE  
Lat 31.09 Long 121.18



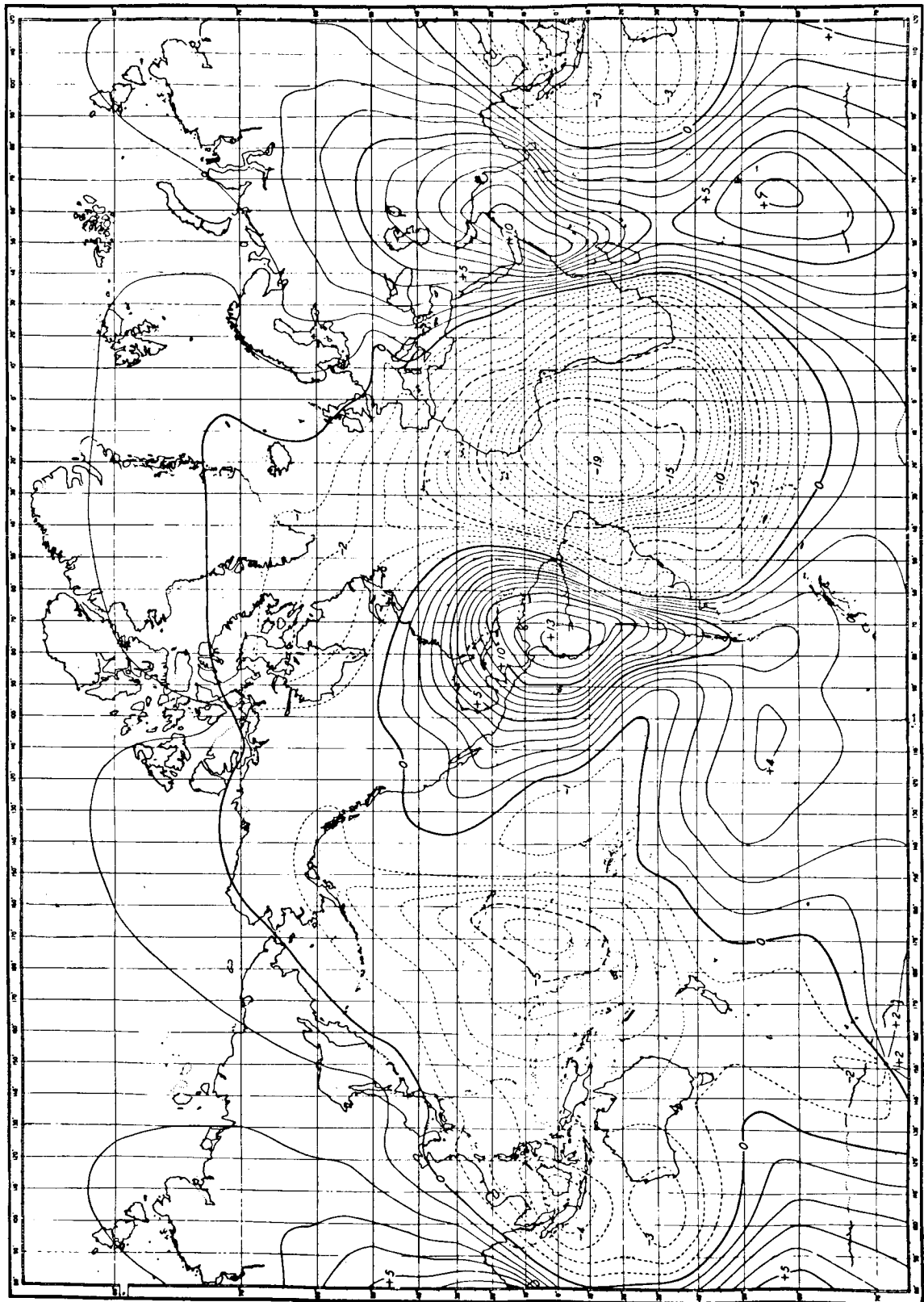
ZUY  
Lat 52.46 Long 104.03



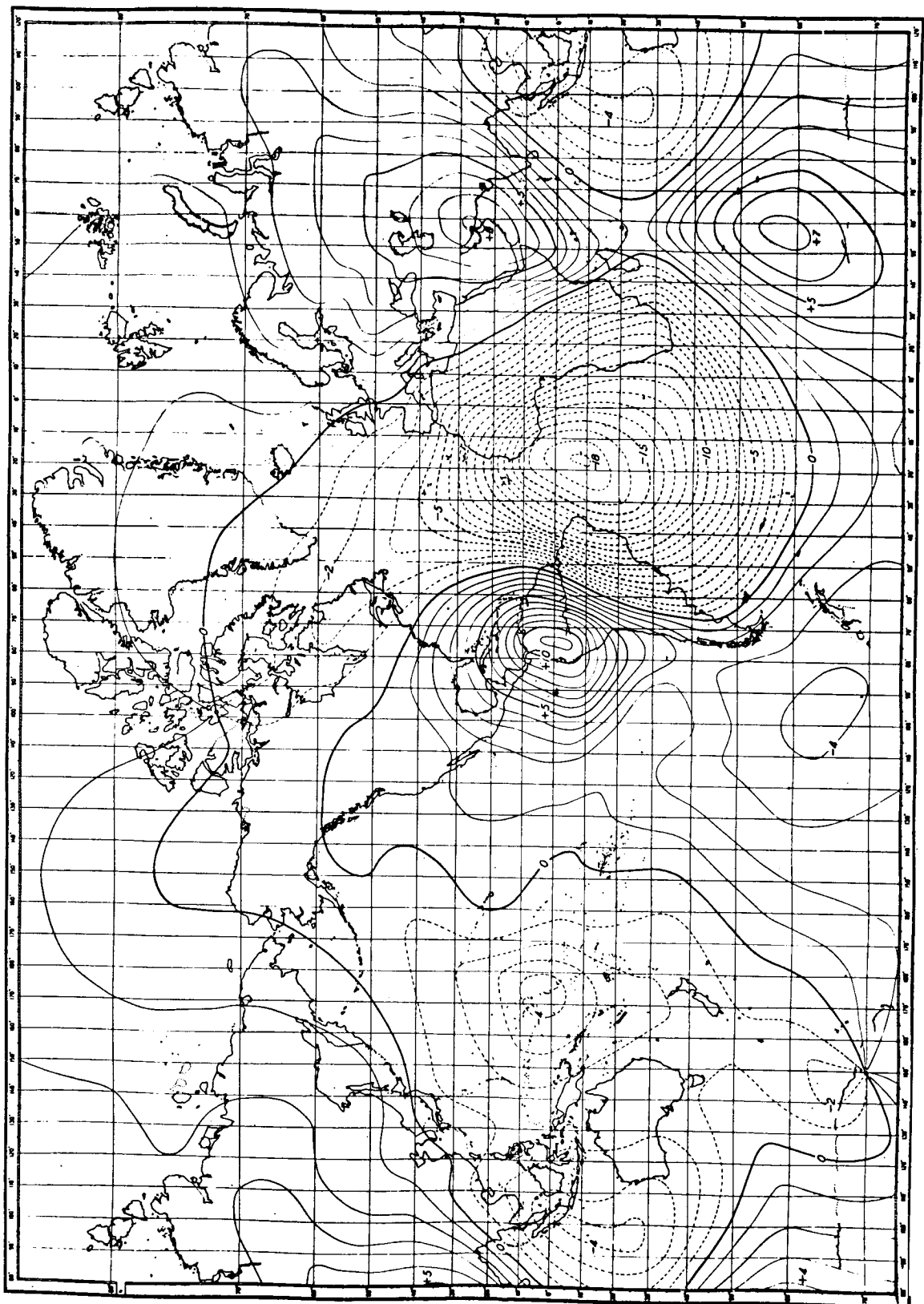
APPENDIX B

Comparison of isoporic charts (1912-1942)

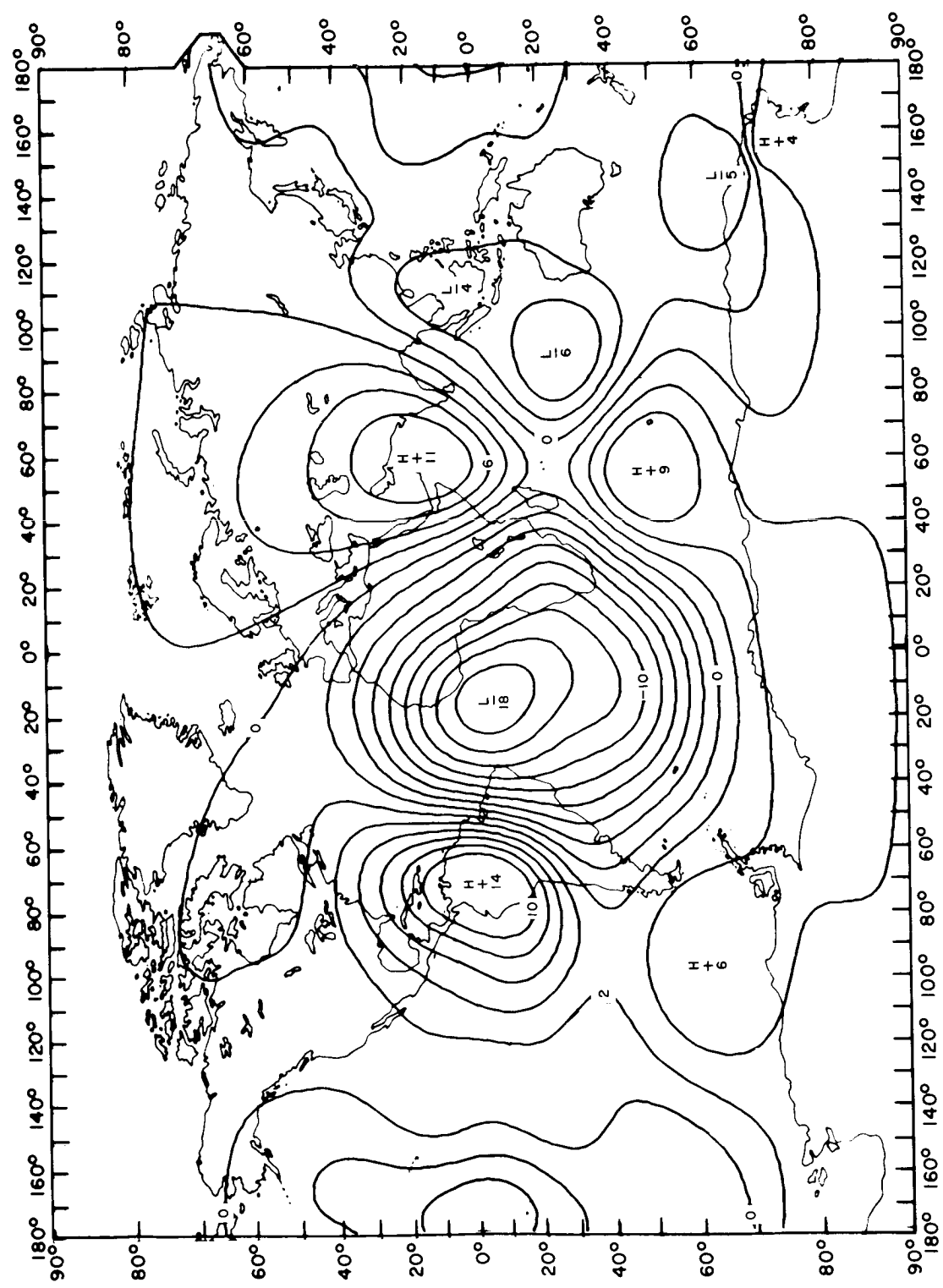
from GSFC(12/66) with those from Vestine et al.(1959)



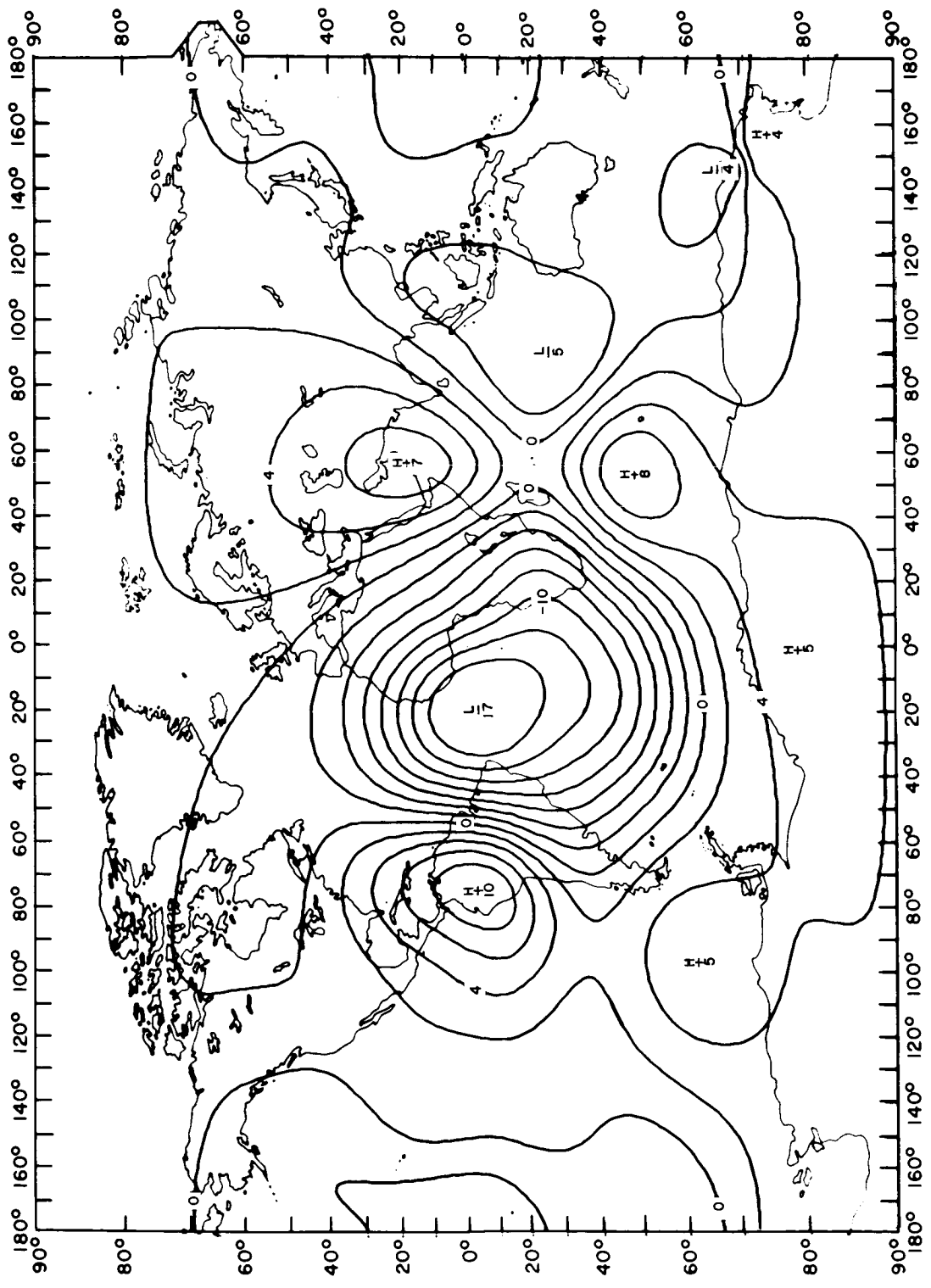
Geomagnetic secular change in minutes per year,  
inclination, epoch 1912.5. Vestine et al. (1959).



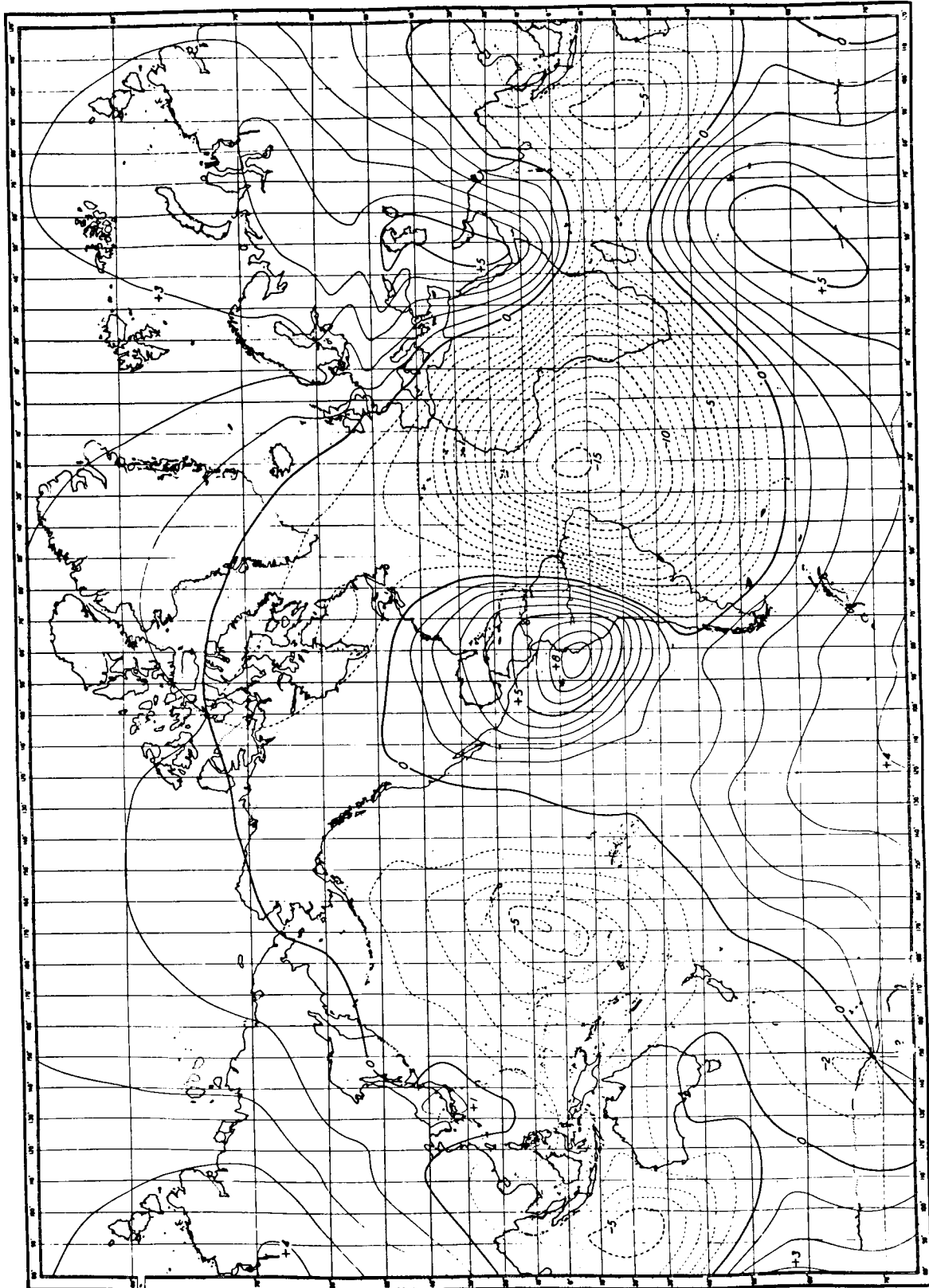
Geomagnetic secular change in minutes per year,  
inclination, epoch 1922.5. Vestine et al. (1959).



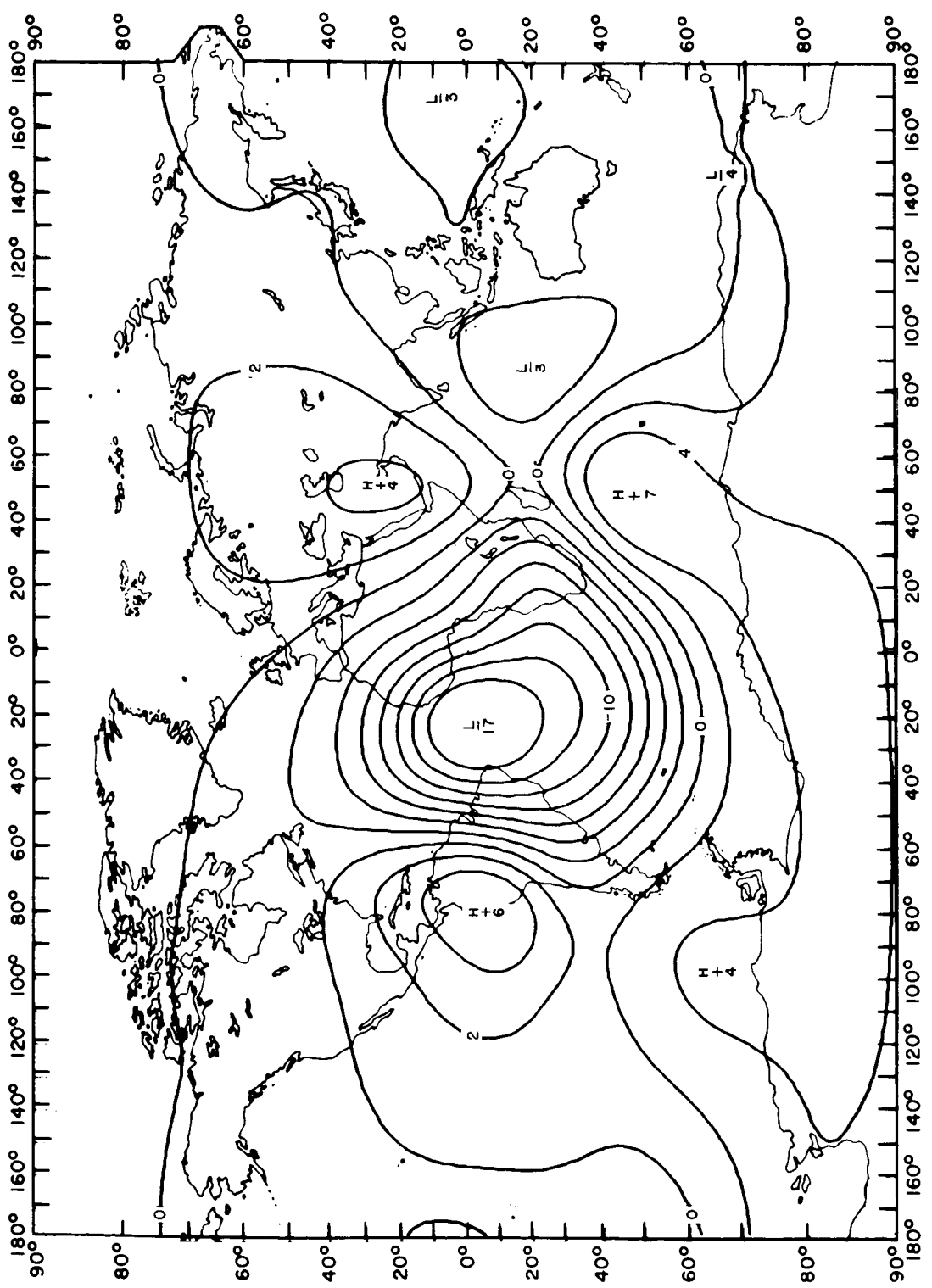
Geomagnetic secular change in minutes per year,  
inclination, epoch 1912.5. GSFC(12/66).



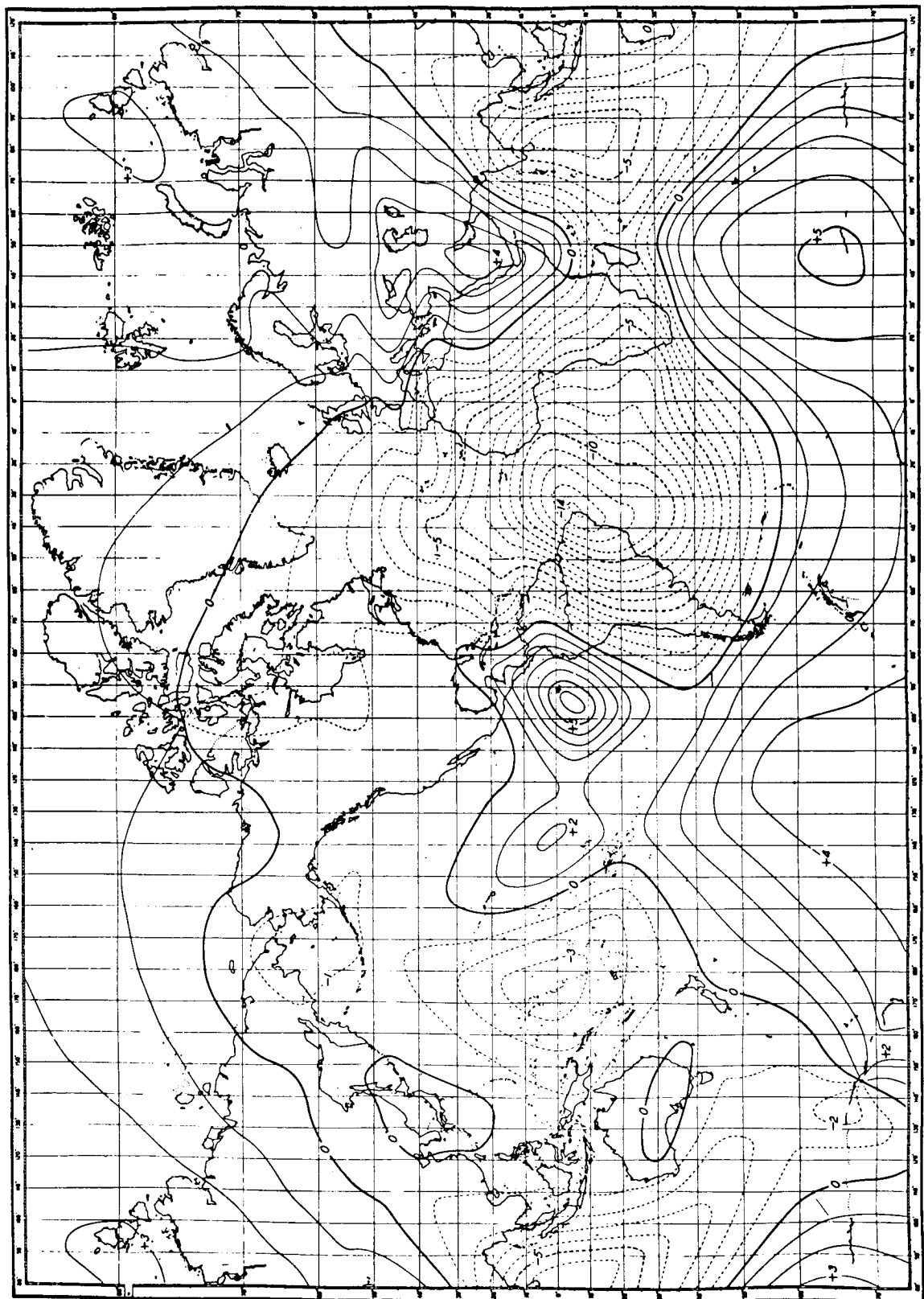
Geomagnetic secular change in minutes per year,  
inclination, epoch 1922.5. GSFC(12/66).



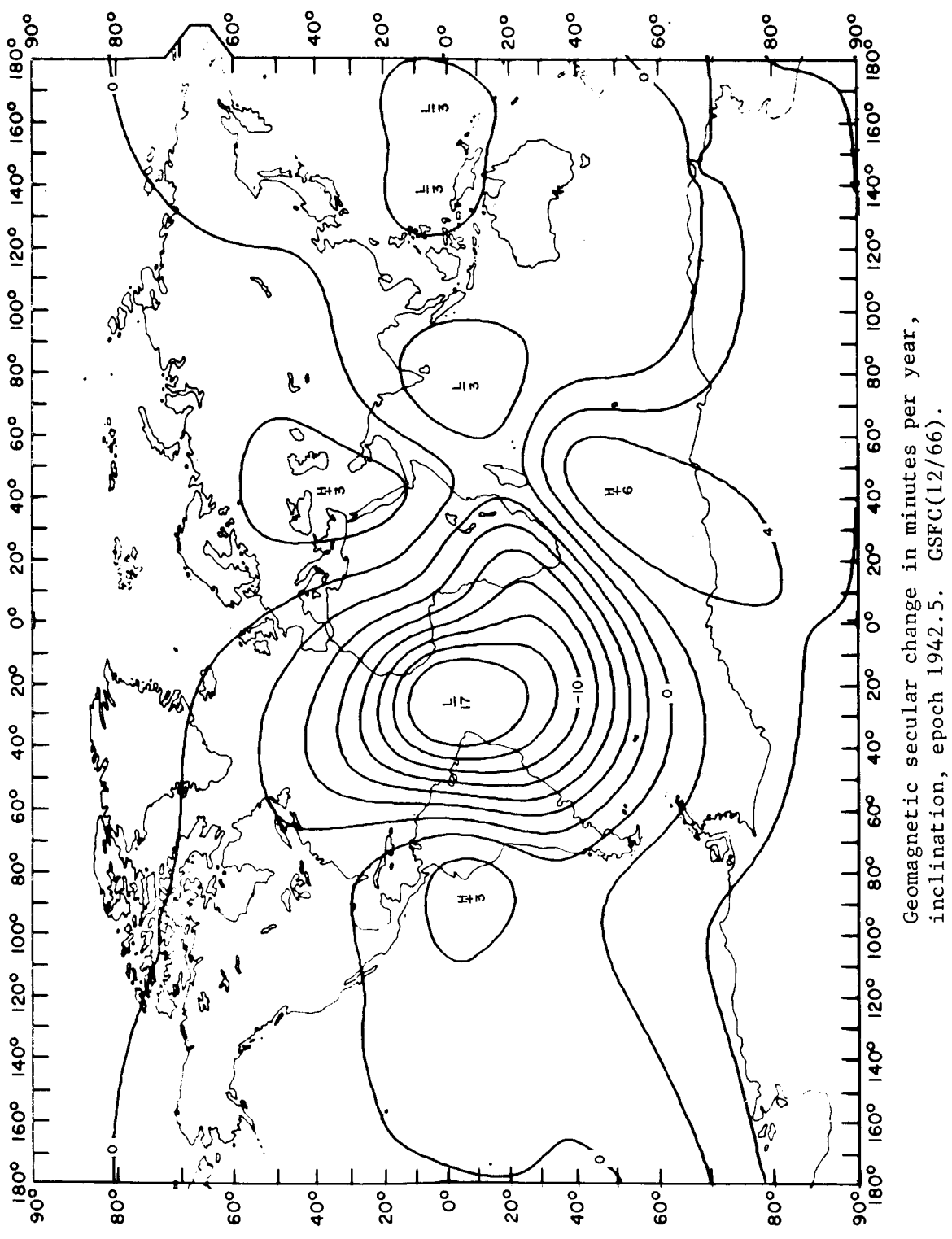
Geomagnetic secular change in minutes per year,  
inclination, epoch 1932.5. Vestine et al. (1959).



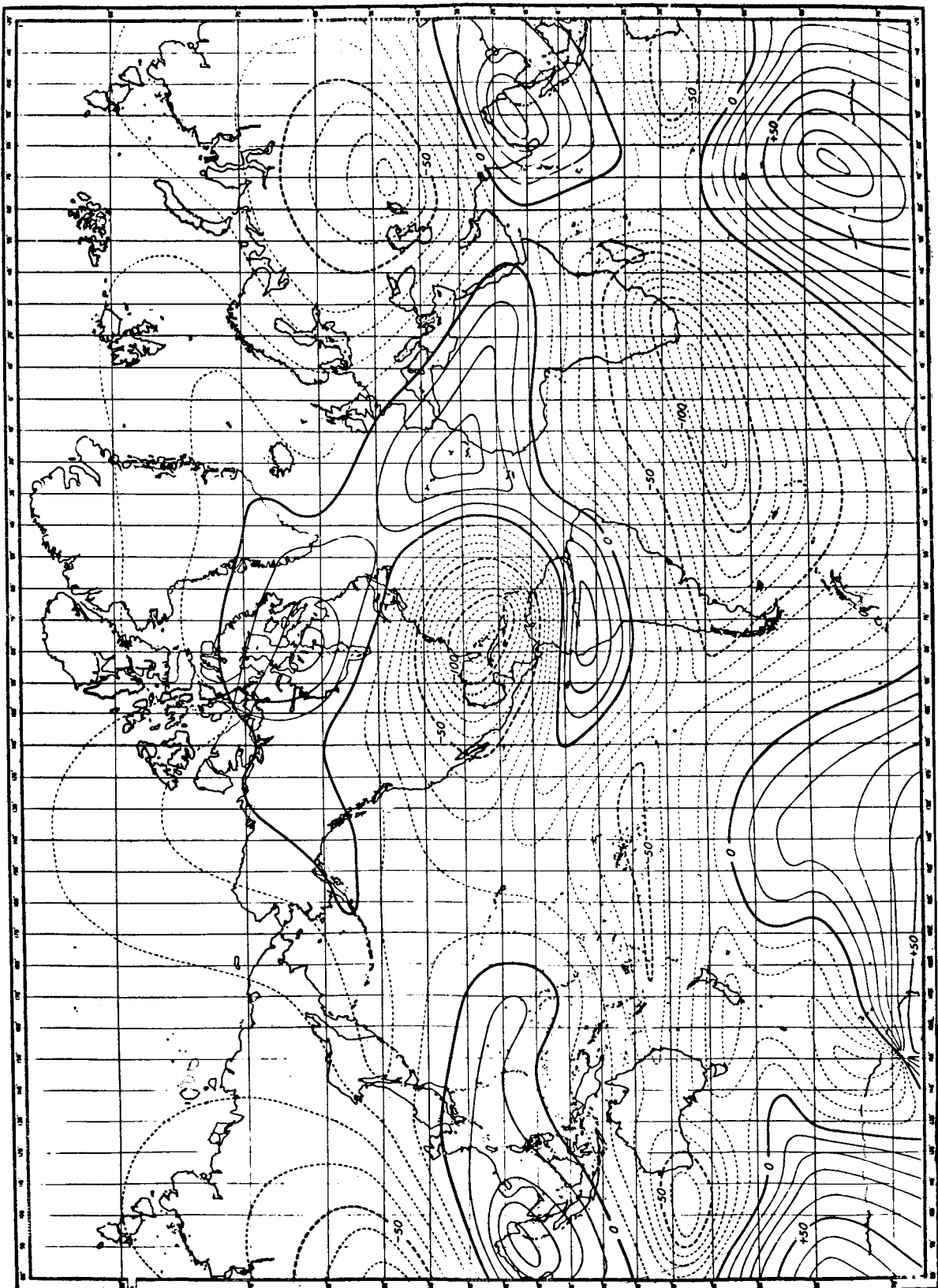
Geomagnetic secular change in minutes per year,  
inclination, epoch 1932.5. GSFC(12/66).



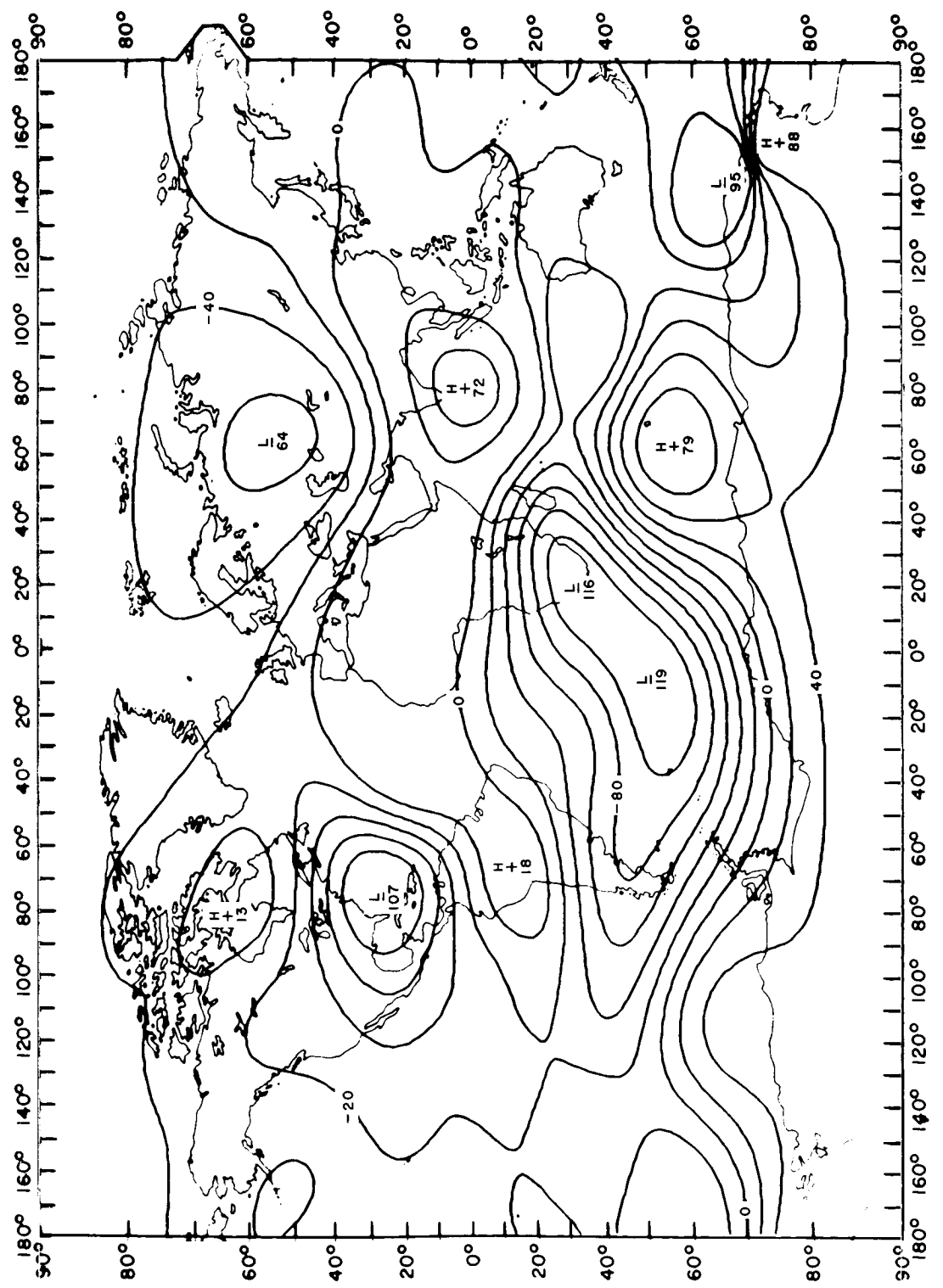
Geomagnetic secular change in minutes per year,  
inclination, epoch 1942.5. Vestine et al. (1959).



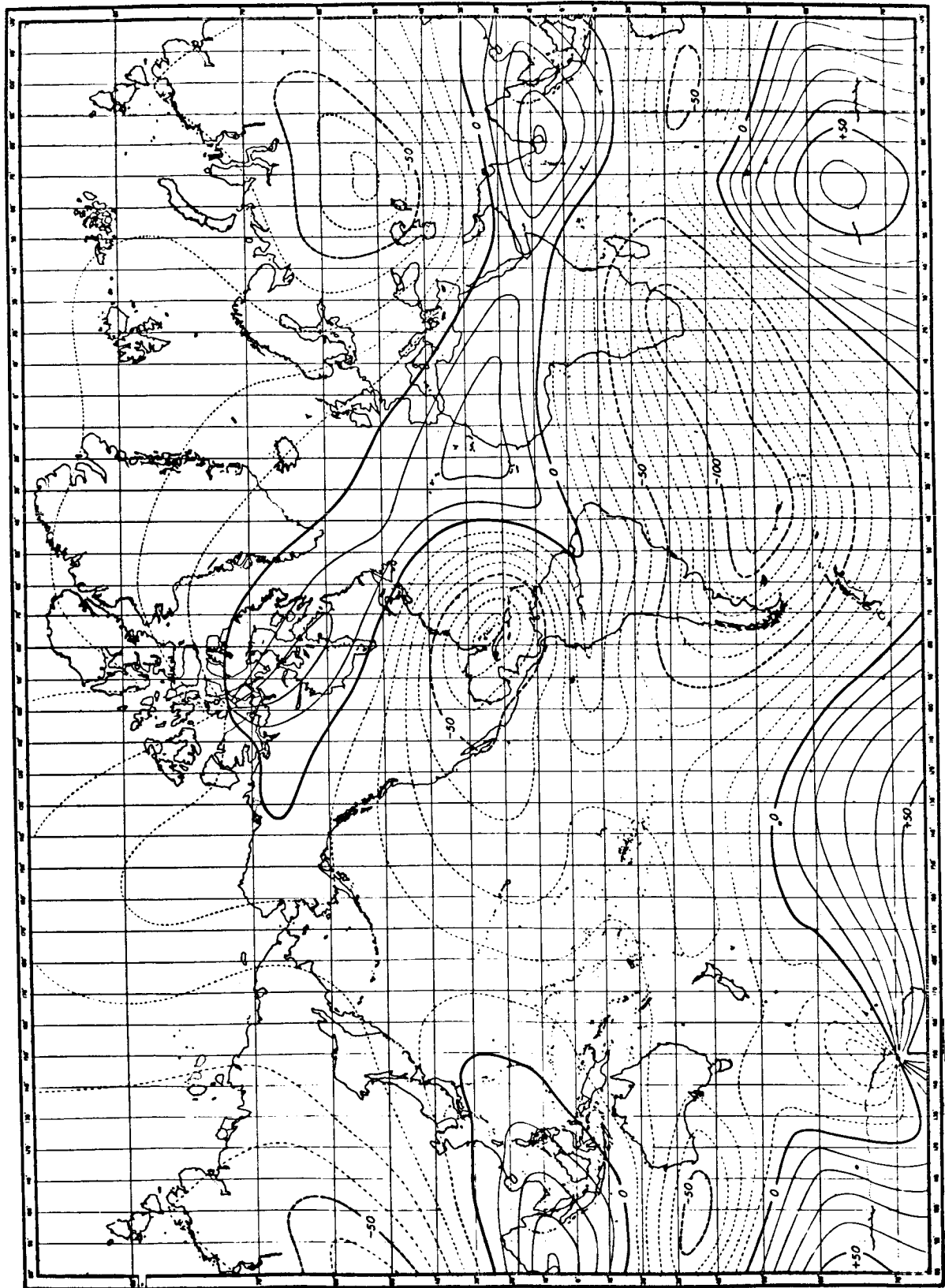
Geomagnetic secular change in minutes per year,  
inclination, epoch 1942.5. GSFC(12/66).



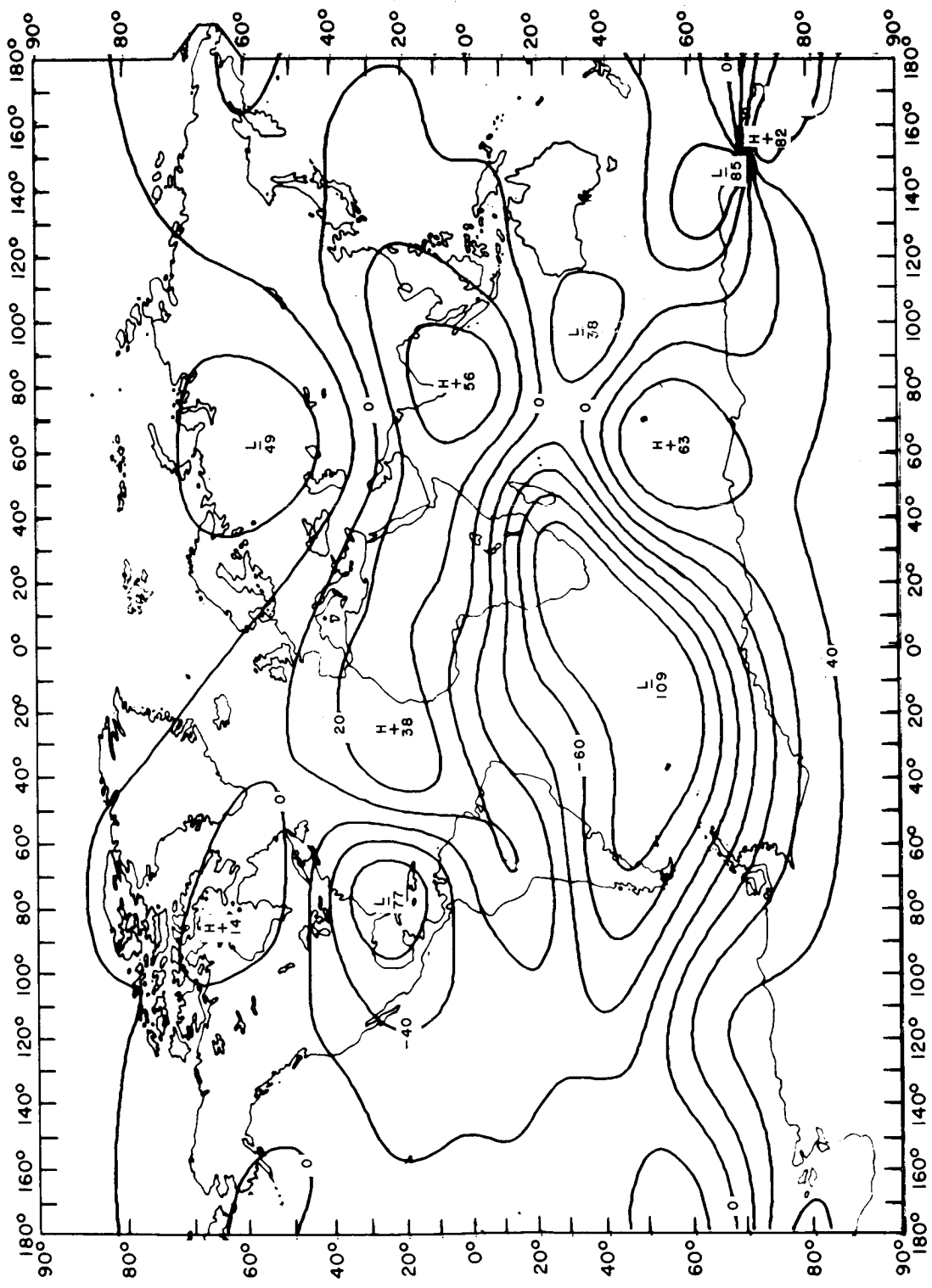
Geomagnetic secular change in gammas per year,  
horizontal component, epoch 1912.5. Vestine et al. (1959).



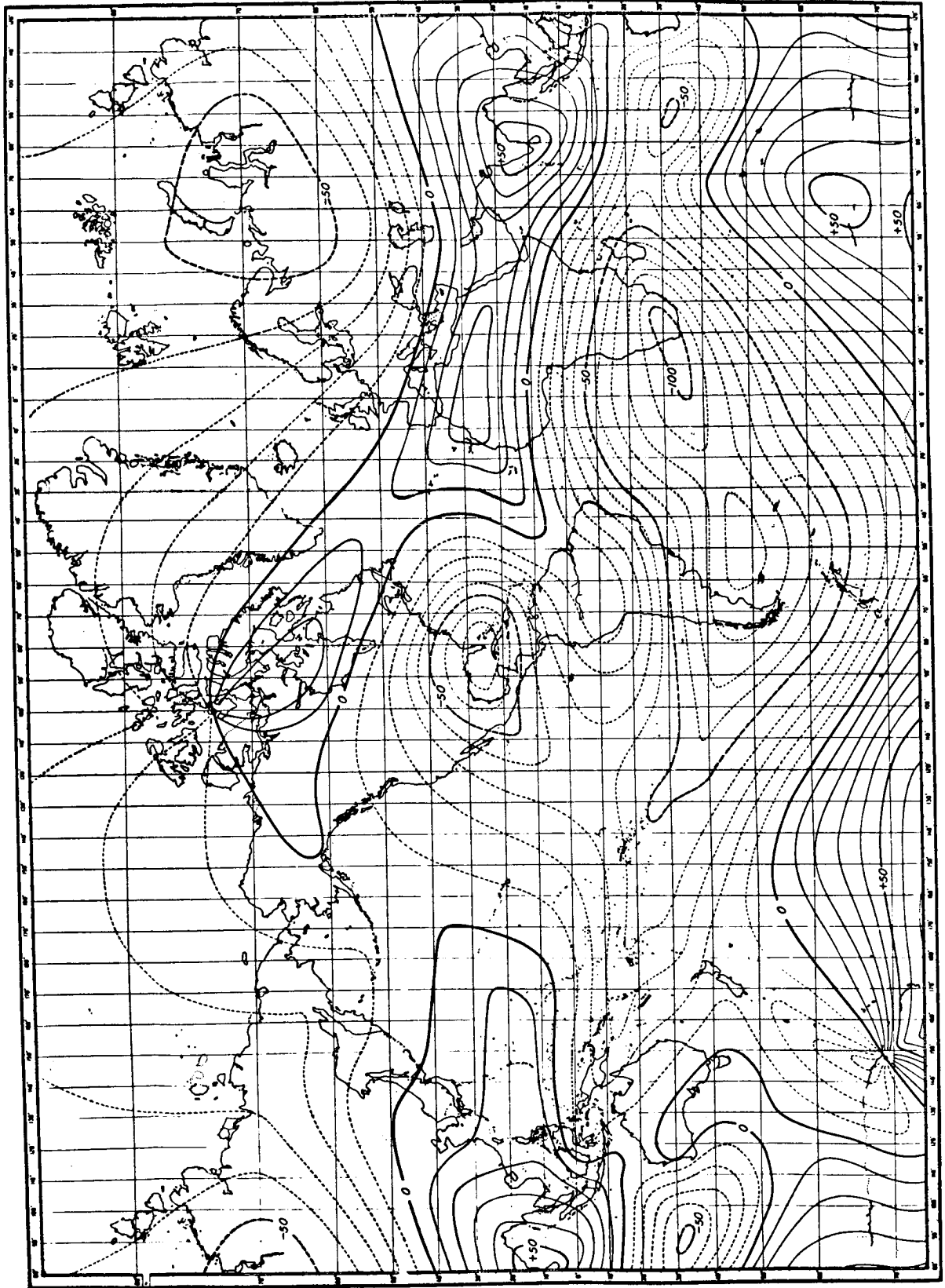
Geomagnetic secular change in gammas per year,  
horizontal component, epoch 1912.5. GSFC(12/66).



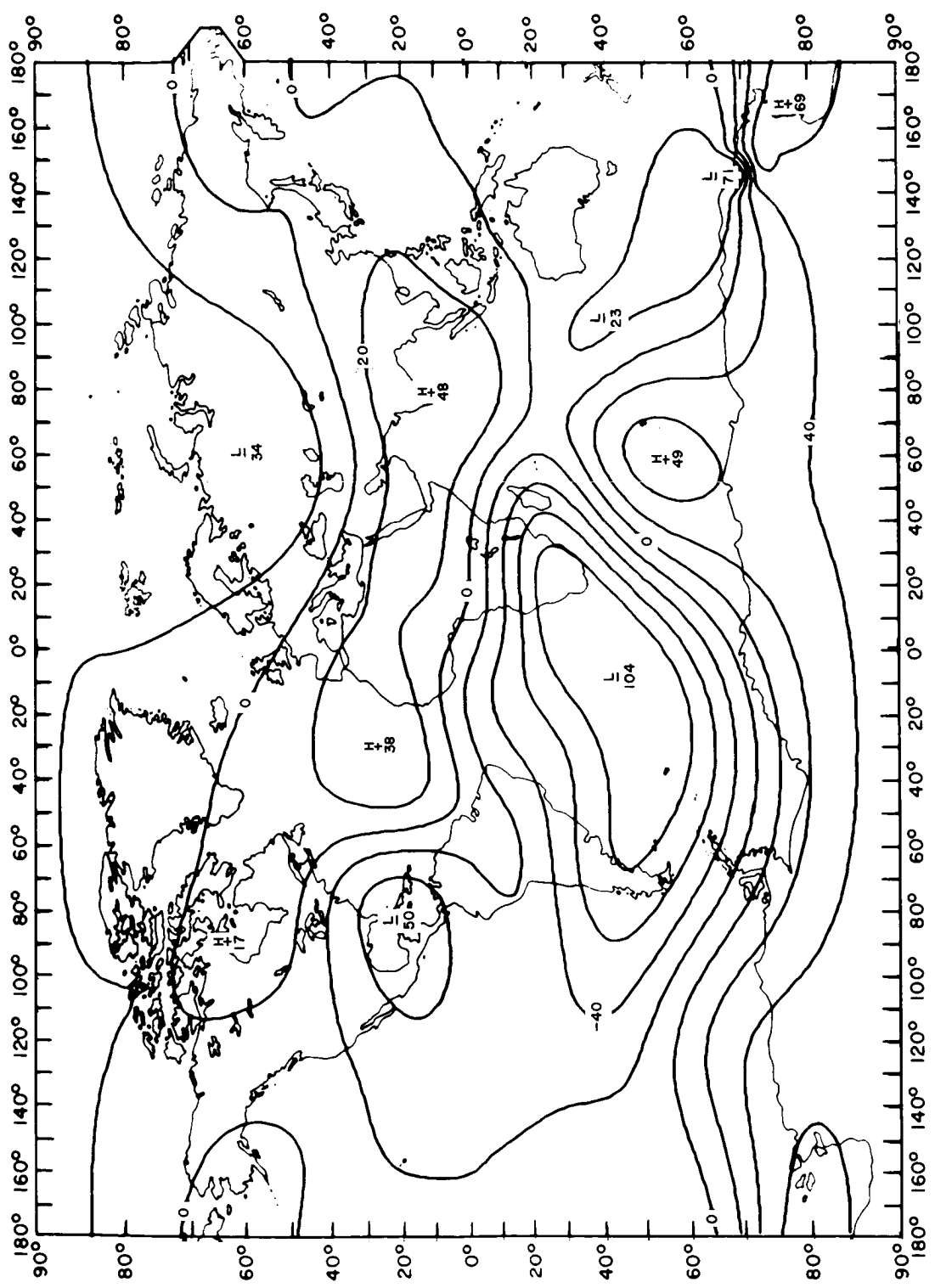
Geomagnetic secular change in gammas per year,  
horizontal component, epoch 1922.5. Vestine et al. (1959).



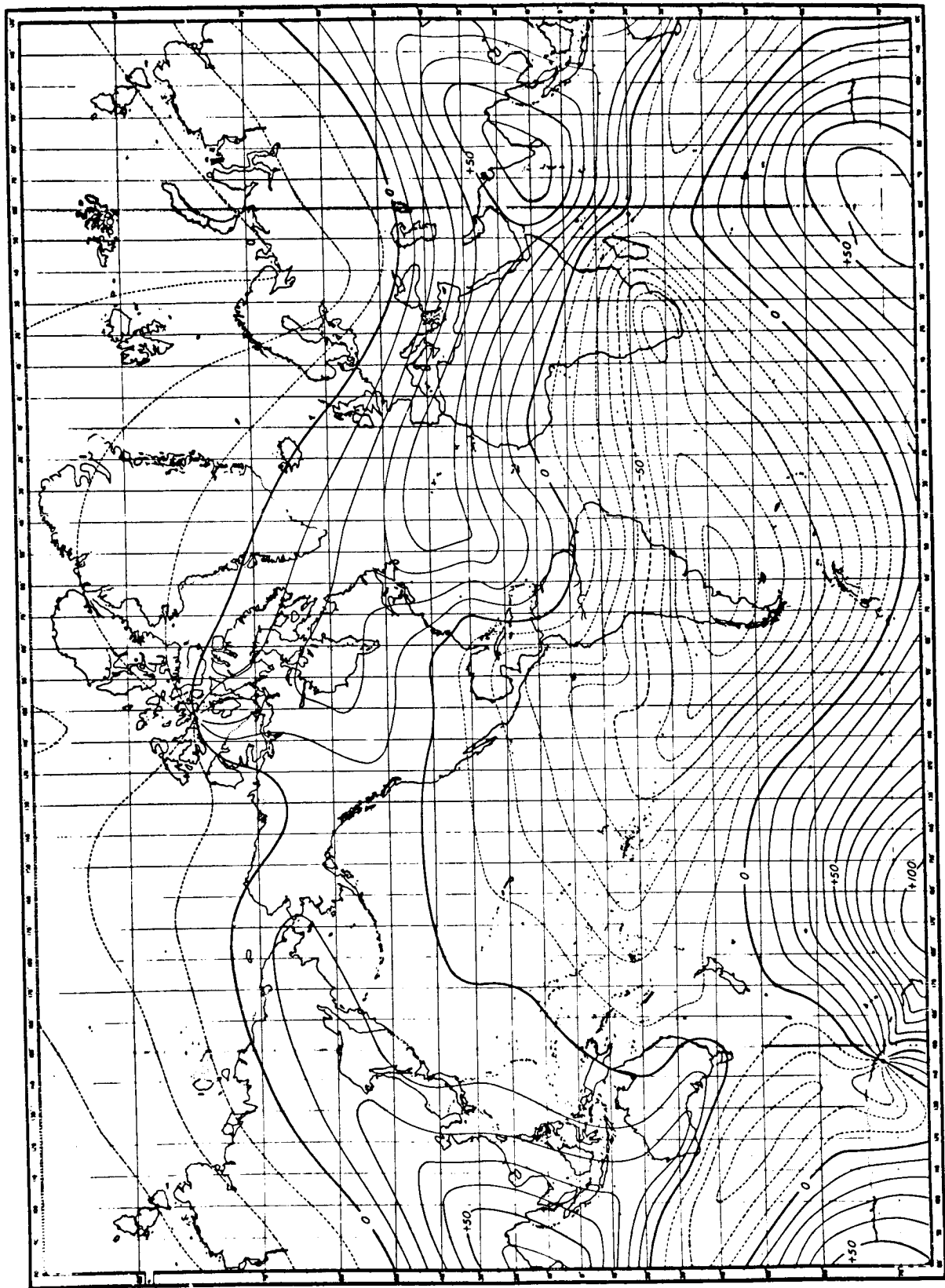
Geomagnetic secular change in gammas per year,  
horizontal component, epoch 1922.5. GSFC(12/66).



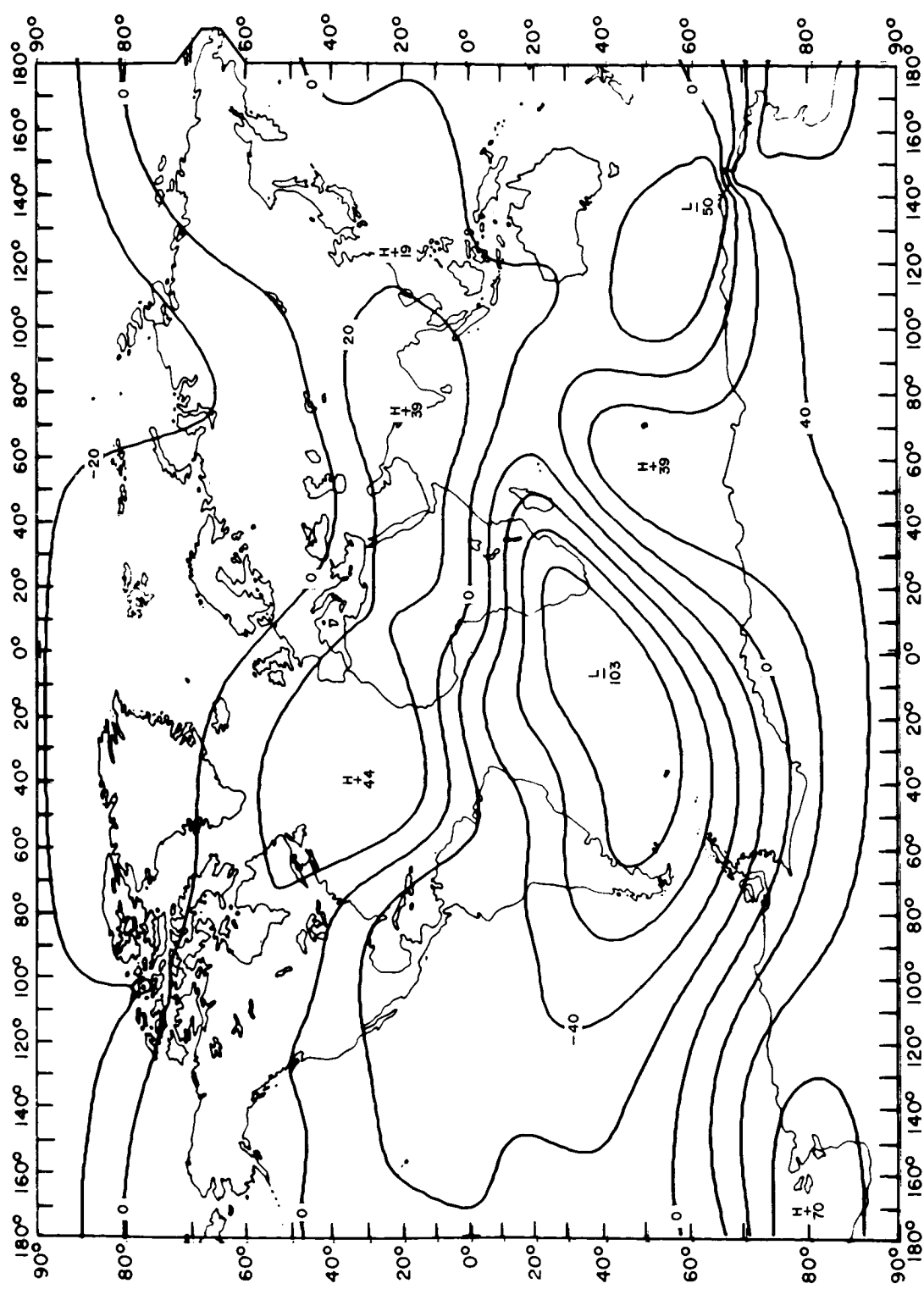
Geomagnetic secular change in gammas per year,  
horizontal component, epoch 1932.5. Vestine et al. (1959).



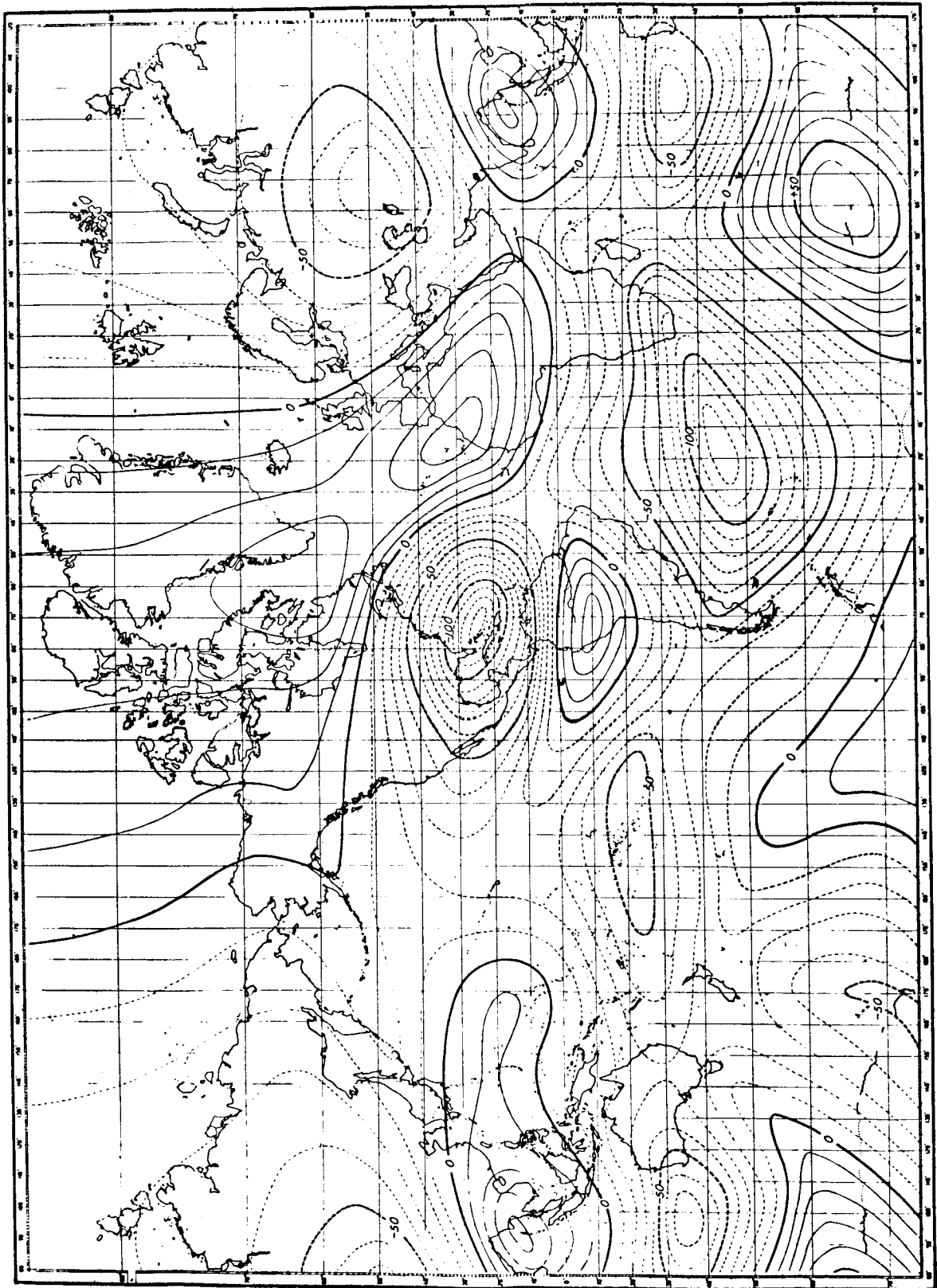
Geomagnetic secular change in gammas per year,  
horizontal component, epoch 1932.5. GSFC(12/66).



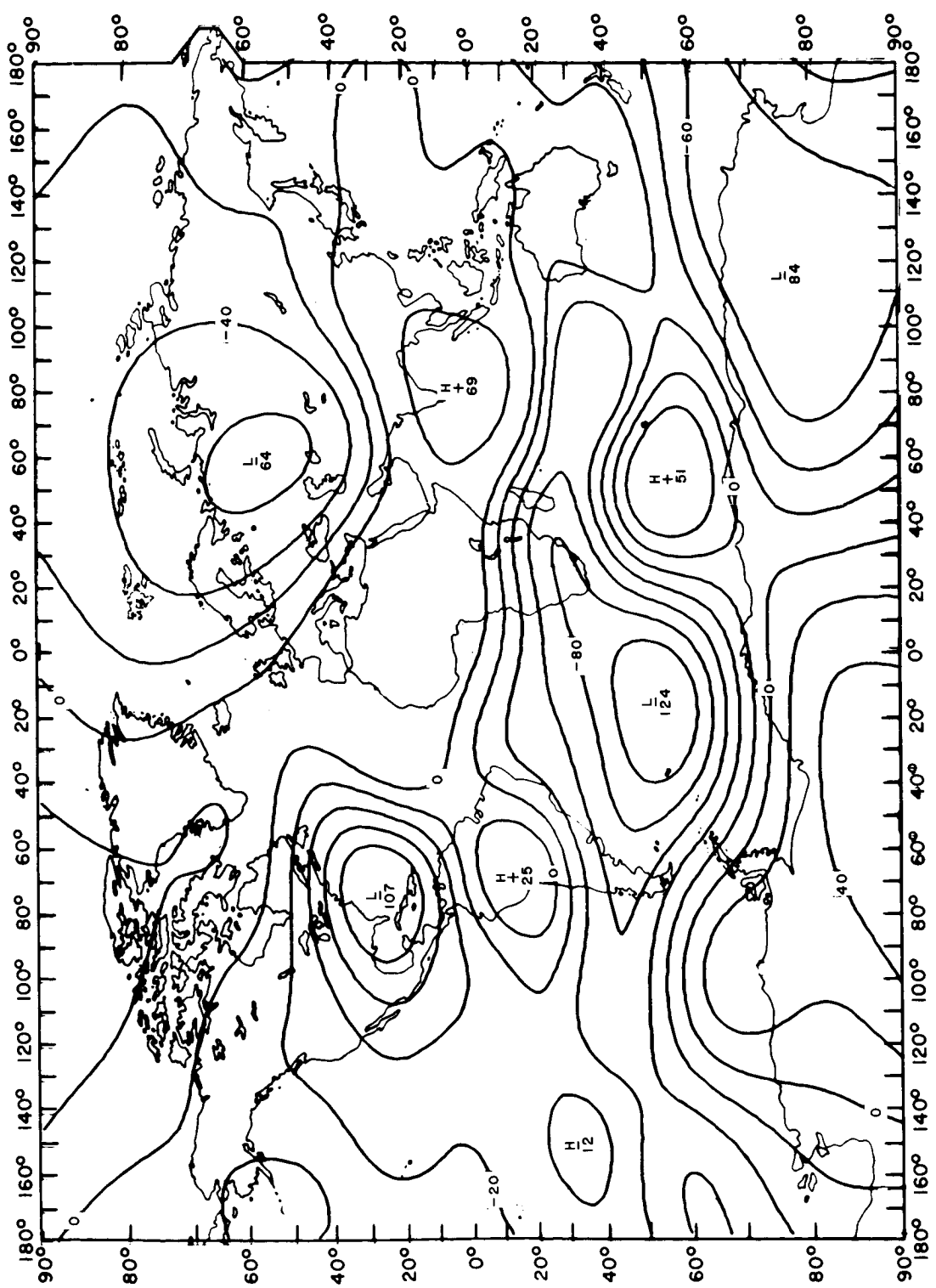
Geomagnetic secular change in gammas per year,  
horizontal component, epoch 1942.5. Vestine et al. (1959).



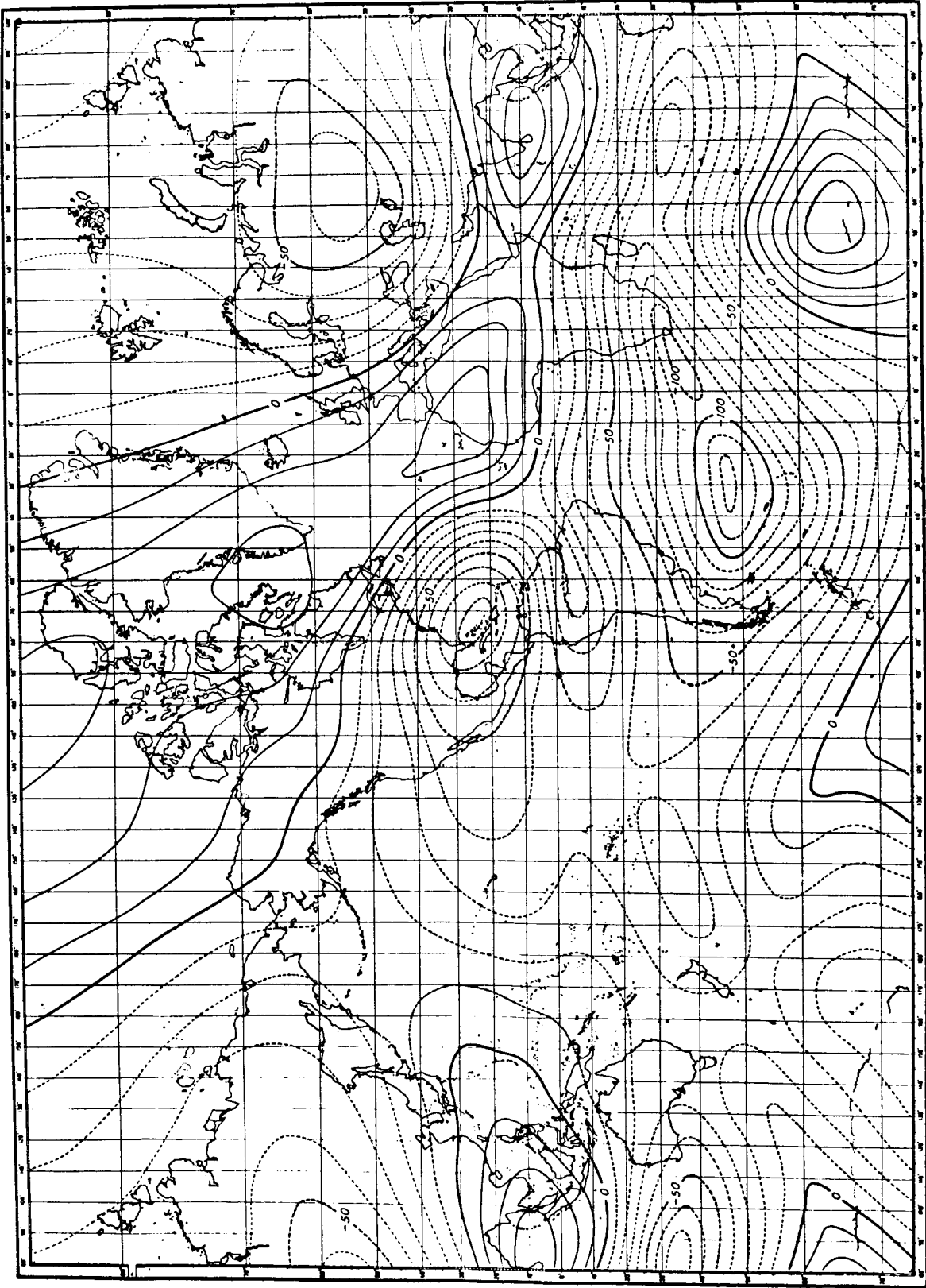
Geomagnetic secular change in gammas per year,  
horizontal component, epoch 1942.5. GSFC(12/66).



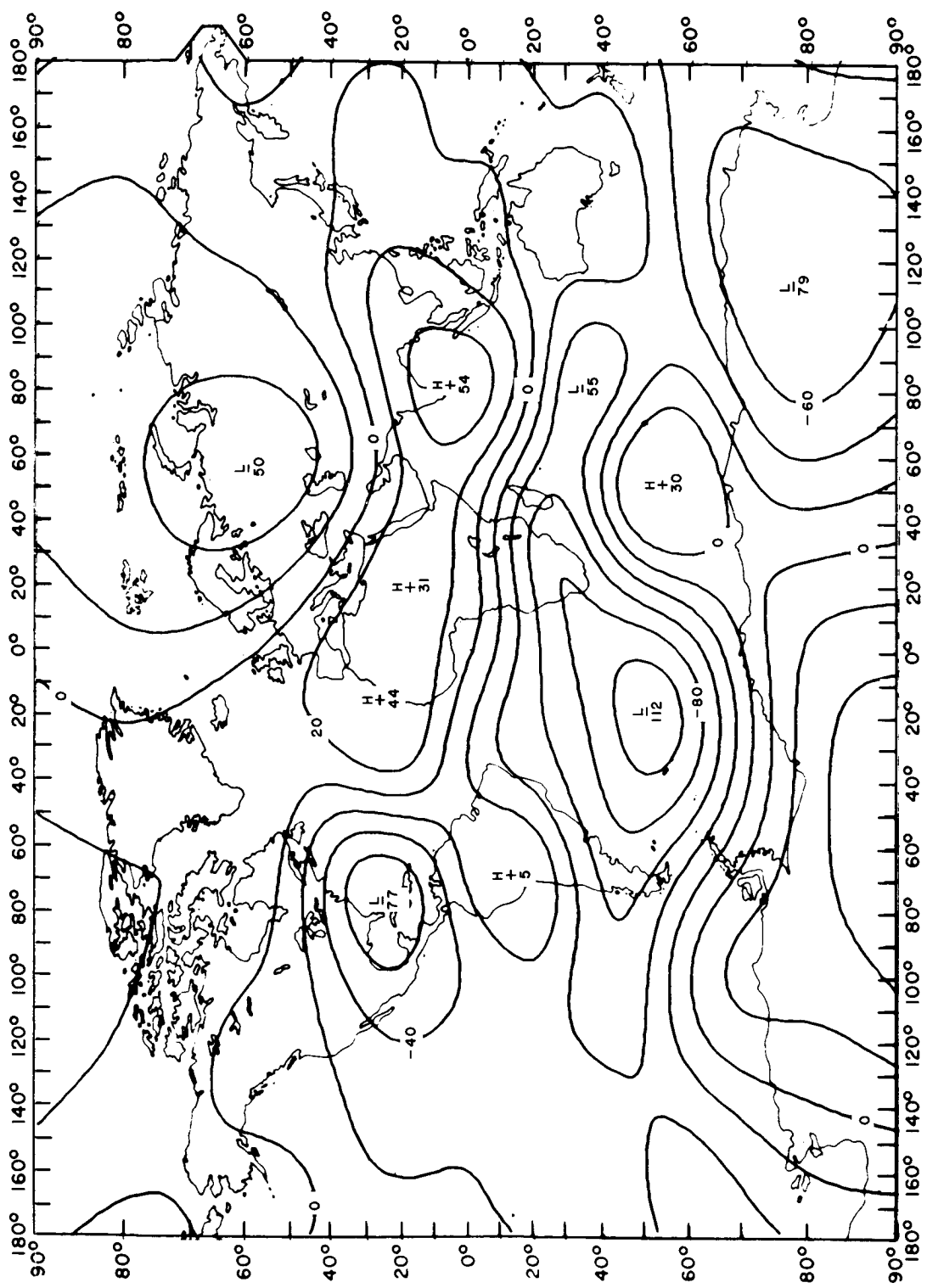
Geomagnetic secular change in gammas per year,  
north component, epoch 1912.5. Vestine et al. (1959).



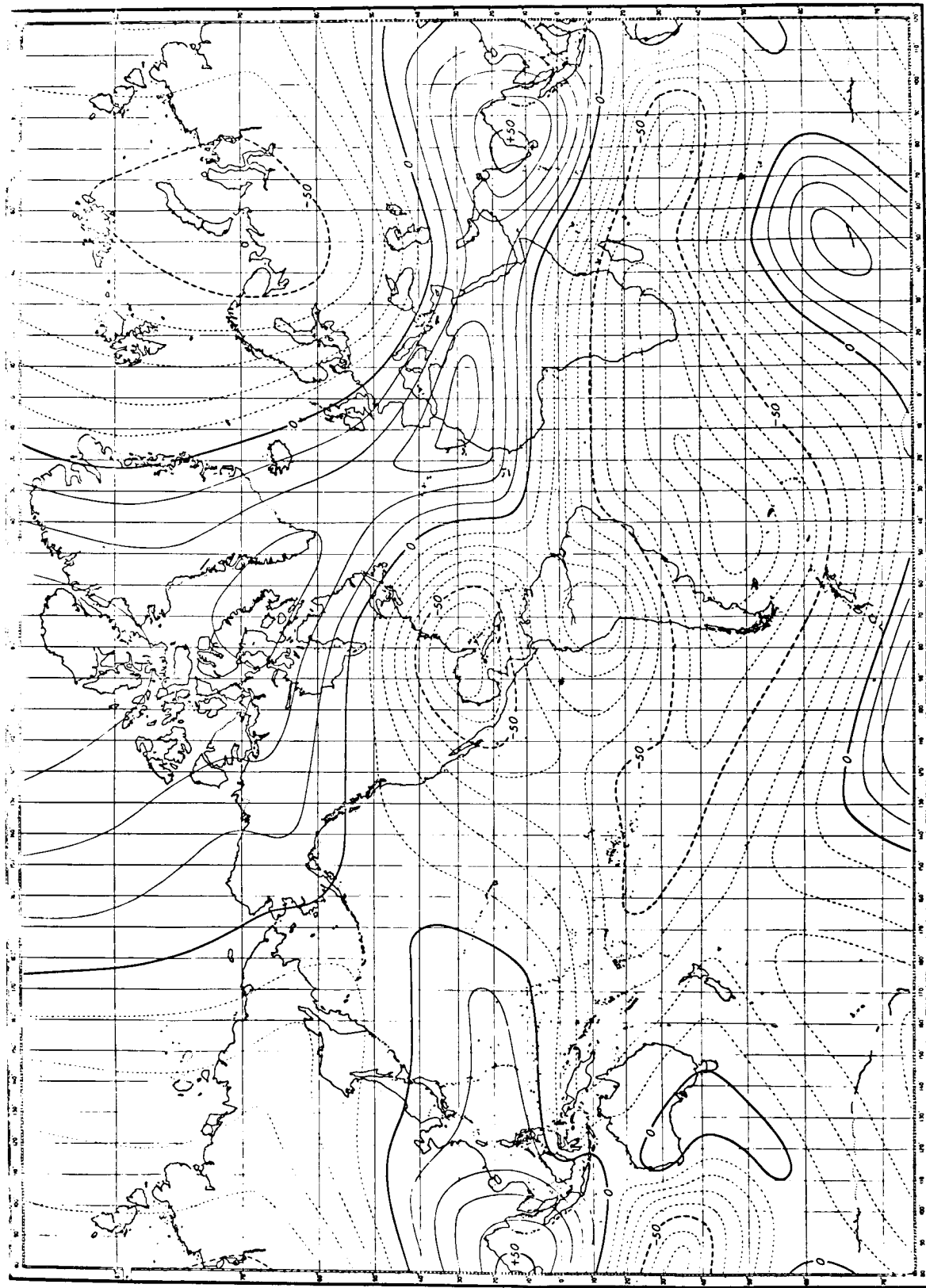
Geomagnetic secular change in gammas per year,  
north component, epoch 1912.5. GSFC(12/66).



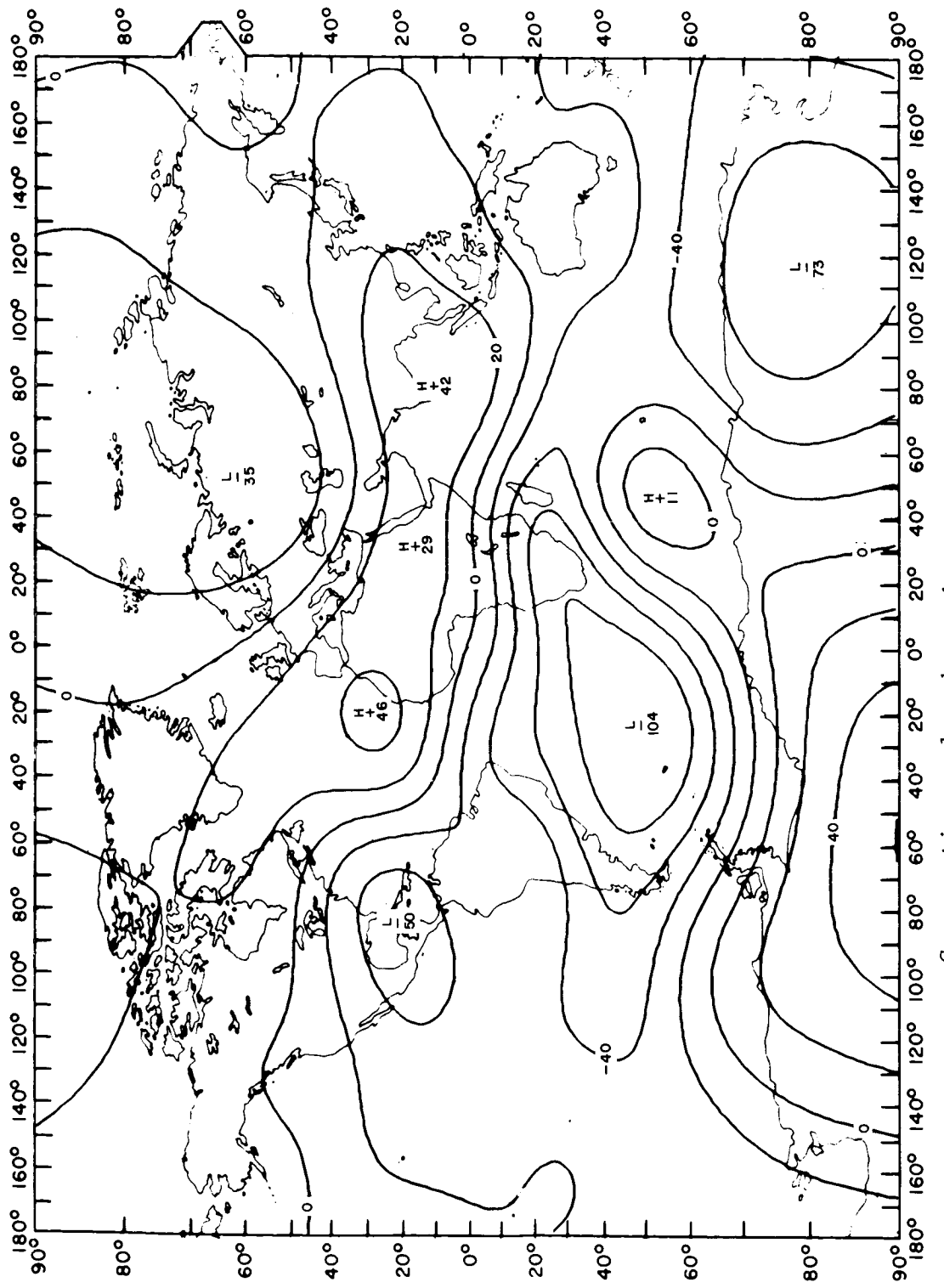
Geomagnetic secular change in gammas per year,  
north component, epoch 1922.5. Vestine et al. (1959).



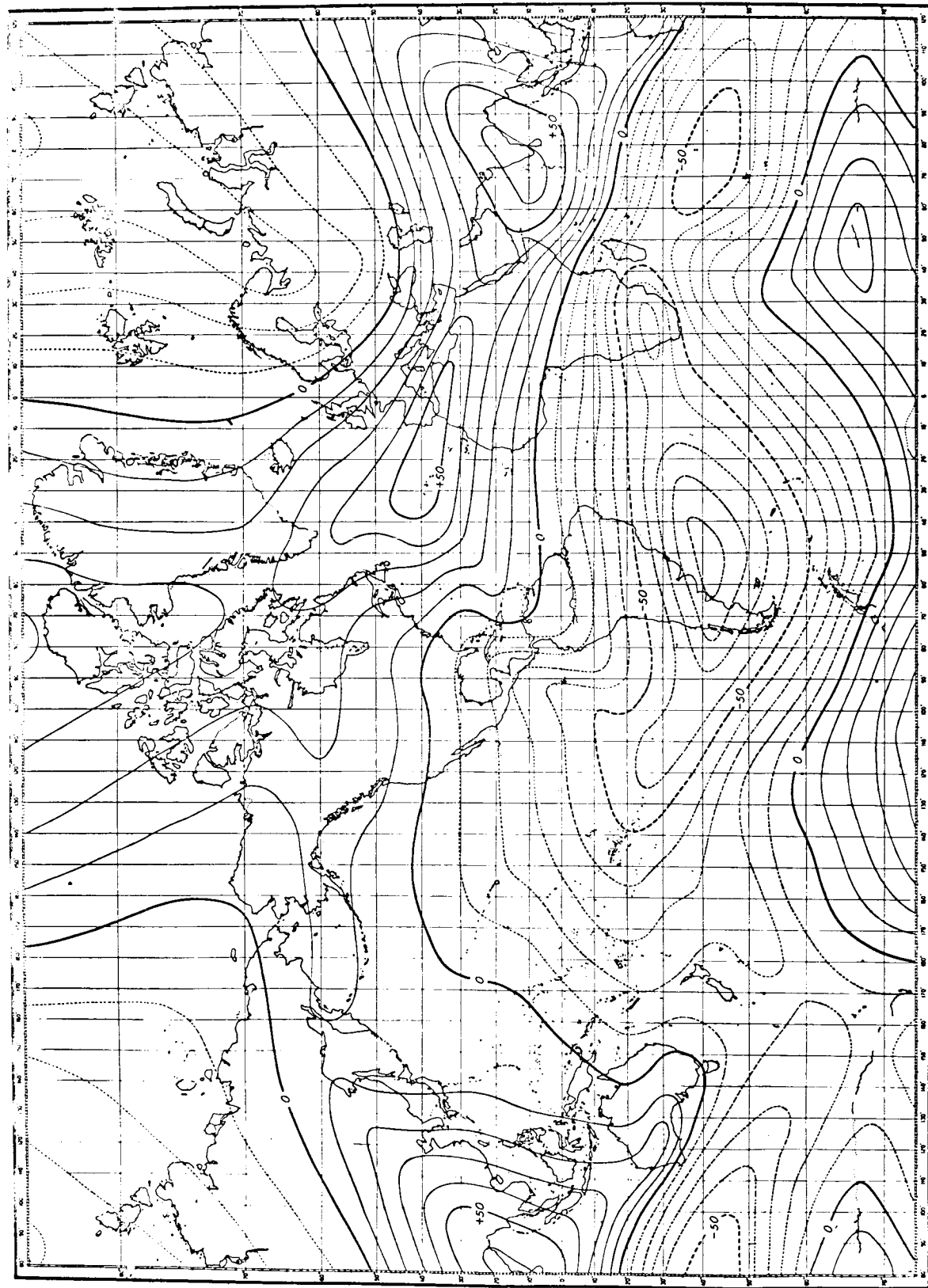
Geomagnetic secular change in gammas per year,  
north component, epoch 1922.5. GSFC(12/66).



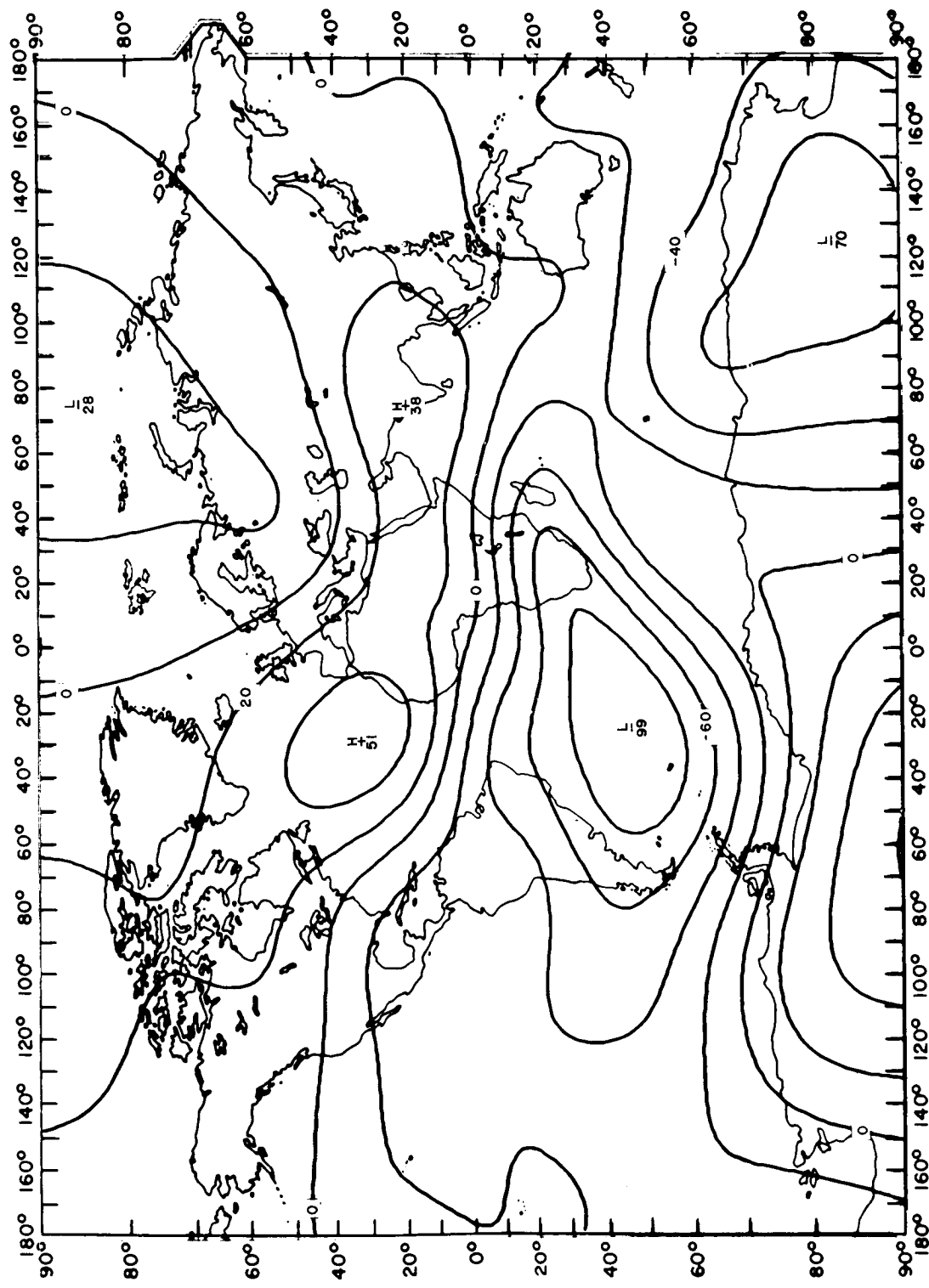
Geomagnetic secular change in gammas Per year,  
north component, epoch 1932.5. Vestine et al. (1959).



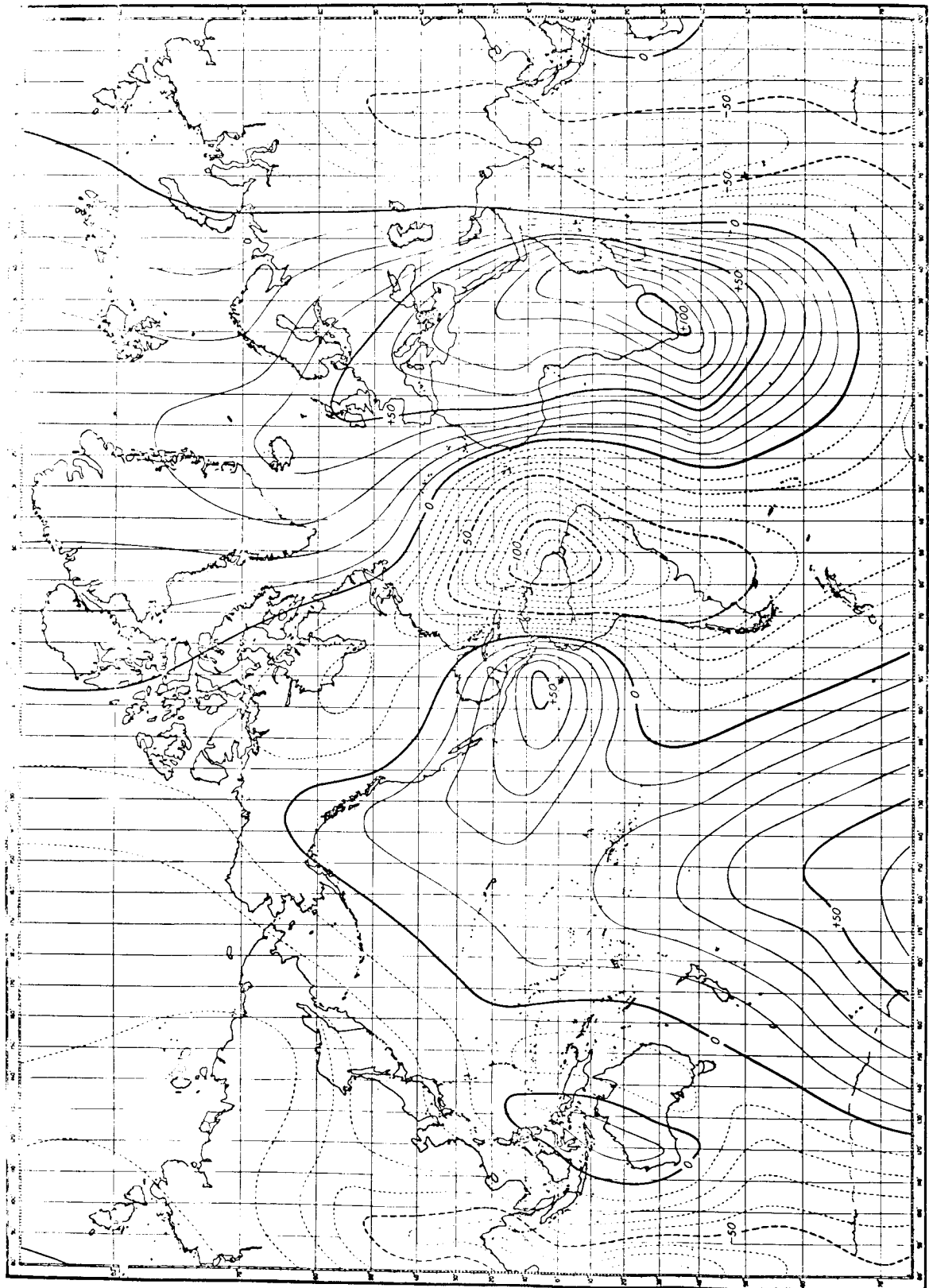
Geomagnetic secular change in gammas per year,  
north component, epoch 1932.5. GSFC(12/66).



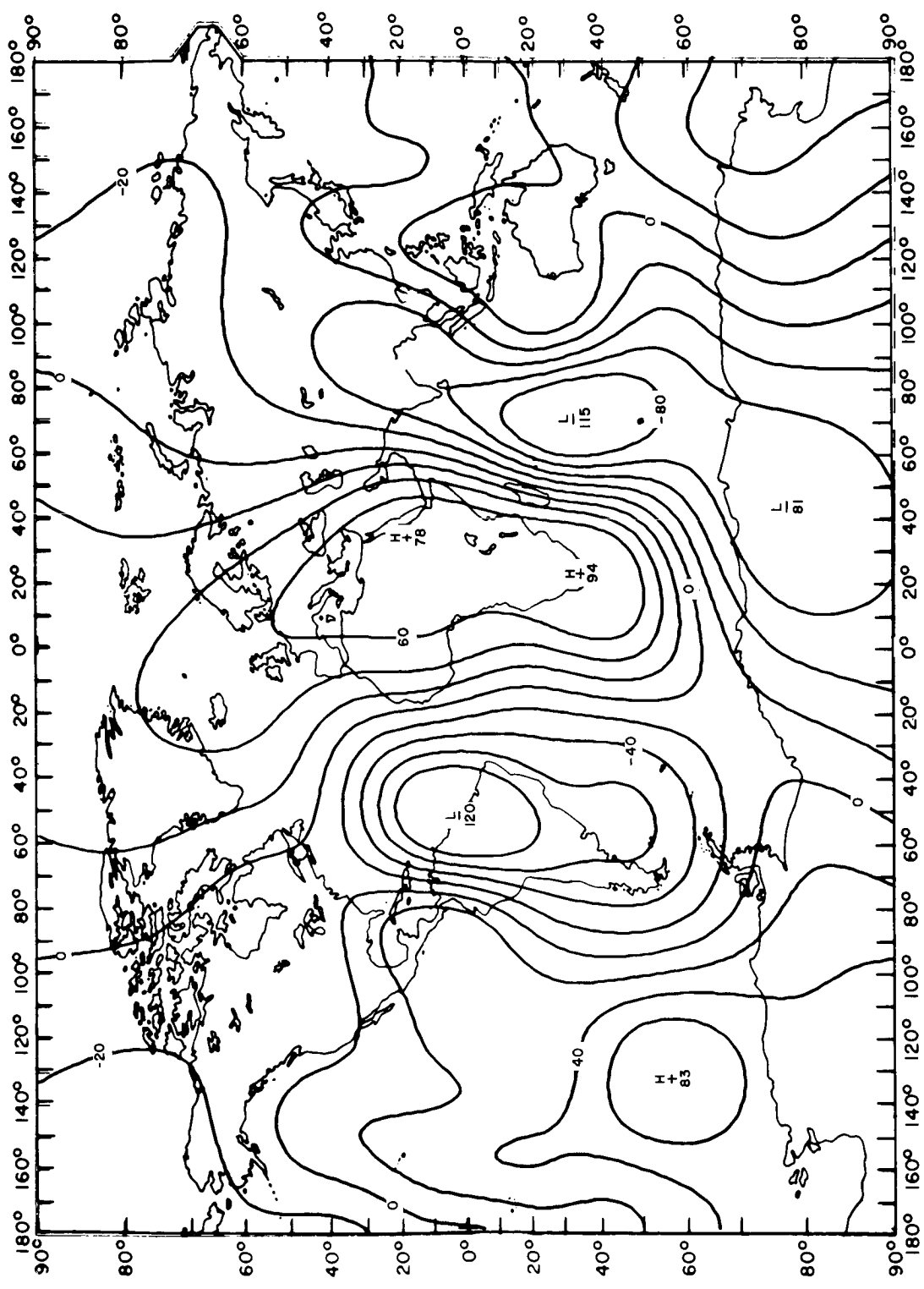
Geomagnetic secular change in gammas per year,  
north component, epoch 1942.5. Vestine et al. (1959).



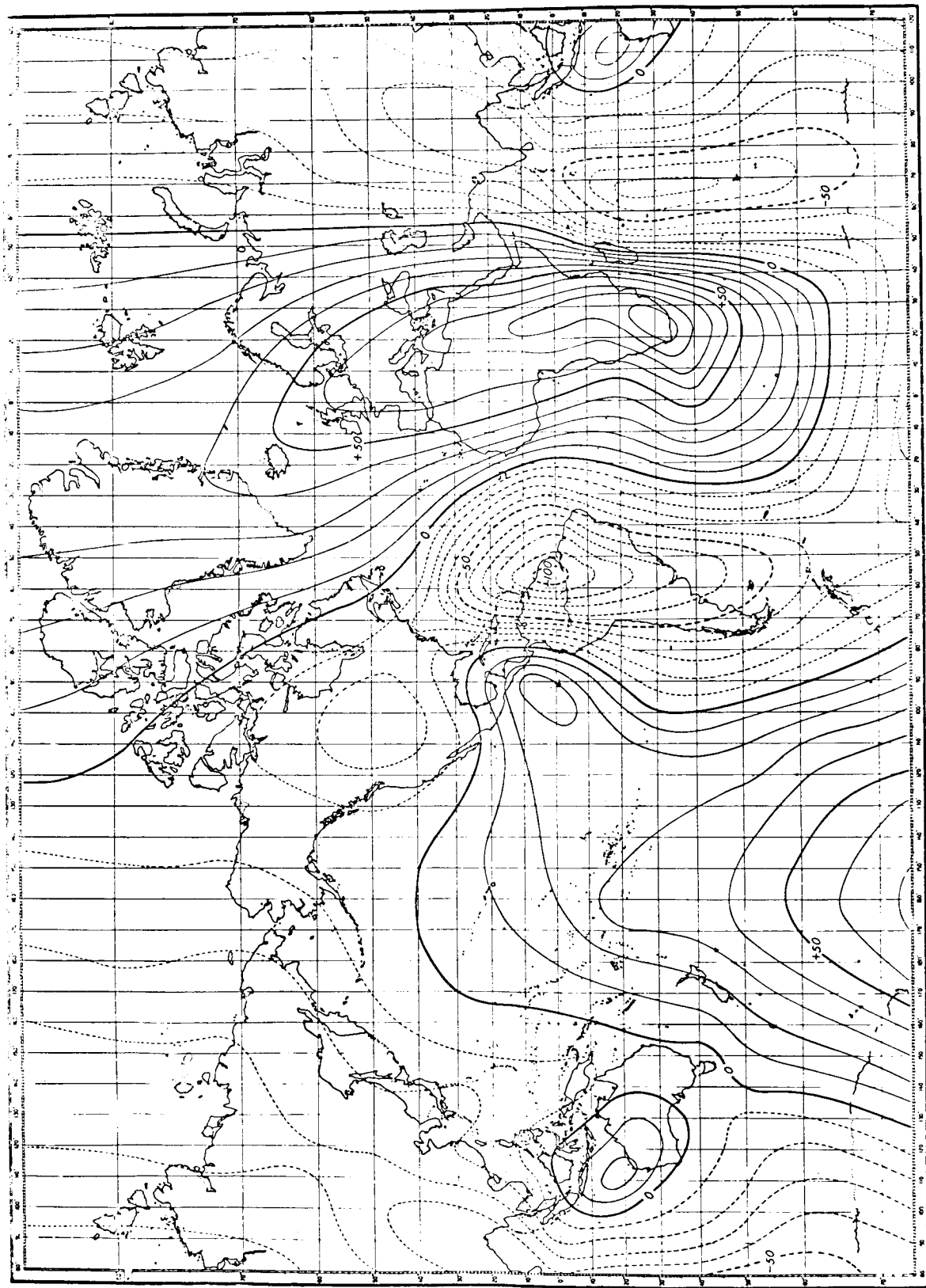
Geomagnetic secular change in gammas per year,  
north component, epoch 1942.5. GSFC(12/66).



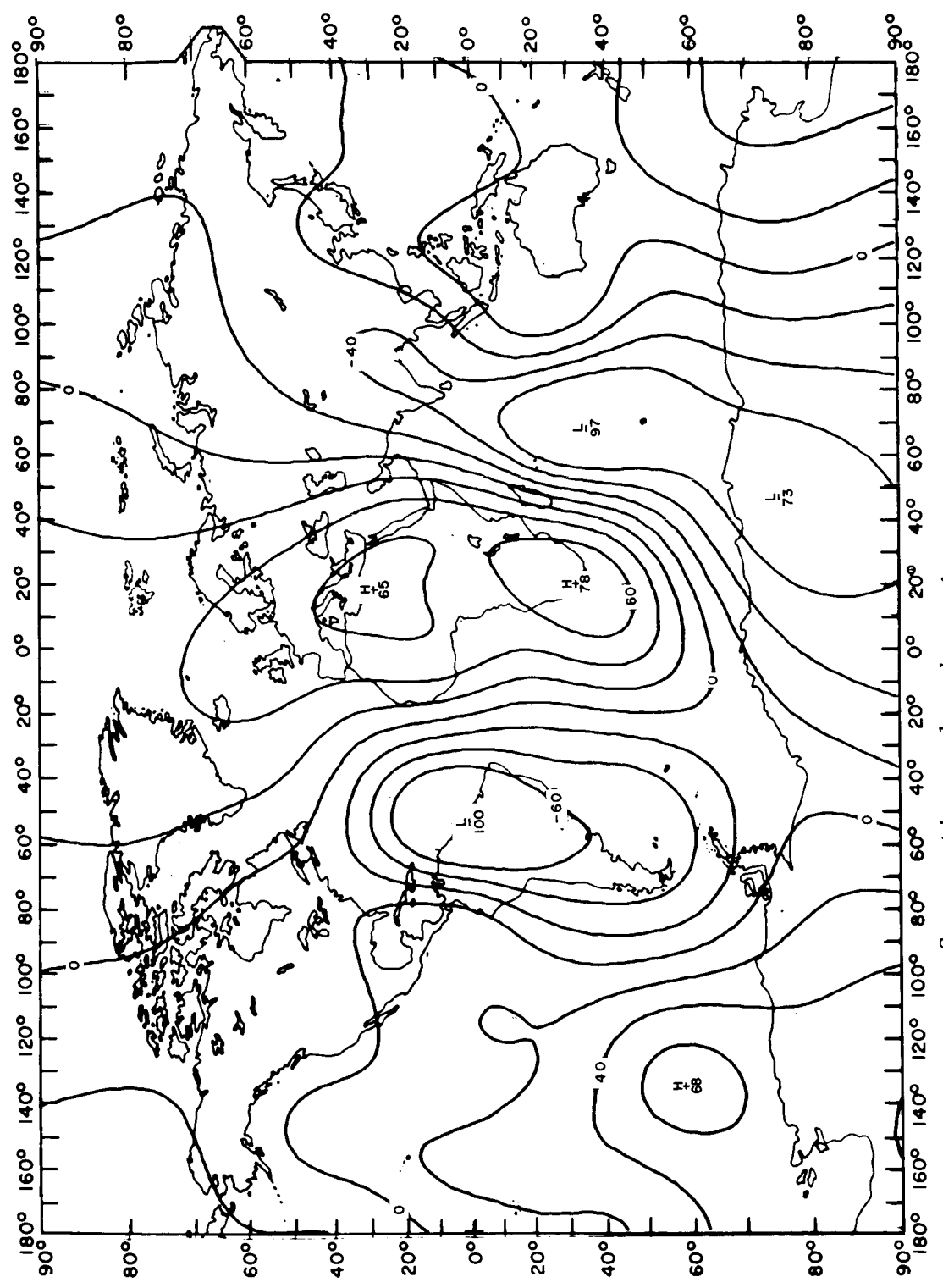
Geomagnetic secular change in gammas per year,  
east component, epoch 1912.5. Vestine et al. (1959).



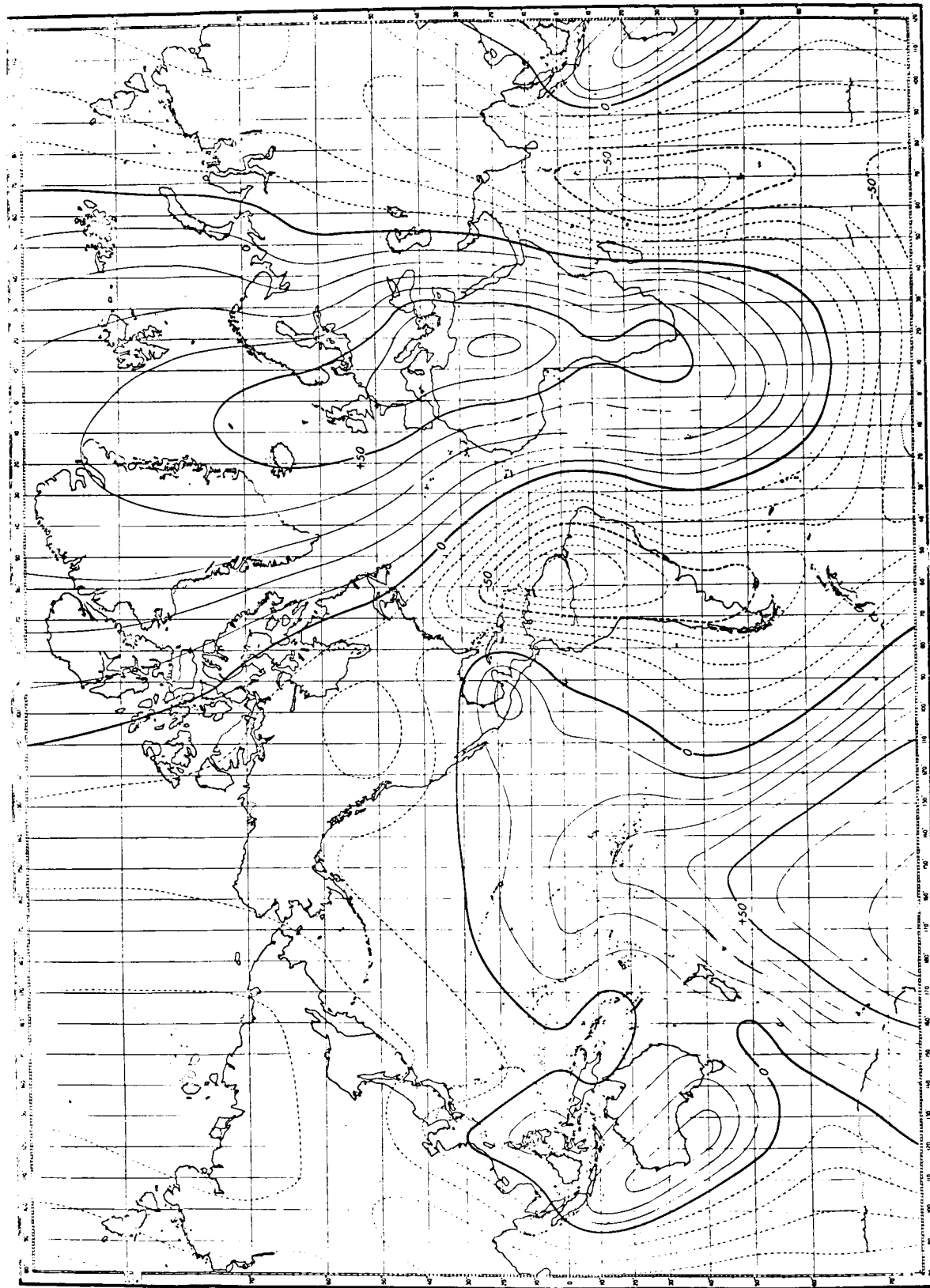
Geomagnetic secular change in gammas per year,  
east component, epoch 1912.5. GSFC(12/66).



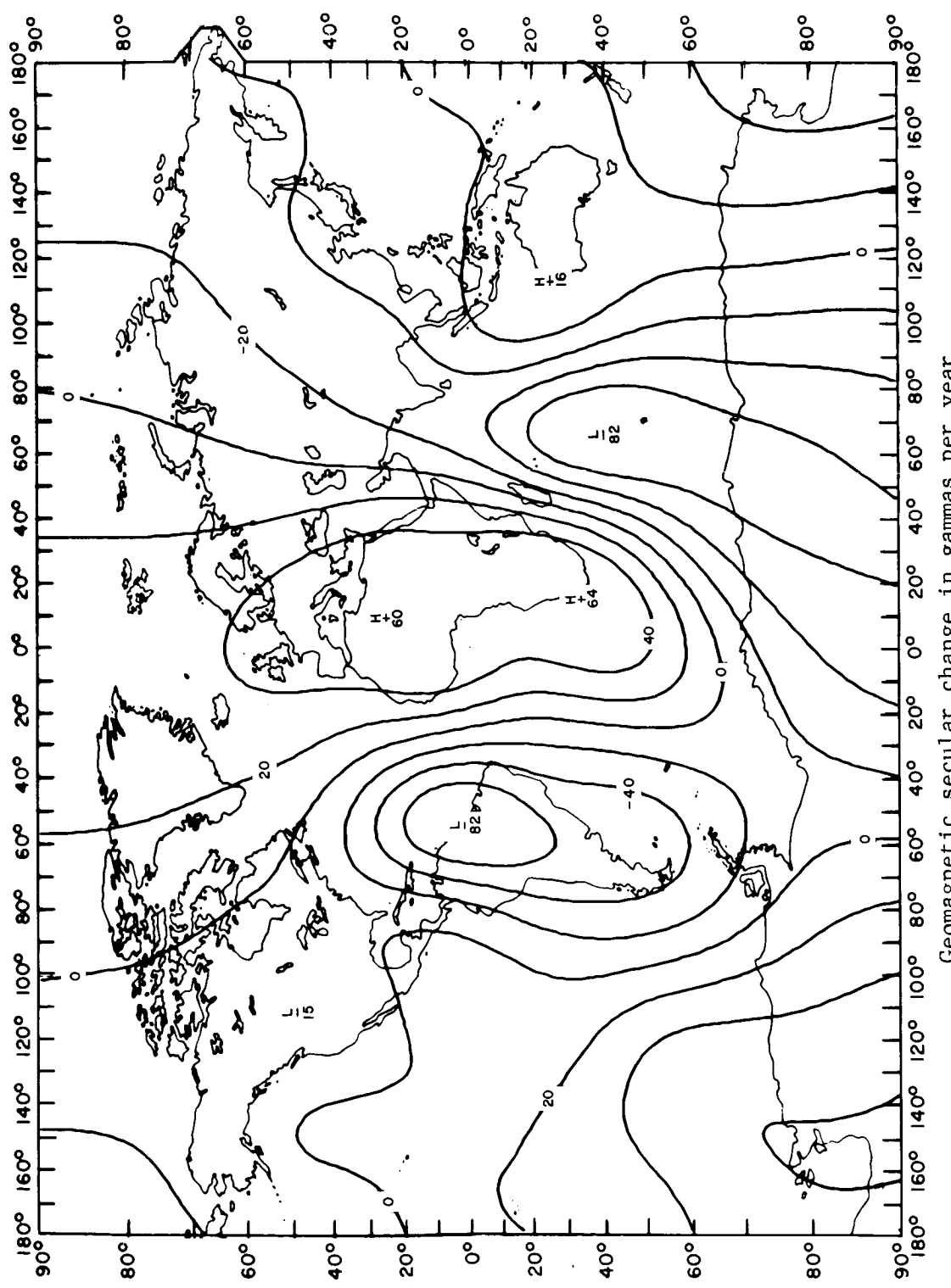
Geomagnetic secular change in gammas per year,  
east component, epoch 1922.5. Vestine et al. (1959).



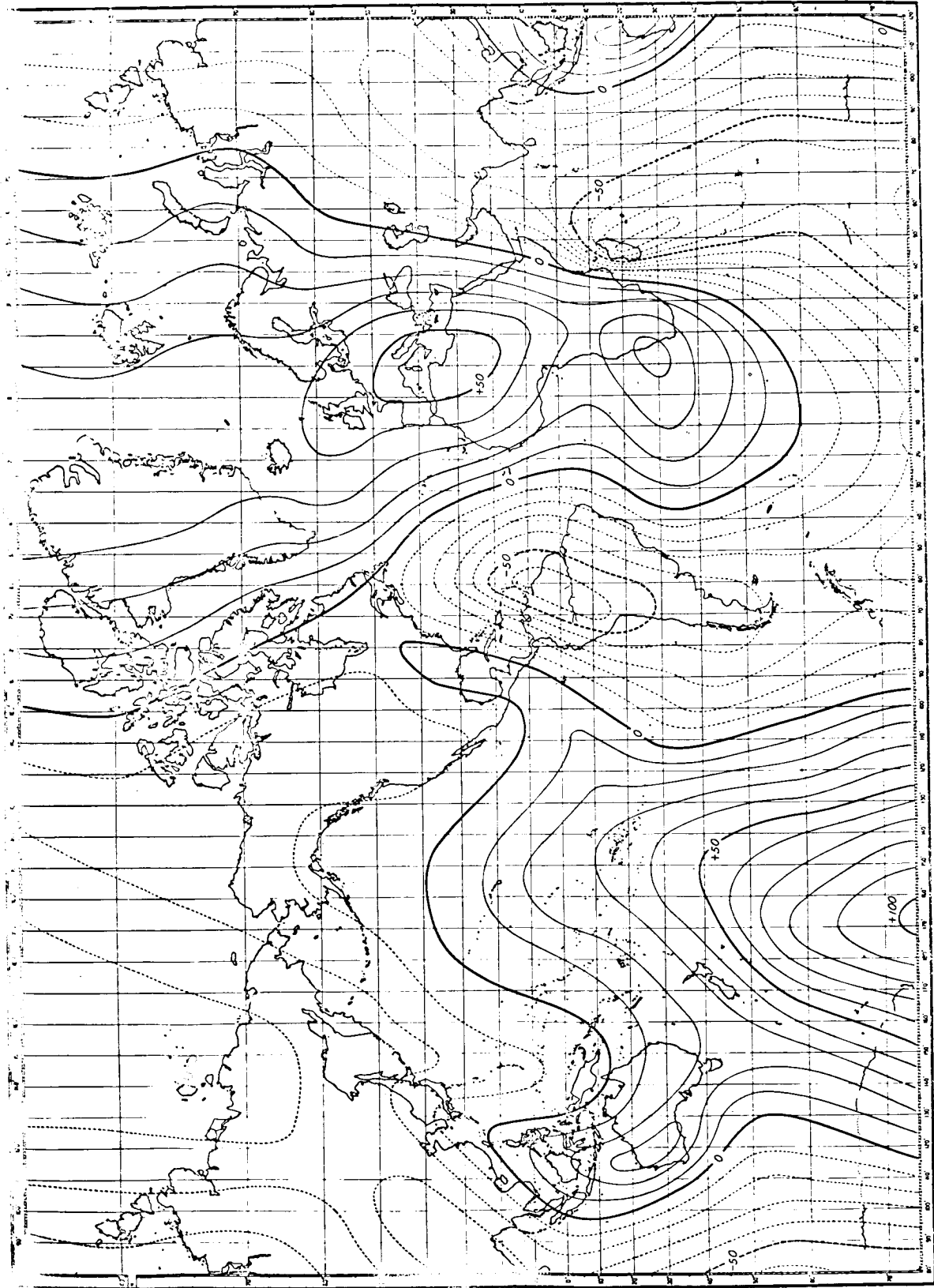
Geomagnetic secular change in gammas per year,  
east component, epoch 1922.5. GSFC(12/66).



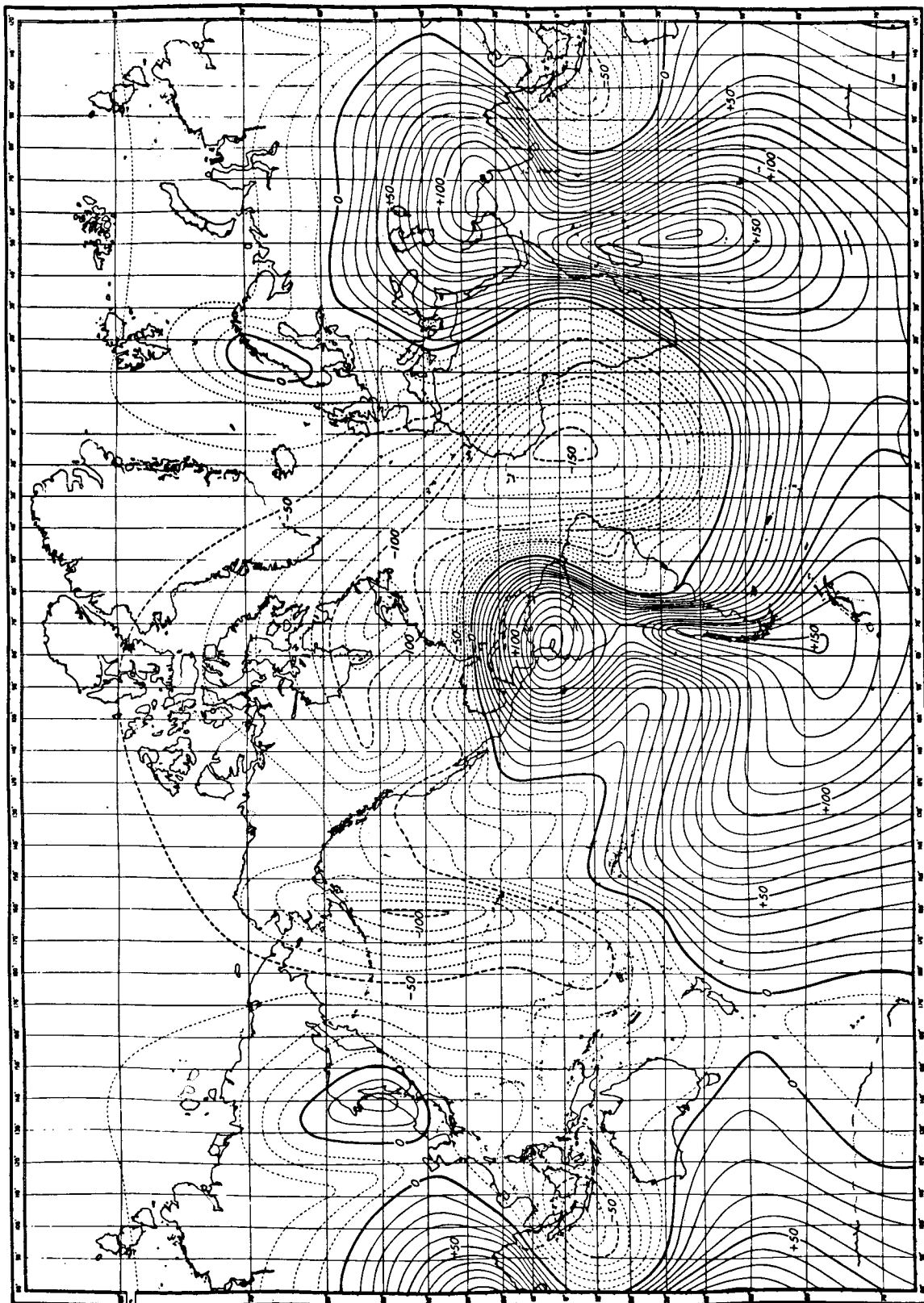
Geomagnetic secular change in gammas per year,  
east component, epoch 1932.5. Vestine et al. (1959).



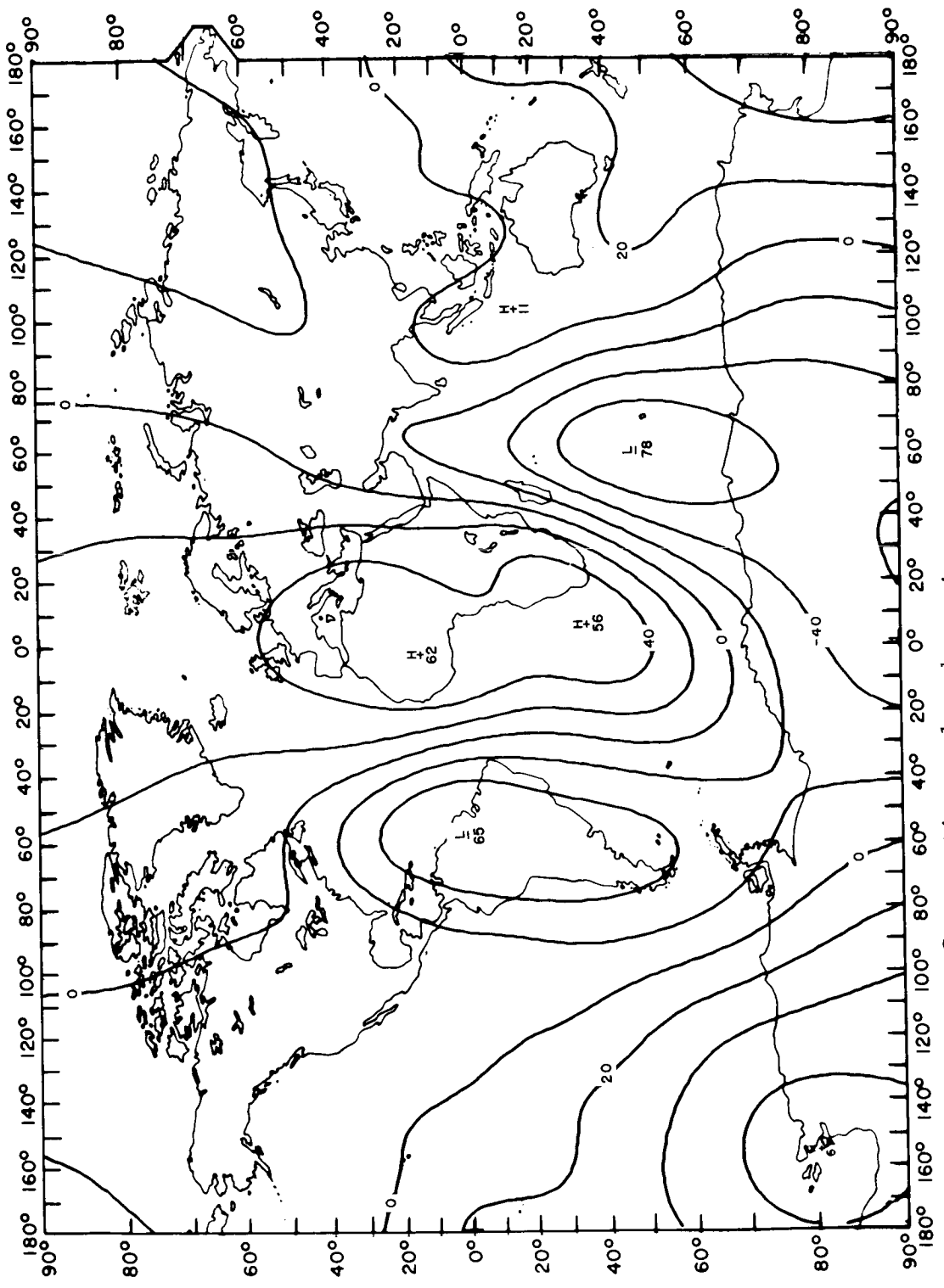
Geomagnetic secular change in gammas per year,  
east component, epoch 1932.5. GSFC(12/66).



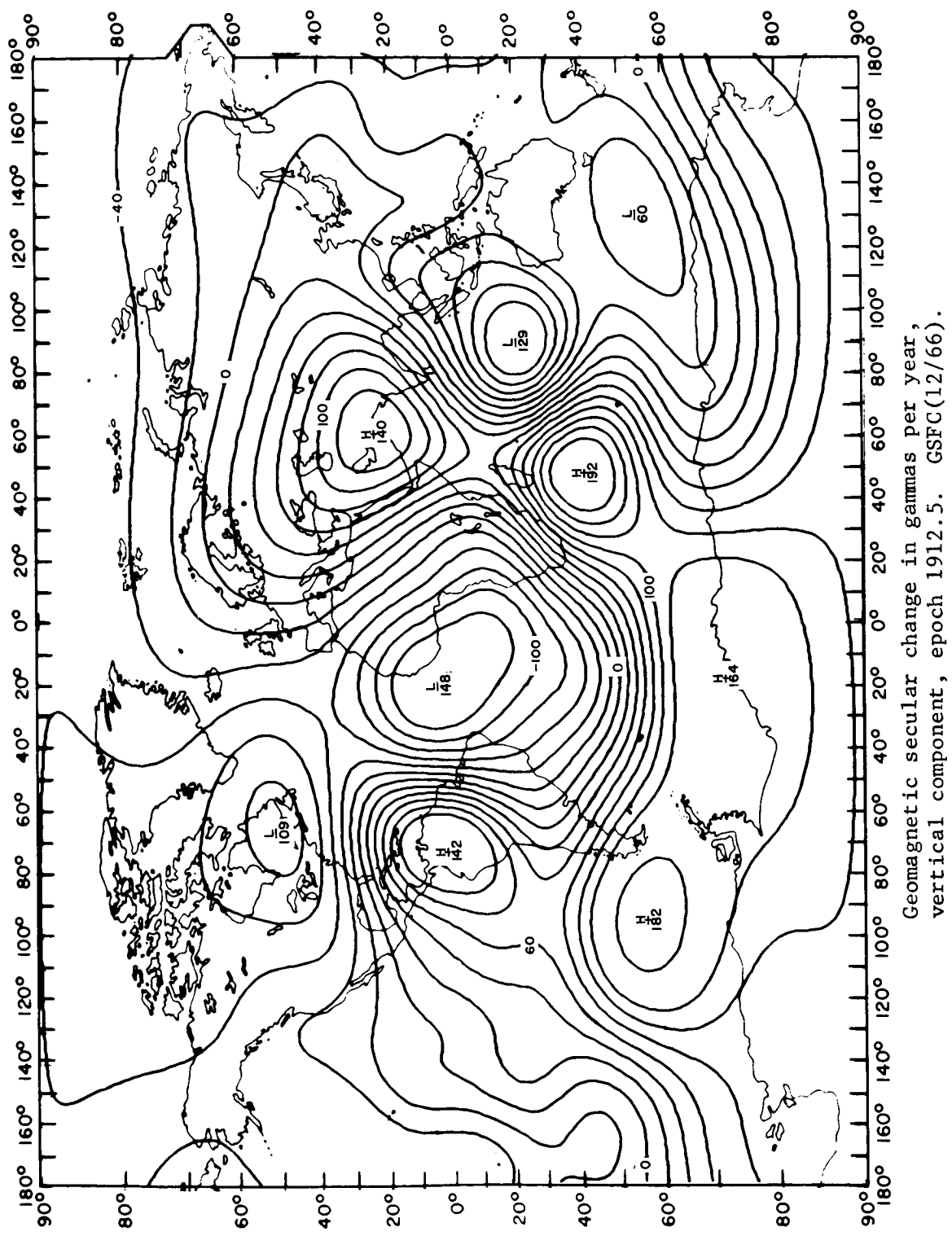
Geomagnetic secular change in gammas per year,  
east component, epoch 1942.5. Vestine et al. (1959).



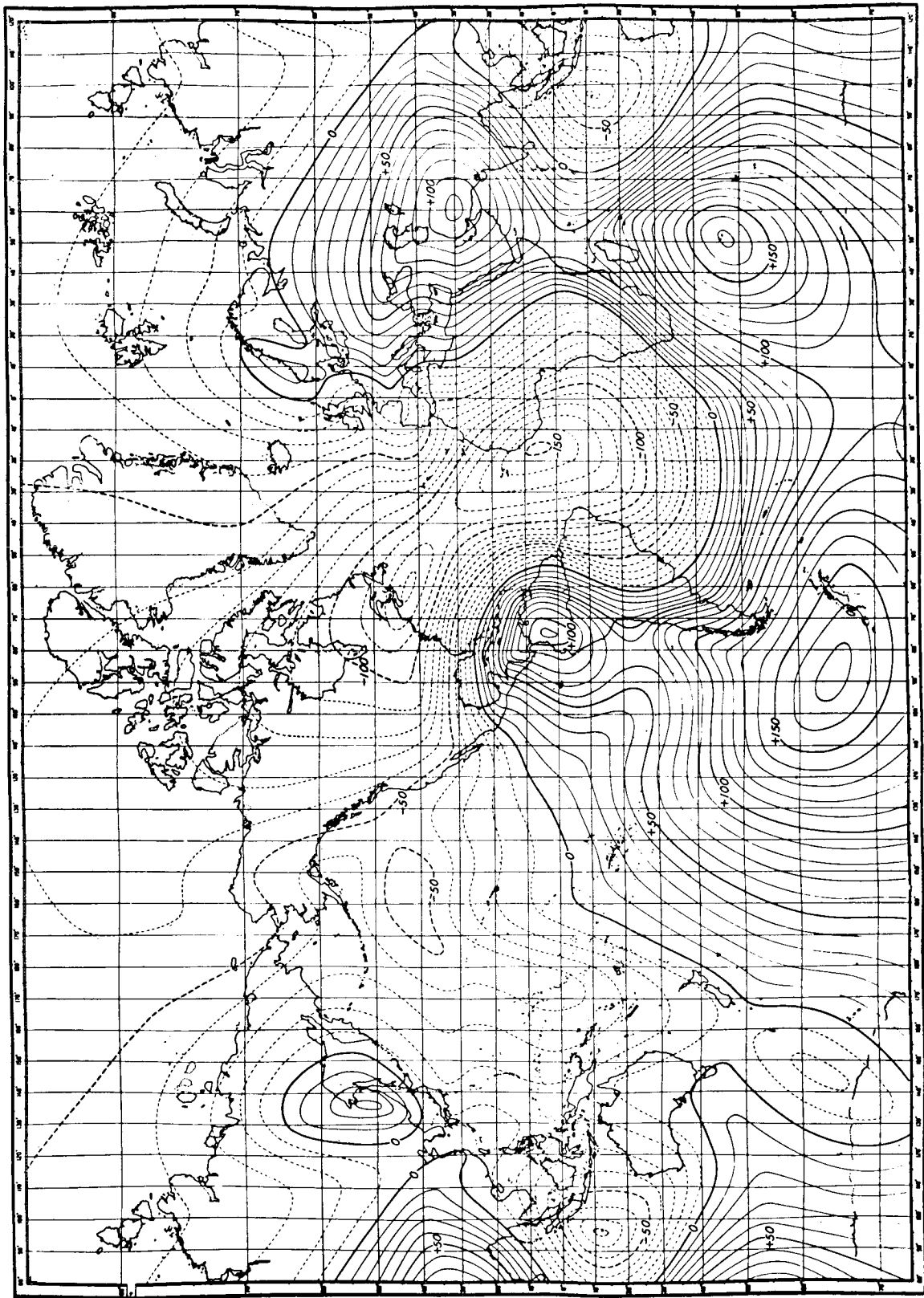
Geomagnetic secular change in gammas per year,  
vertical component, epoch 1912.5. Vestine et al. (1959).



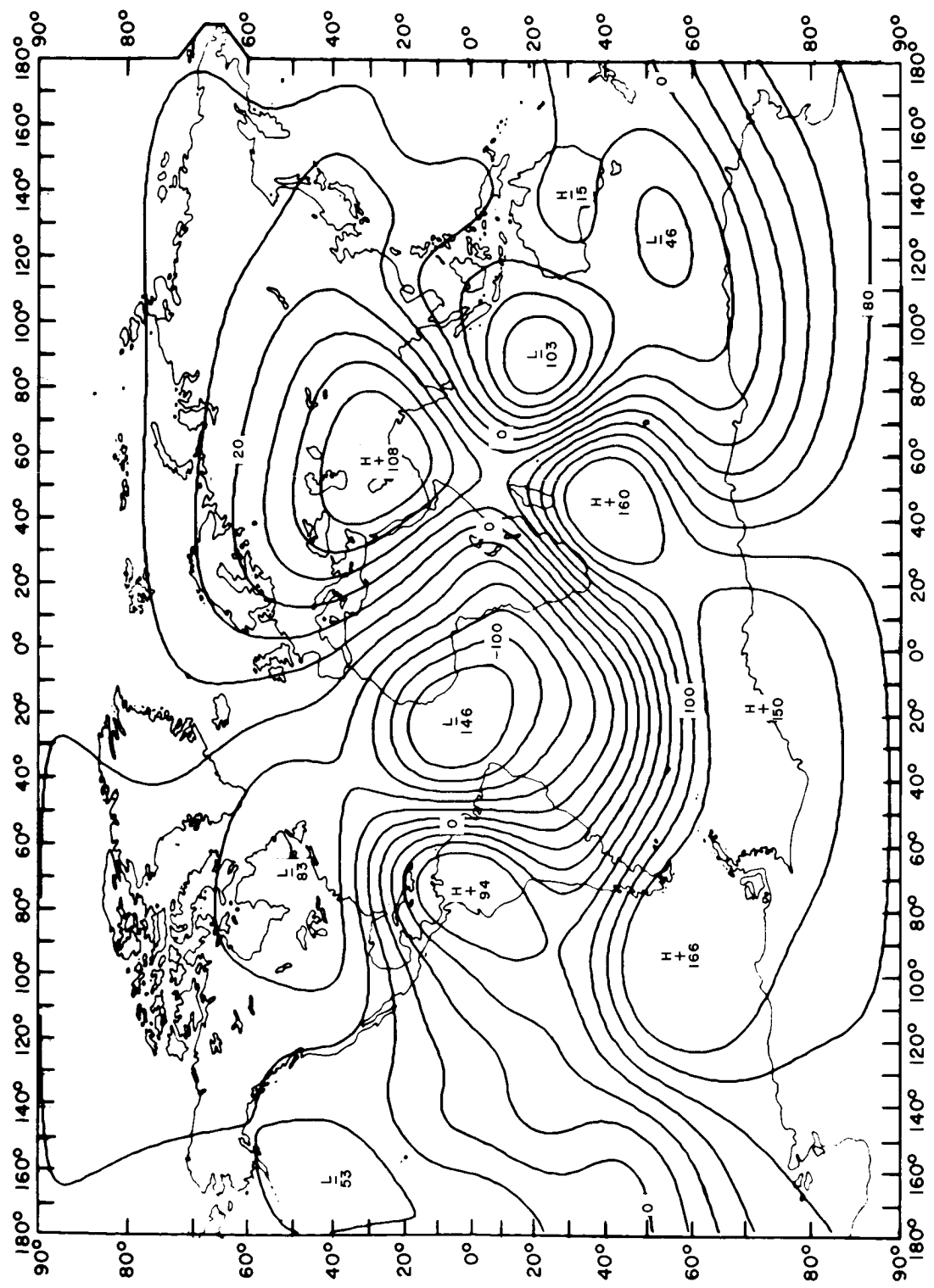
Geomagnetic secular change in gammas per year,  
east component, epoch 1942.5. GSFC(12/66).



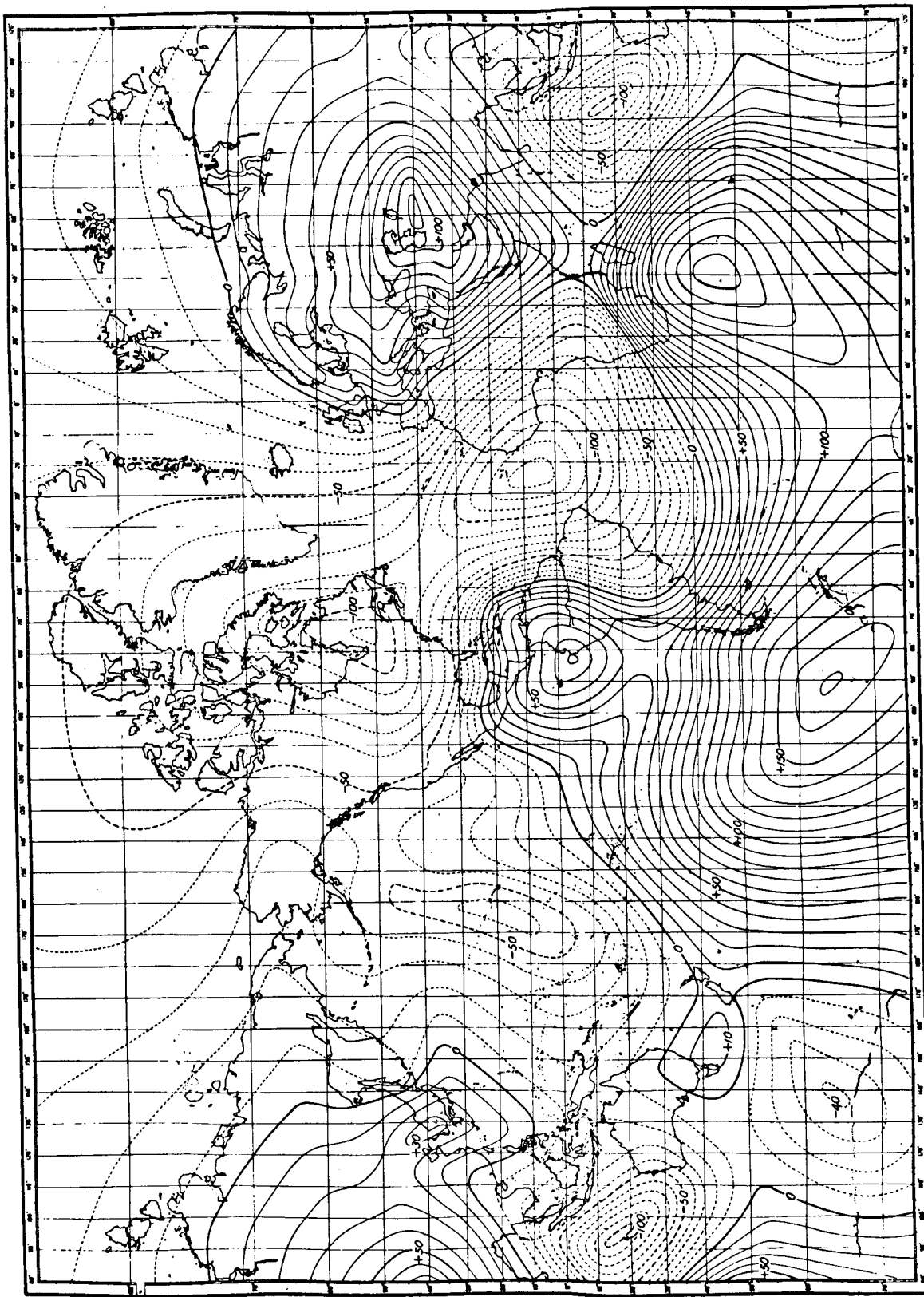
Geomagnetic secular change in gammas per year,  
vertical component, epoch 1912.5. GSFC(12/66).



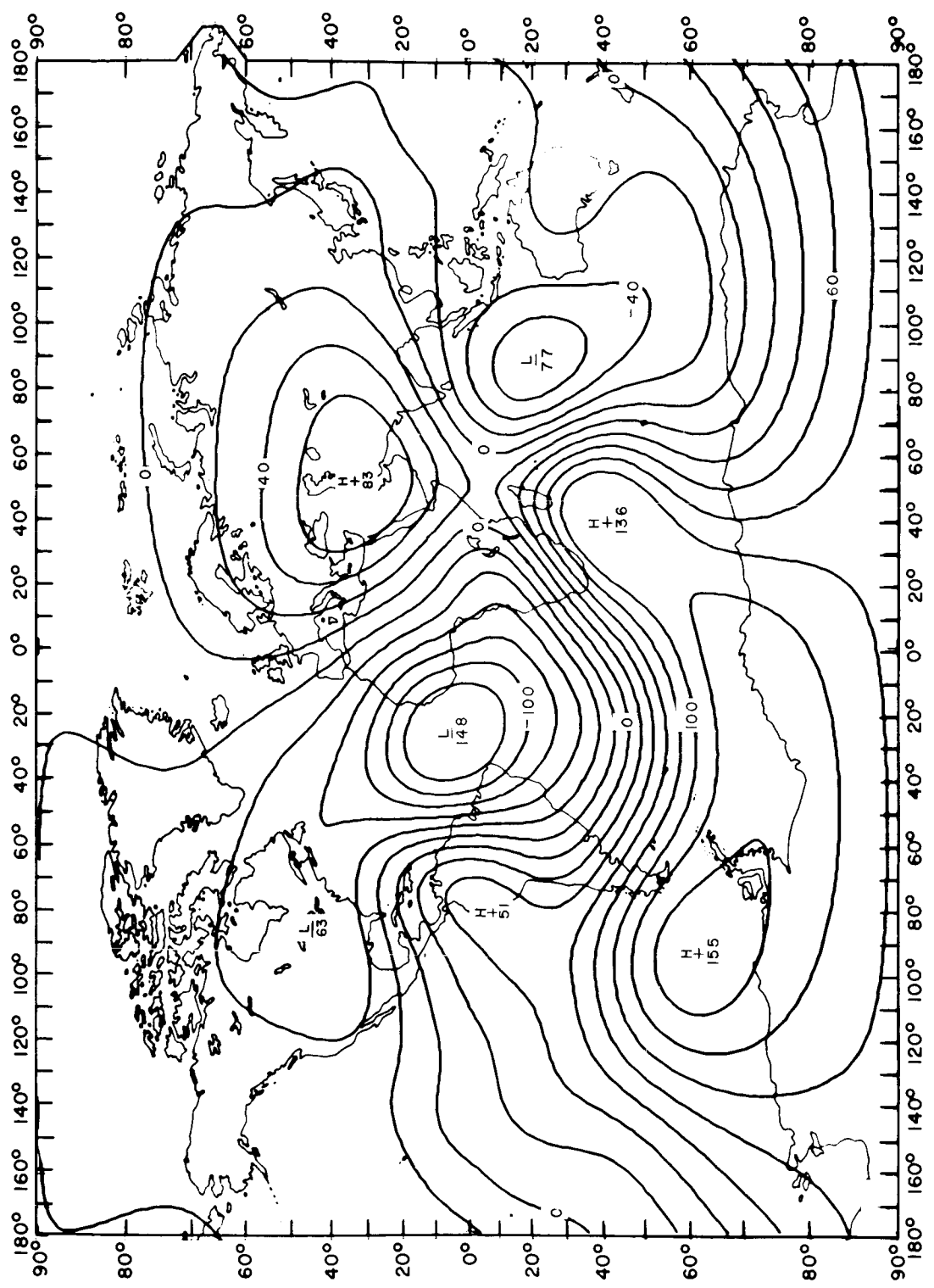
Geomagnetic secular change in gammas per year,  
vertical component, epoch 1922.5. Vestine et al. (1959).



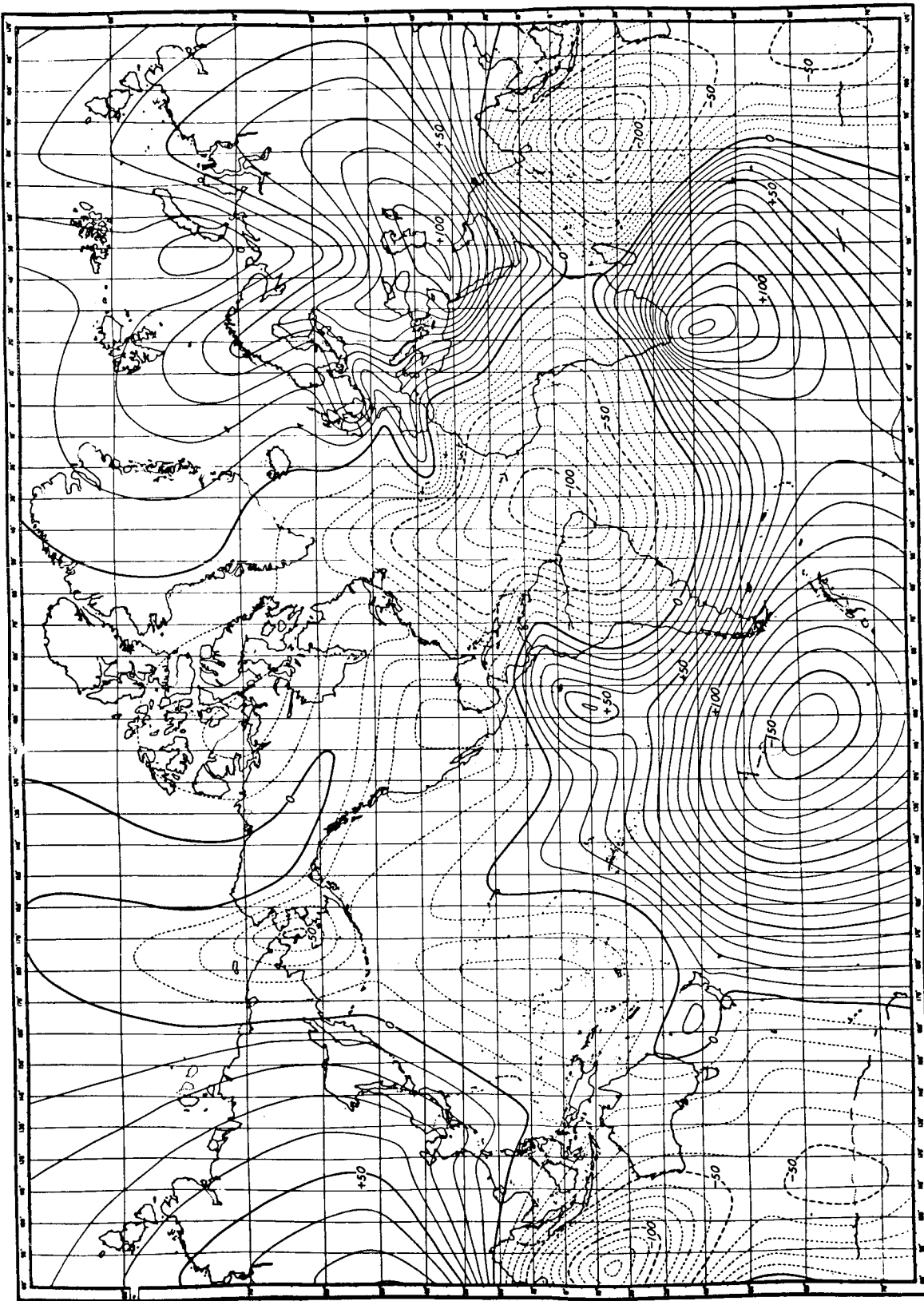
Geomagnetic secular change in gammas per year,  
vertical component, epoch 1922.5. GSFC(12/66).



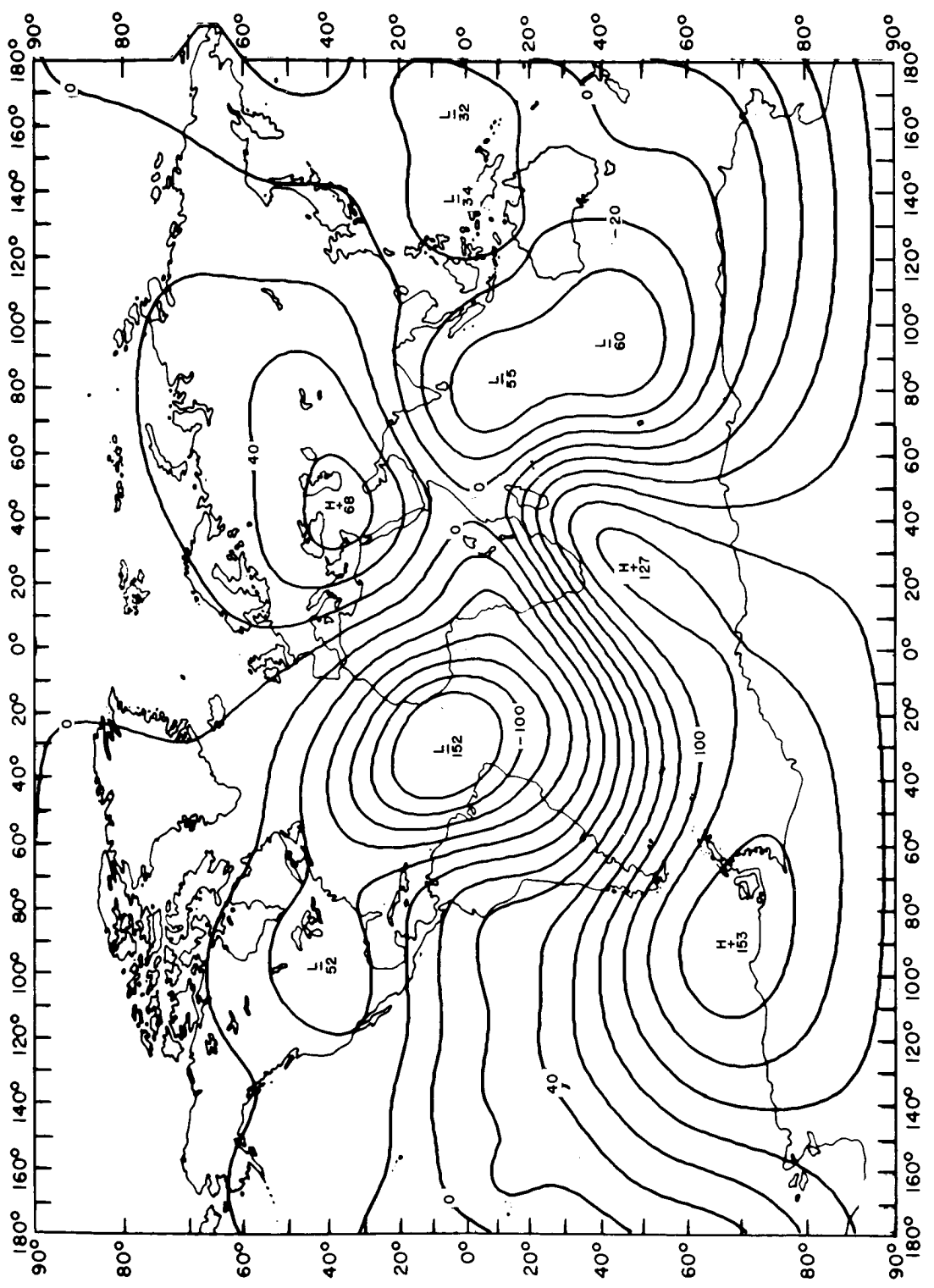
Geomagnetic secular change in gammas per year,  
vertical component, epoch 1932.5. Vestine et al. (1959).



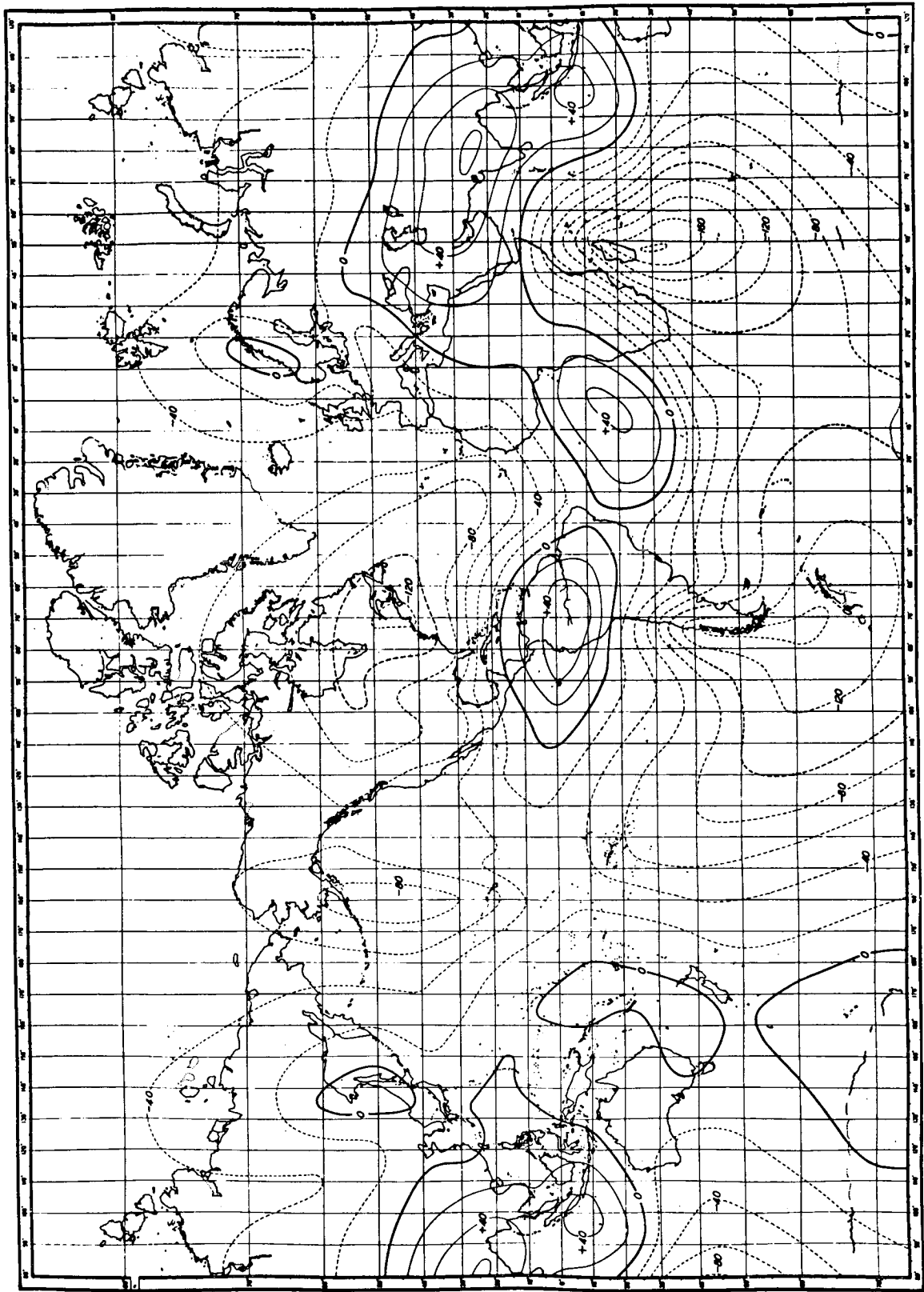
Geomagnetic secular change in gammas per year,  
vertical component, epoch 1932.5. GSFC(12/66).



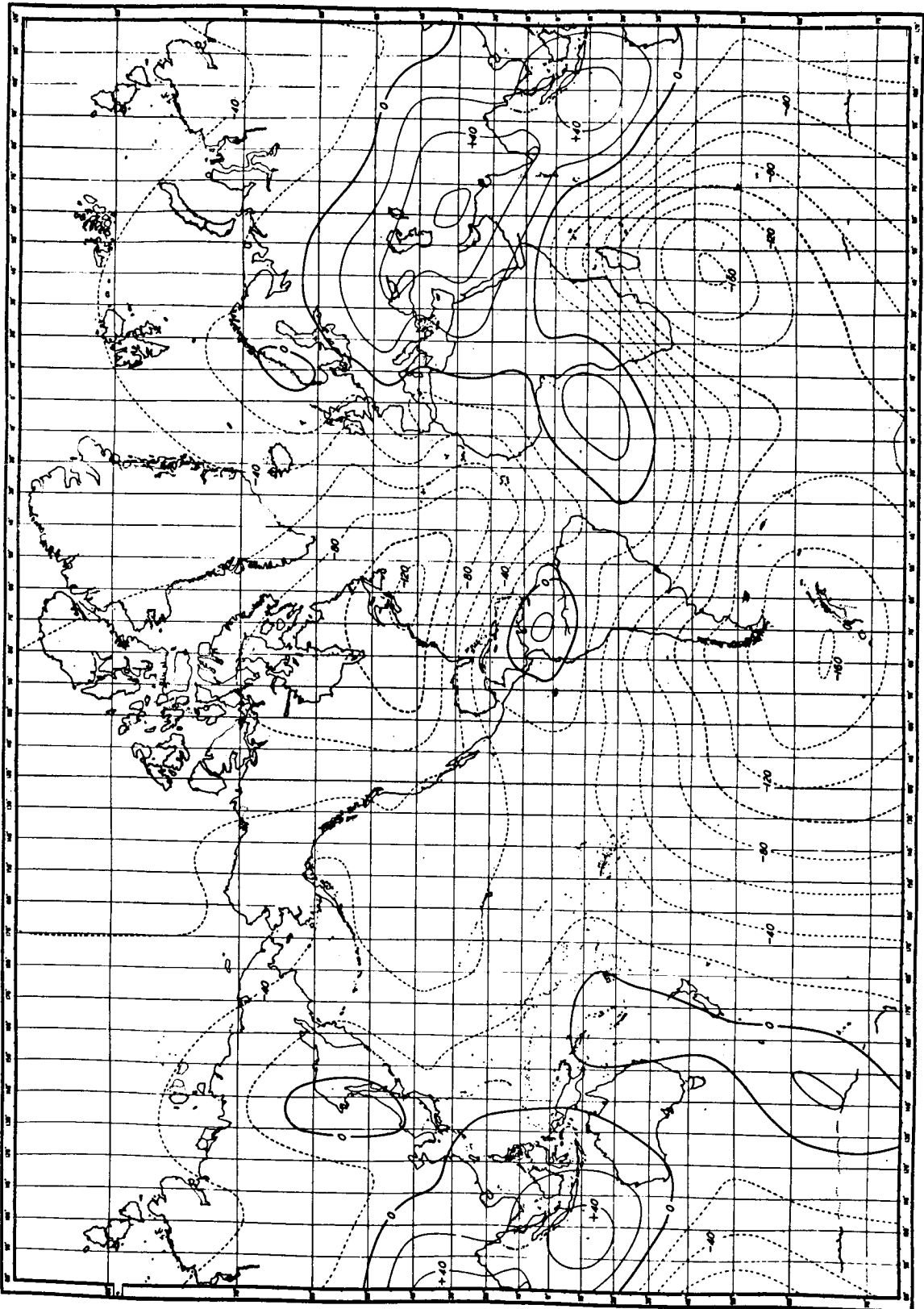
Geomagnetic secular change in gammas per year,  
vertical component, epoch 1942.5. Vestine et al. (1959).



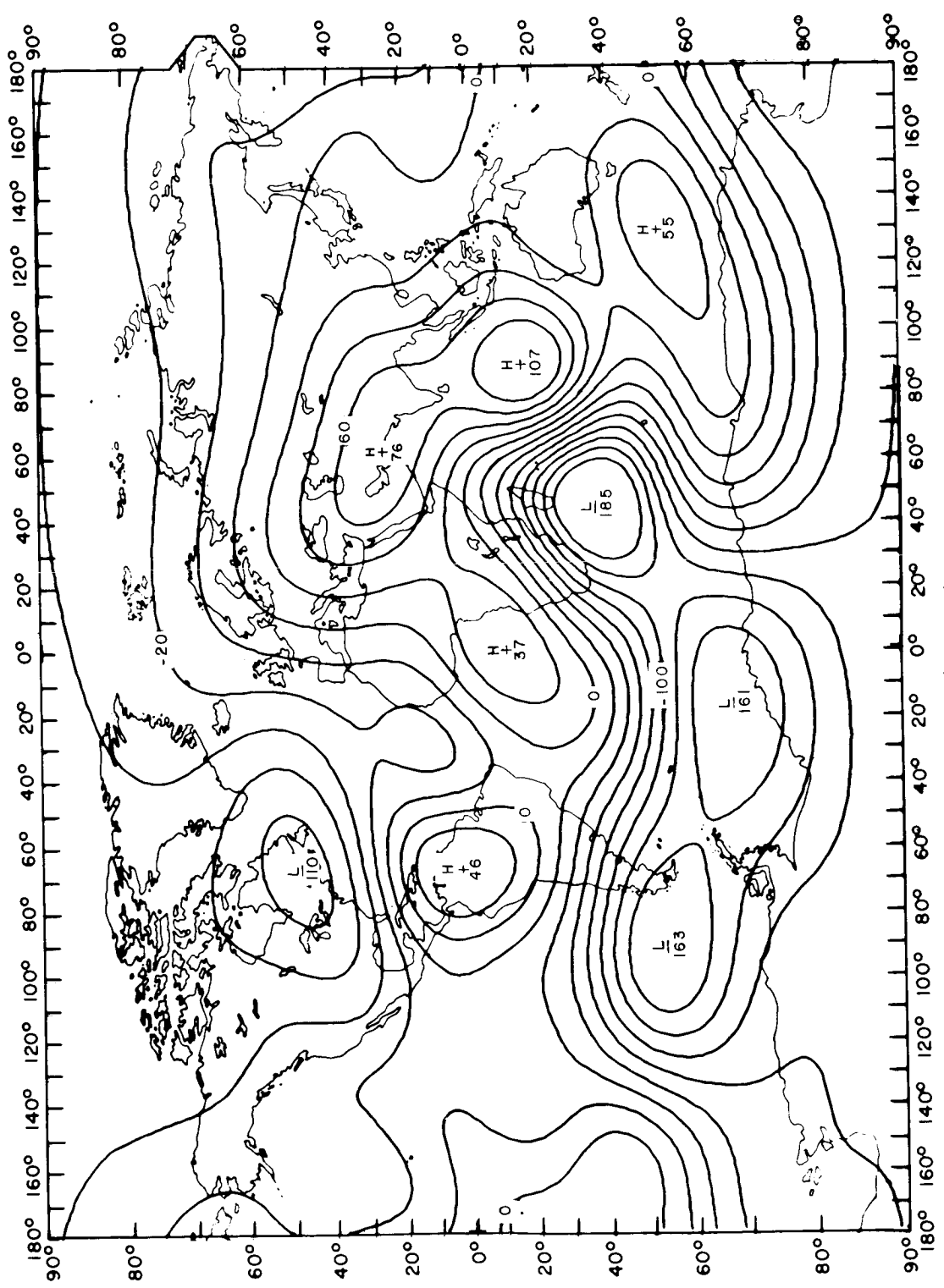
Geomagnetic secular change in gammas per year,  
vertical component, epoch 1942.5. GSFC(12/66).



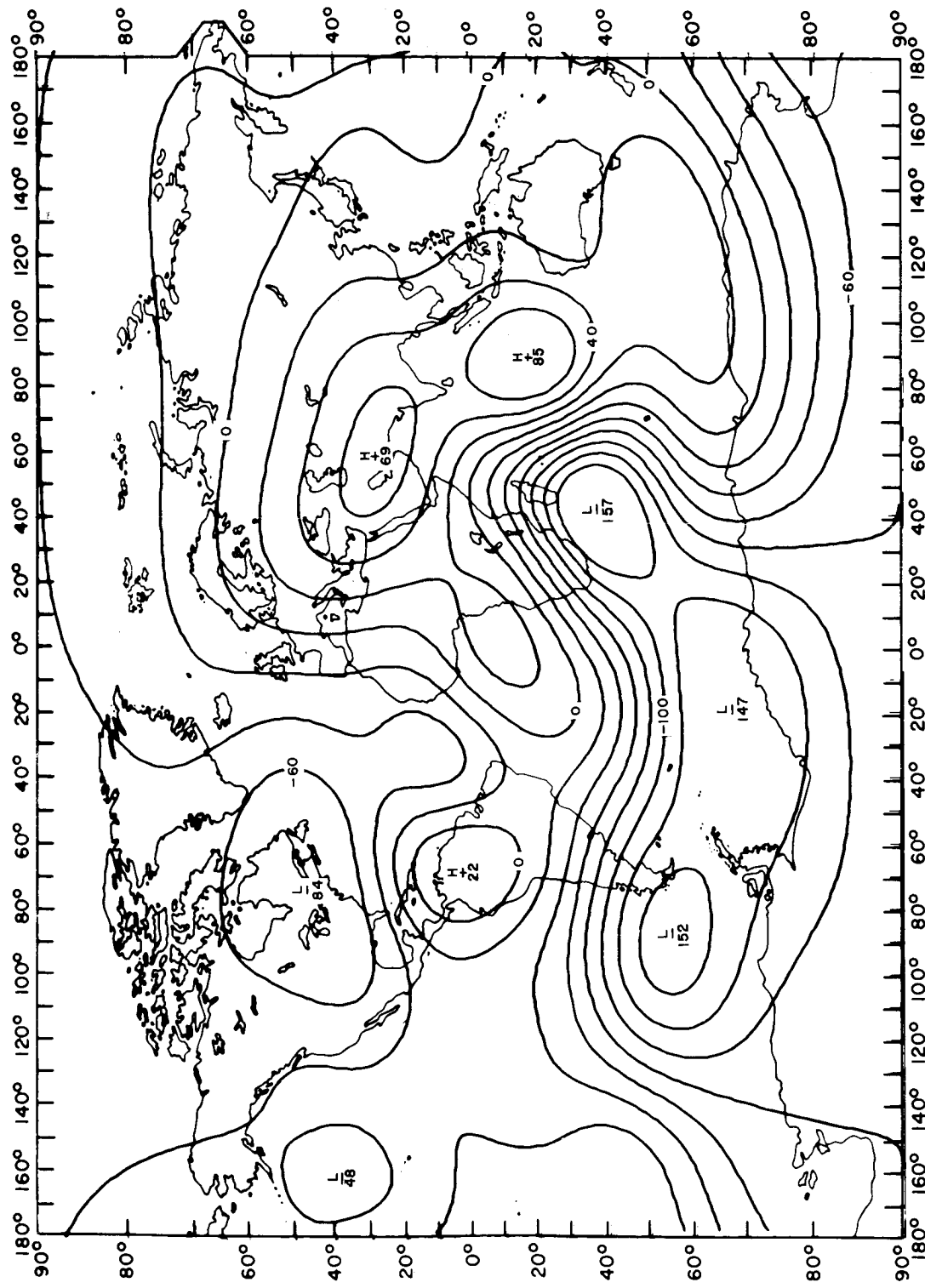
Geomagnetic secular change in gammas per year,  
total intensity, epoch 1912.5. Vestine et al. (1959).



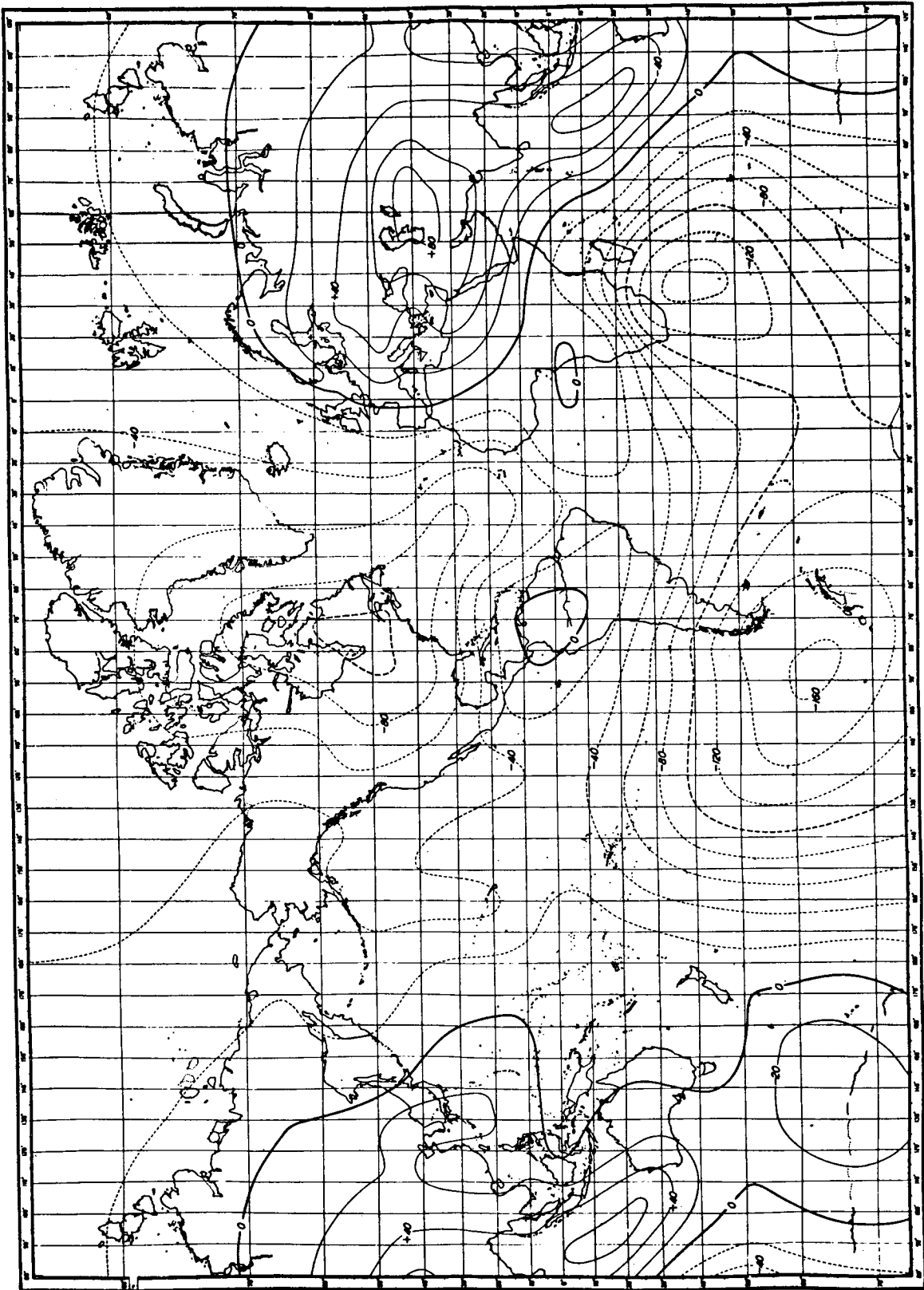
Geomagnetic secular change in gammas per year,  
total intensity, epoch 1922.5. Vestine et al. (1959).



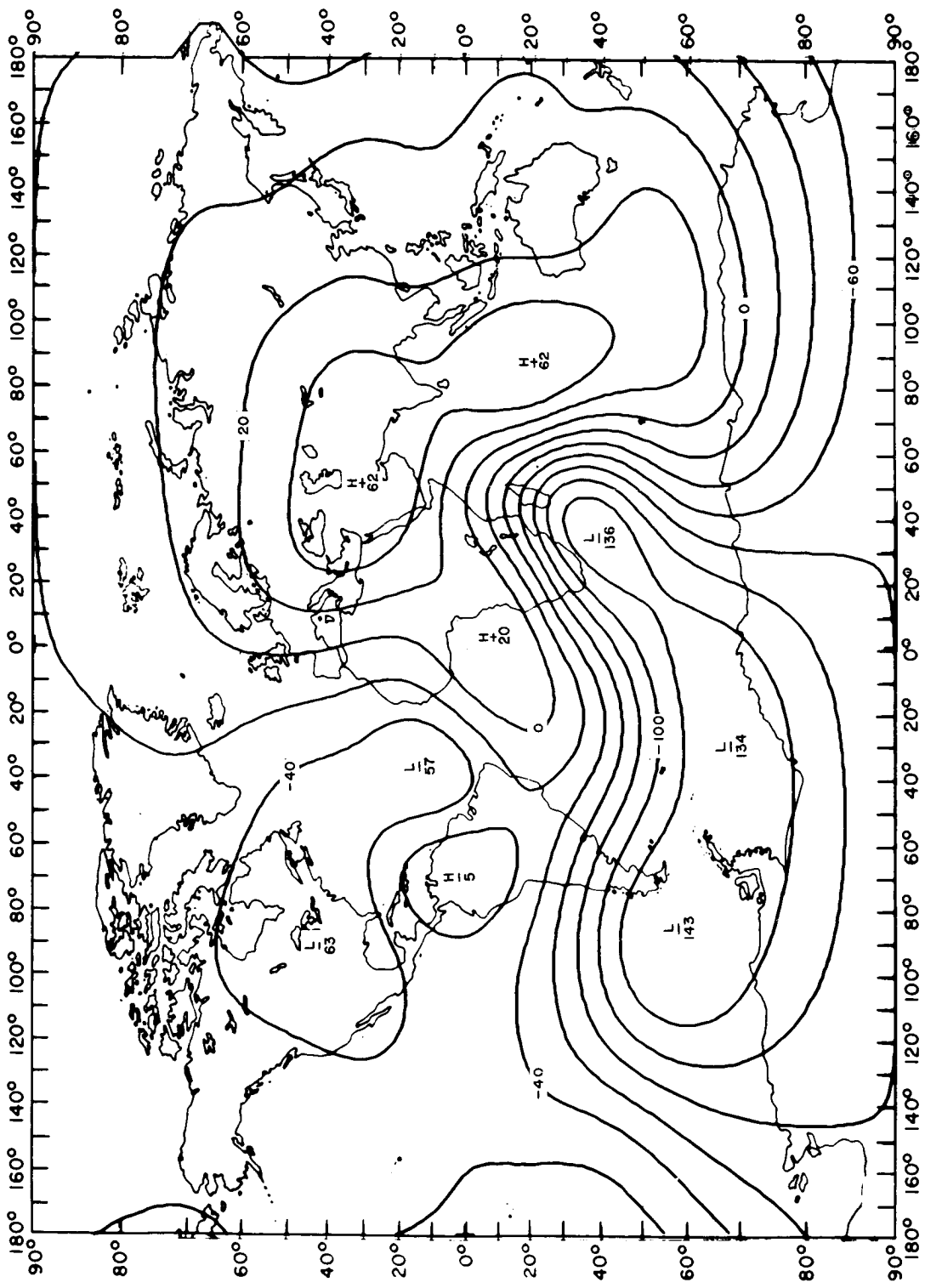
Geomagnetic secular change in gammas per year,  
total intensity, epoch 1912.5. GSFC(12/66).



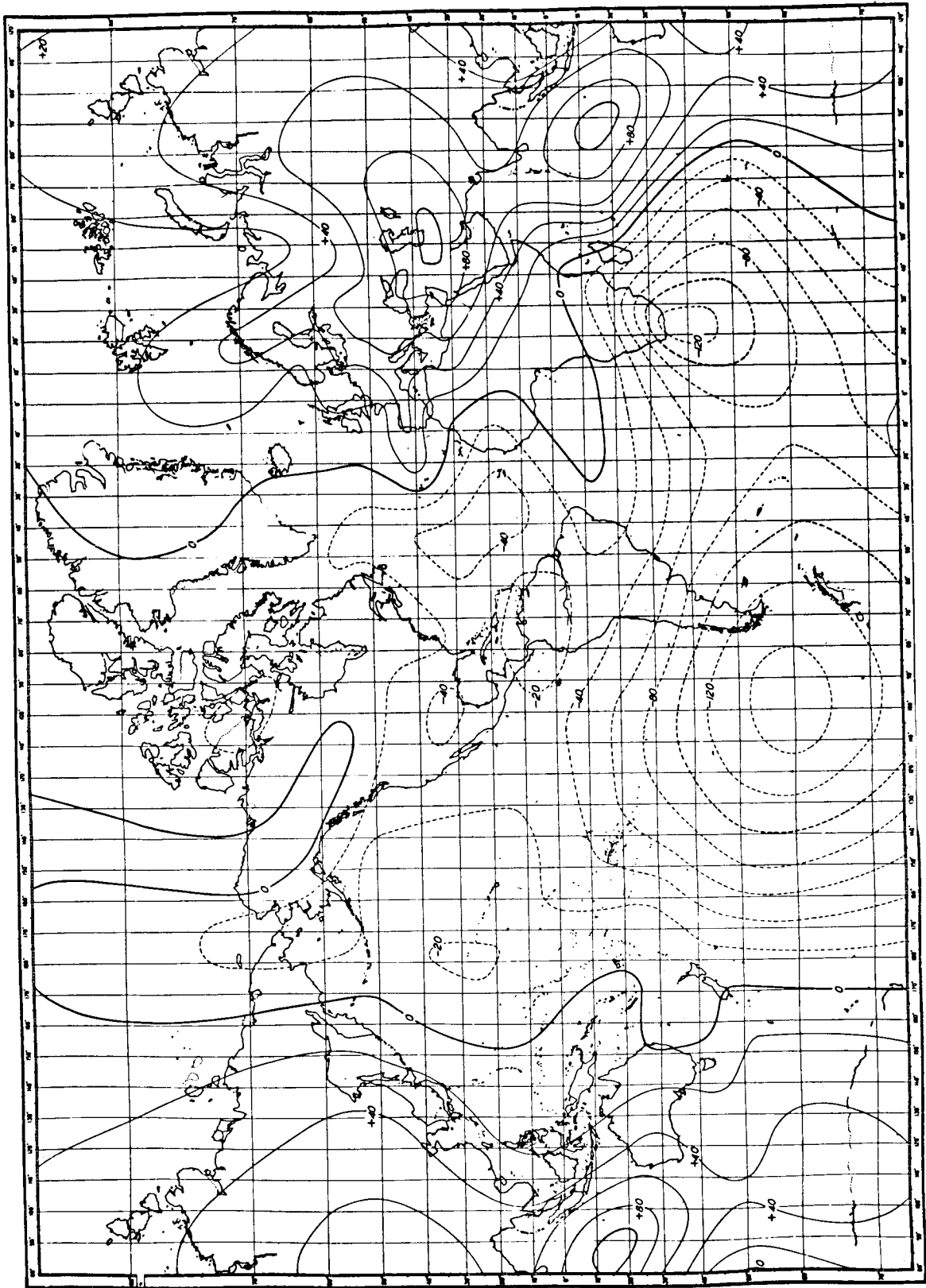
Geomagnetic secular change in gammas per year,  
total intensity, epoch 1922.5. GSFC(12/66).



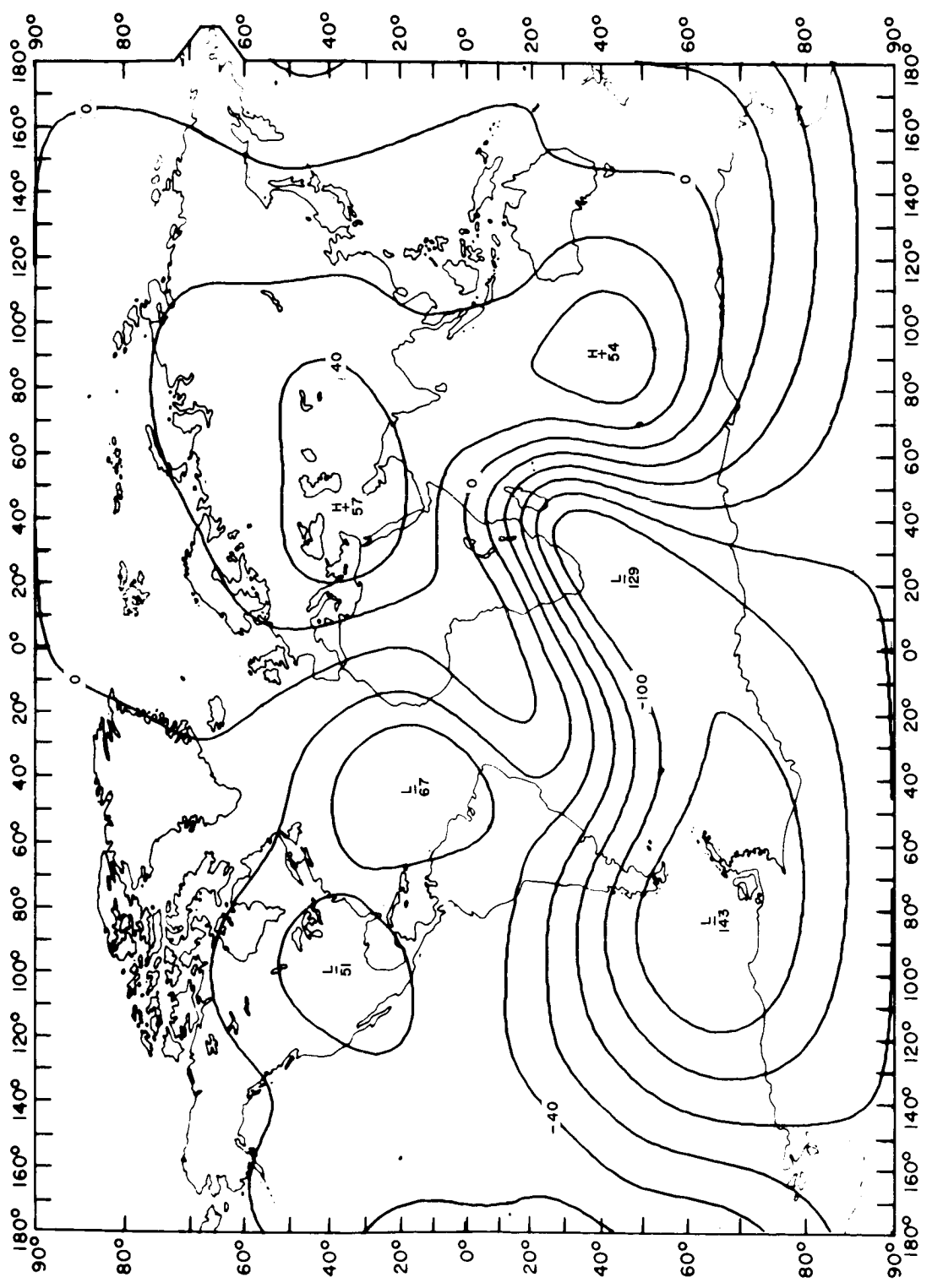
Geomagnetic secular change in gammas per year,  
total intensity, epoch 1932.5. Vestine et al. (1959).



Geomagnetic secular change in gammas per year,  
total intensity, epoch 1932.5. GSFC(12/66).



Geomagnetic secular change in gammas per year,  
total intensity, epoch 1942.5. Vestine et al. (1959).

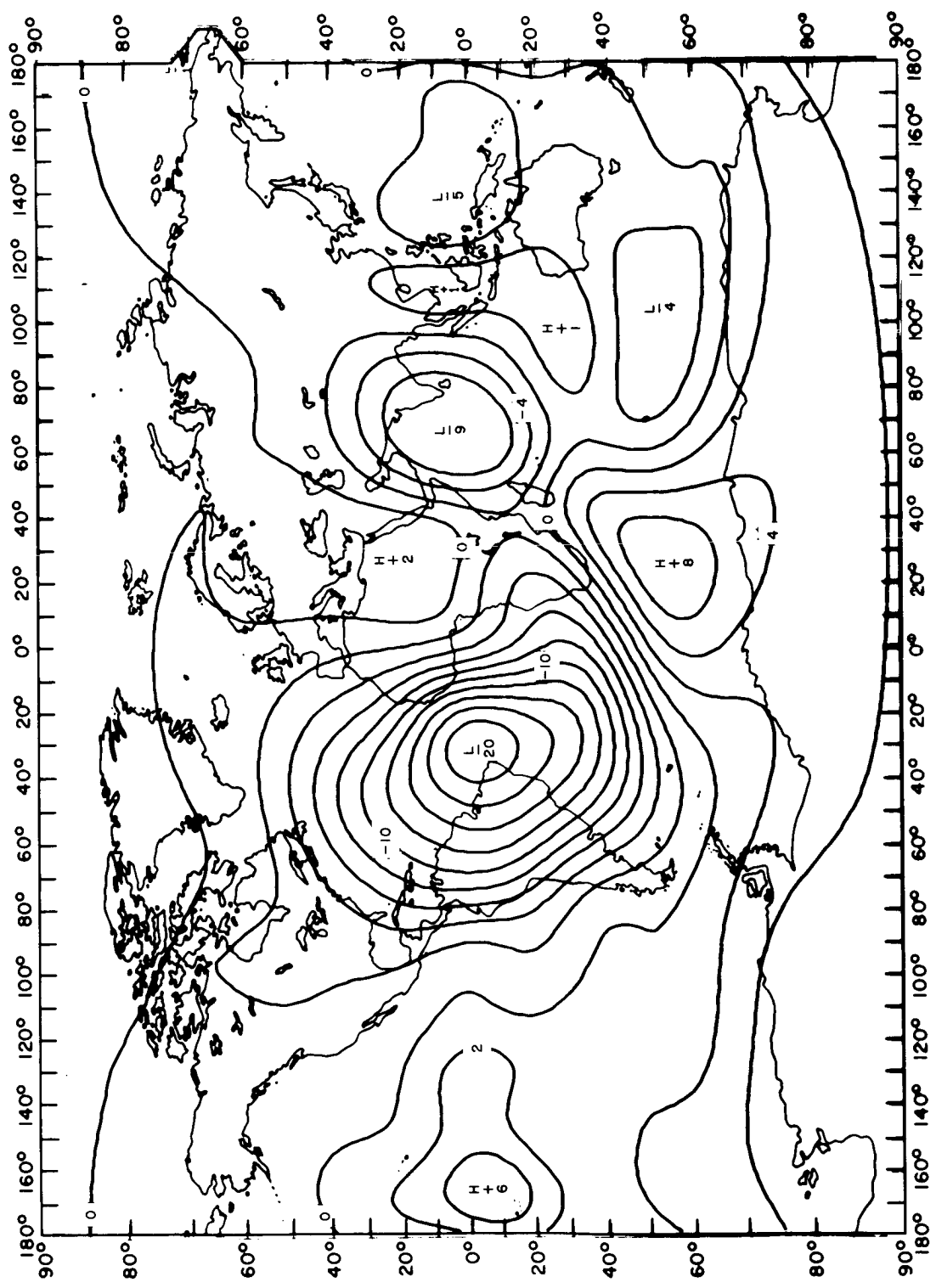


Geomagnetic secular change in gammas per year,  
total intensity, epoch 1942.5. GSFC(12/66).

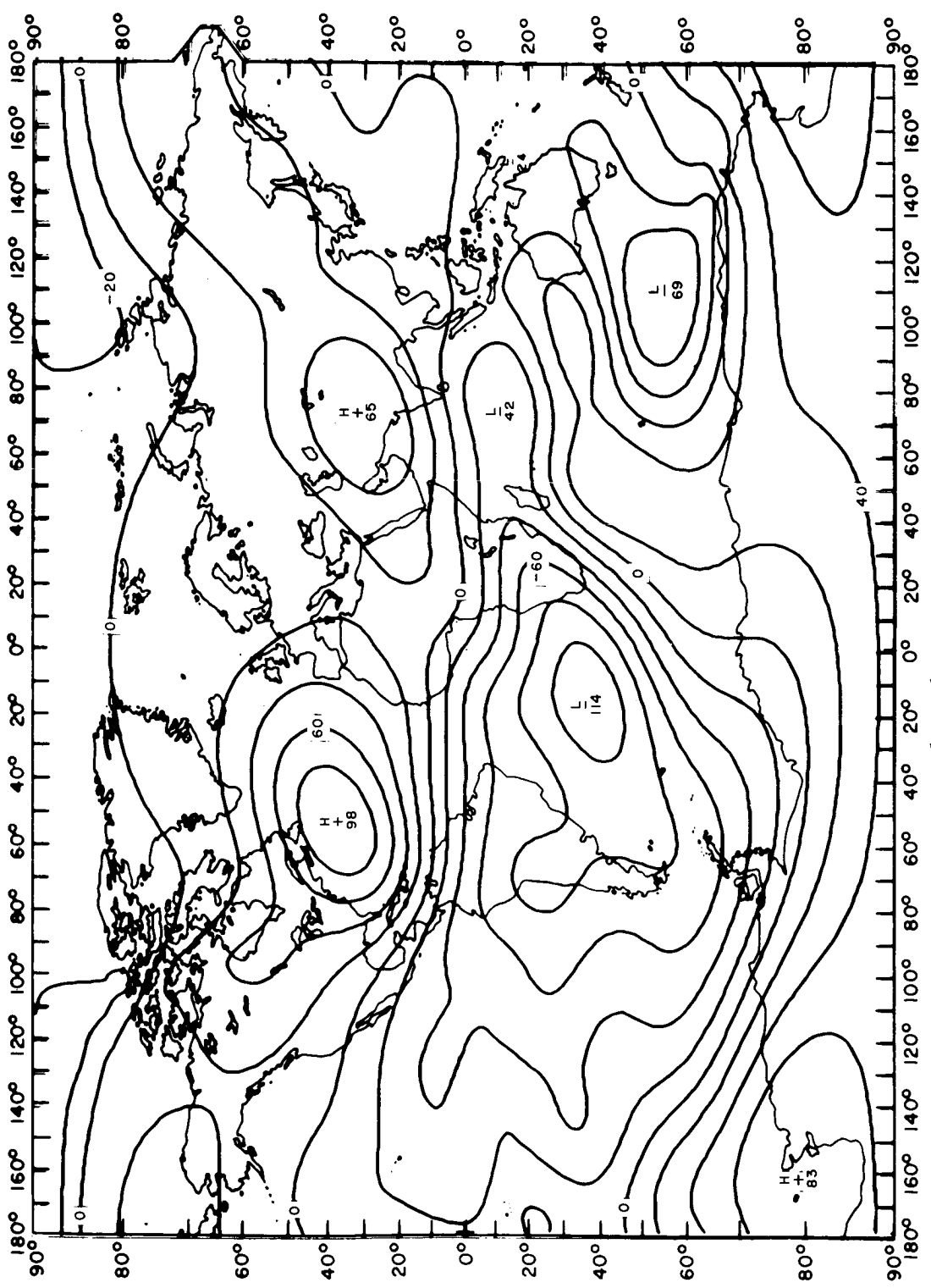
APPENDIX C

Main field component and isoporic charts

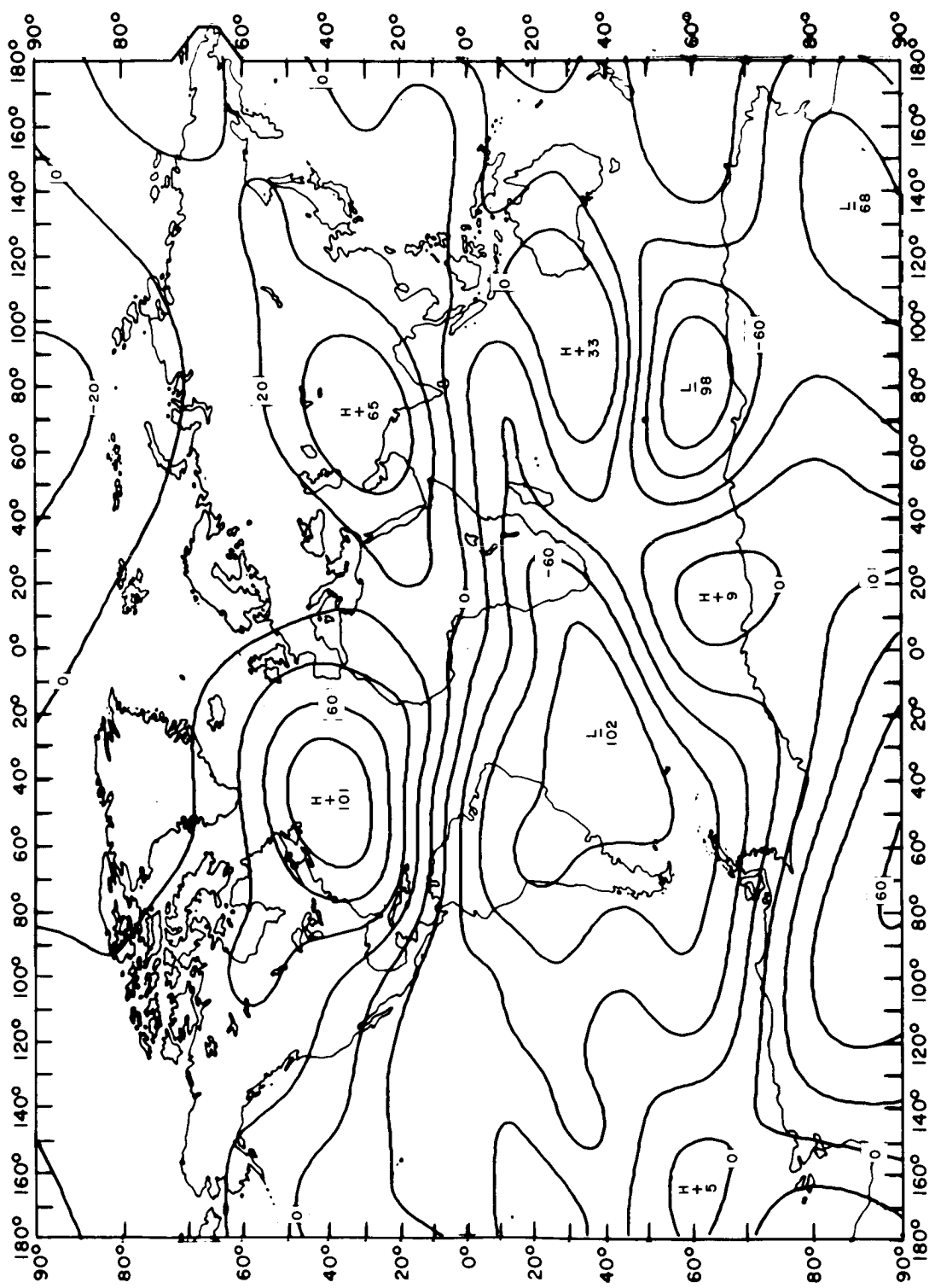
computed from GSFC(12/66) for 1965.0 at the earth's surface



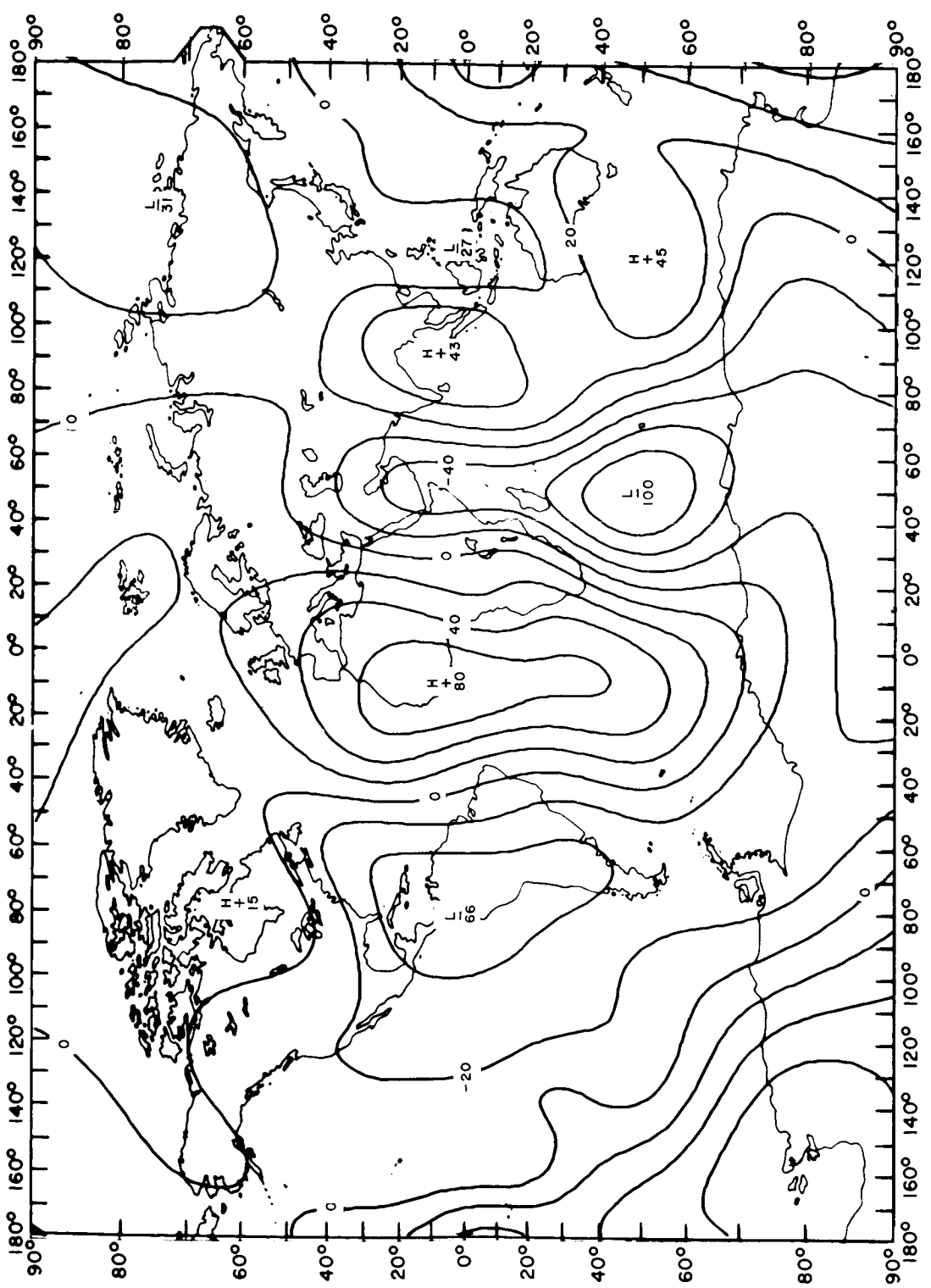
Geomagnetic secular change in minutes per year,  
inclination, epoch 1965.0. GSFC(12/66).



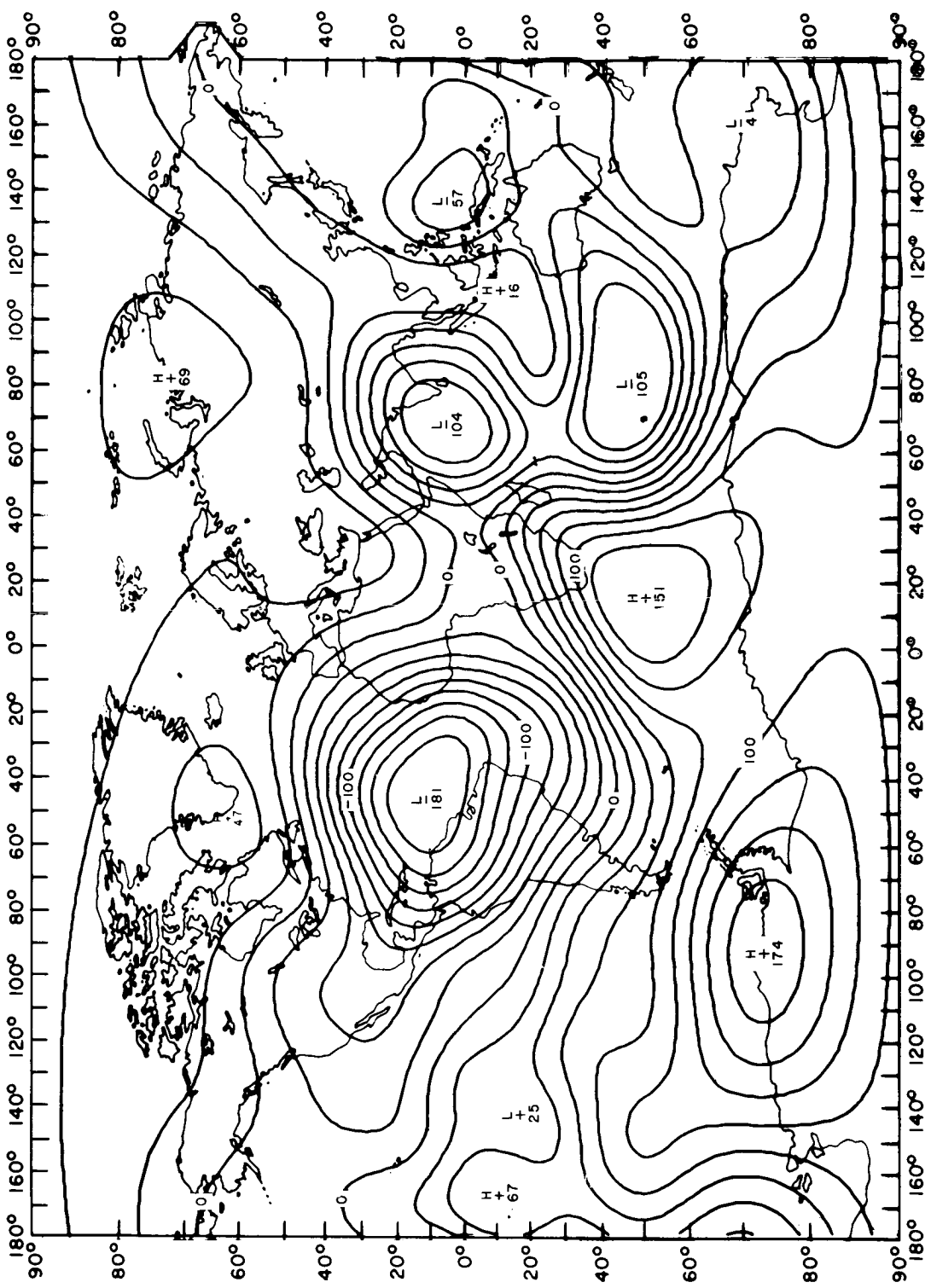
Geomagnetic secular change in gammas per year,  
horizontal component, epoch 1965.0. GSFC(12/66).

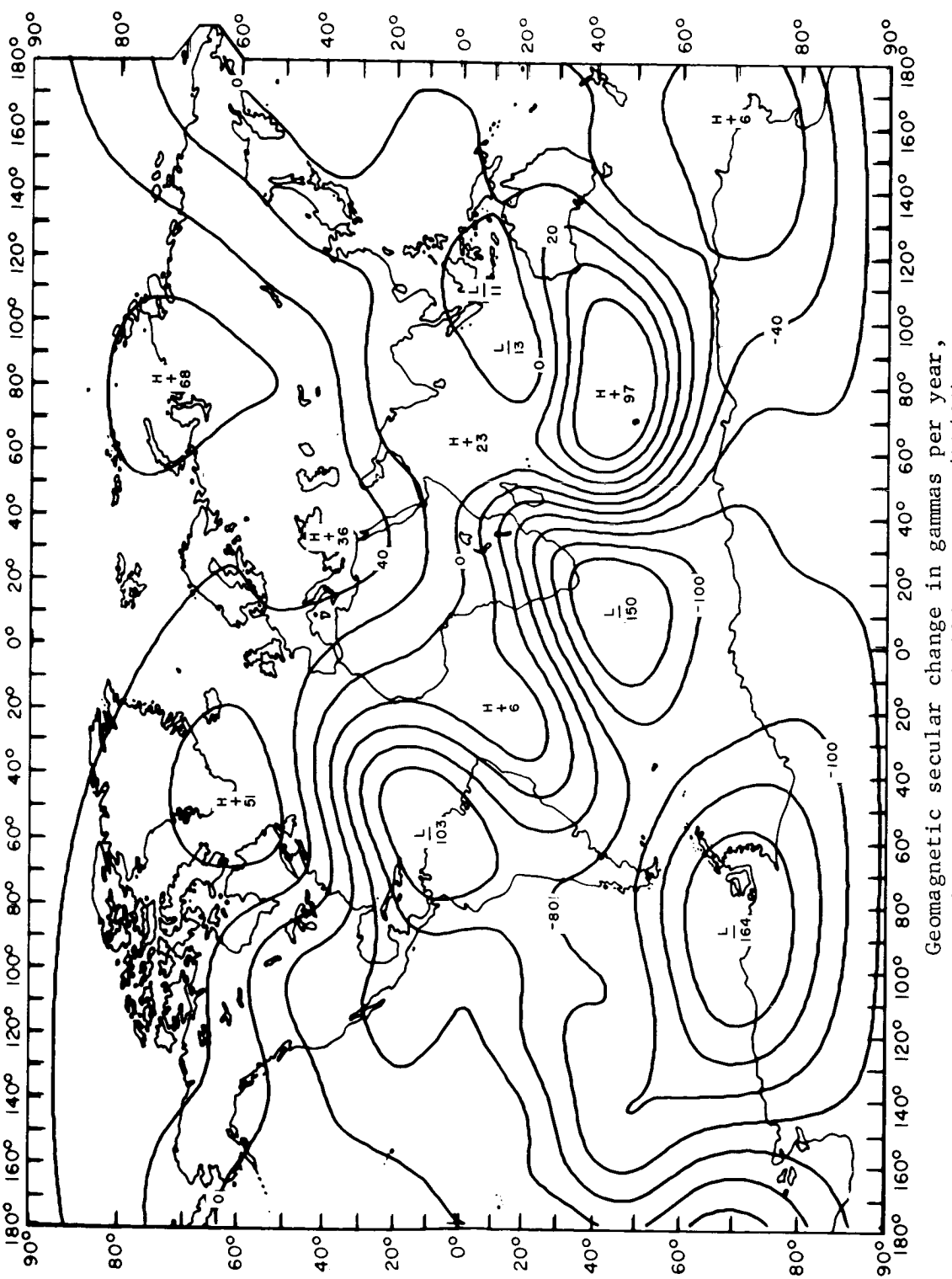


Geomagnetic secular change in gammas per year,  
north component, epoch 1965.0. GSFC(12/66).

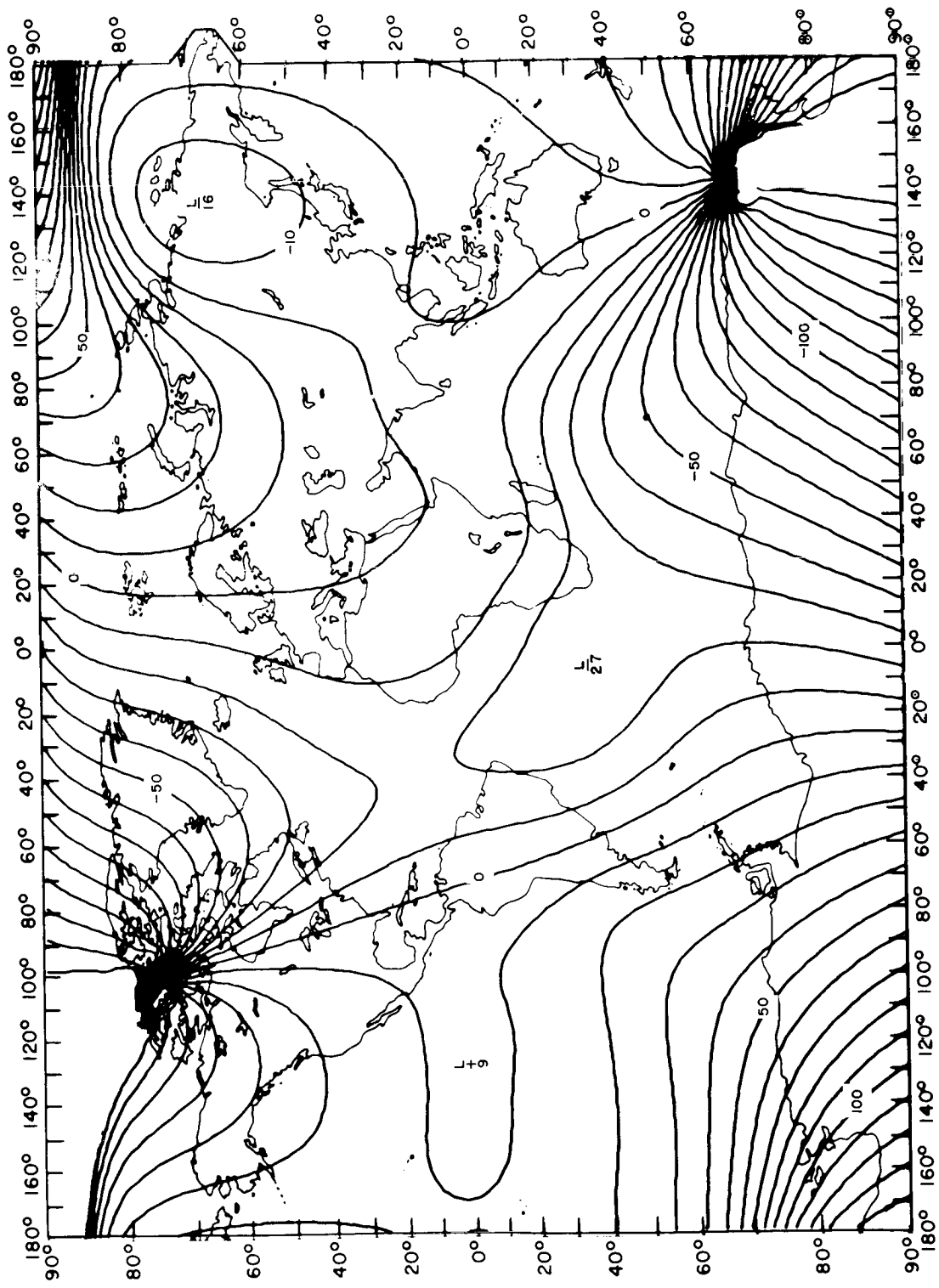


Geomagnetic secular change in gammas per year,  
east component, epoch 1965.0. GSFC(12/66).

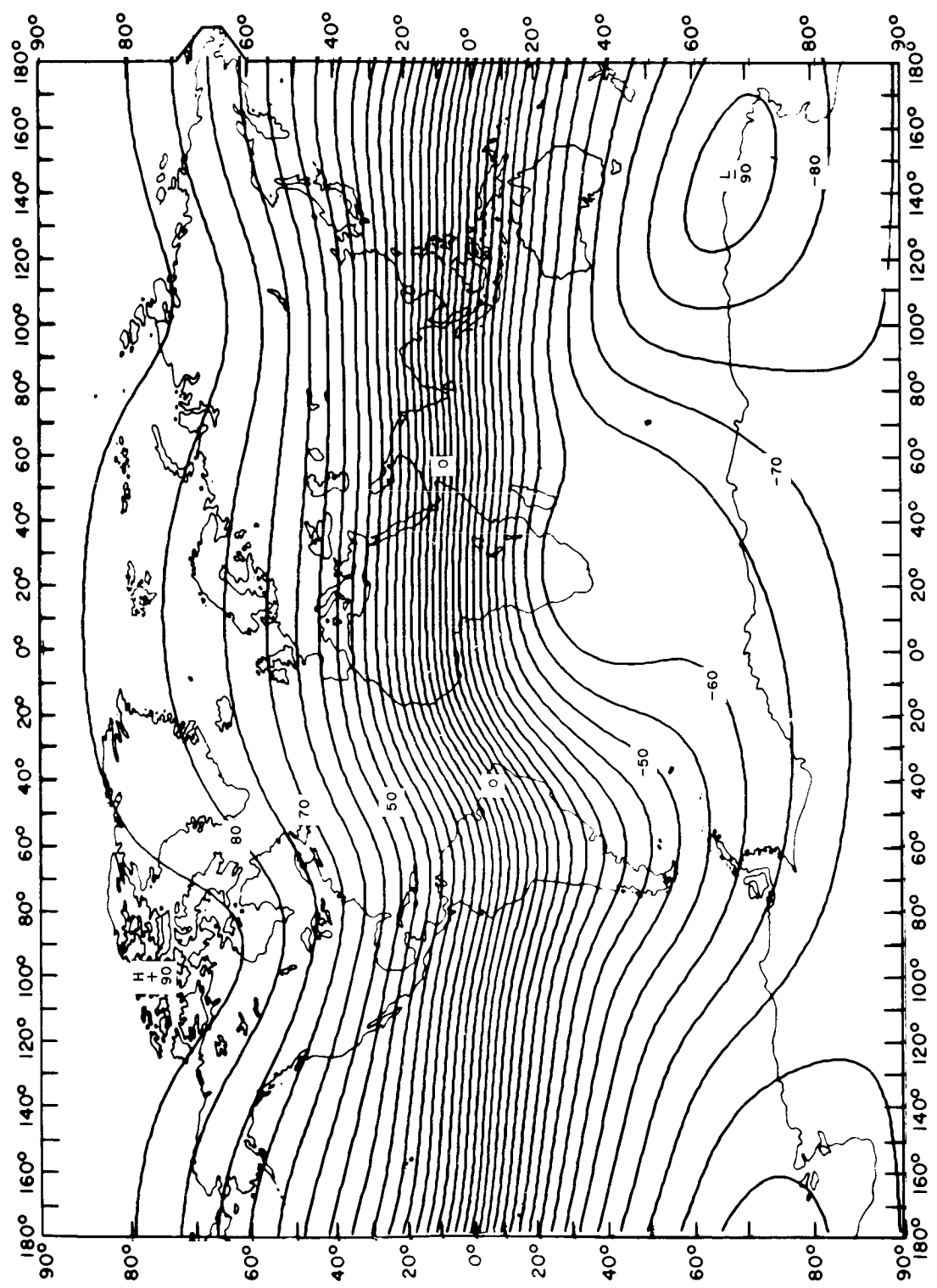




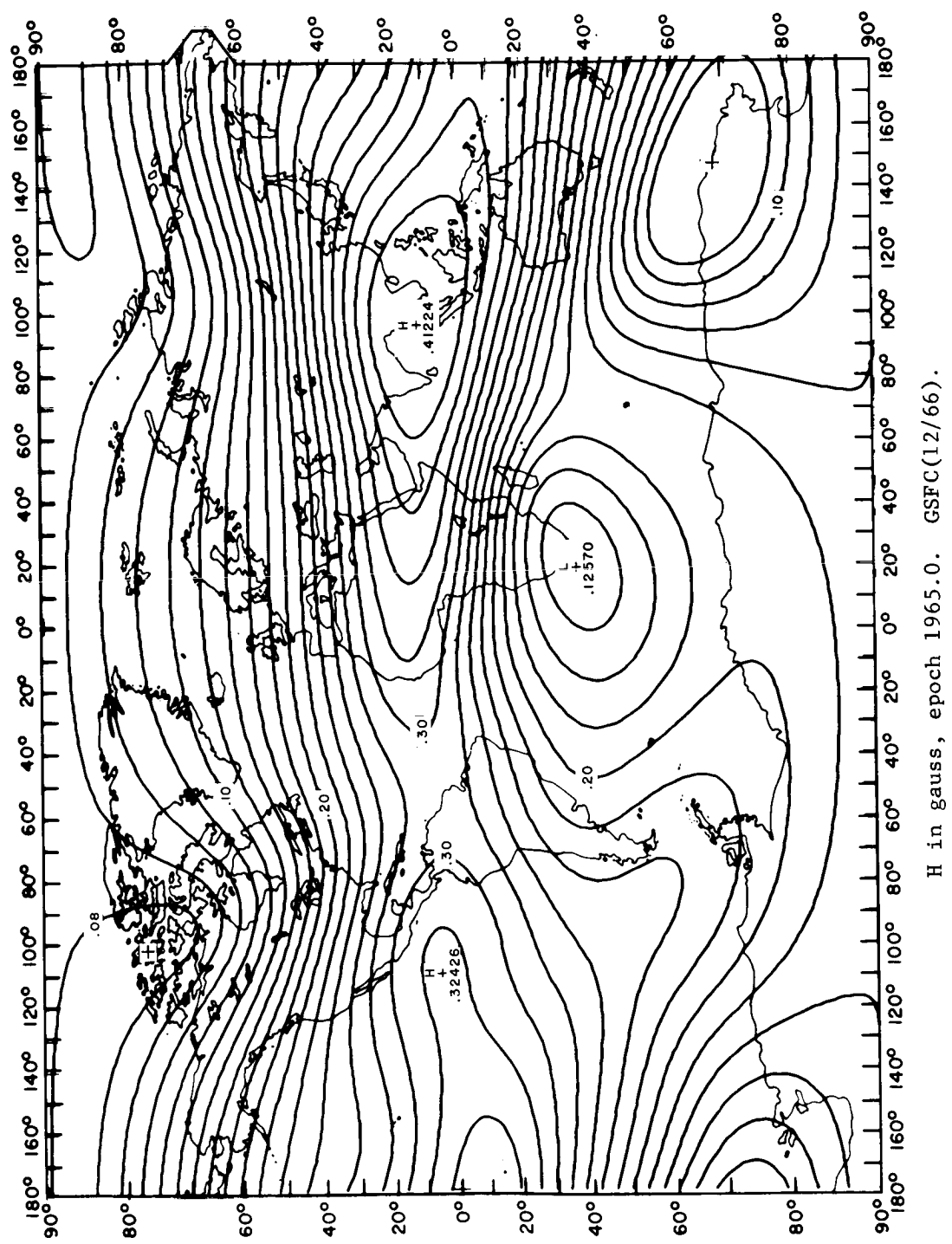
Geomagnetic secular change in gammas per year,  
total intensity, epoch 1965.0. GSFC(12/66).



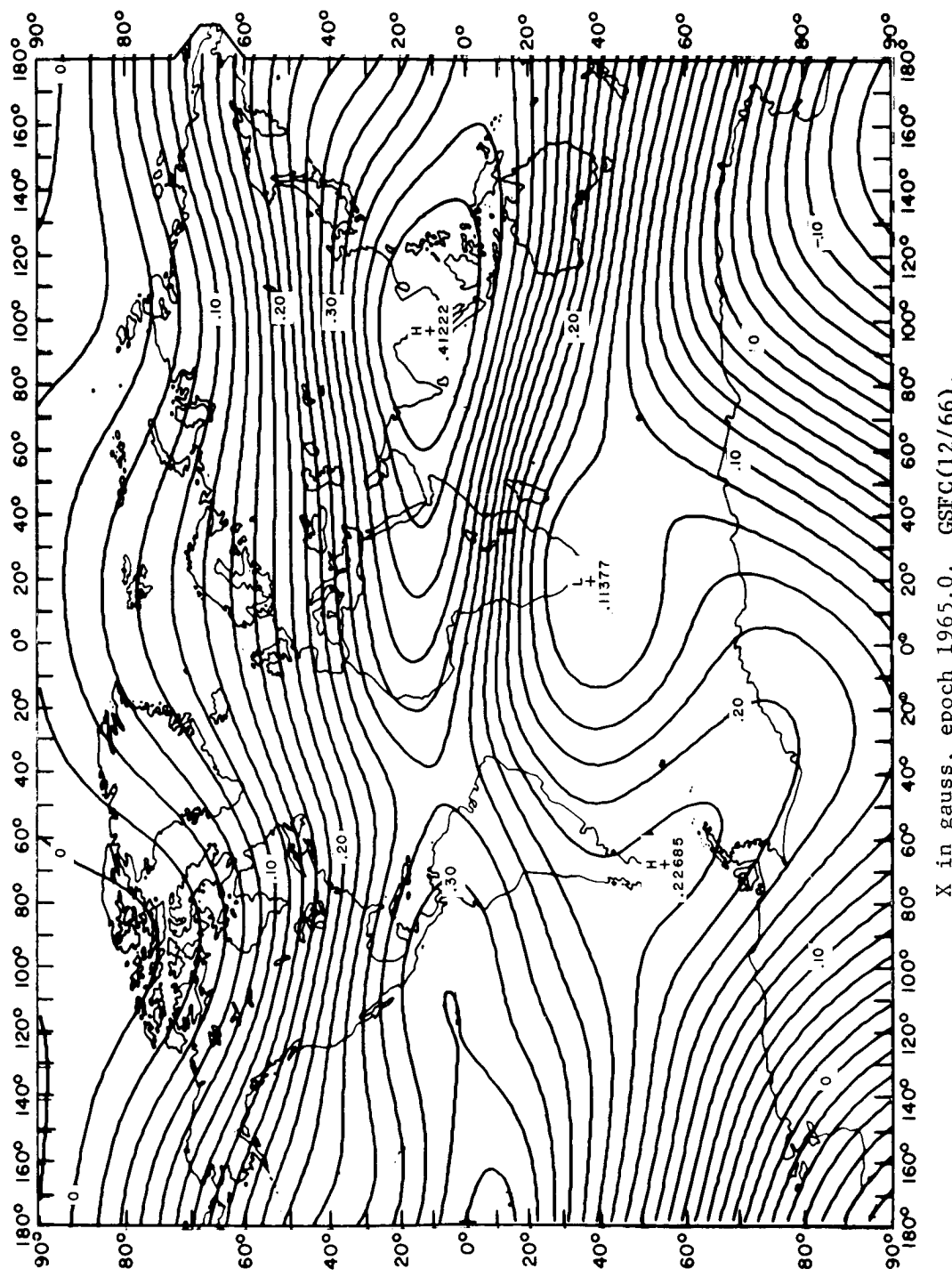
D in degrees, epoch 1965.0. GSFC(12/66).



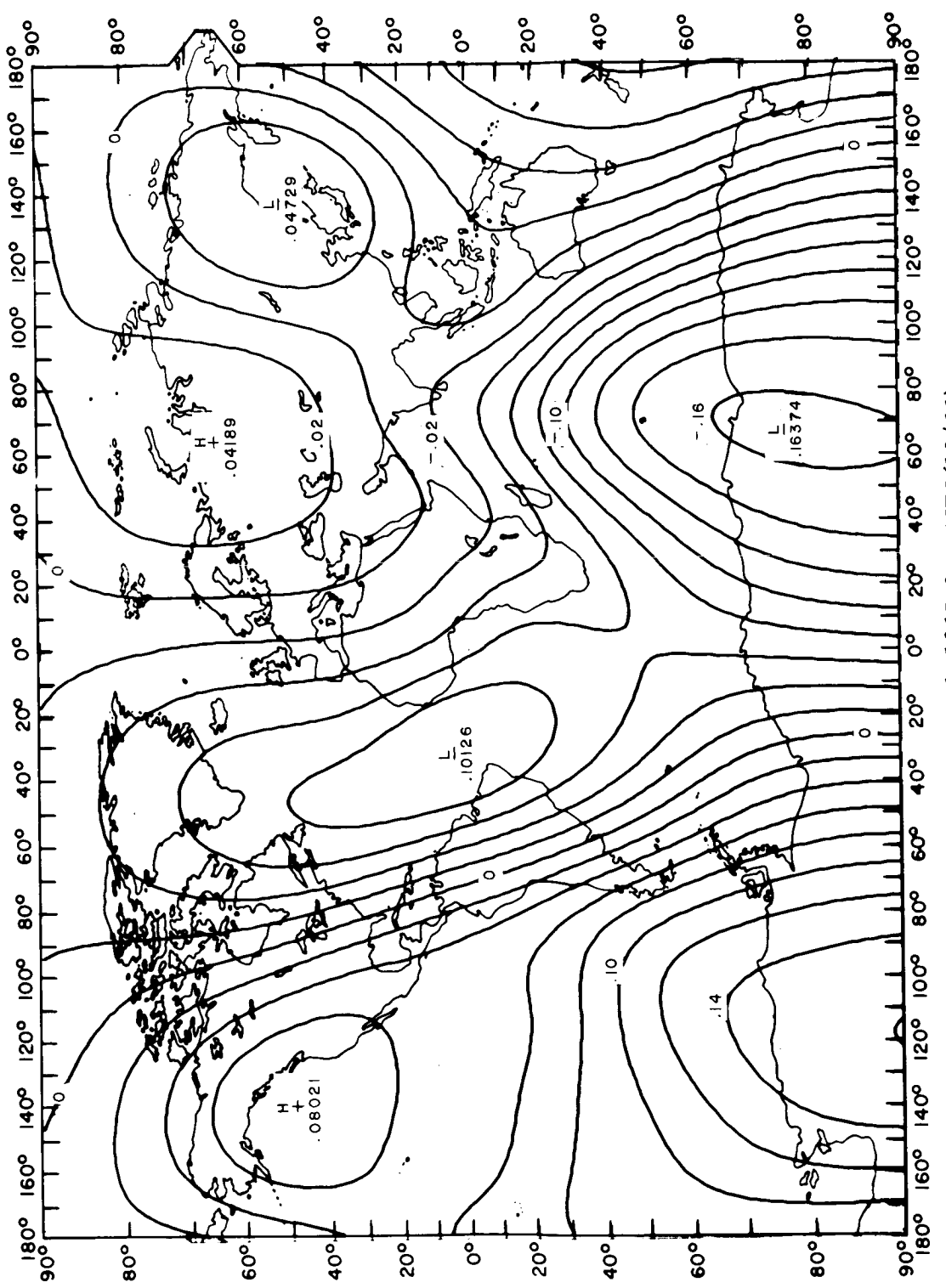
I in degrees, epoch 1965.0. GSFC(12/66).



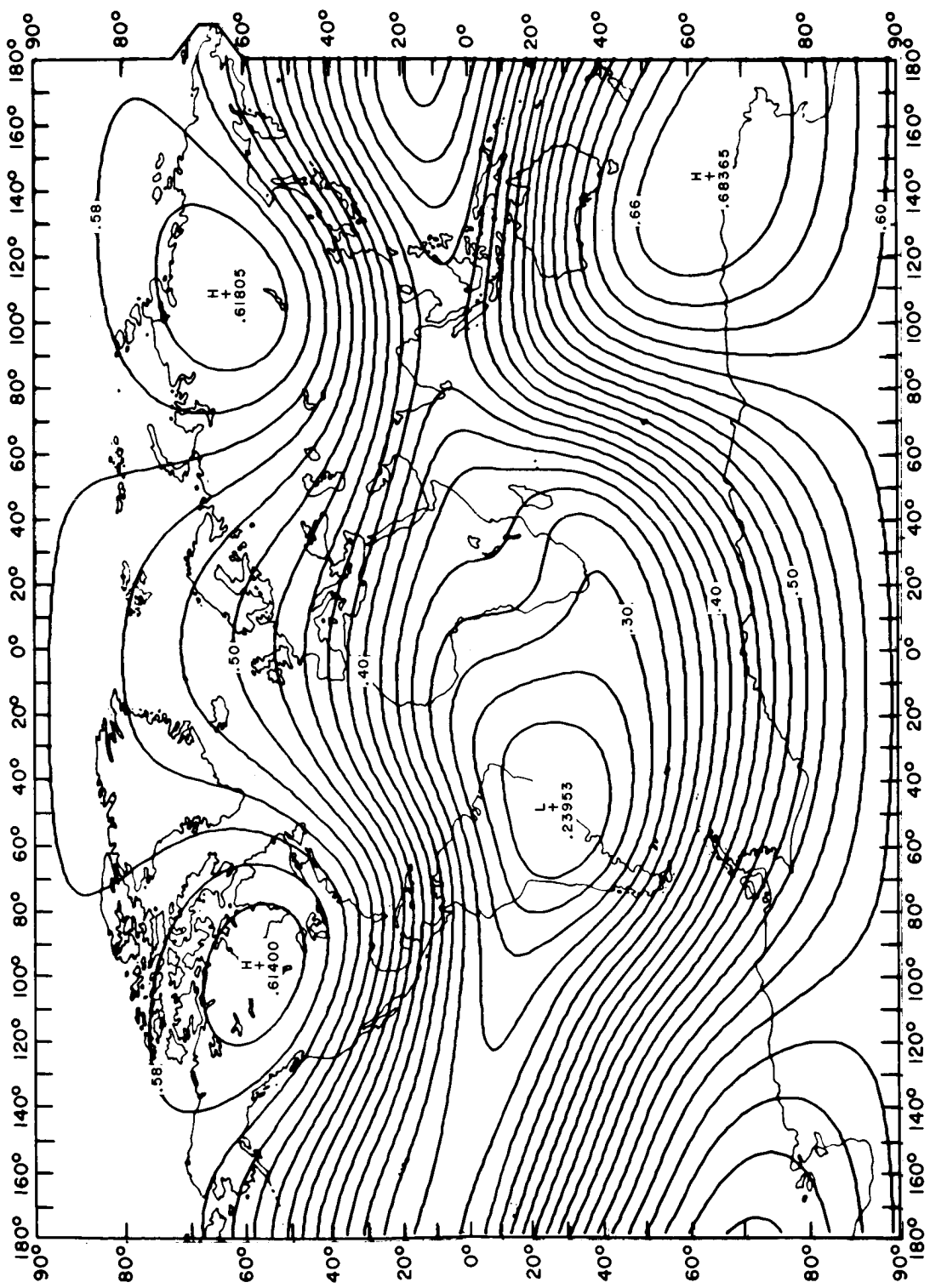
H in gauss, epoch 1965.0. GSFC(12/66).



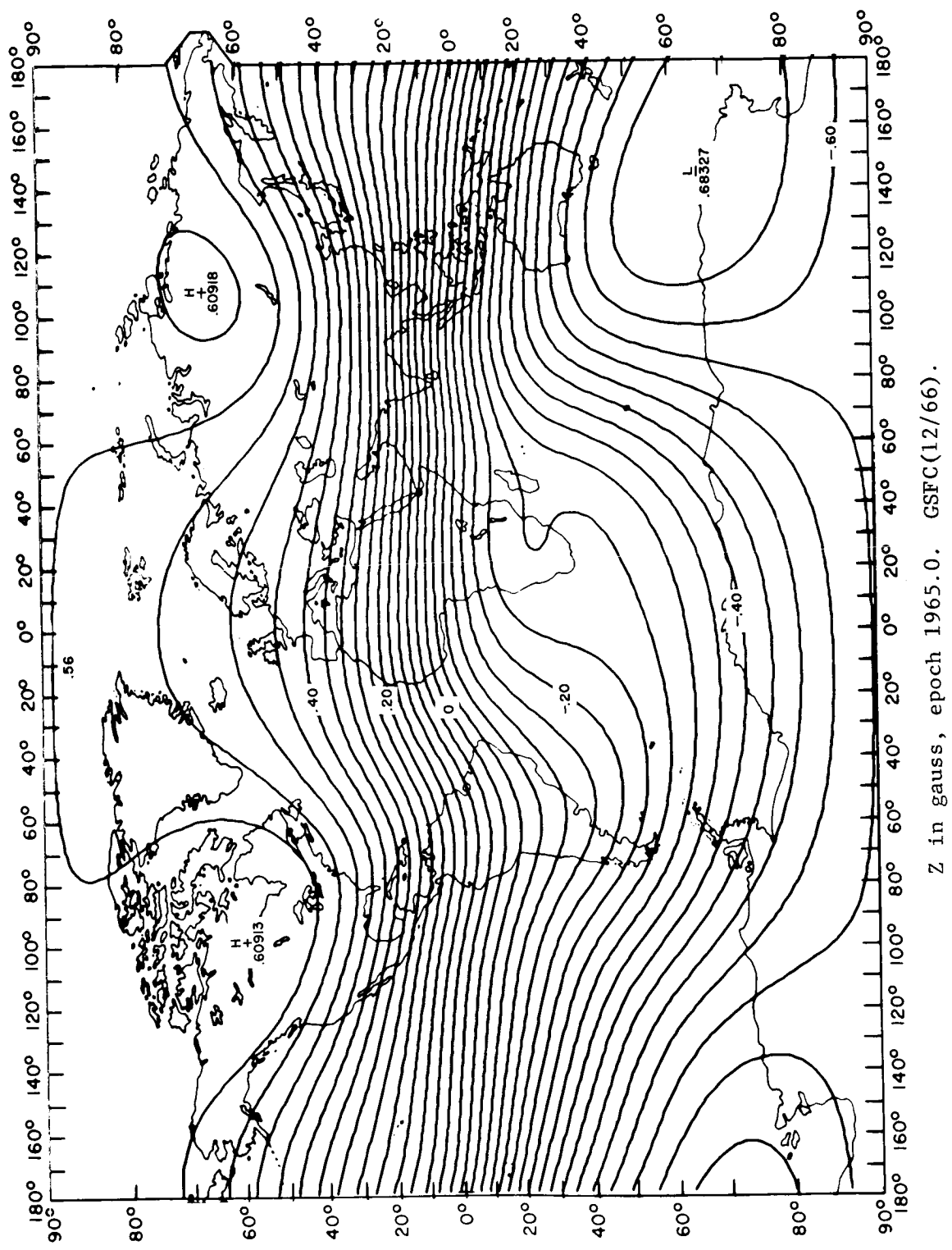
X in gauss, epoch 1965.0. GSFC (12/66).



Y in gauss, epoch 1965.0. GSFC(12/66).



F in gauss, epoch 1965.0. GSFC(12/66).



Z in gauss, epoch 1965.0. GSFC(12/66).